UNIVERSIDADE DE LISBOA
FACULDADE DE CIÊNCIAS
DEPARTAMENTO DE GEOLOGIA

Seismostratigraphic model of the Sines Contourite Drift (SW Portuguese margin) – depositional evolution, structural control and paleoceanographic implications

Sara Morgado Rodrigues

Mestrado em Geologia
Especialização em Estratigrafia, Sedimentologia e Paleontologia

Dissertação orientada por:
Professor Doutor Pedro António Gancedo Terrinha
Doutora Ana Cristina Freixo Pereira Roque

2017

"Voltar ali onde
A verde rebentação da vaga
A espuma o nevoeiro o horizonte a praia
Guardam intacta a impetuosa
Juventude antiga -
Mas como sem os amigos
Sem a partilha o abraço a comunhão
Respirar o cheiro a alga da maresia
E colher a estrela do mar em minha mão."

Sophia de Mello Breyner Andresen

ABSTRACT

The Sines Contourite Drift, located in the Southwest Portuguese margin, is a distal drift of the Contourite Depositional System of the Gulf of Cadiz, built by the influence of the Mediterranean Outflow Water (MOW). This drift is located between 1000 and 2000 m water depth on the Alentejo margin continental slope. The Sines Drift is bounded by four major morphologic features: the 1.4 km high Pereira de Sousa Fault escarpment to the west, the upper continental slope to the east and the Setúbal and São Vicente canyons to the north and south, respectively.

This work presents a seismic stratigraphic analysis and proposes an evolutionary model for the Sines Drift, as well as the identification of its main driving mechanisms and constraints. In pursuing such objectives, the following dataset was used: i) new and unpublished seismic reflection profiles acquired during the MOWER/CONDRIBER cruise in September-October 2014; ii) pre-existent multichannel seismic profiles BIGSETS, STEAM and GSI; iii) SWIM multibeam bathymetry; iv) lithostratigraphic and chronological data from Site U1391 of IODP (Integrated Ocean Drilling Program) Expedition 339 carried out in 2011-2012.

Three evolutionary phases are identified for the Sines Drift development: 1) a sheeted-contourite-drift phase (<5.3-3.2 Ma) built since the Late Miocene by an initially weak flowing MOW; 2) a mounded-contourite-drift phase (3.2-0.7 Ma) from Late Pliocene to Early Quaternary times characterized by a mounded drift in the south and sheeted in the north, with a succession of sinuous N-S paleomoats in the east built as a result of a MOW enhancement; and 3) a plastered-contourite-drift phase from Mid-Pleistocene (0.7 Ma) till the present-day, characterized by the present depositional (sandy-muddy drifts) and erosional (moats) contourite features associated with two major events of MOW intensification.

The growth of the Sines Drift was constrained by seafloor paleomorphologies that resulted from the rifting processes of the Southwest Portuguese margin, inherited from the Mesozoic rifting phases. The paleomorphologies provided accommodation space for drift growth and conditioned its overall architecture. The N-S horsts and grabens built during the Mesozoic rifting confined drift deposition and did not allow its lateral migration.

The formation of the Sines Drift has also been influenced by climatic fluctuations and sea-level changes especially during the Quaternary. The succession of sinuous paleomoats beneath the present-day moat suggests a persistent and northward flowing MOW with several phases of enhancement.

It was also perceived that the São Vicente and Setúbal canyons took most of the downslope sediment supply, as well as the occurrence of mass-movement processes in the west associated with the steep gradient of the Pereira de Sousa escarpment. All these results suggest the Sines Drift had a complex evolution controlled by several factors at different scales.

Keywords: Sines Contourite Drift, Southwest Portuguese margin, Mediterranean Outflow Water, seismic interpretation, IODP Site U1391

RESUMO

Contornitos são corpos sedimentares depositados ou retrabalhados por correntes de fundo que circulam paralelamente aos contornos batimétricos da margem. A formação dos contornitos é afetada, a longo e curto prazo, por fatores externos e/ou internos que podem modificar o padrão de circulação das correntes. Os depósitos contorníticos podem atingir dimensões consideráveis com vários quilómetros de largura e comprimento, os quais conservam informação paleoclimática e paleoceanográfica. Os contornitos também desempenham um papel importante no estudo dos riscos naturais submarinos, associados à ocorrência de deslizamentos, e na indústria de exploração petrolífera, como potenciais reservatórios e selantes.

Um extenso Sistema Deposicional Contornítico (CDS, *Contourite Depositional System*) formou-se no Golfo de Cádis, desde o fim do Miocénico Superior (5.33 Ma), pela ação da Água de Saída Mediterrânica (MOW, *Mediterranean Outflow Water*). Este CDS abrange vários depósitos contorníticos e outras formas sedimentares, deposicionais e erosivas, ao longo da margem continental Sul e Sudoeste Ibérica.

O Contornito de Sines, localizado na margem Sudoeste Portuguesa, é um contornito distal do CDS do Golfo de Cádis. Este corpo situa-se entre 1000 e 2000 m de profundidade na Bacia do Alentejo, com aproximadamente 70 km de comprimento, 40 km de largura, 1 km de espessura, morfologia assimétrica e configuração agradante com inclinação para oeste. O Contornito de Sines está limitado por quatro morfoestruturas: a escarpa da Falha Pereira de Sousa com 1.4 km de altura a oeste, a plataforma continental a este e os canhões de Setúbal e São Vicente a norte e sul, respetivamente.

Este trabalho apresenta uma análise sismostratigráfica e propõe um modelo evolutivo para o Contornito de Sines, além da identificação dos principais mecanismos e constrangimentos que controlaram a sua evolução. Para atingir estes objetivos, recorreu-se ao seguinte conjunto de dados: i) linhas de reflexão sísmica multicanal não publicadas, adquiridas durante a campanha MOWER/CONDRIBER em setembro-outubro de 2014; ii) linhas de reflexão sísmica multicanal, pré-existentes, dos projetos BIGSETS, STEAM e GSI; iii) batimetria multifeixe SWIM e iv) dados litostratigráficos e cronológicos da sondagem U1391 da Expedição 339 do IODP (*Integrated Ocean Drilling Program*), realizada em 2011-2012.

A metodologia utilizada durante este trabalho consistiu em interpretação de estratigrafia sísmica, análise batimétrica, calibração e correlação cronostratigráfica dos horizontes e unidades sísmicas com a sondagem U1391 e representação gráfica das propriedades litológicas e físicas da sondagem referida.

A interpretação sismostratigráfica dos dados apresentados permitiu identificar seis unidades sísmicas (U1 a U6), com idades compreendidas entre o Miocénico Superior e o Presente. Estas unidades foram depositadas sobre uma superfície basal erosiva (B) e estão separadas por cinco horizontes sísmicos (H2 a H6), que marcam descontinuidades na sucessão sísmica. As unidades sísmicas apresentam fácies transparente a maior profundidade, com configuração em cunha, que transita para uma fácies estratificada de elevada amplitude e configuração lobular a menor profundidade.

A análise litostratigráfica da sondagem U1391 permitiu a calibração cronostratigráfica das unidades sísmicas interpretadas, bem como a caracterização da sua litologia. As unidades U2 (onde a sondagem U1391 atingiu a sua máxima profundidade) e U3, situadas entre os 671.5 e 566.1 m de profundidade, têm idades compreendidas entre o Pliocénico Superior e o Quaternário Inferior (3.2-2.5 Ma). Estas unidades são constituídas por vasa carbonatada, de composição dolomítica (~0.87 m) aos 632 m de profundidade e um debrito (~0.35 m) aos 604 m de profundidade. Às unidades U4 e U5, recuperadas entre 566.1 e 196.1 m de profundidade, foram atribuídas idades entre o Pleistocénico Inferior a Médio

(2.5-0.7 Ma) e são constituídas por contornitos finos intercalados por sucessões de vasa carbonatada. A unidade sedimentar mais recente, U6, depositou-se desde o Pleistocénico Médio (0.7 Ma) até ao Presente. A unidade U6 é composta por alternância de depósitos contorníticos finos e grosseiros recuperados entre 196.1 m de profundidade e o fundo oceânico. Estes depósitos apresentam sucessões com bigradação, gradação normal e inversa (separadas por contactos gradacionais, bioturbados e, mais raramente, descontinuidades). Esta unidade contém seis intervalos contorníticos arenosos, areias finas a grosseiras, a 2, 50, 83, 96, 115 e 150 m de profundidade.

Foram identificadas três fases na evolução deposicional do Contornito de Sines: 1) uma primeira fase de contornito com configuração em camada (*sheeted drift)* (<5.3-3.2 Ma), construída desde o final do Miocénico Superior, por uma corrente MOW de fraca intensidade; 2) uma fase de contornito monticular (*mounded drift)* (3.2-0.7 Ma), desde o Pliocénico Superior ao Quaternário Inferior, caracterizada por uma morfologia monticular a sul e agradante a norte, com uma sucessão de paleo-fossas sinuosas ao longo da margem continental a este, que atestam a ocorrência de uma intensificação moderada a elevada da MOW e 3) uma fase final de contornito agradante (*plastered drift),* desde o Pleistocénico Médio (0.7 Ma) até ao Presente, caracterizada pelas atuais formas deposicionais (contornitos argilosos a arenosos) e erosivas (fossas), associadas a dois eventos de intensificação da MOW.

A formação do Contornito de Sines terá tido início no Miocénico Superior, possivelmente após o final da Crise de Salinidade do Messiniano, que afetou a região Mediterrânica entre 5.33 e 5.96 Ma, a qual teve repercussões drásticas para a circulação oceânica entre o Mediterrâneo e o Atlântico. Após a Crise de Salinidade do Messiniano e o restabelecimento da circulação através do Estreito de Gibraltar, a MOW possuía fraca intensidade. A sucessão de paleo-fossas subjacentes à fossa atual sugere uma corrente semipermanente e persistente ao longo da margem Sudoeste Portuguesa, em direção a norte, com vários eventos de intensificação.

A edificação do Contornito de Sines foi constrangida pelas paleo-morfologias do fundo do mar que resultaram dos processos de *rifting*, herdados das fases de *rifting* Mesozóicas na margem Sudoeste Portuguesa. Estas paleo-morfologias forneceram espaço de acomodação para o crescimento do contornito e condicionaram a sua arquitetura deposicional. Os *horsts* e *grabens*, com orientação aproximada N-S, resultantes do *rifting* Mesozóico, confinaram a formação do contornito impedindo a sua migração lateral.

A edificação do Contornito de Sines foi também influenciada por variações climáticas e eustáticas, especialmente durante a sua última fase de desenvolvimento. Durante o Quaternário, os eventos de intensificação da MOW correlacionam-se com dois eventos climáticos do Pleistocénico, registados na região Mediterrânica e nos depósitos contorníticos do Golfo de Cádis: o *Middle Pleistocene Revolution* (0.7-0.78 Ma) e o *Late Quaternary Discontinuity* (0.4 Ma).

Os sedimentos que constituem o Contornito de Sines são maioritariamente sucessões contorníticas de composição carbonatada, com uma maior componente biogénica na primeira fase de desenvolvimento (*sheeted drift*), e uma maior componente siliciclástica (contornitos arenosos), na última fase de desenvolvimento (*plastered drift*). A componente biogénica na primeira fase provavelmente indica a ocorrência de fenómenos de afloramento costeiro e deposição hemipelágica ao longo da margem Oeste Portuguesa, enquanto que a maior contribuição siliciclástica na última fase está associada a eventos de intensificação da MOW. O Contornito de Sines evoluiu de um sistema deposicional inicialmente carbonatado para siliciclástico na última fase de desenvolvimento, testemunhando variações de intensidade da MOW.

Os sedimentos carreados para a margem do Alentejo são maioritariamente fornecidos por deposição hemipelágica, fenómenos de afloramento costeiro e resultante de erosão da margem continental pela

circulação da MOW. O Contornito de Sines não é significativamente afetado por processos gravíticos, sendo registado apenas uma ocorrência no Pliocénico (debrito de ~0.35 m). A baixa incidência de processos gravíticos resulta, provavelmente, da morfologia da margem e da existência dos canhões de Setúbal e São Vicente, que canalizam grande parte do material deslocado. No entanto, existem depósitos de movimento de massa que afetam o sector ocidental do Contornito de Sines, que estão associados ao elevado declive da escarpa da Falha Pereira de Sousa. A formação destes depósitos poderá estar associada a vários fatores intrínsecos e extrínsecos à área em estudo. No que se refere aos fatores intrínsecos, destaca-se a potencial geração de planos de descolamento nas interfaces entre sedimentos contorníticos arenosos e vasosos caso se encontrem sobre pressão, com excesso de fluídos e/ou intercalados por sedimentos menos porosos. No que respeita aos fatores extrínsecos, a atividade sísmica registada na margem Sudoeste Ibérica poderá espoletar a ocorrência de deslizamentos submarinos no Contornito de Sines. Os resultados obtidos sugerem que o Contornito de Sines teve uma evolução complexa, controlada por vários fatores, a diferentes escalas.

Palavras-chave: Contornito de Sines, Margem Sudoeste Portuguesa, Água de Saída Mediterrânica, interpretação sísmica, Sondagem IODP U1391

ACKNOWLEDGMENTS

This study is the result of a long project, which would not have been possible without the support of many people, to whom I will convey my gratitude in this humble acknowledgment.

First, I would like to express my sincere gratitude to my thesis supervisors, Dr. Ana Cristina Roque and Prof. Dr. Pedro Terrinha, for their knowledge and support since the first day. I have been extremely lucky to have had two wise and incredible scientists to guide me through my work. Their insightful comments and thorough review of this thesis has enriched my knowledge on the contourite study field and many others.

The research was carried out at the Marine Geology and Georesources Division of the Portuguese Sea and Atmosphere Institute (DivGM – IPMA). My sincere thanks to all the people in the DivGM division and collaborators, Carlos Ribeiro (*Dr. Calex*), Débora Duarte (*a Pessoa viajante*), Joana Santos, Marisa Loureiro, Susana Muiños, Sónia Silva, Vítor Magalhães, João Noiva, Pedro Brito, Luís Batista, Marta Neres, Margarida Henriques and Rui Quartau, for their numerous advices, help and friendly banter.

My thanks to Dr. Francisco Javier Hernández-Molina (Royal Holloway University of London – RHUL, United Kingdom), Dr. David Casas (Instituto de Ciencias del Mar, Consejo Superior de Investigaciones Científicas – CSIC, Spain) and Dra. Gemma Ercilla (Instituto Geológico y Minero de España – IGME, Spain) for allowing me the use of the seismic profiles acquired during the MOWER/CONDRIBER cruise in 2014, in the scope of the CONDRIBER project.

I acknowledge the support of the Landmark Graphic Corporation via the Landmark University Grant Program.

To my fellow MSc and PhD students, Miguel Santos (*учитель ArcGIS*), Manuel Teixeira (*o vizinho portista*) and João Sá (*portugalský české*) for the help and companionship, despite having their own projects. I am also very grateful to Ana Martins, Sónia Simões, Joana Simões and Sheyla Azevêdo, close friends that will hopefully remain throughout the years.

Last, but not least, I would like to thank my family for their support and undivided attention. Words cannot express how grateful I am to my mother, my father and my twin sister Ana Rita (*meu espelho e meu oposto*), for all the sacrifices they've made in my behalf and for all they have given me over the years.

TABLE OF CONTENTS

LIST OF FIGURES

LIST OF TABLES

LIST OF ABBREVIATIONS

AGC	Automatic Gain Control
AIW	Atlantic Inflow Water
AMOC	Atlantic Meridional Overturning Circulation
CAMP	Central Atlantic Magmatic Province
CDC	Contourite Depositional Complex
CDP	Common Depth Point
CDS	Contourite Depositional System
DS	Descobridores Seamounts
EQD	Early Quaternary Discontinuity
FMS	Formation MicroScanner Sonde
GCCDS	Gulf of Cadiz Contourite Depositional System
GIS	Geographic Information System
GPS	Global Positioning System
GRA	Gamma Ray Attenuation
HLDS	Hostile Environment Litho-Density Sonde
HNGS	Hostile Environment Natural Gamma Ray Sonde
HRLA	High-Resolution Laterolog Array
IODP	Integrated Ocean Drilling Program
IB	Intermediate Branch
LC	Lisboa Canyon
LDW	Lower Deeper Water
LIW	Levantine Intermediate Water
LPD	Late Pliocene Discontinuity
LQD	Late Quaternary Discontinuity
MAD	Moisture and Density
Mbsf	Meters below seafloor
ML	Mediterranean Lower Water
MOW	Mediterranean Outflow Water
MPF	Marquês de Pombal Fault
MPP	Marquês de Pombal Plateau
MPD	Middle Pleistocene Discontinuity
MPR	Middle Pleistocene Revolution

MU	Mediterranean Upper Water
NACW	North Atlantic Central Water
NACWt	sub-tropical North Atlantic Central Water
NACWp	sub-polar North Atlantic Central Water
NADW	North Atlantic Deep Water
NASW	North Atlantic Surface Water
NGR	Natural Gamma Ray
RLB	Rincão do Lebre Basin
PAP	Príncipe de Avis Plateau
PAS	Príncipe de Avis Seamounts
PB	Principal Branch
PSF	Pereira de Sousa Fault
SB	Southern Branch
SC	Setúbal Canyon
SD	Sines Drift
SVC	São Vicente Canyon
SVF	São Vicente Fault
SW	Shelf Waters
WMDW	Western Mediterranean Deep Water
WRMSL	Whole-Round Multisensor Logger
TWT	Two-way time

CHAPTER 1

INTRODUCTION

1.1 Scope and objectives

Contourite drifts are sedimentary products of bottom-currents reworking and shaping continental margins (Rebesco and Stow, 2001). These currents flow parallel to the continental margins building up thick sedimentary features as a result of erosion, transport, reworking and re-deposition of sediments. Contourite drifts can reach up to several kilometers in width and in length, holding important information in their stratigraphic contents. Therefore, contourite drifts represent an important record for paleoceanographic, paleoclimatic and geohazard studies, as well as potential reservoirs for the oil industry (Faugères *et al*., 1993; Mulder *et al.*, 2003; Bryn *et al*., 2005; Laberg *et al.*, 2005; Rebesco, 2005; Shanmugam, 2006; Viana *et al.*, 2007; Rebesco and Camerlenghi, 2008; Brackenridge *et al.*, 2013; Stow *et al.*, 2013; Rebesco *et al*., 2014).

The Contourite Depositional System of the Gulf of Cadiz (GCCDS) has been targeted due to its complex nature and direct relation with the circulation of the Mediterranean Outflow Water (MOW) into the Atlantic Ocean. This CDS results from the dynamics of the MOW since Messinian times, formed by the opening of the Strait of Gibraltar and the end of the Messinian Salinity Crisis (5.33 to 5.96 Ma ago) (Cita, 2001; Bache *et al*., 2012). The GCCDS comprehends contourite drifts in the South and Southwest Iberian margin, namely the Albufeira, Bartolomeu Dias, Faro, Guadalquivir, Huelva, Lagos, Portimão, Sagres and the Sines drifts (e.g. Vanney and Mougenot, 1981; Nelson *et al*., 1993; Sierro *et al*., 1999; Llave *et al*., 2001, 2006, 2007, 2011, 2015; Hernández-Molina *et al.*, 2003, 2006, 2011, 2015; Marchès *et al*., 2007, 2010; Roque *et al*., 2012). The construction of the GCCDS was influenced by several factors associated with its tectonic and climatic settings, seafloor morphology and bottom-current dynamics (Faugères *et al*., 1993; Rebesco and Camerlenghi, 2008; Rebesco *et al*., 2014). The GCCDS is also influenced by the evolution of the Iberian margin through geological times, since it is located near the convergent plate boundary between the Eurasia and the African plate (Gutscher *et al.*, 2002, 2012). Hence, the tectonic setting of the Gulf of Cadiz and the evolution of the Atlantic Ocean are associated with the tectonic features of the study area and affect contourite drift deposition.

The Sines Contourite Drift (SD) belongs to the extensive CDS of the Gulf of Cadiz (Hernández-Molina *et al*., 2015). The SD is a sedimentary body located on the Southwest Portuguese margin, between 1000 and 2000 m water depth on the Alentejo continental slope (Figure 1.1). The SD is bounded by four major morphologic features, the 1.4 km high Pereira de Sousa Fault escarpment to the west, the continental shelf edge to the east, and the Setúbal and São Vicente canyons to the north and south, respectively. The SD consists of Late Neogene to Quaternary contourite deposits (Pereira and Alves, 2010, 2011, 2013; Hernández-Molina *et al*., 2015) and was classified as a plastered drift based on seismic data (Hernández-Molina *et al*., 2015). Mougenot (1976) was the first author to identify the SD, based on seismic reflection profiles and samples of seabed sediments. His work presented the characterization of the main seismic and stratigraphic sequences of the Southwest Portuguese margin, the present-day morphology, structures and the geodynamic evolution of the Portuguese continental shelf. The depositional evolution of the SD is still undefined, with the works of Alves *et al.* (2000, 2003) and Pereira and Alves (2010, 2011, 2013) establishing the stratigraphic record for the older syn-rift sequences in the Alentejo margin and Hernández-Molina *et al.* (2015) studying the GCCDS and its tectonic, sedimentary and

paleoceanographic evidences. Thus, the objective of this work is to propose a seismostratigraphic model for the Sines Contourite Drift, complemented by an analysis of its depositional evolution, structural control and paleoceanographic implications.

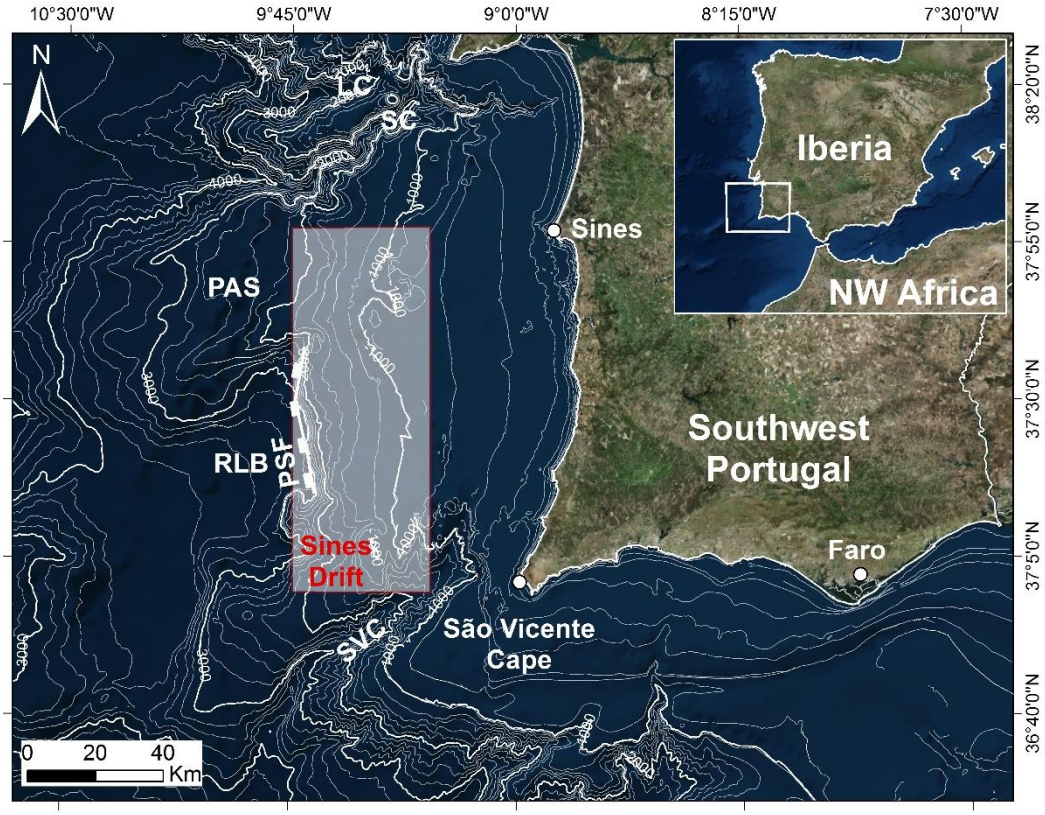

Figure 1.1 – Location of the Sines Drift in the Southwest Portuguese margin, between the Setúbal Canyon (North) and the São Vicente Canyon (South). RLB – Rincão do Lebre Basin; SC – Setúbal Canyon; SVC – São Vicente Canyon; LC – Lisboa Canyon; PAS – Príncipe de Avis Seamounts; PSF – Pereira de Sousa Fault.

1.2 Historical overview on contourite research

Contourite deposits have been the focus of several studies since the 1960's (Figure 1.2). The pioneer works by Heezen and Hollister (1964) and Hollister (1967) established the beginning of a new research field, the study of sedimentary features formed by the influence of contour bottom-currents in the deep-sea.

Contourites were recognized in the seismic record, however their classification and characterization was still poorly defined. McCave and Tucholke (1986) and Faugères *et al*. (1999) established the first classification systems based on seismic features. Other works also focused on seismic reflection profiles to diagnostic drifts, with a comprehensive review of all the known drift types and representative examples (Rebesco and Stow, 2001; Stow *et al*., 2002a,b; Rebesco, 2005; Shanmugam, 2006, 2008; Rebesco and Camerlenghi, 2008). The steady growth of knowledge allowed for a better understanding of the geometry and temporal evolution of contourite processes and led to the definition of Contourite Depositional Systems and Contourite Depositional Complexes (Hernández-Molina *et al.*, 2003; Rebesco and Camerlenghi, 2008). Most of this knowledge emerged from studying contourites formed by the influence of the MOW (García *et al*., 2009; Hernández-Molina *et al.*, 2011, 2015; Roque *et al*., 2012; Rebesco *et al*., 2014; Llave *et al*., 2015). Contourite research also grew in the technological domain, thanks to IODP and ODP Expeditions, such as IODP Expedition 339 in 2011-2012 that focused on the study of MOW paleocirculation along the Iberian margin. These expeditions contributed to a better

knowledge of paleo-climate, oceanic gateways, sea-level and tectonic controls on sediment architecture along continental margins, in the Mediterranean (ODP Leg 107), North Atlantic (IODP 303, IODP 306, IODP 307, IODP 319 and IODP 342), Pacific and Southern Oceans (ODP Leg 181, ODP Leg 194, IODP 317 and IODP 318).

The deep-water processes and environments behind contourite formation in the GCCDS are closely related to the paleoceanography and physical oceanography of the MOW (Nelson *et al.*, 1999) (Figure 1.2). The hydrography of the present MOW and its pathways were laid down by Zenk (1970, 1975), Ambar and Howe (1979) Ambar (1983), Harvey (1982) and Baringer and Price (1999). In the 2000's, the use of floats established precise MOW trajectories and allowed the identification of meddies formation along the Southwest Iberian margin (Bower *et al.*, 1994; Johnson *et al.*, 2002; Ambar *et al.*, 2002, 2008; Serra and Ambar, 2002; Serra *et al.*, 2005).

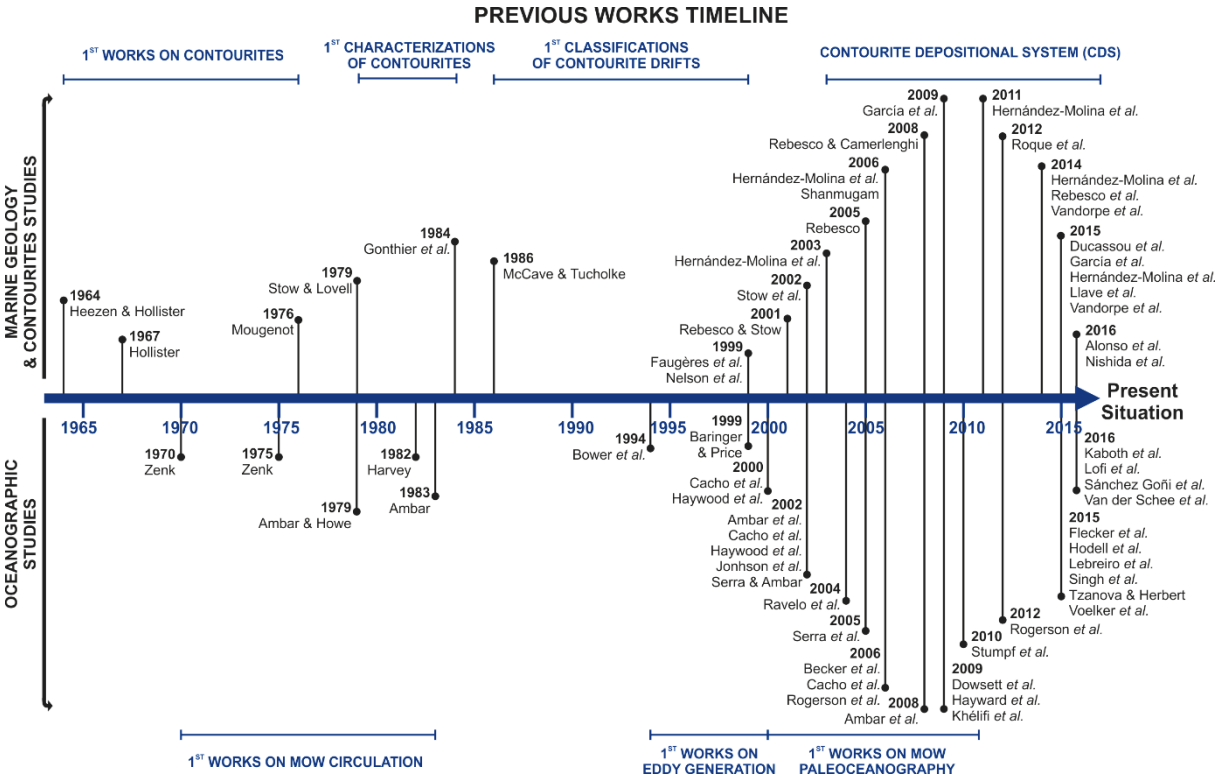

Figure 1.2 – Timeline of previous works made in contourite research till the present-day, with a considerable increase since 1999, depicting the evolution of knowledge and importance in the marine geology and the oceanography study fields.

The circulation of the MOW through the Pliocene and the Quaternary, and its relation to climate changes, has been studied through several methods: i) planktonic and benthic foraminiferal $\delta^{18}O$ records in the Mediterranean Sea (Becker *et al.*, 2006); ii) molecular biomarkers (C_{37} alkenones, *n*-nonacosane and *n*-hexacosanol) together with benthic $\delta^{18}O$ and $\delta^{13}C$ data on the Alboran Sea (Cacho *et al.*, 2000, 2002, 2006); iii) comparison of Nd isotopes, $\delta^{18}O$, Mg/Ca-based temperature and bottom water salinity on the Alboran Sea and Northeast Atlantic margin (Khélifi *et al.*, 2009); iv) Nd and Pb isotope records from authigenic ferromanganese coatings of sediments in gravity cores, on the Gulf of Cadiz and along the Portuguese margin (Stumpf *et al.*, 2010); v) decline and extinction of certain deep-water benthic foraminifers in the Mediterranean Sea and outside this region (Hayward *et al.*, 2009).

The MOW shows a distinct behaviour under different climatic conditions, therefore global climatic indicators were also studied through different approaches and in different regions: i) comparison of oxygen isotopic, $\delta^{18}O$, composition of benthic foraminifera on ODP Site 1014 with $\delta^{18}O$ record from

ODP Site 846, from different regions of the Pacific (Ravelo *et al.*, 2004); ii) analysis of planktic foraminifers and ostracods of sediment records in the North Atlantic Ocean (Dowsett *et al*., 1992) and at IODP Site U1391 in the Southwest Iberian margin (Singh *et al*., 2015); iii) paleoclimate modelling simulations in the Mediterranean and European region, supported by geologic data (Haywood *et al.*, 2000, 2002; Tzanova and Herbert, 2015); iv) parameters from cores of sediment records on the Gulf of Cadiz (grainsize, sediment composition, benthic foraminiferal assemblage and benthic foraminiferal stable isotope analysis) (Rogerson *et al.*, 2006, 2011; Hodell *et al*., 2015; Voelker *et al*., 2015; Kaboth *et al*., 2016; Sánchez Goñi *et al*., 2016);

1.3 Outline at a glance

This dissertation comprises eight chapters:

- **Chapter 1: Introduction**

In the first chapter the character and objectives of this work are outlined, as well as the database, thesis outline and previous contourite works in the Southwest Portuguese margin and Gulf of Cadiz.

- **Chapter 2: Geological Setting**

This chapter focuses on the stratigraphy and tectonics of the study area in the scope of the geodynamic evolution of SW Iberia and Africa-Eurasia plate boundary.

- **Chapter 3: Contourite Deposits in the Seismic Record**

The third chapter presents the characteristics of contourite drifts, their identification in the seismic record and their economic relevance. The different contourite features and factors contributing to contourite formation are also included.

- **Chapter 4: Contourites in Iberia**

The fourth chapter presents the oceanographic setting of the Southwest Iberia margin and a brief overview on the contourite depositional systems of West Iberia and Gulf of Cadiz.

- **Chapter 5: Data & Methodology**

This chapter contains the data used in this work and their provenance, as well as the used methodology and procedures.

- **Chapter 6: Results**

The sixth chapter reports the main results of this study, with a stratigraphic and structural interpretation of the Sines Drift and an analysis of the lithological and geophysical properties from IODP well data.

- **Chapter 7: Discussion**

This chapter discusses the Sines Drift depositional evolution, structural control and the role of bottom-currents and climatic fluctuations.

- **Chapter 8: Conclusions & Future Work**

The last chapter contains the conclusions of this study and suggestions for future works.

CHAPTER 2

GEOLOGICAL SETTING

The SD is located on the Southwest Iberian margin as shown in Figure 2.1 between depths of 1000 and 2000 m. The Southwest Iberian margin has a continental slope gently dipping to the west, cut in the south by the São Vicente Canyon that sources the Horseshore Abyssal Plain, and in the north by the Setúbal and Lisboa Canyons that reach the Tagus Abyssal Plain (Mougenot *et al*., 1979; Alves *et al*., 2003; Terrinha *et al*., 2009; Figure 2.1). The continental margin deepens west of the Pereira de Sousa Scarp to the Tagus Abyssal Plain, at depths of ~5000 m. The Southwest Iberian margin has other prominent features, such as the Príncipe de Avis Seamounts, the Descobridores Seamounts and the Marquês de Pombal Plateau (Mougenot *et al*., 1979).

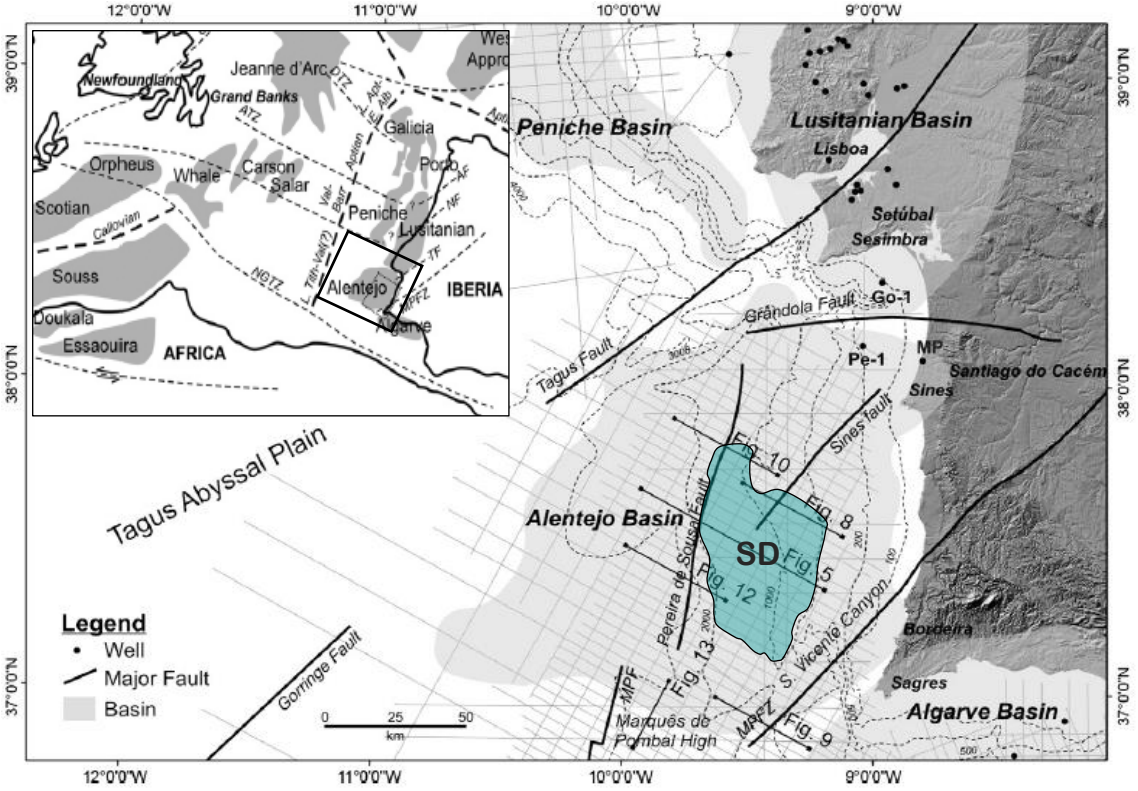

Figure 2.1 – Localization of the Sines Drift and the main Portuguese sedimentary basins and their relation with the other basins in the Central and North Atlantic due to the rifting of the North Atlantic (Pereira and Alves, 2011).

2.1 Geodynamic Evolution of the Southwest Iberian margin

The Southwest Iberian margin is located near the Eurasia-Nubia plate boundary in the North Atlantic. The Iberian margin began to develop during the early stages of continental rifting from the Triassic to the Early Cretaceous, which led to the Opening of the North Atlantic Ocean (Pinheiro *et al*., 1996; Rasmussen *et al*., 1998; Alves *et al*., 2002, 2006, 2009; Figure 2.2). In the Iberian margin, a group of Mesozoic rift basins evolved from south to north: the Algarve, Alentejo, Peniche, Lusitanian, Porto and Galicia Basins, which share a common rift-to-drift evolution insered in the context of the Mediterranean and the Atlantic regions (Alves *et al*., 2009, 2013; Pereira and Alves, 2010, 2011; Ribeiro, 2013b;

Terrinha *et al*., 2013a; Terrinha *et al*., 2013b). The rocks that constitute the basement are part of the Hesperian Massif, which incorporates Precambrian and Paleozoic rocks. During the Cenozoic, the Southwest Iberian margin evolved as a passive margin subjected to various pulses of compression, related to the Alpine Orogeny (Alves *et al*., 2003, 2006; Pereira and Alves, 2011, 2013).

2.1.1 The Late Paleozoic Evolution

- ***The Variscan Orogeny***

The basement of the Southwest Iberian margin is comprised by rocks of the Hesperian Massif, a segment of the Variscan Orogenic Belt that extends all over Europe. The orogenic belt, formed during the Late Paleozoic (Devonian-Permian) by the convergence and collision of two major continents, Laurasia and Gondwana, led to the creation of the supercontinent Pangea (Ribeiro, 2013a). The Paleozoic basement of the Southwest Iberian margin is comprised by deformed and metamorphosed rocks from the South Portuguese Zone (Ribeiro, 2013a).

2.1.2 The Mesozoic Evolution

During the Mesozoic, the Southwest Iberian margin suffered continental rifting, oceanic breakup and subsequent drifting, associated with the opening of the North Atlantic Ocean. The rifting started in the Triassic, leading to the formation of epicontinental seas during Jurassic and Cretaceous times (Ribeiro, 2013b). This process begun with the thinning of the continental lithosphere, which created graben and half-graben structures with the deposition of evaporites and continental deposits, followed by whole lithospheric rupture, which accommodated the initial formation of oceanic lithosphere and the formation and development of a passive margin.

The Iberian margin is considered a type of conjugate magma-poor asymmetric rift margin that recorded the distinct periods of continental extension (Pinheiro *et al*., 1996; Tucholke *et al*., 2007). However, a consensus has yet to be reached regarding the number and magnitude of rifting events, their exact age and more often their regional implications (Pinheiro *et al*., 1996; Alves *et al*., 2009).

It has been considered that the Iberian margin evolved as a conjugate of the Newfoundland and Nova Scotia margins after four rifting events, namely in the Late Triassic, Early-Middle Jurassic, Late Jurassic and Early Cretaceous (Pinheiro *et al*., 1996; Rasmussen *et al*., 1998; Alves *et al*., 2002, 2006, 2009; Figure 2.3). As a result of the Atlantic tectonic extension, the Southwest Iberian margin was segmented in distinct structural domains: the inner proximal margin, the outer proximal margin and the distal margin (Alves *et al*., 2009; Pereira and Alves, 2011, 2013; Figure 2.2).

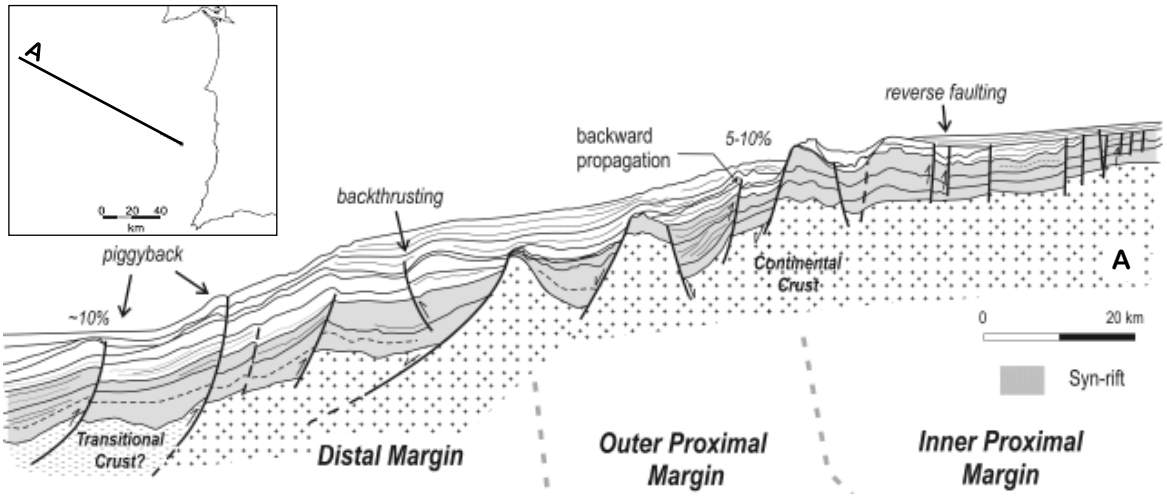

Figure 2.2 – Line drawings depicting the distinct structural domains of the Southwest Iberian margin (Alves *et al*., 2013).

- ***Rift Phase I***

The first rift phase in the Late Triassic (to earliest Jurassic) was established above a pre-existent Paleozoic continental crust (Ribeiro *et al*., 1979). Continental extension begun in the Late Triassic with a wide rift mode in a widespread rift basin between the Labrador and Nova Scotia margin, and from the south (Alentejo) to the north (Galicia) along the margin (Pinheiro *et al*., 1996; Figure 2.3). Subsidence and thinning was accommodated in grabens and half-grabens during this period (Stapel *et al*., 1996), marked by the deposition of continental red beds overlain by successions of Hettangian shales and evaporites (Azerêdo *et al*., 2003). This first phase of extension is synchronous with continental rifting between North Africa and North America (Welsink *et al*., 1989) and between the Labrador margin and the North Sea (Sinclair, 1995).

- ***Rift Phase II***

The second extensional phase is initially marked by magmatic activity from the Rhaetian to the Hettangian. The magmatic activity occurs as dispersed volcano-sedimentary successions throughout the Southwest Iberian margin (in Sesimbra, Santiago Cacém and Algarve Basin) (Ribeiro *et al*., 1979; Azerêdo *et al*., 2003; Martins *et al*., 2008). These volcano-sedimentary successions have ages and geochemical signatures related to the Central Atlantic Magmatic Province (CAMP) (Martins *et al*., 2008).

The second rift phase marks the transition from wide rift to focused extension mode (Tucholke and Sibuet, 2007; Pereira and Alves, 2013), displaying seaward migration of the rift locus and preceding continental breakup (Alves *et al*., 2009). The Early to Middle Jurassic is described as a period when West Iberia and Newfoundland experienced limited epeirogenic subsidence, with minor continental extension (Tucholke and Sibuet, 2007; Pereira, 2013; Figure 2.3). During this phase the Iberian margin recorded a progressive influence of open marine environments with episodes of basin inversion, observed on the Toarcian-Aalenian of the Alentejo Basin (Terrinha *et al*., 2002; Azerêdo *et al*., 2003).

The southern North Atlantic was segmented during continental extension and subsequent seafloor spreading (which also affected the offshore Moroccan and Nova Scotia margins), bounded by first-order transfer faults that formed correlative geodynamic provinces (Tankard and Balkwill, 1989) (Figure 2.3). These transfer zones include the Newfoundland-Gibraltar Transform Zone, the Collector Fault Zone, the Avalon Transfer Zone or the Dominion Transfer Zone and the Messejana-Plasencia Fault Zone (Tankard and Balkwill, 1989; Tucholke and Sibuet, 2007).

- ***Rift Phase III***

The third rifting phase in the Late Jurassic overlays a regional angular unconformity that extends from the Callovian to the Mid-Oxfordian (Azerêdo *et al*., 1998, 2002), which shows a new period of intense tectonic subsidence (Hiscott *et al*., 1990; Cunha *et al*., 2009). As a result, West Iberia developed two major N-S to NE-SW rift axes bound by first order transfer zones (the Aveiro Fault, the Nazaré Fault, the Tagus Fault and the Messejana-Plasencia Fault Zone) (Alves *et al*., 2009; Figure 2.3).

The Late Jurassic is characterized by a transition towards seafloor spreading, with increased seaward thinning of the continental crust, and the main axes of subsidence in the proximal margins of the southern Alentejo and Lusitanian Basins (Alves *et al*., 2009). A moderately long phase of extension continued from the Tithonian to the Berriasian-Hauterivian (Tucholke *et al*., 2007; Bronner *et al*., 2011).

- ***Rift Phase IV***

The final rifting phase occurred in the Early Cretaceous (Berriasian to Aptian-Albian) (Figure 2.3) and is mainly observed on the North Iberian margin with a period of tectonic subsidence followed by formation of oceanic crust (Tucholke *et al*., 2007). The separation of the continental crust between the Galicia Bank and North Newfoundland was completed by the Barremian, but continued till the Aptian-Albian boundary with the exhumation of mantle, when the oceanic breakup occurred (Tucholke et al., 2007; Figure 2.3). Seafloor spreading off the Southwest Iberian margin occurred by late Aptian-Albian times (Tucholke *et al*., 2007).

The Late Cretaceous is marked by the opening of the Bay of Biscay, which exerted significant rotational component on the Iberian microplate (Garcia-Mondejar, 1989). During this period, sediment deposition along the margin was controlled by thermal subsidence, loading and eustasy.

The Late Cretaceous is also marked by magmatic activity, with the intrusion of the alkaline massifs of Monchique, Sines and Sintra, as well as volcanics, dykes and sills in the Lisboa and Algarve regions (Miranda *et al*., 2009, Grange *et al*., 2010).

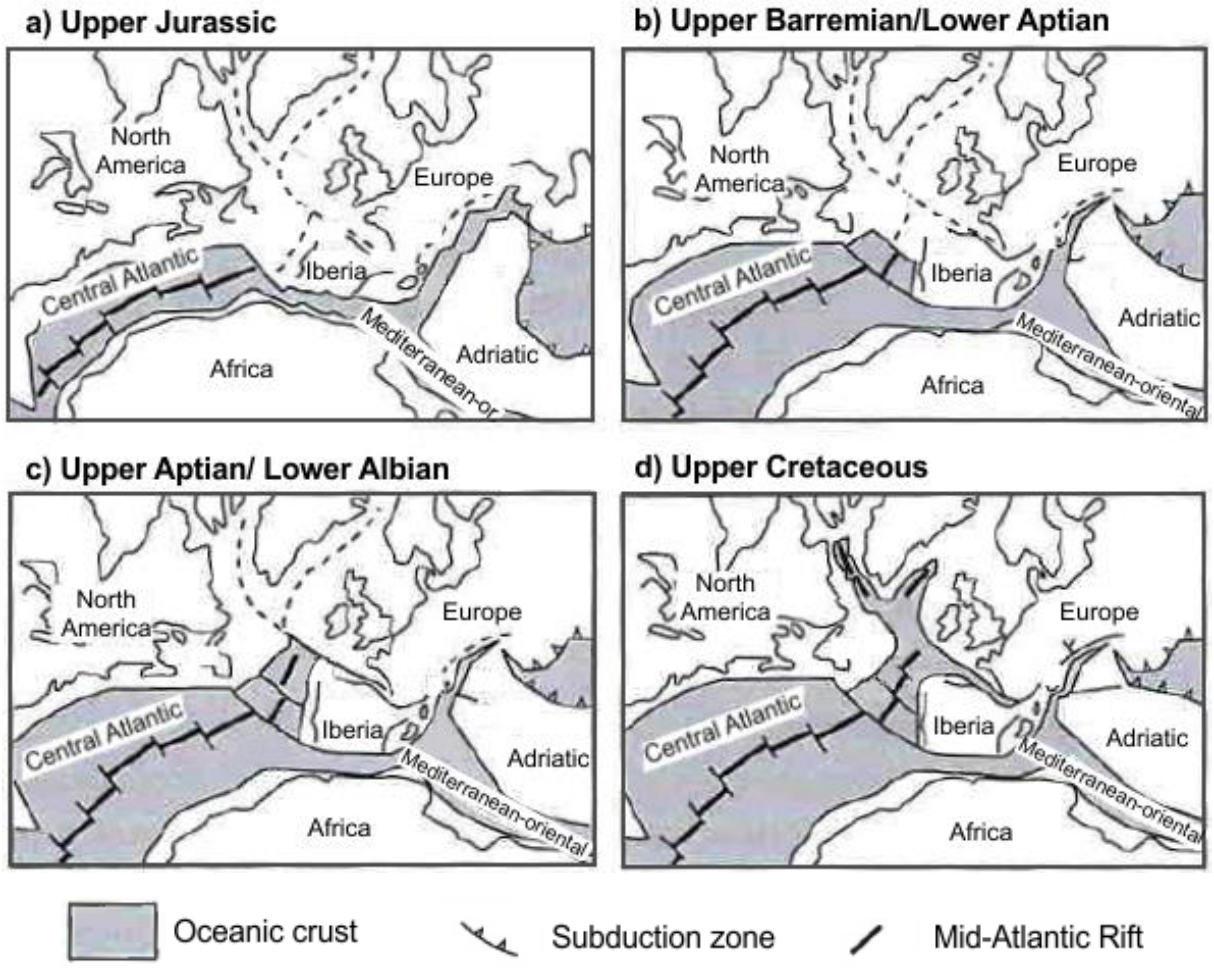

Figure 2.3 – Schematic evolution of the North Atlantic, showing the continental breakup from the Upper Jurassic to the Upper Cretaceous. Modified from Alves *et al*. (2013).

2.1.3 The Cenozoic Evolution

- ***Alpine Orogeny***

The Southwest Iberian margin is a passive margin since the break-up discontinuity in the Early Cretaceous (Alves *et al.*, 2000, 2003). However, the margin is in close proximity to the plate boundary between Eurasia and Africa, thus affected by the collision and compression events of the Alpine Orogeny during the Cenozoic (Pyrenean and Betic phases) (Alves *et al.*, 2003, 2006; Pereira and Alves, 2011, 2013).

- ***Tectonic inversion of the Iberian margin***

The Meso-Cenozoic of the West Iberian margin is marked by several periods of tectonic inversion with ancient and recent features (Mougenot *et al*., 1979; Alves *et al*., 2003, 2009; Terrinha *et al*., 2003, 2013b; Zitellini *et al*., 2004; Neves *et al*., 2009). The most intensive periods occurred from the latest Cretaceous onwards, associated with the collision of the Iberian microplate with the Eurasia and Africa plates (Mougenot *et al*., 1979). Since the Late Cretaceous, nine tectonic phases of shortening, inversion and uplift are recorded, according to Alves *et al*. (2003).

From the Late Cretaceous to the Middle Eocene a significant period of shortening and inversion occurred (Pinheiro *et al*., 1996). This period is associated with N-S to NE-SW convergence towards the Pyrenees, when Iberia was connected to North Africa and the active plate boundary was located at the Bay of Biscay (Mougenot *et al*., 1979; Ribeiro *et al*., 1990). During this period, the proximal margin was also deformed by the intrusion of the igneous bodies of Sintra, Monchique and Sines (Miranda *et al*., 2009).

The Eocene is characterized by a new episode of inversion widely expressed throughout the Iberian margin, caused by a reactivation of the inherited NE-SW rift faults (Mougenot *et al*., 1979). A relatively important period of inversion occurred from the Late Oligocene to the Miocene, associated with the NNE-SSW collision between the Iberian microplate and North Africa, during the Atlas phase of the Alpine Orogeny (Ribeiro *et al*., 1990; Pinheiro *et al*., 1996). In the Miocene, the Alpine compression is also associated with the subduction of the Tethyan oceanic crust in the western Mediterranean and the collision between Iberia and North Africa (Figure 2.4). This led to the formation of the Betic-Rif orogenic arc, the submarine accretionary wedge of the Gulf of Cadiz and the closure of the gateway between the Tethys and the Atlantic Ocean (Gutscher *et al*., 2002, 2012; Gràcia *et al*., 2003a; Cunha *et al*., 2012; Duarte *et al*., 2013; Figure 2.4). Inversion and shortening events continued from the Miocene till the Present along the Southwest Iberia margin, with the reactivation of the NE-SW to WSW-ENE extensional faults (Ribeiro *et al*., 1990; Gràcia *et al*., 2003a; Terrinha *et al*., 2003, 2013b; Zitellini *et al*., 2004; Neves *et al*., 2009).

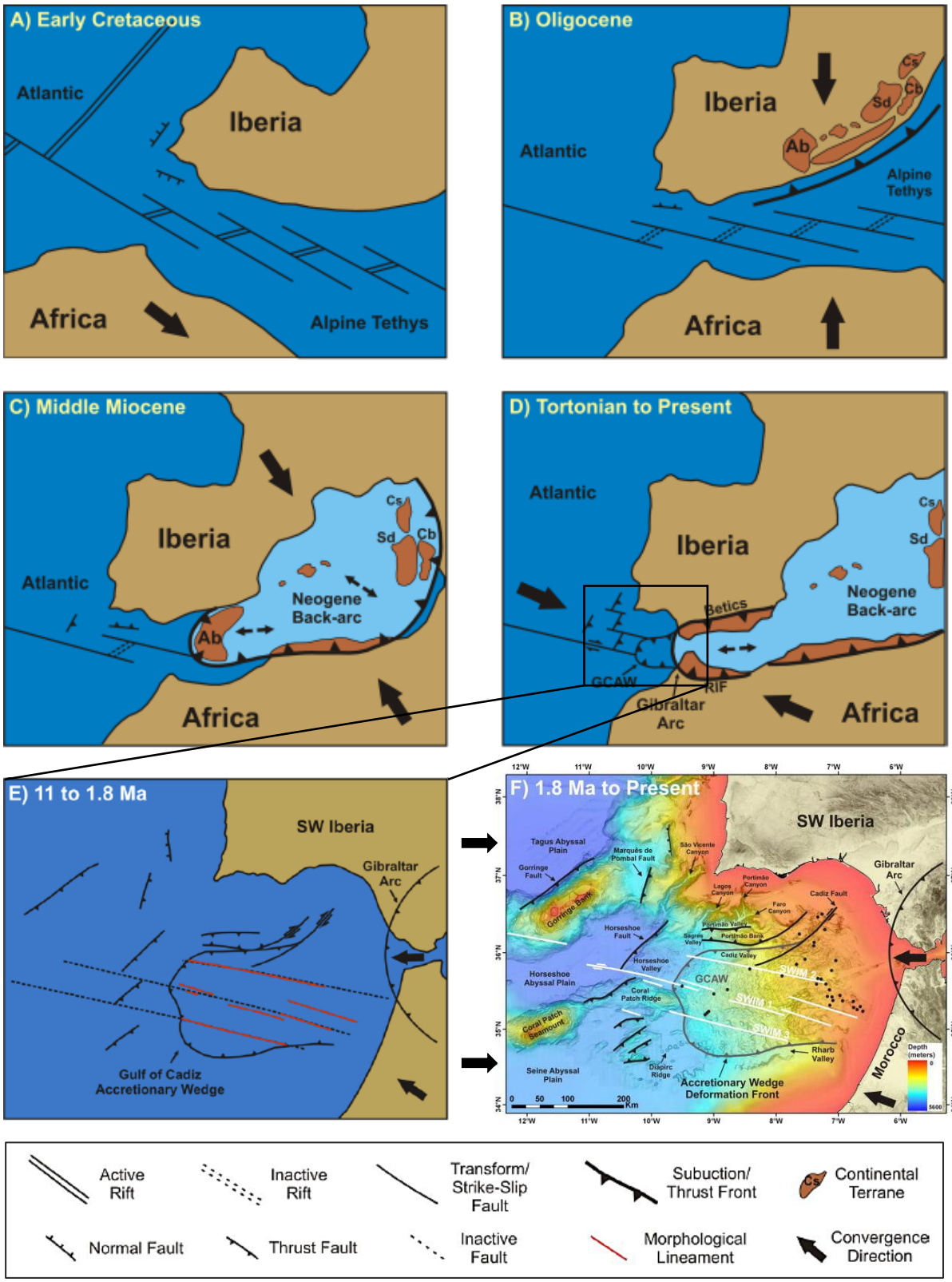

Figure 2.4 – Schematic reconstruction of the tectonic evolution of the Southwest Iberian margin and Western Mediterranean, from the Mesozoic to the Present (Duarte *et al*., 2011).

2.2 Stratigraphy of the Southwest Iberian margin

The sedimentary record of the Southwest Iberian margin spans from Mesozoic to Cenozoic deposits that lay over the Paleozoic deformed basement. The sedimentary fill recorded the evolution of the Iberian margin, from the North Atlantic rifting to the present-day (Hiscott *et al*., 1990; Pinheiro *et al*., 1996; Pereira and Alves, 2011, 2013).

The lithostratigraphy of the Southwest Iberian margin presented here is based on information gathered by Pereira (2013), from outcrops in the areas of Sagres, Bordeira, Santiago do Cacém and Sines, as well as the regional stratigraphy and previous seismostratigraphic studies, exploration wells and dredges samples analysis (Mougenot *et al*., 1979; Hiscott *et al*., 1990; Pinheiro *et al*., 1996; Pereira and Alves, 2010, 2011, 2013; Figure 2.5 and 2.6).

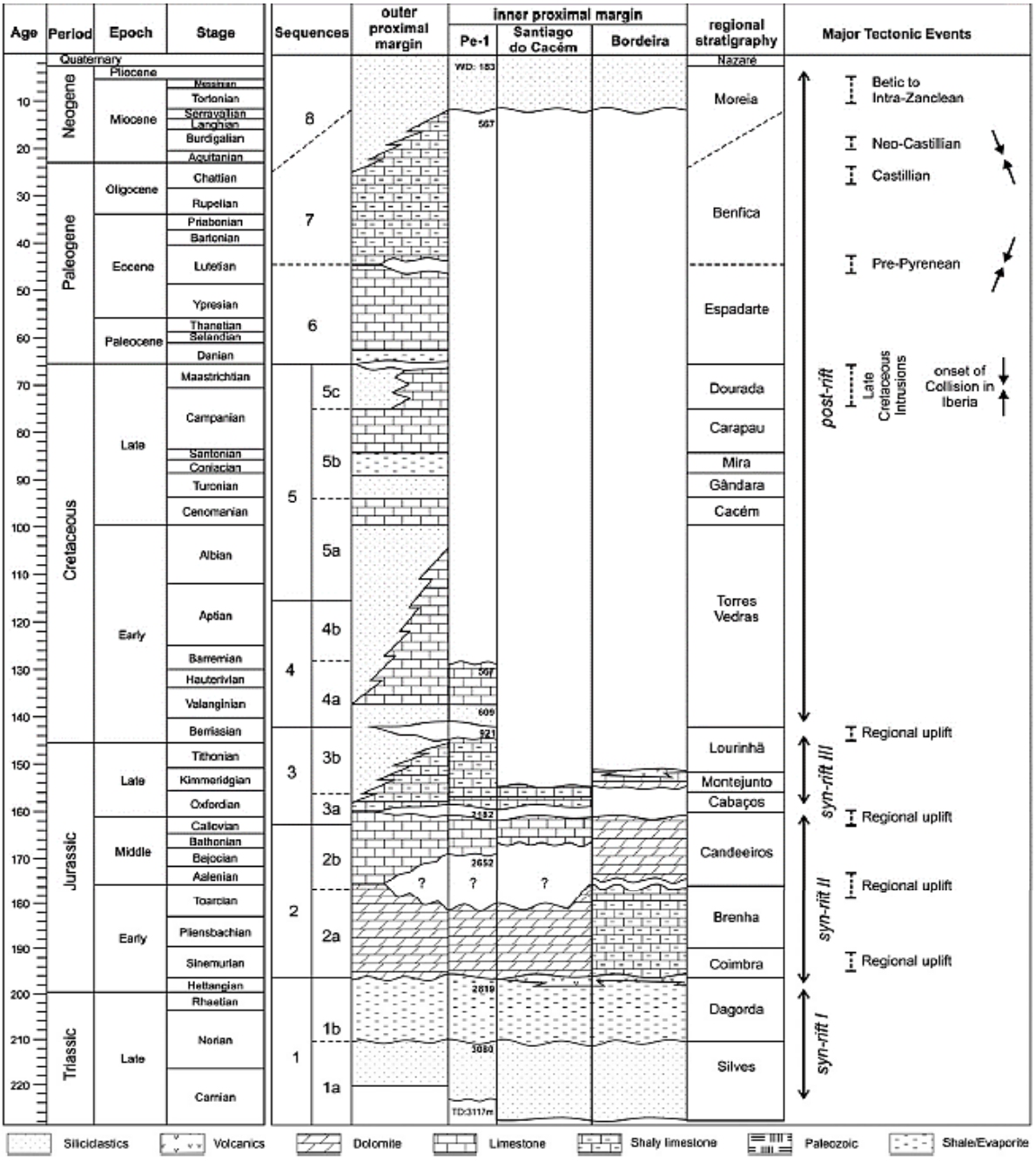

Figure 2.5 – Lithostratigraphy and seismic stratigraphy of the Southwest Iberian margin with the major tectonic events of the Alentejo Basin. From Pereira and Alves (2013), based on Alves *et al*. (2003, 2009), Azerêdo *et al*. (2003) and Rey *et al*. (2006).

2.2.1 The Paleozoic basement

The Paleozoic units in the Southwest Iberian margin are characterized by moderately to highly deformed successions of the South Portuguese Zone (Figure 2.6). These successions occur as outcrops in the Southwest and in Cercal-Rio Mira (Oliveira, 1984). The Southwest includes, from base to top: the Tercenas Formation, the Carrapateira Group and the Brejeira Formation. The Tercenas Formation is characterized as Late Devonian deep marine shales and sandstones. The Carrapateira Group of the Carboniferous comprises:

- The Bordalete Formation, composed by metasedimentary black shales and sandstones interbedded by siliceous nodules;
- The Murração Formation, characterized by silts, limestones and black to red schists and shales;
- The Quebradas Formation, defined by black schists, silts, shales and rare interbedded limestones;

The Brejeira Formation is made of widespread turbidites from the Late Carboniferous. The Cercal-Rio Moura consists of the Volcanic Complex of Cercal and the Mira Formation. The Volcanic Complex of Cercal was formed since the Late Devonian to the Tournaisian(?). The Mira Formation belongs to the Flysch do Baixo Alentejo Group and is characterized by turbidites in the Namurian, conglomerates and sporadic interbedded limestones.

2.2.2 The Mesozoic deposition

The Mesozoic deposits of the Southwest Iberian margin, which recorded the syn-rift phases, are initially represented by Late Triassic fluvial red beds with rarer marls and dolomites of the Silves Formation, above a regional angular unconformity and the deformed Late Paleozoic (Oliveira, 1984; Ribeiro *et al*., 1987; Inverno *et al*., 1993, Azerêdo *et al*., 2003; Figure 2.5). These deposits are observed at the Telheiro beach and in Bordeira. The Silves Formation is overlain by the extensive continental Dagorda Formation, characterized by evaporites, dolomites, marls and shales from the Norian to the Hettangian (Oliveira, 1984; Ribeiro *et al*., 1987; Inverno *et al*., 1993; Azerêdo *et al*., 2003; Figure 2.5 and 2.6).

The transition to the second rift phase in the Early Jurassic is marked by the evolution of the Central to North Atlantic, with the setting up of widespread shallow marine conditions and the formation of carbonate successions (Azerêdo *et al*., 2003). In the Alentejo Basin, this event is marked by the occurrence of low energy dolomitic carbonate ramps of the Coimbra Formation (Azerêdo *et al*., 2003; Figure 2.5). This early inclusion of marine deposits is preceded by the occurrence of magmatic activity of the CAMP, marking the initiation of an extensional rift phase in the Rhaetian-Hettangian (Martins *et al*., 2008). The Southwest Iberian margin in the Pliensbachian is marked by a new period of tectonic subsidence (Cunha *et al*., 2009) with the accumulation of deep-water sediments and marly limestones in the southern Alentejo Basin, the Forno unit (Oliveira, 1984; Ribeiro *et al*., 1987). Other areas of the Alentejo Basin are characterized by dolomites (Inverno *et al*., 1993).

The continuous deepening of the margin associated with a period of tectonic latency, resulted in the formation of a carbonate ramp along the margin, and by the Toarcian-Aalenian a period of regional uplift in Southwest Iberia resulted in a hiatus (Ribeiro *et al*., 1987; Terrinha *et al*., 2002). Deposition begun again in the Bajocian, when the carbonate ramp became shallower and the landward domains were uplifted to exposure, which resulted in the extensive unconformity from the Mid-Callovian to the Early Oxfordian (Azerêdo *et al*., 1998, 2002, 2003). In Bordeira, the carbonate ramp includes Toarcian(?)-Callovian dolomites (Dolomias Inferiores unit), while in Santiago do Cacém the Bathonian-Callovian was constrained to open shallow marine limestones with marls and dolomites, the Rodeado and Monte Branco Formations (Inverno *et al*., 1993).

The Late Jurassic is marked by a new rift phase and tectonic subsidence in the margin (Mougenot *et al*., 1979; Hiscott *et al*., 1990; Cunha *et al*., 2009). The Late Callovian to Middle Oxfordian interval is characterized by a widespread angular unconformity at the base (Azerêdo *et al*., 1998, 2002). In Santiago do Cacém the Oxfordian-Kimmeridgian is characterized by the Deixa-o-Resto Formation with an angular unconformity at the base and a succession of polygenic conglomerate and marine limestones and marls (Inverno *et al*., 1993). In Bordeira, the basal unit (probably Kimmeridgian) is comprised by limestones, dolomites and shales of the Zimbreirinha, overlain by a coral bearing unit (Três Angras Formation), covered by volcanic tuffs, limestones and conglomerates (Ribeiro *et al*., 1987).

In the Alentejo Basin, the basal Oxfordian units are correlated to the Cabaços Formation (Figure 2.5), of lacustrine to shallow marine marls and limestones (Azerêdo *et al*., 2002; Pereira, 2013), while the Oxfordian-Kimmeridgian is characterized by deep-marine to transitional limestones associated with the period of maximum subsidence (Alves *et al*., 2009). The Late Jurassic deposits in the Alentejo Basin are characterized by shallow marine sandstones, pelagic limestones and marls (Inverno *et al*., 1993; Figure 2.5). The Late Kimmeridgian-Berriasian interval is absent in Santiago do Cacém and Bordeira (Ribeiro *et al*., 1987; Inverno *et al*., 1993), however offshore dredges collected shallow marine limestones and dolomites, that mark this interval as a major subsidence period (Mougenot *et al*., 1979).

The final rift phase is marked by an angular unconformity in the Berriasian, related to a shift in the nature and architecture of the depositional units and in the locus of active rift subsidence (along the principal N-S axis on the margin) (Pinheiro *et al*., 1996; Rey *et al*., 2006; Alves *et al*., 2009, 2013). In the Alentejo Basin this period is absent, but exploration wells in the Southwest Iberian margin revealed siliciclastics and carbonates that are roughly correlated to the fluvial-deltaic and shoreline siliciclastics of the Torres Vedras Formation, north of the Lusitanian Basin, and to the shallow marine limestones of the Cascais Formation, south of the Lusitanian Basin (Mougenot *et al*., 1979; Mougenot, 1989).

The Berriasian-Aptian in the Iberian margin is characterized at its top by a widespread unconformity, the breakup unconformity (Tucholke *et al*., 2007). Afterwards, the conjugate Iberia-Newfoundland margins evolved as drifting tectonic plates and deposition was mainly controlled by eustasy, periods of post-rift compression and sediment input into the inherited accommodation space and on the oceanwards domains (Mougenot *et al*., 1979; Alves *et al*., 2009, 2013; Neves *et al*., 2009; Cunha *et al*., 2010). The final period of the Cretaceous (Campanian) is marked by the occurrence of magmatism with the intrusions of Monchique, Sines and Sintra (Miranda *et al*., 2009; Grange *et al*., 2010).

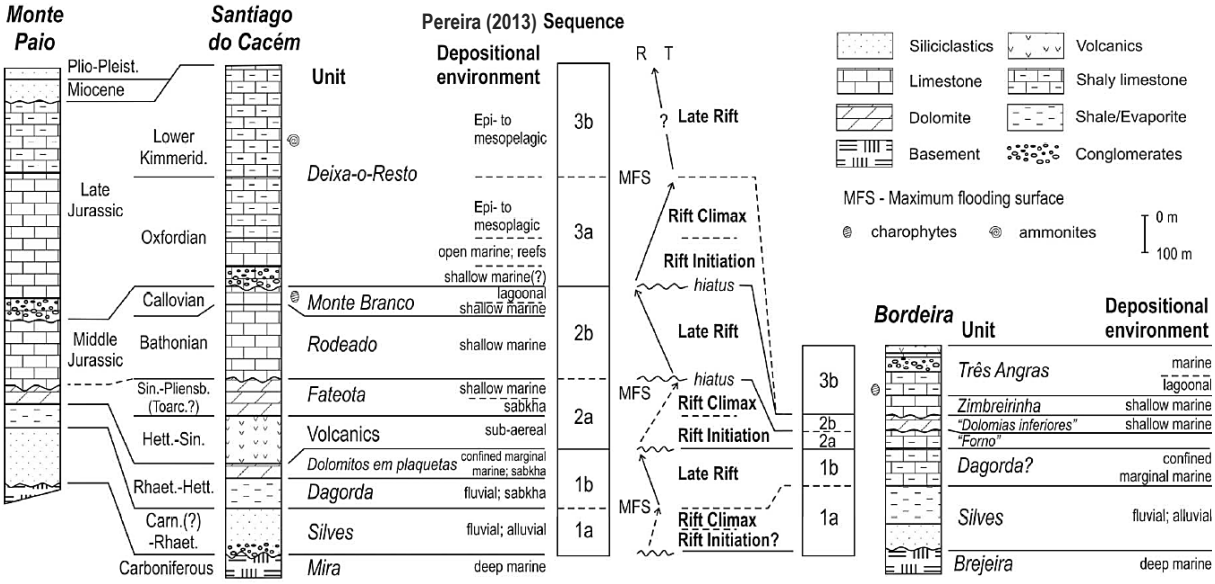

Figure 2.6 – Schematic lithostratigraphy, depositional environments and T-R trends from outcrops at Monte Paio, Santiago do Cacém and Bordeira. From Pereira (2013).

2.2.3 The Cenozoic deposition

The Cenozoic in the Alentejo Basin is comprised by Paleogene to Quaternary sediments. These sediments are sourced by the surroundings areas and by canyon sediment bypass, from the Cenozoic continental depocenters (Oliveira, 1984; Alves *et al*., 2003). The canyon sediment bypass is related to the Lisboa and Setúbal Canyons to the north and the São Vicente Canyon to the south, which control the sediment input into the margin (Llave *et al*., 2006; Pereira and Alves, 2010; Valadares, 2012).

The Paleogene in the offshore is characterized by limestones, dolomites and continental to shallow marine siliciclastics assigned to the Benfica and Moreia Formations (Mougenot *et al*., 1979; Figure 2.6). The Eocene is possibly characterized by mass-movement deposits associated with the margin inversion, (Mougenot *et al*., 1979), while the Oligocene is marked by a widespread erosion surface, which resulted from tectonic uplift of the margin, and is subsequently covered by fault-bounded successions due to a rise of sea-level from the Chattian onwards (Alves *et al*., 2000).

The Neogene is marked by several phases of inversion from the Burdigalian to the Miocene, with deposition of shallow marine siliciclastics. Afterwards, from the Pliocene to the Pleistocene, deep-water limestones and marls were deposited above (Mougenot *et al*., 1979). According to the present knowledge, the formation of a Contourite Depositional System in the Southwest Iberian margin and Gulf of Cadiz began when the Strait of Gibraltar opened, following the end of Messinian Salinity Crisis (5.33 to 5.96 Ma; Cita, 2001; Bache *et al*., 2012). The establishment of this gateway allowed the exchange between Mediterranean and Atlantic water masses and the formation of a complex drift system on the South and Western Iberian margin (Hernández-Molina *et al*., 2006; 2015).

2.2.4 Magmatism

The West Iberian margin is considered a typical magma-poor rifted margin with distinct and widespread cycles of magmatic activity throughout the Mesozoic:

1) The tholeiitic cycle (203-198 Ma), represented by extrusive lava flows in Algarve, Bordeira, Santiago do Cacém and Sesimbra (Martins *et al*., 2008) and the Messejana-Plasencia doleritic dyke system (Silva *et al*., 2008). This is associated with the Central Atlantic Magmatic Province (CAMP) (Verati *et al*., 2007).
2) The early alkaline cycle (146-142 Ma), represented by the occurrence of alkaline magmatism in the center of the Lusitanian Basin (Grange *et al*., 2008).
3) The transitional cycle (135-130 Ma), which occurs mainly in the Lusitanian Basin and in Algarve, as dykes of dolerites, gabbros and diorites. Minor hypovolcanics also occur in Nazaré and Montejunto (Miranda *et al*., 2009).
4) The alkaline cycle (100-71 Ma), which occurred in two pulses: the Foz da Fonte, Paço d'Ilhas and Ribamar as part of the sill and dyke complex of Mafra (100 Ma) (Miranda *et al*., 2009) and the Lisboa Basaltic Complex (73 Ma), intrusive Sines, Sintra and Monchique massifs (84-71 Ma) (Miranda *et al*., 2009; Grange *et al*., 2010).

The first three cycles are associated with the main phases of continental rifting, while the fourth cycle is associated with the post-rift evolution of the West Iberian margin (Pinheiro *et al*., 1996).

CHAPTER 3

CONTOURITE DEPOSITS IN THE SEISMIC RECORD

3.1 Bottom-Currents

Bottom-currents can shape the seafloor by eroding, re-suspending and transporting sediments. This type of current is influenced by several forces that can alter current speed and direction. The erosive, transport or deposition capacity of bottom-currents varies in time and along their track, forming what is known as drifts, and particularly contourites (Figure 3.1).

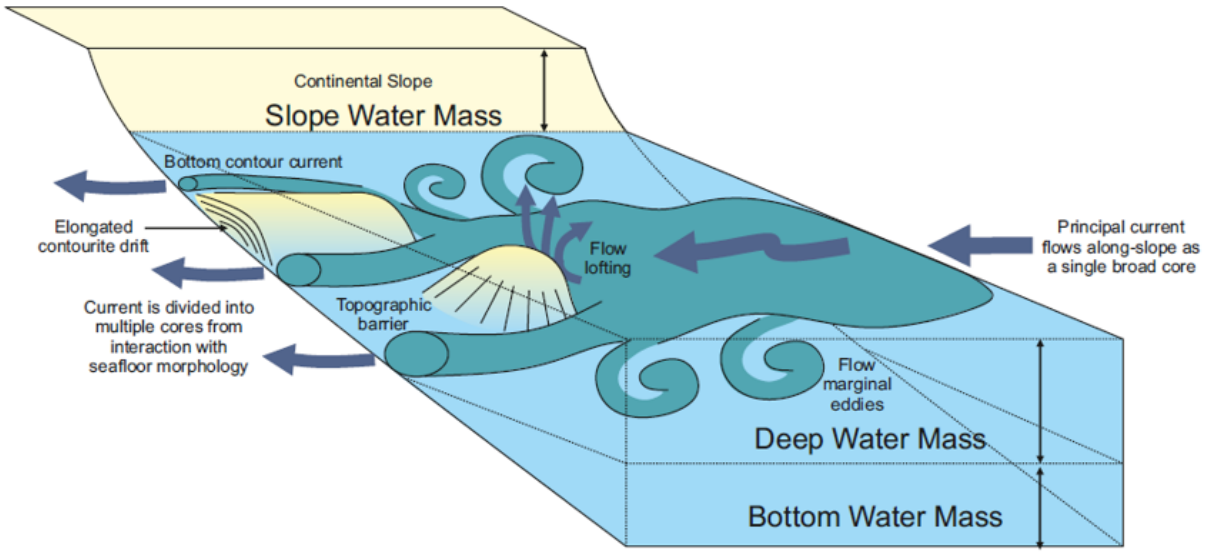

Figure 3.1 – Diagram of the main bottom-current features and interaction between bottom-currents and local topography. Modified from Stow *et al.* (2008).

Bottom-current is a generic term that includes different types of currents (Stow *et al*., 2008; Shanmugam, 2008). Most bottom-currents start as density currents sinking to their buoyancy level. These currents are mainly unidirectional subsurface currents in contact with the seafloor. They follow a quasi-geostrophic balance and a quasi-steady flow that can be affected by tides, seasonal changes or migrating eddies (Shanmugam, 2008; Zenk, 2008). Thus, their direction is subparallel to the seafloor topography, flowing alongslope as a single broad core, branding them as "contour-currents" (Stow *et al.*, 2008; Figure 3.1).

Not all currents are directly involved in contourite formation and a few play only a secondary role. The different currents involved in contourite construction are described as follows (Shanmugam, 2008):

- **Contour-currents:** with a net flow alongslope, subparallel to the topographic contours. Despite their path, they can also flow upslope, downslope, around and over topographic obstacles or irregularities. The Coriolis force and the meridional distribution of continents force the intensification of these currents along the western and eastern boundaries of the oceans;
- **Abyssal currents** (also named "ocean currents"): characterized as equivalent of large-scale bottom-currents flowing in the bottom-deep sea, below the edge of the continental slope, with the topography and the Coriolis force playing an important role in determining their pathway;

- **Thermohaline currents:** formed as a result of uneven density distributions and variable temperature and salt content in the water masses. The horizontal transport of a water mass determines the oceanic conveyor-belt, called the Meridional Overturning Circulation on the Atlantic Ocean (AMOC) (Figure 3.2);
- **Geostrophic currents:** characterized by long-lasting equilibrium conditions between the horizontal pressure gradient and the Coriolis force. The flow is forced to follow the bathymetric contours, since these currents have zero vertical velocity;
- **Deep-water currents:** formed by deep-water tidal currents in submarine canyons, long-wave baroclinic currents (internal waves, tides, solitary waves) and tsunami-related traction currents.

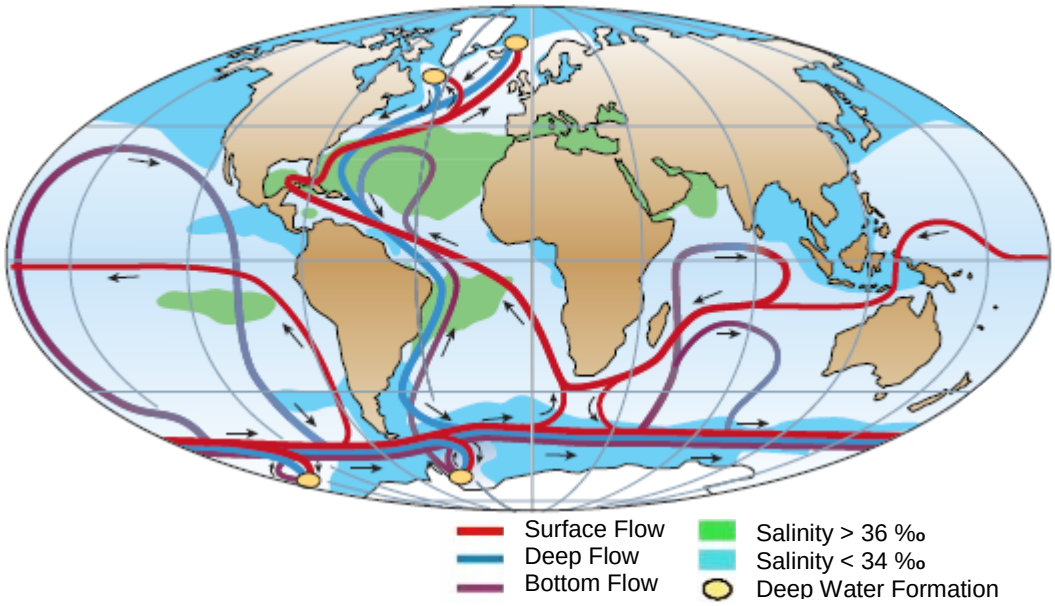

Figure 3.2 – Representation of the global oceanic conveyor-belt and the so called Atlantic Meridional Overturning Circulation (Rahmstorf, 2002, 2006).

Two other processes occur interstratified with the processes involved in contourite formation, although they are not related to the construction of contourites:

- **Upwelling:** which involves the rise of deep-water masses, and produces bottom-currents against topographic barriers and continental margins, mainly at low latitudes;
- **Downwelling:** characterized by a downward transport of cooled water masses from the surface. This transport occurs mainly at polar latitudes, resulting in bottom-currents (not necessarily at the ocean margins, therefore it does not affect the seafloor sometimes).

3.2 Contourites

Contourites are sediments deposited on continental margins or ocean basins, due to the effect of bottom-currents and several processes (such as tides, internal waves, barotropic waves, dynamic instabilities and gravitational flux) on the seafloor (Stow *et al.*, 2002b; Rebesco, 2005; Faugères and Stow, 2008). Contourite deposition often involves multi-phase entrainment, long distance transport, and interaction among depositional processes induced by the various types of bottom-current (McCave, 2008; Stow *et al.*, 2008). Yet, the different types of bottom-currents are known to influence to a greater or lesser extent many depositional environments. They affect various types of sediment, both during and after deposition. Thus, it is generally accepted that contourite sedimentary facies also include sediments,

usually interbedded, that are not deposited under the influence of bottom-currents (Figure 3.3). The occurrence of sediments other than contourites is due to the interaction between alongslope, downslope and pelagic processes. Turbidites, for example, can occur frequently within contourite successions, even if the bottom-current influence is large enough to control the overall geometry of the deposits and generate a contourite drift (Faugères *et al.*, 1999; Rebesco, 2005; Rebesco *et al.*, 2014).

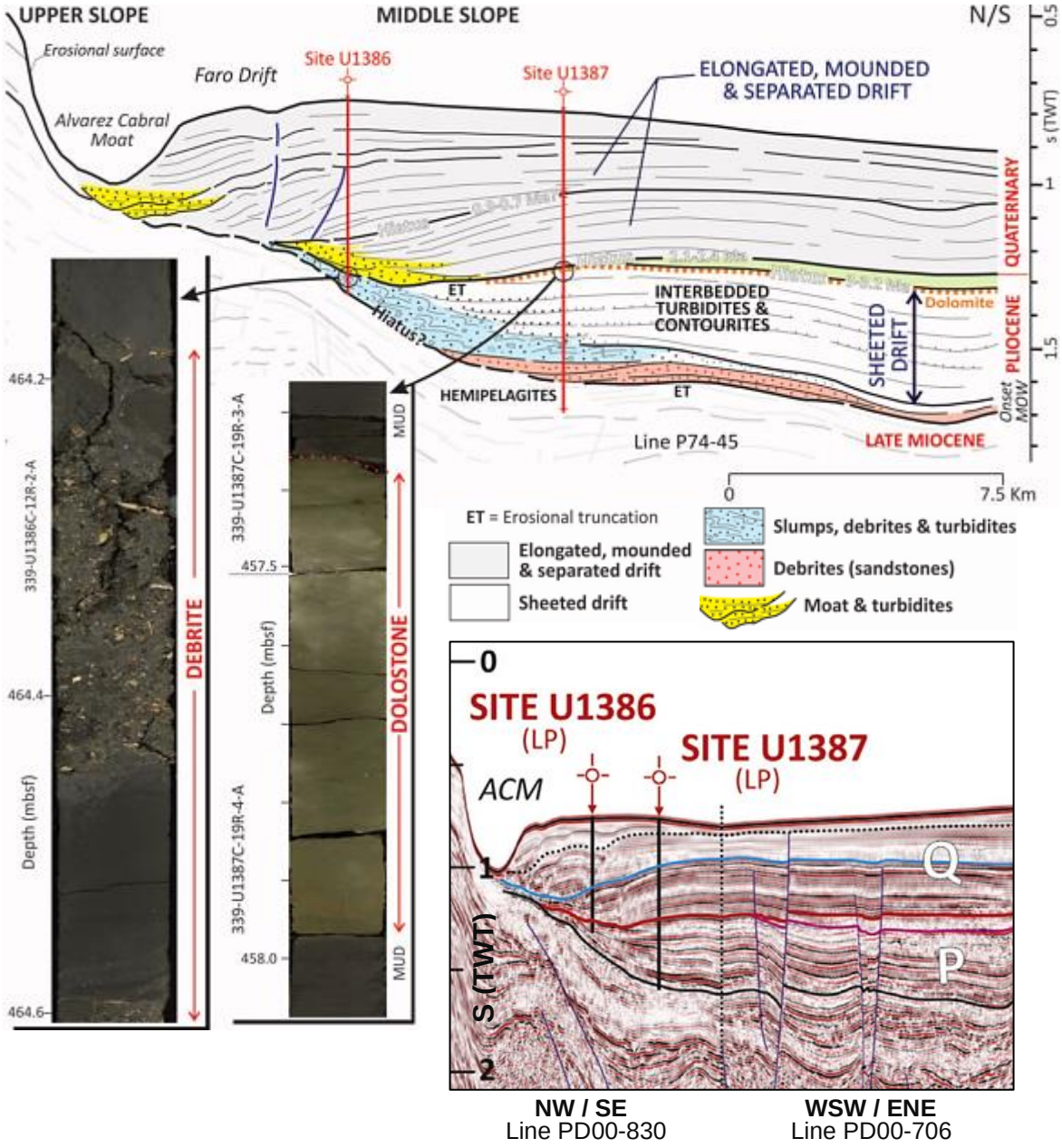

Figure 3.3 – Examples of other sediment facies interbedded with contourite facies at Expedition 339 Sites U1386 and U1387 in the Faro Drift, Algarve Basin (adapted from Hernández-Molina *et al.*, 2014a, 2015).

Bottom-currents are capable of building thick and extensive accumulations of sediments, if a significant sediment input is available, from the abyssal floor to the outer shelf (Faugères and Stow, 2008). The term contourite drifts should be used for sediment accumulations deposited, or significantly affected, by currents flowing along the contours. However, it was highlighted already that different types of bottom-current exist and therefore, the term contourite drifts should be used for sediment accumulations deposited by bottom-currents in general.

3.3 Depositional and erosional features related to bottom-currents

The formation of contourites along any continental margin involves the construction of several erosional and depositional features. When alongslope processes dominate over other processes, such as mass wasting, turbidity currents or pelagic settling, erosional and depositional features are formed as a result of bottom-current variations (Figure 3.4 and 3.5) and are usually linked to a Contourite Depositional System (CDS). If this CDS is distinct but connected within the same water mass, it can be considered a Contourite Depositional Complex (CDC) (Hernández-Molina *et al.*, 2003, 2006). The formation of a CDS ends when the transport capacity of the bottom-current diminishes till it no longer dominates over other depositional processes. Therefore, mixing with other deep-water facies types occurs, with the formation of erosional and depositional features at different scales, from small crossbed layers to large sediment drifts (Rebesco, 2005; Rebesco *et al.*, 2014).

In the seismic record, contourites are easy to recognize due to unambiguous diagnostic criteria at the mesoscale. The classification of contourite drifts, established by Faugères *et al.* (1999) and Rebesco *et al.* (2014), focuses on the definition of different drift types by location, morphology and drift development for each geological and hydrological context. These classifications are not mutually exclusive, due to gradation and overlap between all types and mixed drifts (Figure 3.5 and 3.6). Most drifts have sheeted or mounded morphology, but the mounded forms are also further classified based on other physiographic features (Faugères *et al.*, 1999). Large-scale surface and linear erosional features are also common, usually associated with contourite deposits. Surface features are reported as terraces or abraded surfaces, while linear features are channels, moats or marginal valleys (Figure 3.4 and 3.6).

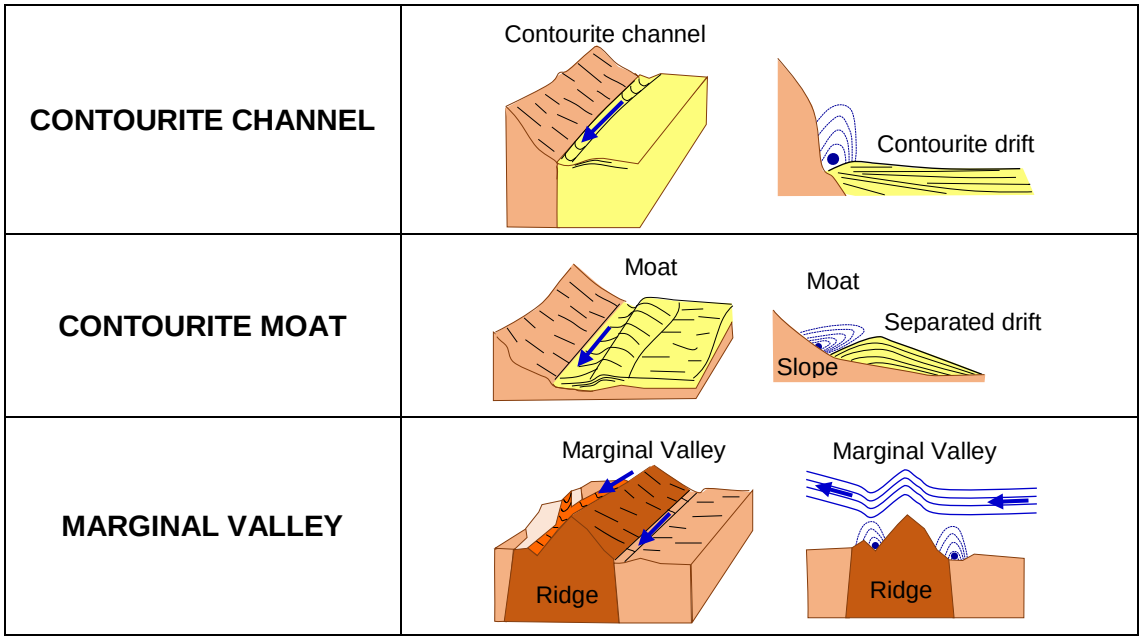

Figure 3.4 – Main characteristics of linear large-scale contourite erosional features Rebesco *et al*. (2014).

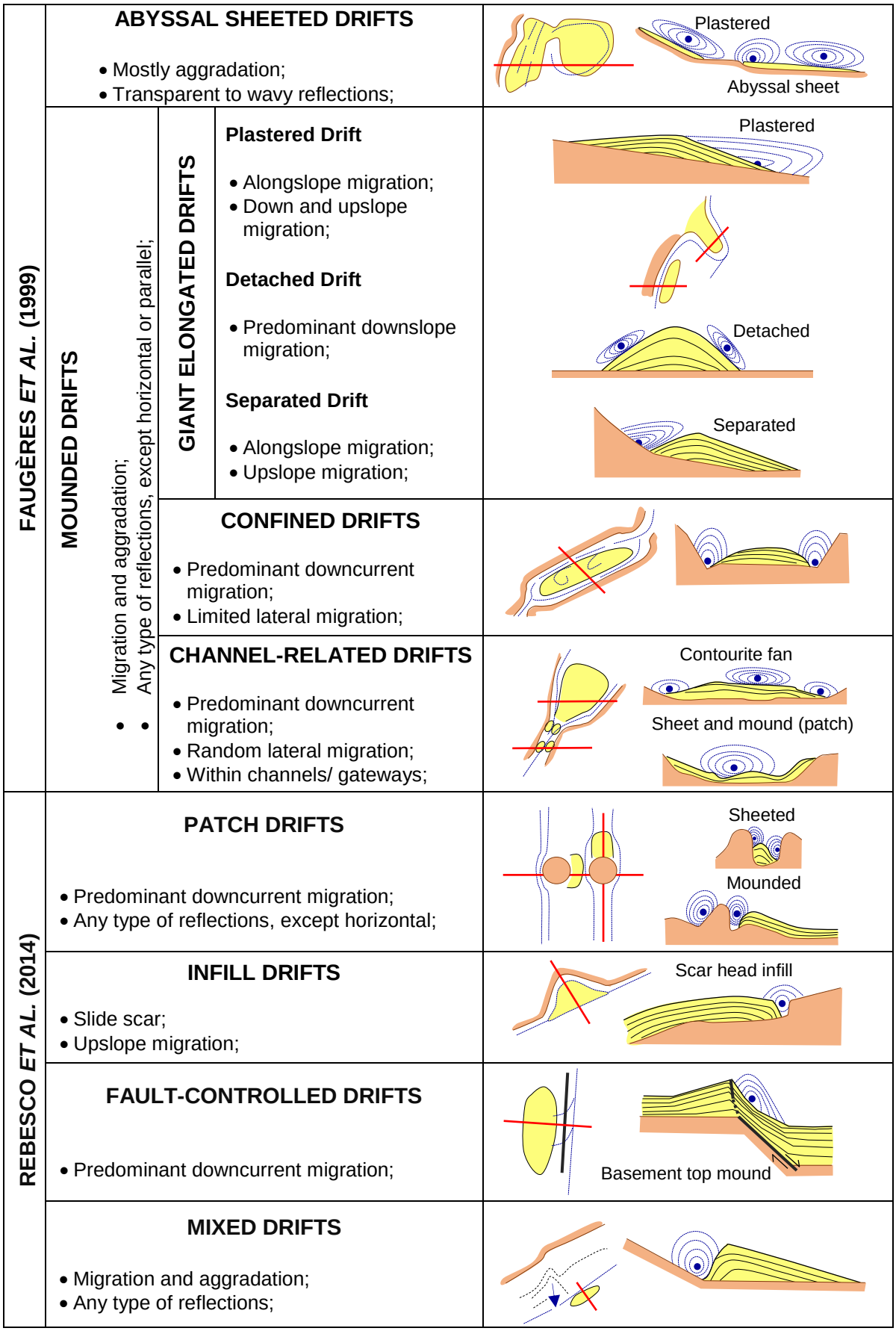

Figure 3.5 – Drift classifications and related bottom-current paths. Modified from Faugères *et al.* (1999) and Rebesco *et al.* (2014).

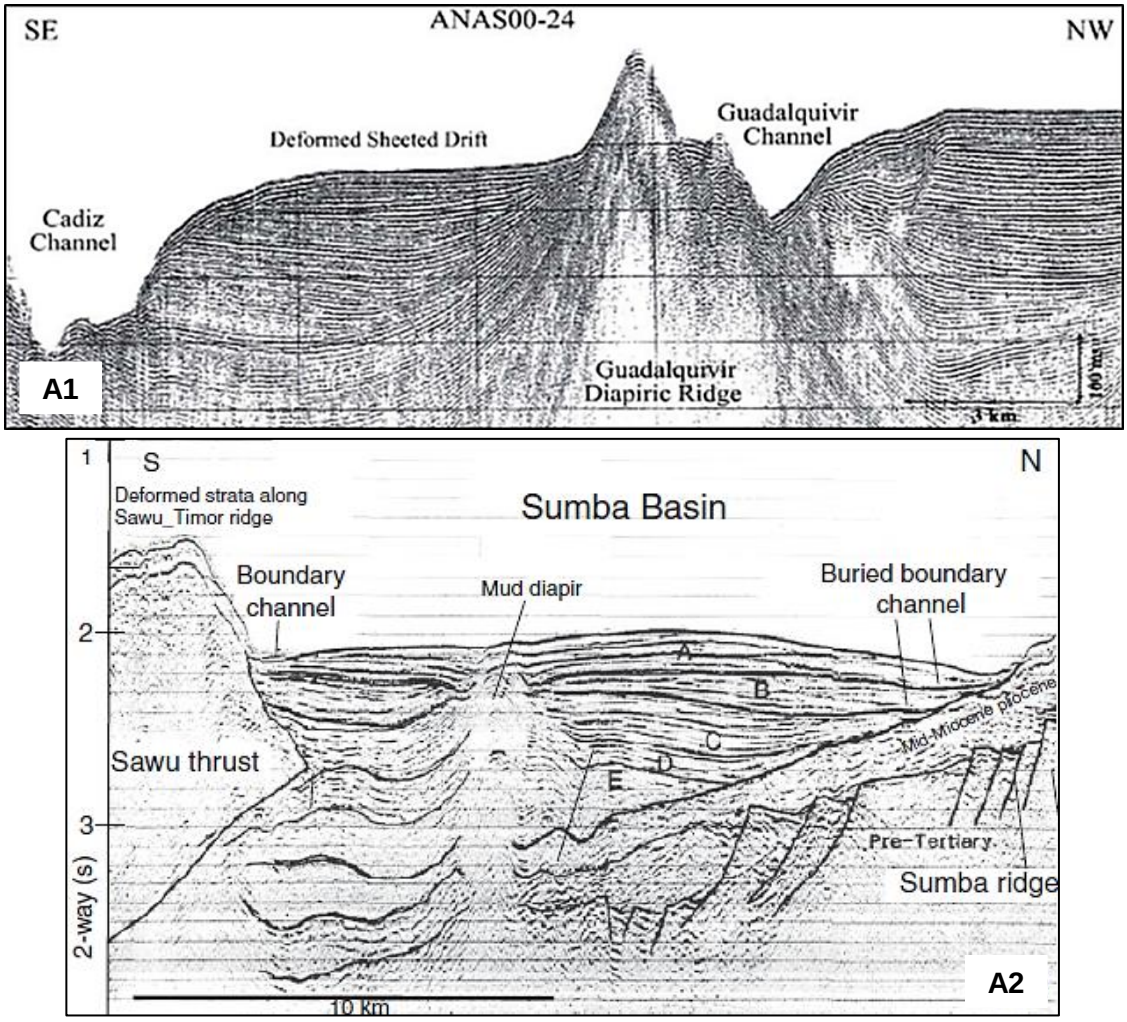

Figure 3.6 – Seismic profiles examples of different drift types and large-scale features: (A1) sheeted drift and contourite Guadalquivir and Cadiz channels, bound by the Guadalquivir Diapiric Ridge, in the Gulf of Cadiz (Hernández-Molina *et al.*, 2006); (A2) confined Sumba Drift in the forearc Sunda Basin, Indonesia (Reed *et al*. 1987).

3.4 Identification of Onshore Contourite Features

Contourites have been identified mostly in the North and South Atlantic basins, usually associated with deep water masses (e.g. North Atlantic Deep Water or Antarctic Bottom Water). However, contourite features have also been described in the Mediterranean, Indian, Pacific, Arctic and Antarctic basins in different settings and associated with either deep-intermediate or shallow water masses (Faugères *et al.*, 1999; Rebesco *et al.*, 2014; Figure 3.8).

While their identification in the offshore has been rather successful, the detection of contourite deposits in the onshore sedimentary record is extremely difficult since it is not possible to identify their overall morphology. Their identification in the onshore geological record is also obscured by the occurrence of geological processes such as bioturbation, sedimentation, erosion, compaction, tectonics and metamorphosing (Rebesco and Camerlenghi, 2008; Rebesco *et al.*, 2014). The identification of contourite outcrops needs to consider the context behind their formation, associated with the paleogeographic and tectonic frameworks. The most ancient records of contourites come from the Cambro-Ordovician to the Neogene (Figure 3.7), trending in an east-westward tendency across the globe, associated with the evolution of the Paleo Tethys Ocean (Huneke and Stow, 2008; Rebesco *et al.*, 2014; Figure 3.8).

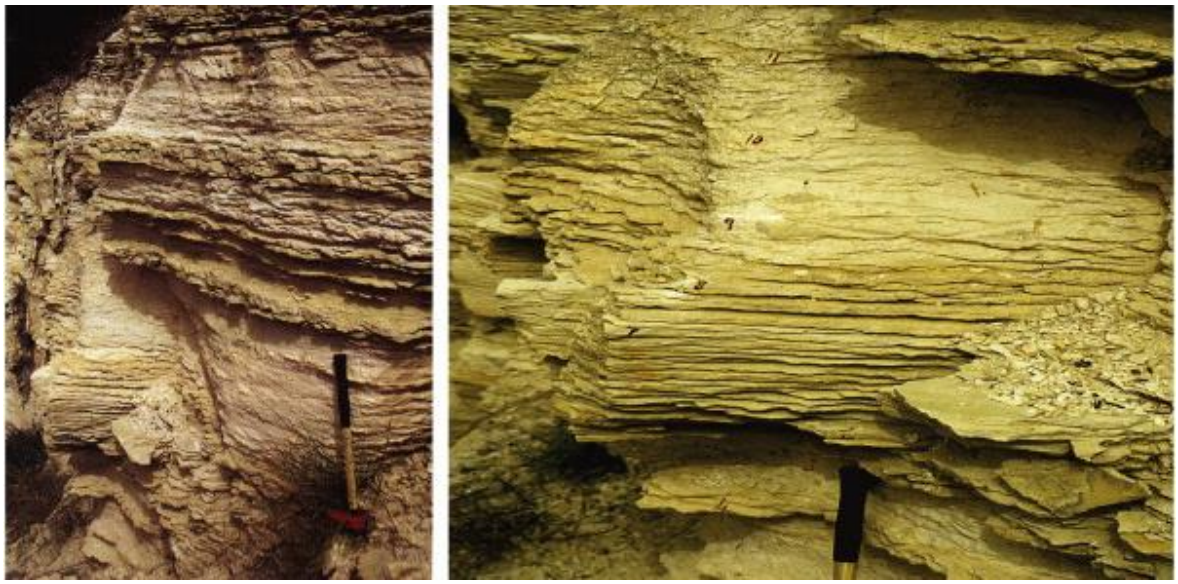

Figure 3.7 – Ancient contourite outcrops of the *Lefkara* Formation, Cyprus (Paleogene to Early Neogene). From Rebesco *et al.* (2014).

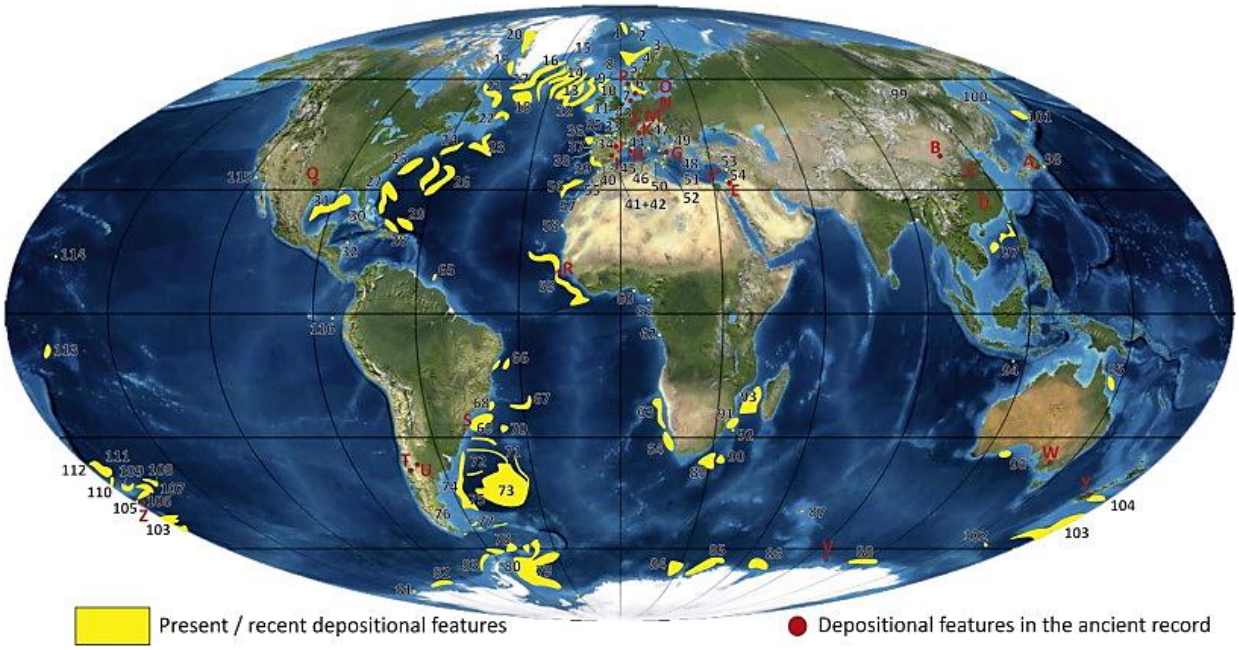

Figure 3.8 – Compilation of contourite deposits in the offshore (yellow areas) and contourite outcrops in the sedimentary record (red dots). From Rebesco *et al.* (2014).

3.5 Contourite Drifts: Economic and Oceanographic Relevance

Contourites have been given growing attention in three main research areas, paleoceanography and paleoclimatology, hydrocarbon exploration and slope stability.

The academy is by far the field that has given greater interest and contributions to the study of contourites. Contourites were usually confined to more academic studies in the past, since they were rarely associated with hydrocarbon bearing reservoirs and most of the hydrocarbon reserves found in deep-waters were related to turbidite reservoirs (e.g. Viana *et al.*, 2007; Viana and Rebesco, 2007; Viana, 2008). In more recent years, the number of contourite systems identified in deep-water settings

has increased, (Faugères *et al.*, 1993; Rebesco *et al*., 2014) and sandy contourites have been discovered during IODP Expedition 339 in 2011-2012 (Brackenridge, 2014; Stow *et al*., 2014), which shows their potential to act as reservoirs and seals. As a result, the economic value of contourites increased and the petroleum industry started to invest in the research of contourites (Rebesco, 2005; Shanmugam, 2006; Stow *et al.*, 2013; Brackenridge *et al.*, 2013). The economic interest in contourites has gradually increased thanks to the academic research and the need to investigate hydrocarbon reservoirs other than the classic turbidites (Viana *et al*., 2007; Rebesco *et al.*, 2014).

In parallel with the petroleum industry uses, two other main research areas are depicted as having considerable importance: paleoceanography-paleoclimatology and slope stability. The paleoceanographic record, driven by climate changes, can be studied through contourite deposits (Faugères *et al*., 1993; Rebesco *et al.*, 2014). The sedimentary stacking pattern of contourite drifts change due to important paleoceanographic, climatic or sea-level fluctuations, which affect sediment influx and deposition. Therefore, their stacking pattern can be used to identify phases and modifications of oceanic current activity, as well as the factors that induce local- and global-scale variations in thermohaline circulation, fundamental to understanding climate changes (Faugères *et al*., 1999; Rebesco *et al*., 2014).

The analysis of slope stability in areas affected by contour-currents and contourite deposition is another important aspect to study (Rebesco and Camerlenghi, 2008). Vigorous contour-currents can locally erode the seafloor, provoking sediment instability and triggering potentially hazardous mass-flow events (Mulder *et al.*, 2003; Laberg *et al.*, 2005; Viana *et al.*, 2007). Several studies have shown that contourites act as a predispositioning factor for slope instability. For example, the development of the Storegga Slide in Norway. The Storegga slide corresponds to a collapse of ~290 km along the Norwegian margin on an area of ~3500 km^3 (Bondevik *et al*., 2012). This event was triggered in the Holocene by seismic activity or methane hydrates dissociation (Bünz *et al*., 2003; Lisa, 2014). However, it was also shown that contourites with high mud content, plasticity and water content worked as weak layers for shear stress movements and predisposed the occurrence of the Storegga slide (Bryn *et al*., 2005).

CHAPTER 4

CONTOURITES IN IBERIA

4.1 Oceanography of SW Iberia

The present oceanic circulation in the Gulf of Cadiz is motivated by the exchange system established between the Atlantic Ocean and the Mediterranean Sea through the Strait of Gibraltar (Baringer and Price, 1999). This gateway allows the exchange between the warm saline Mediterranean Outflow Water (MOW) and the overlying Atlantic Inflow Water (AIW) (Ambar *et al*., 2002; Serra *et al*., 2005).

The AIW is a 0-500 m layer formed by the North Atlantic Surface Water (NASW), which flows from the surface to approximately 100 m depth with temperatures above 16ºC and salinity of 36.40‰, and by the North Atlantic Central Water (NACW), which flows between 100 and 700 m depth with temperatures of 11-17ºC and salinity of 35.6-36.5‰ (Criado-Aldeanueva *et al.*, 2006). The NASW has its origin in shallow NACW that was modified by air-sea interactions (Criado-Aldeanueva *et al*., 2006). The NACW is comprised by two distinct layers: the northward upper layer of sub-tropical origin (NACWt) at >45ºN (with 12.2-18.5ºC and 35.66-36.75‰) and the southward lower sub-polar layer (NACWp), which prevails up to 35ºN (with 4-12ºC and 34.96-35.66‰) (Pérez *et al*., 1993; Fiúza *et al*., 1998; Mason *et al*., 2006; Padin *et al*., 2011). Over the continental shelf of the Gulf of Cadiz, warmer and fresher Shelf Waters (SW) have been detected at the surface with temperatures of 14-18ºC and salinity of 35.9-36.5‰ (Criado-Aldeanueva *et al*., 2006).

The Mediterranean Water is originated in the Mediterranean Sea as a result of higher evaporation than precipitation and runoff, consisting of the mixture of two water masses from the Mediterranean Basin, the Levantine Intermediate Water (LIW) and a small component of the Western Mediterranean Deep Water (WMDW). The constricted basin and arid climate provides the necessary conditions for the formation of warm, dense saline water of 13ºC and 36.5‰ (Ambar and Howe, 1979). The WMDW is formed in the Gulf of Lion, filling the Mediterranean Basin below 500 m water depth, and flows around the Iberian Peninsula and the Balearic Islands, before exiting by the Alboran Sea and through the Strait of Gibraltar. The LIW is formed in the eastern Mediterranean Basin, and flows between 150 and 500 m water depth, over the upper and mid-continental slopes, through the Sicilian Strait, towards the Alboran Sea and Strait of Gibraltar (Millot 1999, 2009).

The MOW is restricted to a core approximately 10 km wide as it passes through the Strait of Gibraltar (Ambar and Howe, 1979). The MOW accelerates through the Strait of Gibraltar (reaching velocities up to 250 cm s^{-1}) as a warm (13ºC) and dense (37‰) water mass and forms a turbulent gravity driven flow before sinking downslope towards northwest (Ambar and Howe, 1979; Mulder *et al*., 2003; García *et al*., 2009; Figure 4.1). The MOW sinks as a result of its high salinity and the seafloor morphology at the exit of the Strait of Gibraltar. In the Gulf of Cadiz, the MOW begins to raft above the NADW and deflects northward due to the Coriolis force (Zenk 1970, 1975; Baringer and Price, 1997; Ambar *et al.*, 1999). The MOW can exceed 80 km in width and forms a broad water mass along the continental slope, with lower velocities of 80-40 cm s^{-1} towards northwest (Baringer and Price, 1997). The MOW's reaches its lowest velocity (about 10 cm s^{-1}) on the South Iberian margin (Ambar and Howe, 1979) due to diapiric ridges oblique to its flow direction (Nelson *et al*., 1993). Eventually, it settles as an intermediate contour-current offshore the Cape São Vicente, between 400 and 1400 m water depth.

The MOW's main water core is separated into two major cores and two minor ones (westwards of 6º20' – 7º W), which flow at different depths with distinct oceanographic properties (Zenk 1970; Ambar and Howe, 1979; Ambar *et al*., 2002). The two major cores are the Mediterranean Upper Water (MU) and the Mediterranean Lower Water (ML), and the minor cores are the Shallow Core and the Deep Core (Zenk 1970; Ambar and Howe 1979; Ambar *et al*., 2002, 2008; Figure 4.1). The MU is a warmer and more saline water (13–14ºC and 35.7-37‰) than the ML (10.5–11.5°C and 36.5–37.5‰) and flows northward, along the continental slope of southwest Iberia, between 600 and 1000 m depth, but centered at 700-800 m depth. The ML flows northwest between 1000 and 1300 m depth, stabilizing around 1200-1300 m depth with 20-30 cm s^{-1} velocity average (Bower *et al.*, 2002; Llave *et al*., 2007b). At 7ºW, a branch detaches from the southern part of the ML to veer off towards southwest. At 7º 20'W, the ML is divided into three distinct branches: the Southern Branch (SB), the Principal Branch (PB) and the Intermediate Branch (IB). They flow in a general northwestern direction and join around 8º 20'W (Llave *et al*., 2007b; García *et al*., 2009; Figure 4.1).

The Shallow Core flows between 400 and 600 m depth along the continental slope of southwest Iberia, and possesses higher temperatures than the Deep Core (Ambar *et al*., 2002, 2008). The Deep Core is recognized from the Portimão Canyon to Cape São Vicente, between 1300 and 1600 m depth (Ambar *et al*., 2002, 2008; Bower *et al*., 2002). The Deep Core branch is detached from the ML in association with pulses of dense water, forced to descend to greater depths due to interaction with the canyon topography (Bower *et al.*, 2002; Ambar *et al.*, 2008). Both the Portimão Canyon and Cape São Vicente act as a source of meddies formation. The Portimão Canyon is a source of meddies detached from the Deep Core and found downstream from the canyon, while Cape São Vicente is a source of meddies detached from the ML (Ambar *et al.*, 2002, 2008; Serra *et al.*, 2005).

Underneath the MOW, the North Atlantic Deep Water (NADW) from the Greenland-Norwegian Sea flows southward at depths >1500 m. This water is characterized as a cold (3º-8ºC) and less saline (34.95–35.20‰) water mass (Reid, 1979). In the Gulf of Cadiz, the NADW is joined by part of the MOW, flowing southwards down the eastern part of the Atlantic Ocean (Reid, 1979).

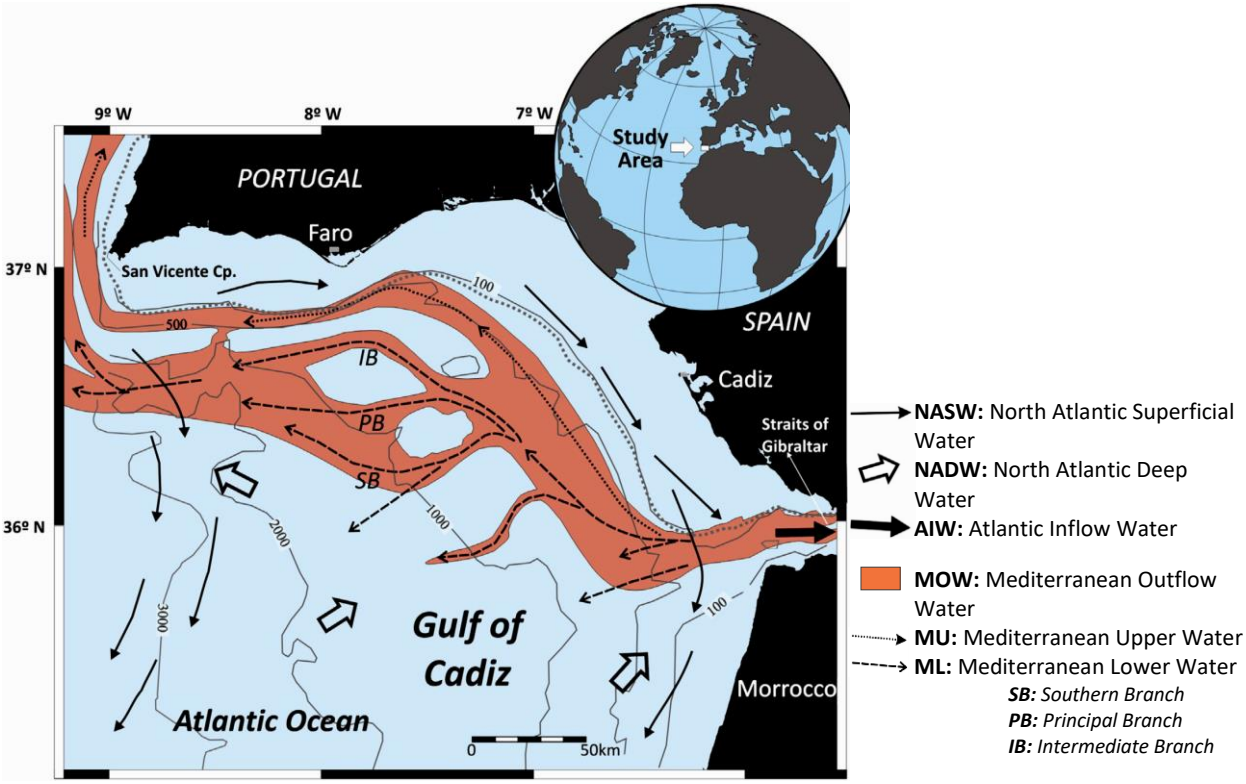

Figure 4.1. – Main water masses flowing around the Iberian Peninsula (Stow *et al*., 2013).

4.1.1 Pliocene-Quaternary Paleoceanography of the MOW

While present-day MOW circulation is well constrained, the paleoceanography of the MOW is still poorly known. The interaction between the MOW and the Atlantic Ocean is marked by the Messinian Salinity Crisis, an event during which the Mediterranean Sea underwent desiccation. Data from the Mediterranean Basin pinpoints the Messinian Salinity Crisis between 5.96 and 5.33 Ma (Cita, 2001; Bache *et al*., 2012). The occurrence of the Messinian Salinity Crisis in the Miocene is associated with several events of tectonic activity and sea-level and climatic fluctuations, which led to the closure of the Strait of Gibraltar and the isolation of the Mediterranean Basin in multiple stages (Bache *et al*., 2012). The Messinian Salinity Crisis ended with the Zanclean flood, which signified the beginning of water masses exchange between the Mediterranean and the Atlantic (Garcia-Castellanos *et al*., 2009). Several authors also suggest water formation in the Mediterranean Basin after an influx of Atlantic water into the basin, around the Early to Mid-Pliocene (Hsü *et al*., 1973; Llave *et al*., 2011; Bache *et al*., 2012).

The circulation of the MOW through the Pliocene and Quaternary, and its relation to past climatic conditions, was studied through several methods, previously mentioned in Chapter 1. With the establishment of the MOW circulation in the Early Pliocene, climatic fluctuations influence and cause variations. Climatic fluctuations are responsible for the formation of two periods of cooler, saltier and more oxygenated Mediterranean deep water, with an enhanced circulation regime: the first period at, 3.4-3.0 Ma, occurred moderately close to the onset of the Northern Hemisphere glaciations (3.1-2.7 Ma) (Hayward *et al*., 2009; Khélifi *et al*., 2009); and the second period, at 1.3-1.0 Ma, corresponds to the Mid-Pleistocene Transition (1.2-0.55 Ma) (Hayward *et al*., 2009). These variations are characterized by MOW enhancement during glacial times, with a saltier, denser and more vigorous lower branch of the MOW (Cacho *et al*., 2000, 2002; Hernández-Molina *et al*., 2003, 2006; Rogerson *et al*., 2005; Llave *et al*., 2006; Voelker *et al*., 2006; Toucanne *et al*., 2007; García *et al*., 2009; Kaboth *et al*., 2016). While during the interglacials, a weaker MOW was split into several branches (Stow *et al*., 2002c). A few authors also propose highly dynamic outflow waters, with up and downslope movements on numerous timescales, in response to the density contrasts between the Atlantic and the Mediterranean water masses and their relation to climatic changes (Rogerson *et al*., 2005, 2012).

4.2 Contourites in the Iberian margin

The MOW has affected the Iberian margin since the Late Miocene and its interaction with the seafloor developed erosional and depositional features. This current has affected the sediments deposited in this region and lead to the formation of variable drifts from the Strait of Gibraltar to the Northwest Iberian margin (the Albufeira, Bartolomeus Dias, Faro, Guadalquivir, Huelvas, Lagos, Portimão and Sagres drifts; in the Camarinal and Spartel sills and around the Galicia Bank; Vanney and Mougenot, 1981; Llave *et al*., 2001, 2006, 2007, 2011; Hernández-Molina *et al*., 2003, 2006, 2011, 2015; Roque *et al*., 2012; Figure 4.2). Therefore, this complex sedimentary system is referred to as the Gulf of Cadiz Contourite Depositional System (GCCDS) (Hernández-Molina *et al*., 2003, 2006).

The occurrence of contourite deposits in the West Portuguese margin is scarce and poorly characterized, with a few examples identified near structural highs and geomorphologic irregularities (Alves *et al*., 2003; Badagola, 2008). Their development is associated with the circulation of the MOW or the deeper NADW (Hernández-Molina *et al*., 2011). The Sines Drift is one of the main features of the GCCDS in the Southwest Portuguese margin, firstly identified by its general plastered morphology and stratified acoustic character (Mougenot, 1989; Hernández-Molina *et al*., 2015). Moreover, Hernández-Molina *et al*. (2011) has made a numeric simulation of bottom-current velocities (at regional scale) to detect

potential zones for drift formation in the West Portuguese margin. The results include the Extremadura Spur, off Porto at the continental slope and off Aveiro at the continental rise (Figure 4.2).

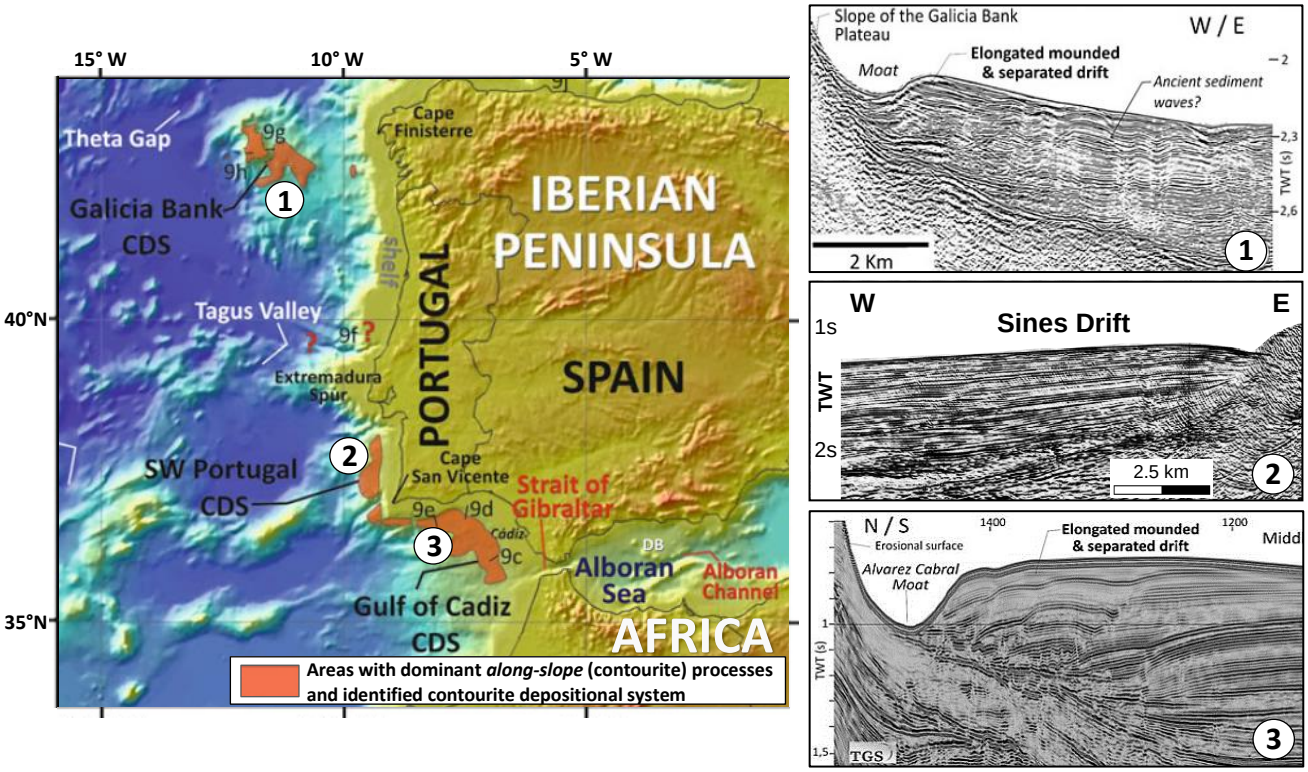

Figure 4.2 – Examples of contourite drifts identified from the Galicia Bank (1) to the Western Iberian margin (2) and the Strait of Gibraltar (3). Modified from Hernández-Molina *et al*. (2011), with seismic profiles from Hernández-Molina *et al*. (2011) and Alves et *al*. (2003).

4.3 Contourite Depositional System of the Gulf of Cadiz

The GCCDS is well characterized in the South Iberia margin (Figure 4.3). Many authors have studied its erosional and depositional features (e.g. Gonthier *et al.*, 1984; Nelson *et al.*, 1993, 1999; Llave *et al.*, 2001, 2006, 2007b, 2011, 2015; Stow *et al.*, 2002c, 2013; Hernández-Molina *et al.*, 2003, 2006, 2014a,b, 2015; Mulder *et al*., 2003, 2006; Roque *et al.*, 2012; Brackenridge *et al.*, 2013). The features in the eastern Gulf of Cadiz are associated with the erosive capacity of the bottom water mass and its interaction with local seafloor morphology. In this area, laterally extensive abraded surfaces are moving to discrete contourite channels, where diapiric structures control bottom-current flow. The northern Gulf of Cadiz is linked with contourite moats and large-scale depositional features (Figure 4.3). Depositional features, such as contourites, also occur along the Iberian margin. These features have distinct but similar characteristics, related to the decrease in transport capacity of the MOW and the increasing distance from the Strait of Gibraltar (Hernández-Molina *et al.*, 2006, 2015).

The main depositional features in the GCCDS are sediment wave fields, sediment lobes, mixed drifts, plastered drifts, elongated mounded and separate drifts and sheeted drifts. The main erosional features identified are contourite channels, furrows, marginal valleys and moats. Their characteristics and distribution along the margin define five morphosedimentary sectors (Hernández-Molina *et al.*, 2006; Figure 4.3): 1) proximal scours and ribbons sector; 2) overflow sedimentary lobes sector; 3) channels and ridges sector; 4) contourite drifts sector; 5) submarine canyons sector. The main characteristics of each sector are reviewed herein.

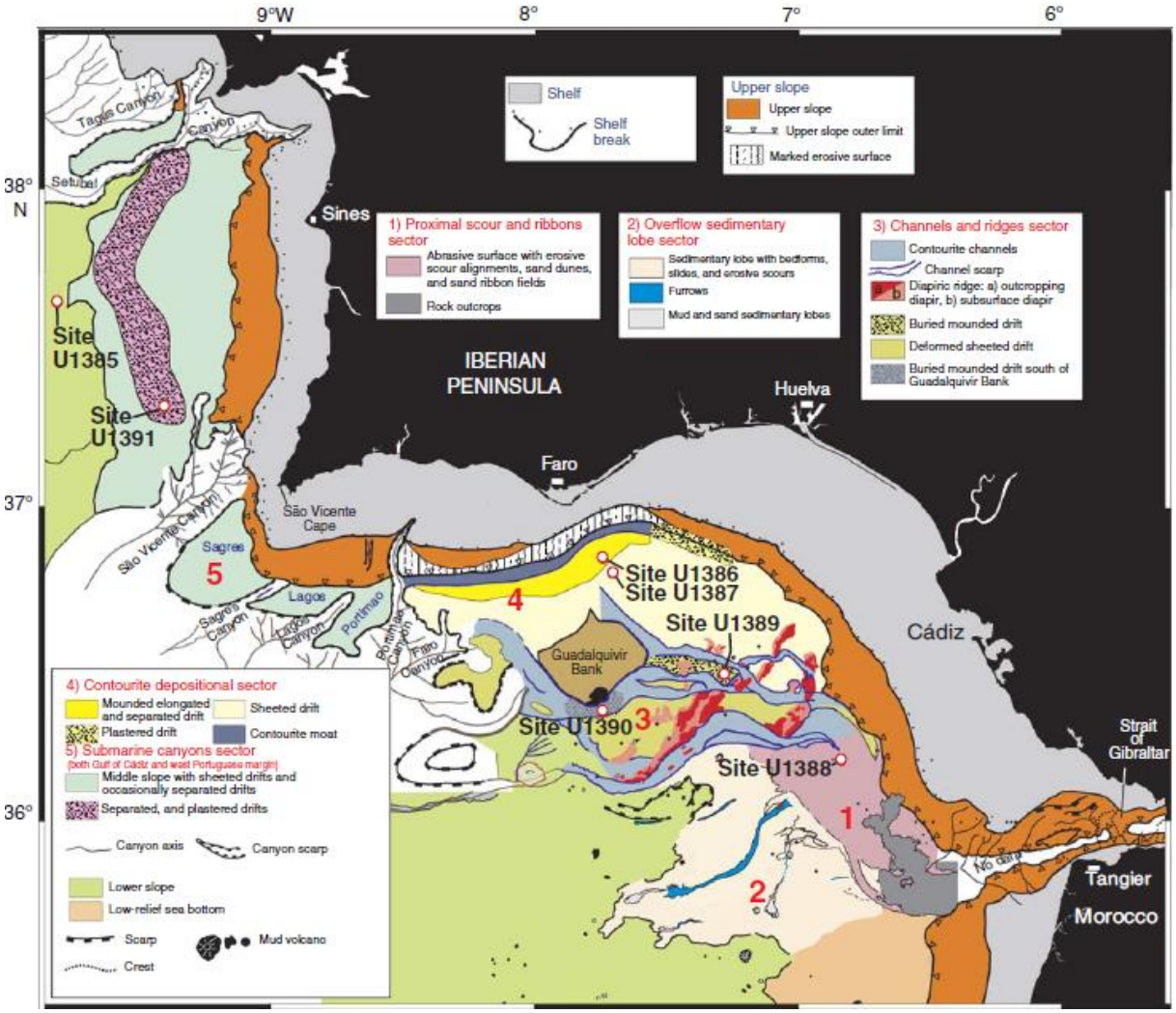

Figure 4.3 – GCCDS sectors differentiated by large-scale erosional and depositional features (Hernández-Molina *et al*., 2006).

Sector 1: Proximal scours and ribbons sector

The sector 1 of the GCCDS is located near the Strait of Gibraltar. It is characterized by high energy bottom-currents (Kenyon and Belderson, 1973) and gravity-driven overflow features (Mulder *et al.*, 2003). The turbulent and gravity-driven cascade of the MOW over the Camarinal Sill, which is the sill that separates the Mediterranean and the Atlantic Ocean, led to the formation of two deep erosional channels and outcrop features (Hernández-Molina *et al.*, 2014b; Figure 4.4). Recent campaigns have identified additional drift features, with plastered drifts along the upper slope and two mounded drifts on two broad erosional terraces (Hernández-Molina *et al*., 2014b, 2015). These terraces form a major abraded surface, from 500 to 800 m water depths, dominated by erosional processes (Hernández-Molina *et al.*, 2014b).

Closer to the Strait of Gibraltar, the region is characterized by rock outcrops on the seafloor and coarse grained sediments (Mulder *et al.*, 2003). These features suggest a highly vigorous current regime along the route of the MOW proximal to the Strait of Gibraltar. Although, there are depositional features in this sector, which suggest a reduction in MOW velocity (and sediment transport capacity) away from the Strait of Gibraltar towards northwest and laterally from the MOW's core to the east and west (Mulder *et al.*, 2003). Gravel and sand lag deposits give way to sand ribbons and wave deposits (Mulder *et al*., 2003). The orientation of all features follow the route of the MOW alongslope, as it leaves the Strait of Gibraltar towards west and bends northward due to the Coriolis force.

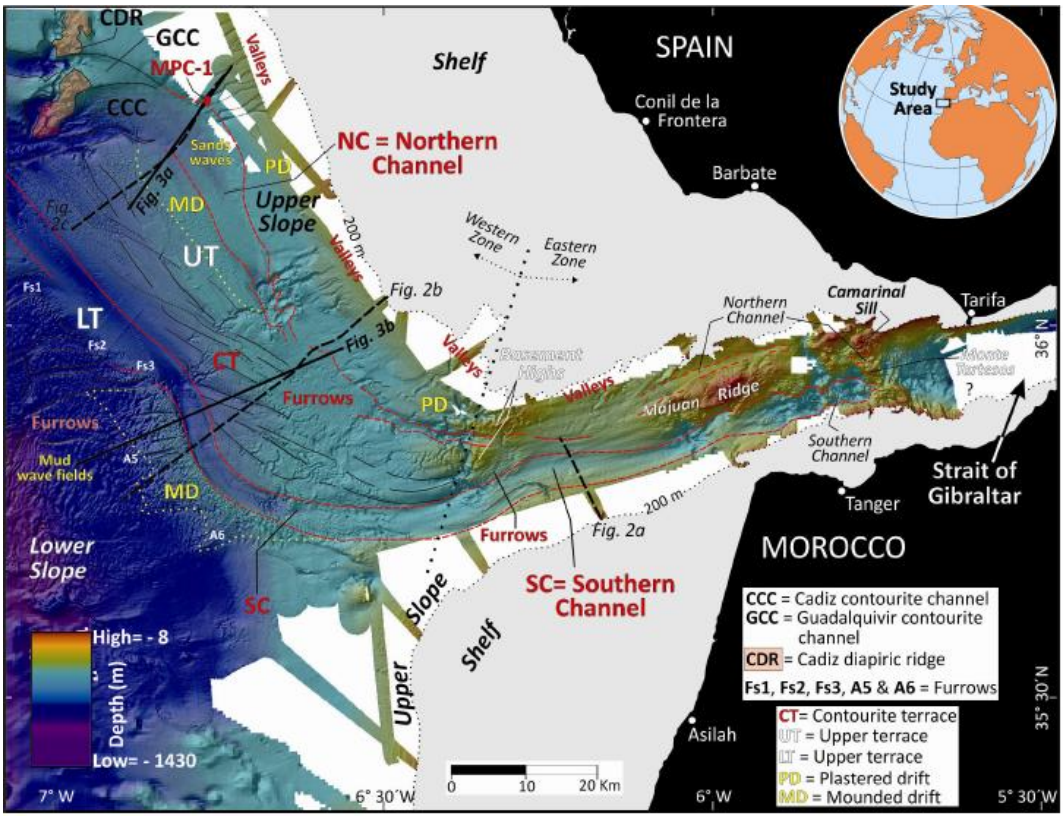

Figure 4.4 - Swath bathymetry with the location of the main depositional and erosional features at the exit of the Strait of Gibraltar (Hernández-Molina *et al*., 2014b).

Sector 2: Overflow sedimentary lobes sector

Sector 2, characterized by overflow sedimentary lobes, is located downslope and seaward of the first sector, between 800 and 1600 m water depth. This sector is characterized by sand-rich contourite deposits, with sedimentary wave fields, downslope orientated channels, furrow erosive features and associated depositional lobes (Hernández-Molina *et al*., 2006, 2014b; Hanquiez *et al*., 2010). The main depositional feature is a large contourite drift, located near the border with Sector 1. This large contourite is topped by an extensive sediment wave field (Figure 4.5). These sediment wave fields are incised by a series of downslope orientated channels and furrows. The largest channel is the Gil Eanes Channel, with an extension of 40 km and a reach of 1200 m water depth (Nelson *et al.*, 1993). The Gil Eanes Channel and two major channels are U-shaped in cross section, with bioclastic sands in their axes and sediment lobe deposits at their terminus. These lobe deposits are thought to be formed by incision and induced gravity processes, related to a periodic deepening of the MOW (Rogerson *et al.*, 2012). Other features in this sector include mud volcanoes, topographic highs on the seafloor that can redirect channels and that have important roles as conduits for gas migration (Hanquiez *et al.*, 2010).

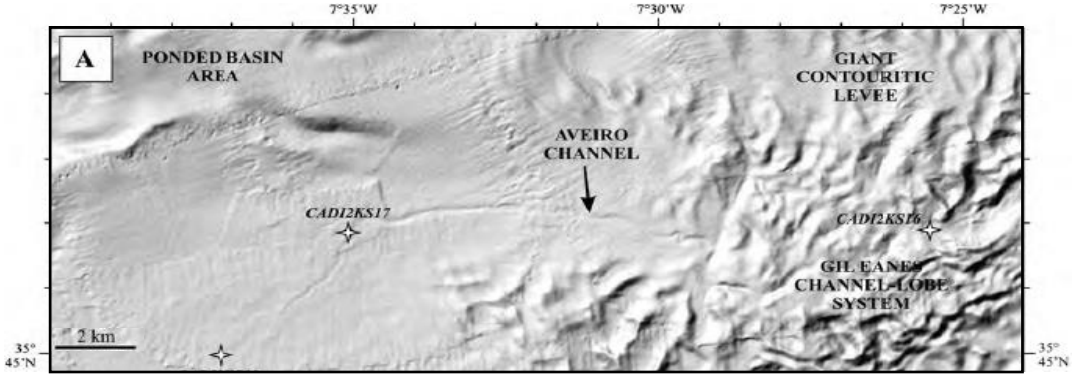

Figure 4.5 – High-resolution bathymetry of the Aveiro channel-lobe depositional system located in sector 2 of the GCCDS (Hanquiez *et al*., 2010).

Sector 3: Channels and ridges sector

The channels and ridges sector is located northwest of the first sector. This sector is characterized by diapiric ridges orientated NE-SW, perpendicular to the MOW flow, and tectonic basement highs. The interaction between the MOW's branches with the seafloor creates the distinct channels in this sector (Nelson *et al.*, 1993, 1999). This also provokes a morphological enhancement of the MOW branches, which leads to a higher erosional capacity. The major channels are named from the upper continental slope seaward: Gusano, Huelva, Diego Cao, Guadalquivir and Cadiz channels, with lengths over 100 km (Hernández-Molina *et al.*, 2006; Stow *et al.*, 2013; Figure 4.6). Unlike the channels and furrows in Sector 2, these contourite channels tend to be sinuous and asymmetrical in cross section (Stow *et al.*, 2013). The channels incise the upper slope sheeted drifts, mid-slope deformed sheeted and buried mounded drifts (Llave *et al*., 2007a; Figure 4.6).

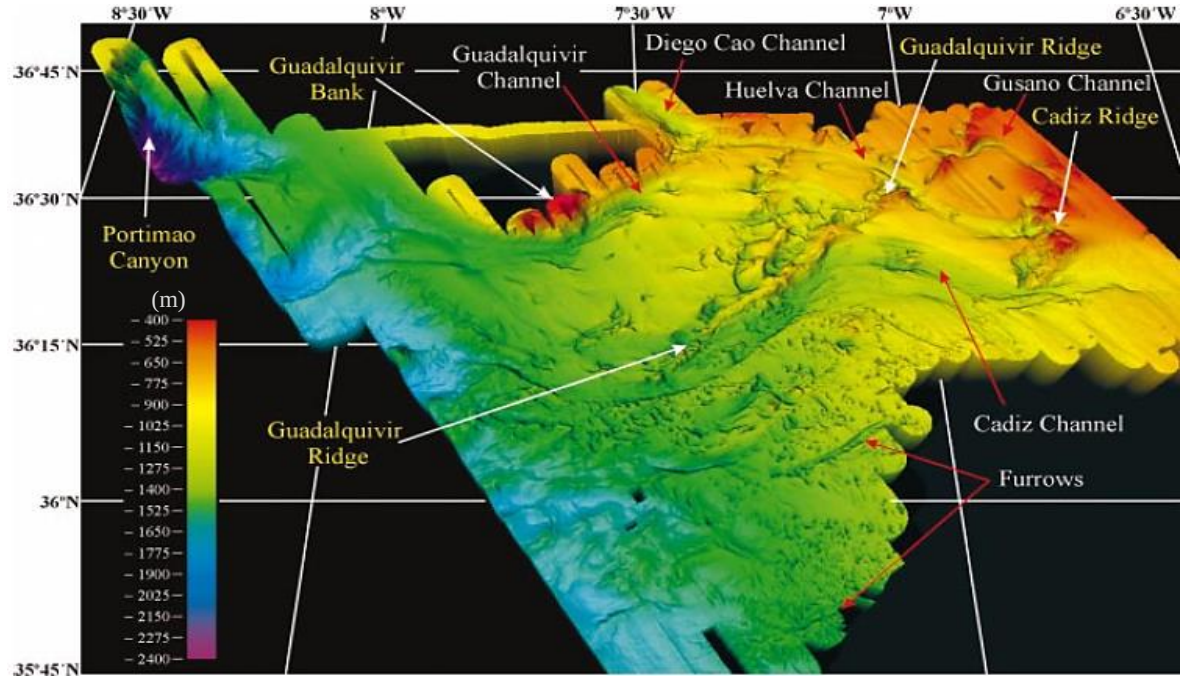

Figure 4.6 - Three-dimensional model from swath bathymetry with the main erosional features (contourite channels and furrows) and diapiric ridges of the Gulf of Cadiz (Hernández-Molina *et al*., 2003).

Sector 4: Contourite drifts sector

The contourite drifts sector is located in the West and South Iberian continental margin. The fourth sector has been recognized by the occurrence of contourite drifts (Mougenot and Vanney, 1982; Faugères *et al.*, 1984; Gonthier *et al*., 1984). This sector is characterized by high sediment thickness, and hence shows a clear record of the influence of the MOW in the North Atlantic Ocean (Llave *et al*., 2001, 2010, 2015; Roque *et al.*, 2012; Stow *et al.*, 2013; Hernández-Molina *et al.*, 2014b, 2015).

The largest feature in this sector is the Faro-Albufeira elongated mounded drifts, and the related Alvares-Cabral contourite moat, which separates these features from the continental slope and funnels the MOW westward (Figure 4.7). These drifts show upslope progradation patterns and laterally extensive erosional discontinuities, which can be linked with fluctuations in the intensity of the MOW (Llave *et al.*, 2001; Roque *et al*., 2012). Downslope, associated with the Faro-Albufeira elongated mounded drifts, are a set of aggradational sheeted contourite drifts: the Faro-Cadiz and the Bartolomeu Dias drifts (Hernández-Molina *et al*., 2006; Llave *et al*., 2011; Roque *et al.*, 2012).

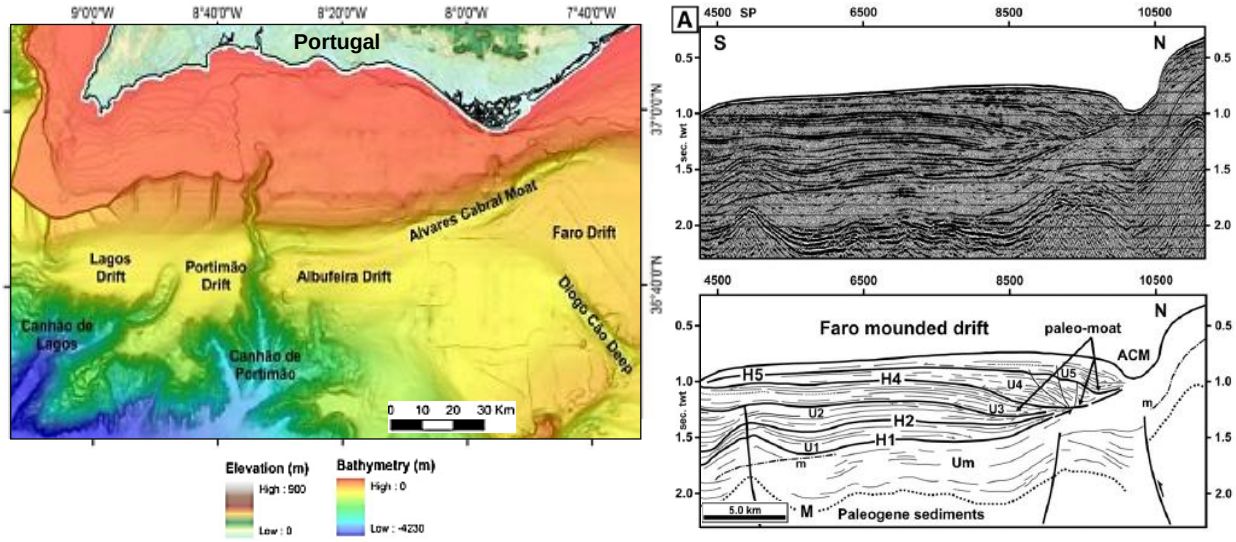

Figure 4.7 – Bathymetric map and seismic profile with interpretation of the main depositional (Faro mounded drift) and erosional (Alvares-Cabral moat) features in the South Iberian margin. Modified from Roque *et al.* (2012).

Sector 5: Submarine canyons sector

The submarine canyons sector is the western most sector of the GCCDS, mainly dominated by downslope erosive features and muddy plastered and sheeted contourite drifts (Hernández-Molina *et al*., 2006; Roque *et al.*, 2012; Figure 4.8). The largest feature in this sector is the São Vicente Canyon, orientated downslope (NE-SW), although other canyons also form significant features on the sea bed, the Portimão, the Lagos and Sagres canyons (Llave *et al.*, 2001; Hernández-Molina *et al.*, 2015). These canyons are surrounded by the Lagos, Portimão and Sagres sheeted drifts. These drifts are characterized by muddy sediments interbedded with sand-rich downslope deposits (Llave *et al*., 2001).

This sector differs from Sector 4 due to the capture of the MOW as it flows over the Portimão Canyon. This implicates a reduction in bottom-current velocity and a decrease in average grain size across the canyon (Mulder *et al*., 2006; Marchès *et al*., 2010). This reduction has important implications for the controls on contourite sand and mud deposition and downslope/alongslope process interaction. Afterwards, the MOW flows towards southwest or turns north and flows along the West and Northwestern Iberian margin (Zenk 1970, 1975; Baringer and Price, 1997; Ambar *et al.*, 1999). In the north, the MOW flows along the seafloor, leading to the formation of contourite drifts on the Galician and Cantabrian continental margins (Hernández-Molina *et al.*, 2011).

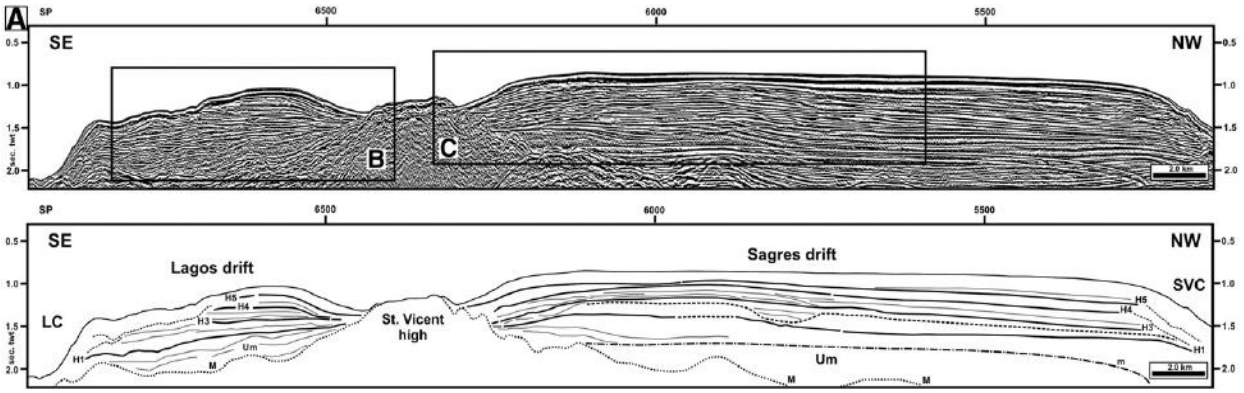

Figure 4.8 – Seismic profile with interpretation of the Lagos and Sagres drifts, separated from the São Vicente High by moats and bound by the Lagos Canyon (LC) and São Vicente Canyon (SVC), respectively (Roque *et al*., 2012).

CHAPTER 5

DATA & METHODOLOGY

5.1 Dataset

The dataset used in this work consists of: i) unpublished seismic reflection profiles acquired in 2014 in the scope of the MOWER/CONDRIBER project, ii) seismic reflection profiles acquired in other academic surveys (BIGSETS, STEAM) and oil-industry survey (GSI), iii) downhole logging data acquired during the Integrated Ocean Drilling Program (IODP) Expedition 339 at Site U1391, iv) lithological, chronological and physical properties data from this Site, v) stratigraphic and logging data from Pescada-1 oil-well, and vi) SWIM multibeam bathymetry (Zitellini *et al*., 2009; Figure 5.1).

5.1.1 Seismic reflection data

The seismic reflection profiles used in this work were obtained either during several academic cruises, namely MOWER/CONDRIBER, STEAM 94 and BIGSETS 98, or in oil-industry surveys as GSI 84 (Figure 5.1). The acquisition parameters of each seismic reflection survey are compiled in Table 5.1.

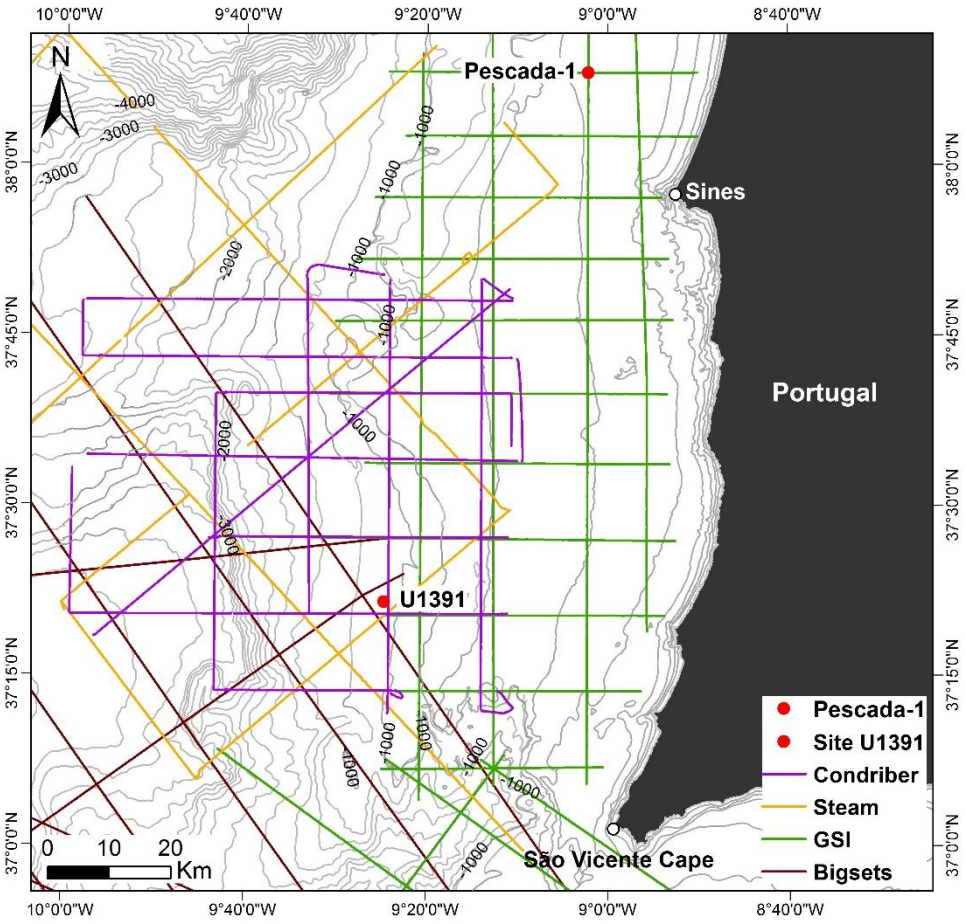

Figure 5.1 – Location of the seismic datasets and IODP Site U1391 used in this work: CONDRIBER, STEAM, GSI and BIGSETS.

Table 5.1 – Acquisition parameters of each seismic survey: CONDRIBER, STEAM, GSI and BIGSETS (Steam report, 1994; Alves *et al.*, 2000; Zitellini *et al*., 2001; Informe Técnico Campaña Mower, 2014).

Dataset	Year	Research Vessel	Streamer Length	Source	Total volume	Shot Interval	Channels	Channel Interval	Sample Rate	Total Seismic
CONDRIBER	2014	RV Sarmiento de Gamboa	250 m	8 G-GunII Sercel airguns	910, 610 in^3 (2000 psi)	50 m	3 (40 hydrophones per group)	50 m	0.5 ms	785 km
STEAM 94	1994	MV Zirfae	-	1 Airgun	10 in^3	25 m	12	25 m	0.5 ms	-
GSI 84	1984	MV P.E. Haggerty	3000 m	Airgun array	2775 in^3 (2000 psi)	25 m	120 (27 hydrophones per group)	-	2 ms	4600 km
BIGSETS 98	1998	RV Urania	1200 m	4 Sodera SSI GI-GUN airguns	150-250 in^3	25-50 m	48	25 m (group interval)	1 ms	2715 km

5.1.2 Pescada-1 oil-well data

Oil industry well Pescada-1 data was attained from other works (Matias, 2002; Batista, 2009) to correlate the older seismic horizons. The well is located southwest of Setúbal (38º08'7.1"N, 09º02'8.6"W) on the continental shelf beneath 148.41 m of water depth and reached 3082.44 m in depth (Table 5.2).

Table 5.2 – Coring summary of the oil industry well Pescada-1 (extracted from Matias, 2002; Batista, 2009).

Coring Summary	Pescada-1
Longitude	09º02'8.6"W
Latitude	38º08'7.1"N
Water depth (m)	148.41 m
Total penetration (mbsf)	3082.44 m
Total length of cored section (m)	2951.7 m

5.1.3 IODP Expedition 339 well data

As part of the IODP Expedition 339 from 16th November 2011 to 16th January 2012, six sites were drilled across the Gulf of Cadiz and West Portuguese margin to research the influence of the Mediterranean Outflow Water on global circulation and climate.

This study focus on Site U1391, drilled on the Southwest Iberian margin on the Sines Drift (37º21.5322′N, 9º24.6558′W) (Figure 5.1). Three holes were drilled at Site U1391: U1391A, U1391B and U1391C. The Site penetrated 671.5 mbsf (meters below seafloor), beneath 1073.7 m of water depth and cored a total of 1378.1 m with a recovery of 958.57 m, which corresponds to 92.3% (Table 5.3). During IODP Expedition 339, several analyses were carried on-board and downhole, including detailed visual assessment, smear slide analysis, sediment samples, physical properties and downhole logging measurements.

In the present work, downhole logging measurements, physical properties and grain size data from Site U1391 were used to provide information about the lithostratigraphy, the chronostratigraphy and the

petrophysical properties of the drilled sediments. IODP Expedition 339 core datasets are available at IODP's online database: http://iodp.tamu.edu/index.html. The tools and methods used during Expedition 339 to acquire the core data are reviewed herein.

High-resolution non-destructive measurements of physical properties of sediments at Site U1391 include gamma ray attenuation (GRA) bulk density, *P*-wave velocity and magnetic susceptibility in 2.5 cm steps on the Whole-Round Multisensor Logger (WRMSL). Natural gamma ray (NGR) was measured on whole-round core sections at 10 and 20 cm spacing. Also, discrete *P*-wave velocities were measured on working-half sections and in Hole U1391A on every other section. However, the measurements were only considered viable for the upper 50 mbsf. Moisture and density (MAD) samples were obtained for every other section of each core in Holes U1391A and U1391C. Finally, color reflectance spectrometry and split-core pointlogger magnetic susceptibility were obtained for every section of each hole in 5 cm steps (Expedition 339 Scientists, 2012).

The downhole logging measurements had to account for the placement of the pipe (the so called "baseline") at 98.9 mbsf. The logging operations deployed two tool strings, the triple combination and the Formation MicroScanner Sonde (FMS). These tool strings also included Hostile Environment Natural Gamma Ray Sonde (HNGS), High-Resolution Laterolog Array (HRLA) and Hostile Environment Litho-Density Sonde (HLDS). The tool string reached the bottom of the hole at 671.5 mbsf and logging was made with multiple passes up to the seafloor.

Table 5.3 – Coring summary of the three drilled holes at IODP Site U1391: U1391A, U1391B and U1391C (extracted from Expedition 339 Scientists, 2012).

Coring Summary	Hole U1391A	Hole U1391B	Hole U1391C
Longitude	9º24.6601′W	9º24.6604′W	9º24.6468′W
Latitude	37º21.5392′N	37º21.5288′N	37º21.5286′N
Water depth (m)	1073.7	1073.3	1073.3
Total penetration (mbsf)	353.1	353.5	671.5
Total length of cored section (m)	353.1	353.5	331.5
Total core recovered (m)	342.62	346.93	269.02
Core recovery (%)	97.03	98.14	81.15

5.2 Methodology

5.2.1 General concepts of seismic reflection

Seismic reflection is a geophysical method capable of obtaining data and acoustic 2D images of the geology under the seafloor. This method is based on the generation and detection of acoustic waves, which propagate through different geological layers. The process begins with the generation of a short pulse of sound (shot) from a source, for example an airgun. The released energy generates acoustic waves that travel through the water and rock layers. The acoustic waves will be reflected on different interfaces, due to acoustic impedance contrasts (Yilmaz, 1987; Sheriff and Geldart, 1995):

$$I = \rho \times V \qquad \text{Equation 1}$$

Where I represents the acoustic impedance, ρ the density (g/cm^3) and V the velocity (m/s).

Subsequently, the reflected waves will be recorded at the surface by seismic receivers, for example hydrophones in the offshore acquisition (Sheriff and Geldart, 1995; Figure 5.2). The records will be processed and transformed into seismic profiles, images used to interpret the stratigraphy and geometry of the subsurface layers of the surveyed area.

5.2.2 Seismic Data Acquisition and Processing

The datasets used in this work form a heterogeneous group with different sources, acquisition parameters and seismic processing. This variability produces inconsistencies for the coverage of the study area and for the characteristics of each dataset (such as seismic processing, vertical and horizontal resolution, quality and positioning system). Therefore, this variability can constrict the results and conclusions obtained in the present work. Also, the older seismic profiles (GSI) correspond to digitalized paper formats, TIFF to SEG-Y (Batista, 2009). This transformation inserts a boundary for the application of further geological or geophysical software.

And finally, another factor that can cause inconsistencies in seismic interpretation is the resolution *vs*. depth penetration challenge. A seismic dataset is always characterized by two distinct but related properties: resolution and penetration depth (Sheriff and Geldart, 1995). These properties are conditioned by the frequency of the signal and by the type of acoustic source. In seismic reflection, depth is measured in two-way travel time (in milliseconds or seconds) and it corresponds to the time the sound waves take since they leave the source, reflect on an interface and return to the receiver. With depth, the frequency of the signal decreases while velocity and wavelength increase. Therefore, seismic resolution will decrease and high frequencies will be preferably reflected on shallower reflectors while low frequencies reflect on deeper levels (Sheriff and Geldart, 1995). A seismic survey is a compromise between these two properties, since it favours one and damages the other. Therefore, the acquisition and the seismic processing must consider the objectives of the survey. If a seismic survey has good resolution, it uses high frequencies and therefore does not reach the lower layers of the subsurface (Figure 5.2).

The seismic datasets used in this study have good penetration with medium (BIGSETS and GSI, up to 10 km depth) and high (CONDRIBER and STEAM, up to 4 km depth) resolution. The acquisition specifications of the CONDRIBER seismic survey are displayed in Appendix 10.1.

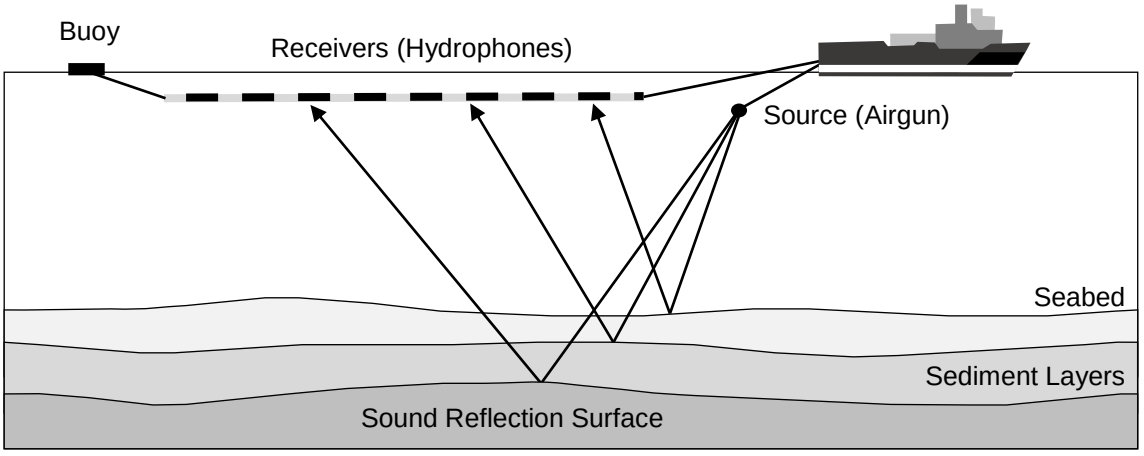

Figure 5.2 – Example of offshore seismic reflection survey with classic source and receivers' geometry. Modified from FLCT Services Ltd. (2009).

- ***Processing steps***

The aim of seismic data processing is to increase the signal-to-noise ratio, and thus improve the vertical resolution of the individual seismic traces (Sheriff and Geldart, 1995). The CONDRIBER survey is constituted by 16 multichannel high (to medium) resolution 2D seismic profiles, obtained with an airgun source during the MOWER/CONDRIBER cruise in 2014. The CONDRIBER data was processed by the Instituto de Ciencias Marinas in Barcelona (ICM-CSIC). The processing steps applied are outlined below (Informe Técnico Campaña Mower, 2014; Appendix 10.1).

The processing flow begun by extracting the navigation of each shot and channel through *export headers* from *Seisee*. This step allows the calculation of the common depth point (CDP), of each profile, on the program *CDP3*. This sequence results in a SEG-Y file with shot, channel, CDP and UTM coordinates of each CDP and shot in the headers of the traces.

The next step was the application of a noise filter. The noise of the SIG streamer usually comes with the same signal and other times with inverted signal due to multiple noise sources. Therefore, same signal noise auto-eliminated itself when the polarity of one of the channels was switched and summed. The noise with inverted signal was eliminated by applying a Matlab script (*Seg4king*), which replaced, for a certain time of the trace, values which are higher than a certain magnitude of the previous and next traces, for the measurement of these.

The main processing flow was developed on the software *Hotshot*. *Hotshot* can create referenced bitmaps, which allow the digitalization of the seafloor depth and elimination of the water column. Afterwards, the signal of the reflections from channels 2 and 3 was switched (with function *VNEG*), since the channels had inverted polarity (regarding the reflections of channel 1).

The next step was the application of a function (*RABAL*) to equalize channels and shots, followed by high-pass filtering to eliminate frequencies lower than 30 Hz. Filtering was also employed through several band-pass filters, progressively applied since the seafloor:

- 0 ms: 75 - 240 Hz;
- 100 ms: 25 – 180 Hz;
- 1000 ms: 25 - 100 Hz;
- 9000 ms: 20 - 100 Hz;

Afterwards, a Mute removed the signal of channel 3 below 0.4 seconds.

The profiles with sedimentary cover undertook another processing sequence: the elimination of the first 150-200 ms (below the seafloor) of channels 1 and 2, to give more rebound to the high frequencies of channel 3. This sequence was followed by Sort and Stack of the traces by order of the shot, or by CDP's for the more superficial profiles.

The next step was the application of a new equalization of the traces and resampling at 1 ms (since the originals are sampled at 500 μs). Afterwards, it was necessary to apply an Automatic Gain Control (AGC) with a window of 0.7 seconds to normalize the traces. The last step was a Shift to eliminate the first 50 ms of the file and to allow synchronization between register and trigger. Finally, the resultant SEG-Y file was written.

The use of different processing steps can constrain the quality of the seismic profiles and cause imprecisions during seismic interpretation. This also shows in the display of the seismic data and when attempting a seismic to well tie.

5.2.3 Seismostratigraphic Calibration Method

To take full advantage of Site U1391 physical properties data and to calibrate the well data with the crossing seismic profiles, it is possible to create a model of the seismic trace: the synthetic seismogram. A synthetic seismogram is a concept manufactured from sonic (or velocity) and density logs, which is compared to seismic data to identify reflections of particular interest (Sheriff and Geldart, 1995; Hardage, 2007). This process can also distinguish primary reflections from multiples or other events.

First, the logs have to be converted from functions of depth to functions of vertical seismic travel time (Yilmaz, 1987; Holstein, 2007). This transformation is applied by a simple equation:

$$D = V \times t \qquad \text{Equation 2}$$

Where D represents depth (m), V the velocity (m/s) and t the seismic travel time (second).

Secondly, the sonic and density logs have to be multiplied to create a log of the acoustic impedance (Equation 1). This time-based impedance is converted into a series of reflection coefficients (Equation 3) (Yilmaz, 1987):

$$R = \frac{I_1 - I_2}{I_1 + I_2} = \frac{\rho_1 V_1 - \rho_2 V_2}{\rho_1 V_1 + \rho_2 V_2} \qquad \text{Equation 3}$$

R – Seismic reflection coefficient;
ρ_1 – bulk density of the layer above the reflection interface (g/cm^3);
ρ_2 – bulk density of the layer below the reflection interface (g/cm^3);
V_1 – velocity of the layer above the reflection interface (m/s);
V_2 – of the layer below the reflection interface (m/s).

An estimated seismic wavelet is convolved with the reflectivity model to obtain a synthetic seismogram (Figure 5.3). Afterwards, the synthetic seismogram can be compared with the real seismic traces near the well for interpretation purposes and if necessary, to apply editing. Editing involves shifting the synthetic seismogram up and down in the time scale to determine the time shift required to position the synthetic seismogram with optimal alignment of reflection peaks and troughs with the seismic traces (Sheriff and Geldart, 1995). Other corrections are progressively applied until the synthetic model is considered sufficiently adjusted to the seismic trace (Anderson and Newric, 2008). As with all types of modelling, the result is not unique, since it is possible that another different model could produce an equally good match.

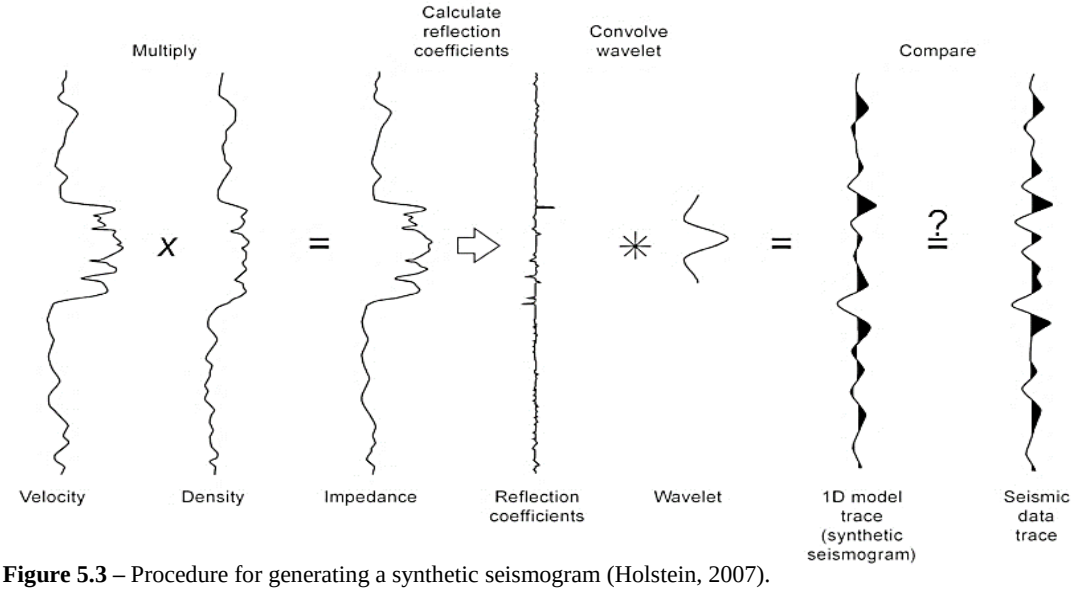

Figure 5.3 – Procedure for generating a synthetic seismogram (Holstein, 2007).

Site U1391 has velocity (from DSI Tool, km/s) and density (g/cm^3) logs available. These logs were edited for bad intervals and outliers, mostly identified at the top and the bottom portions of the data. Kingdom software (*SynPAK* module) generates a synthetic seismogram by following the process mentioned above (Figure 5.3 and 5.4). The wavelet chosen was minimum phase with the following parameters: 20 Hz for F1, 25 Hz for F2, 75 Hz for F3 and 240 Hz for F4. The chosen frequencies consider the band-pass filters applied during the CONDRIBER seismic processing and also the start of logging measurements, which register from the baseline (98.9 mbsf) to the bottom of the hole (671.5 mbsf). However, it is generally preferable to extract the wavelet from the seismic data to be matched (Sheriff and Geldart, 1995; Anderson and Newric, 2008). The synthetic seismogram obtained is presented in normal and reverse polarity, alongside the velocity (km/s) and the density (g/cm^3) logs, as well as the acoustic impedance and the resistivity (ohm.m) logs created, shown in Figure 6.2. This Kingdom software license does not possess the tools necessary to apply editing or other corrections to the synthetic seismogram. Therefore, the interpretation and calibration of said model with the real seismic traces (from the intersected seismic profiles: CL06 or BS19) cannot be completed. But an example of this process can be seen below (Figure 5.4).

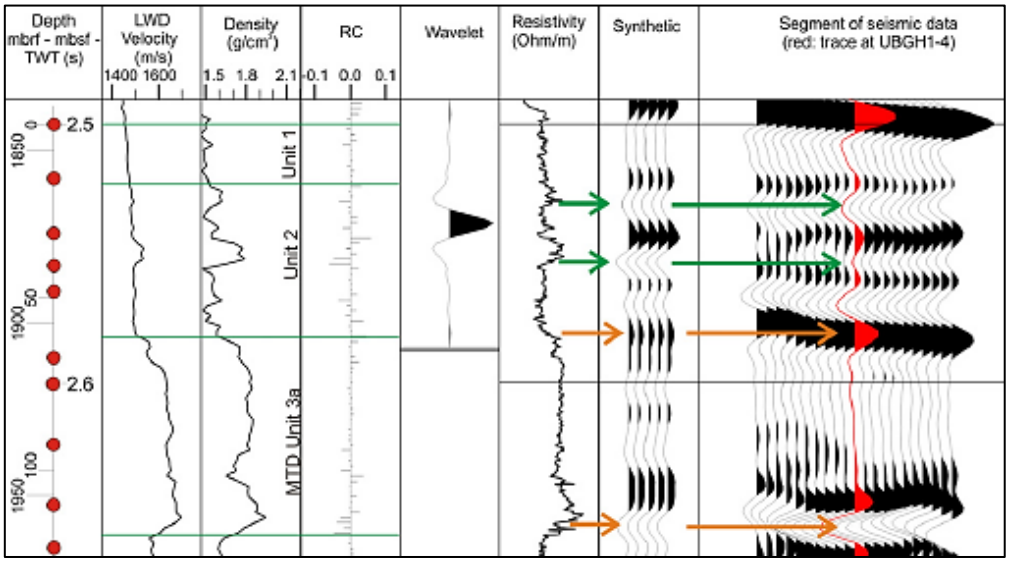

Figure 5.4 – Example of synthetic seismogram using the P-wave velocity (obtained from Logging-While-Drilling, LWD) and bulk density logs from the Ulleung Basin Gas Hydrate Drilling Expedition 1 Site UBGH1-4, in 2007 in the Ulleung Basin, offshore Korea and a seismic wavelet extracted from 3-D seismic data (Scholz *et al*., 2012).

The lack of calibration between seismic reflections and the resulting seismogram can also derive from other factors:

- A synthetic is an estimate of the seismic image if the imaging ray path travelled vertically downward from a source and then reflected vertically upward along the same travel path to a receiver located exactly at the source position. While seismic profile traces are a composite of several field traces, which represent wave field propagation along multiple oblique ray paths between sources and receivers (Sheriff and Geldart, 1995);
- The effects of the near surface are not considered for a synthetic seismogram, since the velocity and density logs themselves are not recorded over shallow depths (since logging usually starts after the placement of the pipe). Although this effect can be corrected with co-derived velocity and density measurements to create relatively continuous profiles (Cunningham and Droxler, 2000; Anderson and Newric, 2008). This factor also considers the alteration caused by drilling and drilling fluid invasion, which damage the rocks and therefore affect the measurements and representations of the petrophysical properties (Hardage, 2007).

5.2.4 Seismostratigraphic Correlation Method

Seismostratigraphic correlation uses the data provided by seismic profiles and wells to establish temporal or lateral relations between stratigraphic units or between their bounding discontinuities, and can be applied for lithostratigraphic correlation or chronologic correlation studies (Vail *et al*., 1977; Snedden and Sarg, 2008).

Lithostratigraphic correlation establishes a relation between strata or units with compatible lithological characteristics, without considering an equivalence in the geologic time scale (Vail *et al*., 1977; Mitchum *et al*., 1994). Lateral relation between lithostratigraphic units implicates recognizing lateral continuity and using consistent and unambiguous stratigraphic markers, which are the most reliable method to establish a relation.

Chronologic correlation assumes the occurrence of geologic time equivalence between stratigraphic units, even with different lithology (Vail *et al*., 1977). This concept implicates knowing the age of the correlated units to establish relations between stratigraphic units of the same area and between units with the same geologic time interval. This is also used to ascertain the position of a unit in the chronostratigraphic table at a global scale (Vail *et al*., 1987).

In seismic interpretation, correlation is simply the identification of seismic units or discontinuities based in similarities between character reflection and their arrival time in a crossing point of two or more seismic profiles (time-tie) (Sheriff and Geldart, 1995; Snedden and Sarg, 2008). This process was chosen since the synthetic seismogram created above was not used to tie seismic and well data. IODP's database has a time-depth checkshot chart available for Expedition 339, Site U1391. Site U1391 time-depth chart and the stratigraphic events identified by Hernández-Molina *et al.* (2015) allow a correlation with the intersected seismic profiles, CL06 and BS19 (Table 5.4).

Table 5.4 – Time-depth chart created from U1391 time-depth checkshot data and from the main stratigraphic discontinuities mentioned in Hernández-Molina *et al*. (2015).

IODP U1391	Depth (mbsf)	Depth (m)	Two-way travel time (ms)
Seafloor	0	1073.43	1430
LQD	91	1164.43	1610
MPD	196.1	1269.53	1700
EQD	566.1	1639.53	2020
BQD	575	1648.43	2050
LPD	633.2	1706.63	2100
Bottom of hole	671.5	1744.93	2170

5.3 Seismic stratigraphy interpretation

Interpretation of seismic reflection profiles involves a stratigraphic analysis and, if possible, calibration or correlation with lithological chronostratigraphic data (Vail *et al*., 1977; Snedden and Sarg, 2008). This method applies geological concepts of stratigraphy on the seismic data. The key concepts of seismic stratigraphy were defined in the Memoir 26 of American Association of Petroleum Geologists entitled "*Seismic stratigraphy: Applications to hydrocarbon exploration"* (Payton, 1977). This approach focuses on distinctive criteria available on seismic reflection data to interpret depositional sequences, geometry relations, geologic information, eustatic variations and tectonic events.

The concept of **depositional sequence** is outlined as a stratigraphic unit composed of genetically related strata (Figure 5.5), bounded by unconformities or their correlative conformities (Sloss, 1963). This concept is based on the repetitive nature of geological and sedimentary events and assumes chronostratigraphic significance for depositional sequences and their boundaries. Although not all reflections are generated by geological interfaces (such as coherent noise patterns: multiples or diffractions). This methodology defines the depositional sequence boundaries as discontinuities or correlative conformities, which represent marks of erosion or non-deposition, sometimes associated with a hiatus (a lapse of time that separates rocks of different ages, measured at the scale of the basin, Mitchum *et al.*, 1977a,b).

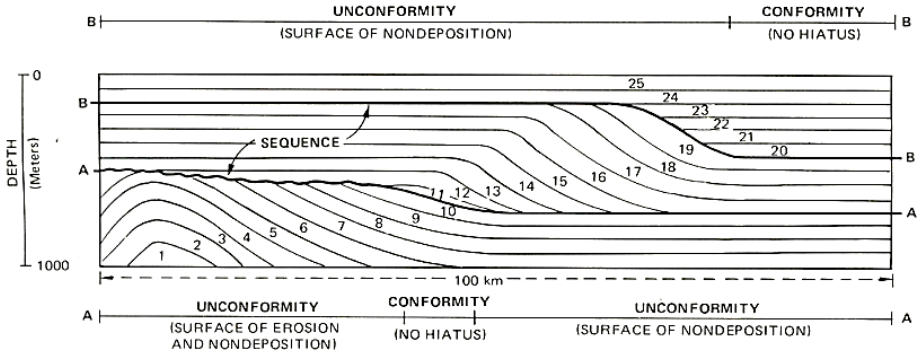

Figure 5.5 – Example of depositional sequence, limited by bounded unconformities and their relative conformities (surfaces A and B) and reflectors terminations (adapted from Mitchum *et al.*, 1977b).

A **seismic sequence** is a depositional sequence identified on a seismic section (Mitchum *et al*., 1977a, b). This concept defines a succession of reflections as genetically related strata, bounded at the top and base by surfaces of discontinuity (surfaces A and B in Figure 5.5), marked as reflection terminations (Mitchum *et al*.,1977c). However, the conventional concept of seismic sequence and the terminology involved is not fully applicable to contourite studies (Nielsen *et al*., 2008). The conventional concept of seismic sequence implies that sequences and their strata are formed as a result of base-level changes and downslope shelf-to-basin sediment transport, while contourites are mainly formed by bottom-currents regimes and sediment pathways orientated parallel to the continental margins. Also, the unconformities that bound the sequences are inferred to be autocyclic and result from foreseeable changes in accommodation space, while unconformities in contourites result from a non-predictable pattern related to variations in current regime (Nielsen *et al*., 2008).

Therefore, it is preferable to use the term **seismic succession**, as suggested in Nielsen *et al*. (2008). Seismic successions are not associated with any specific depositional environment to denote a stratigraphic subdivision of a drift succession. The separation of seismic successions is based on the analysis of reflection terminations and internal reflectors patterns, using the traditional techniques introduced by Mitchum *et al.* (1977a,b,c). These concepts allow the definition of seismic succession as a three-dimensional unit, limited by stratigraphic discontinuities and composed by a group of reflections, whose parameters diverge from the adjacent successions. This differentiation is drawn by seismic facies, a group of seismic parameters used to characterize a seismic succession and individualize it from the adjacent successions.

5.3.1 Seismic Facies Analysis

Seismic facies analysis is the description and geological interpretation of seismic reflection parameters, such as the geometry and character of the reflections, the internal configuration and the external form. The analysis of several parameters results in a coherent structural interpretation, providing considerable information on the depositional environment and geology of the subsurface (Mitchum *et al*. 1977a,b).

- ***Reflection Terminations***

Considering the geometric relations between reflections, five types of terminations can be identified to define discontinuities or limits of seismic upper and lower units: onlap, downlap, toplap, truncation (erosional or structural) and concordance. Baselap can also be defined if onlap and downlap are indistinguishable. Their presence indicates an important transition and depositional hiatus, as a result of erosion or non-deposition.

Top-discordant relations include truncation or toplap (Figure 5.6). **Truncation**, erosional and structural, is a relation characterized by an abrupt lateral ending of the reflections against a discordant surface. It could be generated as a result of water currents action or due to tectonic tilting of a sequence, followed by erosion over large areas or confined to the flanks of submarine channels. **Toplap** is characterized as the termination of reflections, interpreted as strata, against an overlying surface. Toplap is usually formed due to non-deposition hiatus and minor erosion.

Base-discordant relations include onlap and downlap (Figure 5.6). **Onlap** corresponds to a relation where seismic reflections are interpreted as initially horizontal strata terminating progressively on top of a dipping surface, or as initially inclined strata terminating progressively up dip against a surface of higher dip. These terminations are associated with seafloor irregularities, caused by non-depositional hiatus or by deposition on tilted blocks. **Downlap** is characterized as initially dipping strata terminating downdip against an initially dipping or horizontal surface, and results from non-deposition hiatus.

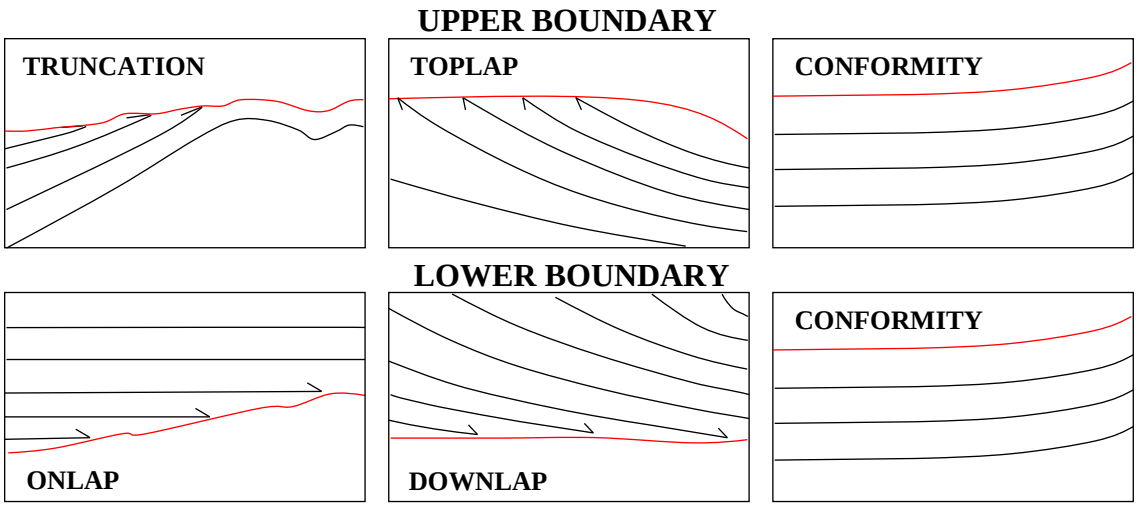

Figure 5.6 – Seismic reflection terminations, according to Mitchum *et al*. (1977b), from Roque (2007).

- ***Reflection Configurations***

The overall geometry of a seismic facies unit consists of the internal reflection configuration and the external form of the unit. The identification of different reflection configurations indicates a geological variation in the seismic unit and carries geological significance (Mitchum *et al.*, 1977c). The variations are identified by the following parameters: reflection continuity, amplitude, frequency and signature.

Continuity is identified by lateral juxtaposition of successive reflections of the same horizon and is related to the physical continuity of the strata. Therefore, continuous reflections suggest widespread, uniformly stratified deposits. Continuity of a given horizon is interpreted as preservation of the depositional conditions with no main changes in the energy of the environment.

Amplitude is associated with the maximum amplitude of the reflected wave, which is dependent on the velocity and density contrasts through each individual interface and the spacing between interfaces (high

amplitudes reflect high acoustic impedance). If a high amplitude reflection diminishes rapidly, it usually indicates a high energy depositional environment and the opposite suggests a large continuity of the formations and a stable depositional environment.

Frequency is the time interval between two successive reflections. The frequency reflects the instrumental seismic characteristics but it is also influenced by other factors such as the thickness of the layered deposits and the presence of fluids. There is an inverse relation between strata thickness and reflection thickness: high frequencies correspond to thin strata.

- ***Internal Reflection Configurations***

Considering the geometric relations between reflections, the description and interpretation of internal reflection configurations begins with simple patterns and continues to the more complex. The configurations occur as a result of the depositional rate, energy, lithology, erosion, deformation and paleomorphology of the basin (Mitchum *et al.*, 1977c).

The **parallel** and **subparallel** (even or wavy) patterns (Figure 5.7) refer to high amplitude, continuous and parallel reflections. These patterns suggest uniform depositional rates on a steady subsiding shelf or stable basin plain setting.

The **divergent** pattern (Figure 5.7) is related to a wedge-shaped sequence of seismic horizons. It suggests lateral variations in depositional rates or the progressive tilting of the depositional surface.

The **chaotic** pattern (Figure 5.7) is identified by discontinuous, discordant and disordered reflections. This pattern suggests a high energy setting with variable depositional conditions and it is generally found in slump structures, erosion derived deposits, cut-and-fill channel complexes and zones highly affected by faults or folds.

The **transparent** pattern (Figure 5.7) is characterized by the total or partial absence of reflections or by the lack of lateral continuity. This pattern is associated with homogeneous rocks, highly deformed or metamorphosed rocks, salt features and large igneous bodies. Although thick and seismically homogeneous sequences of shales or sandstones can also appear reflection-free.

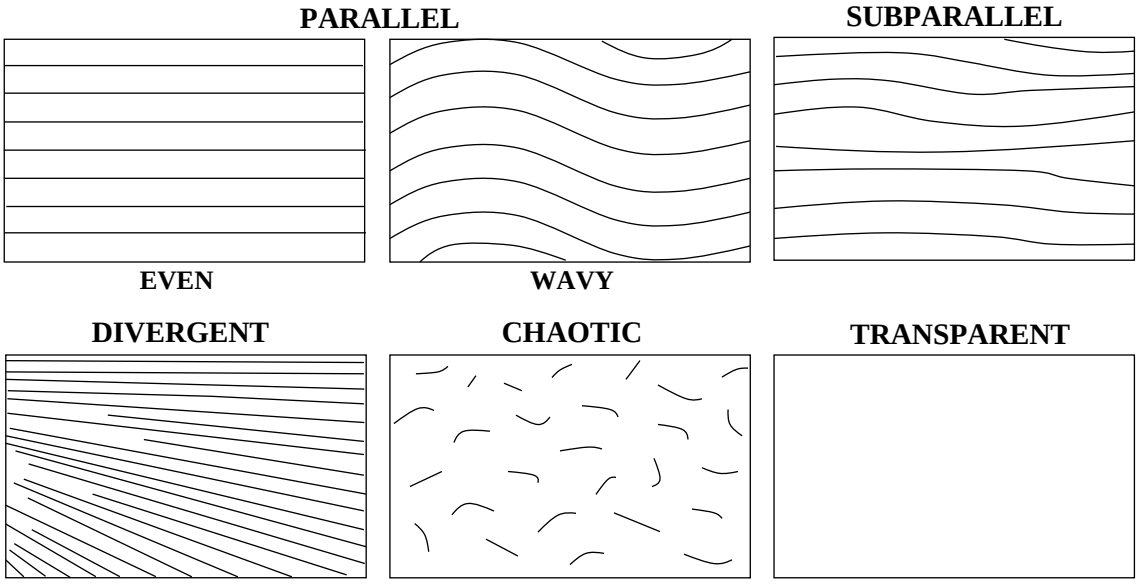

Figure 5.7 – Seismic internal reflection patterns, according to Mitchum *et al*. (1977c).

The most common depositional features observed in seismic profiles are clinoforms, represented by complex reflection configurations.

Prograding clinoforms configurations correspond to packages of oblique to sigmoidal shaped reflections. These configurations are interpreted as strata where significant deposition occurred as a result of prograding or lateral sedimentation outbuilding. There are several sub-types of prograding configurations, such as sigmoid, oblique, tangential and parallel, sigmoid-oblique, shingled and hummocky (Figure 5.8). The differences in prograding clinoform patterns occur due to variations in the depositional rate and water depth, and a wide variety of environmental settings is possible.

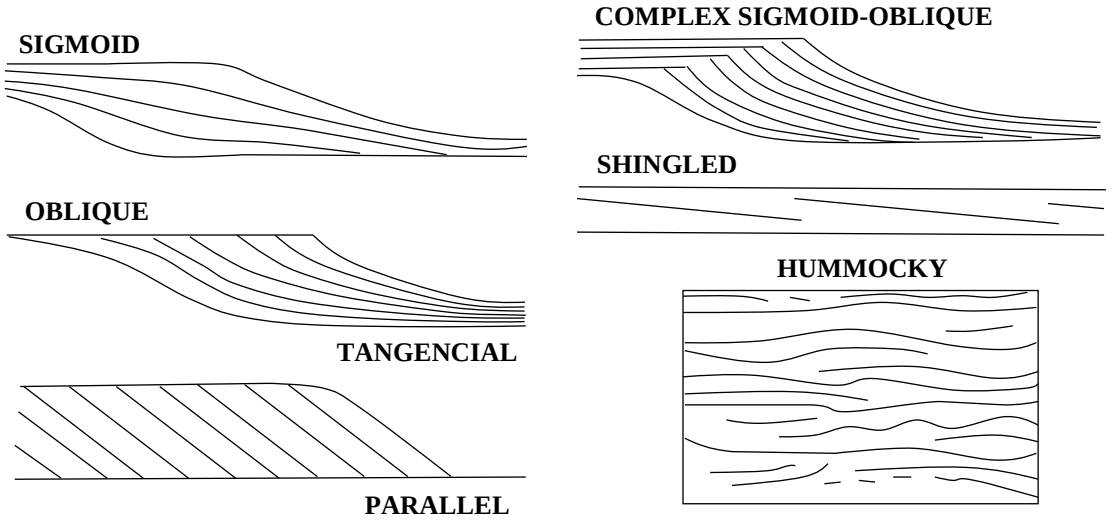

Figure 5.8 – Seismic internal reflection patterns of prograding clinoforms (from Mitchum *et al.*, 1977c).

Sigmoid progradational configuration (Figure 5.8) is an S-shaped clinoform, interpreted as thin, gently dipping strata at the top and base with a thicker, steeper intermediate sector. This configuration suggests a low energy setting with low sediment supply, relatively rapid basin subsidence and/or rapid sea-level rise.

Oblique progradational configuration (Figure 5.8) is interpreted as steep-dipping strata with a toplap termination at or near a horizontal or subhorizontal upper boundary and a downlap termination against the lower boundary. New strata build almost entirely laterally in a depositionally downdip direction, as a result of the foreset steepness.

In the **tangential oblique progradational** pattern (Figure 5.8), the dip decreases gradually in the foreset, forming concave-upward strata that change into a gently dipping bottomset strata. The strata become thinner towards the lower boundary, with downlap terminations.

In the **parallel oblique progradational** configuration (Figure 5.8), the foreset strata maintain a relatively steep dip from top to bottom and terminate with a high angle by downlap at the lower boundary. The oblique progradation configuration is related to high energy sedimentary settings with a high sedimentary supply, slow to no basin subsidence and a still stand of the sea-level, which allows sedimentary bypass or scouring of the upper depositional surface.

The **complex sigmoid-oblique progradational** configuration (Figure 5.8) is a complex prograding clinoform, defined by a combination of variably alternating sigmoid and oblique progradational configurations in the same seismic unit. This variation suggests alternating up-building and depositional bypass on a high energy regime.

Shingled progradational configuration (Figure 5.8) is a thin prograding pattern, generally with parallel upper and lower boundaries and gently dipping parallel internal reflectors, which are oblique and terminate by toplap and downlap. This pattern suggests the formation of depositional units prograding into shallow water.

The **hummocky clinoform** configuration (Figure 5.8) is characterized by irregular and subparallel reflection segments forming a rather irregular hummocky pattern, with non-systematic reflection terminations and splits. This configuration is interpreted as strata forming small, interfingering clinoforms lobes, which build into shallow water in a prodelta or inter-deltaic setting.

- ***External Form***

The interpretation of depositional sequences comprehends an understanding of three-dimensional external forms and an association to different seismic facies units. Therefore, the external form is used to individualize a seismic unit, characterized by variable extent and geometry. Several external forms can be distinguished: sheet, sheet drape, wedge, bank, lens, mound and fill (Figure 5.9). External shapes such as **sheets**, **wedges**, **lens** and **banks** (Figure 5.9) can reach large sizes and display parallel, divergent or prograding patterns as internal reflection configurations.

Sheet drapes are generally related to the deposition of pelagic or hemipelagic sediments on the underlying topography in a low energy, deep-marine environment.

Mound shapes are interpreted as strata that forms build ups, elevations or prominences. Mounds can have different origins as a result of carbonate edifications or diapirs. These shapes have usually small dimensions with diverse internal configurations.

Fill patterns correspond to strata filling a negative-relief feature in the underlying strata. These deposits can have different internal configurations, such as onlap, chaotic, prograding and divergent. Fill deposits can reach over large areas (from meters to kilometres) when in a basin context or be smaller (from centimeters to meters) when in the dependency of a channel.

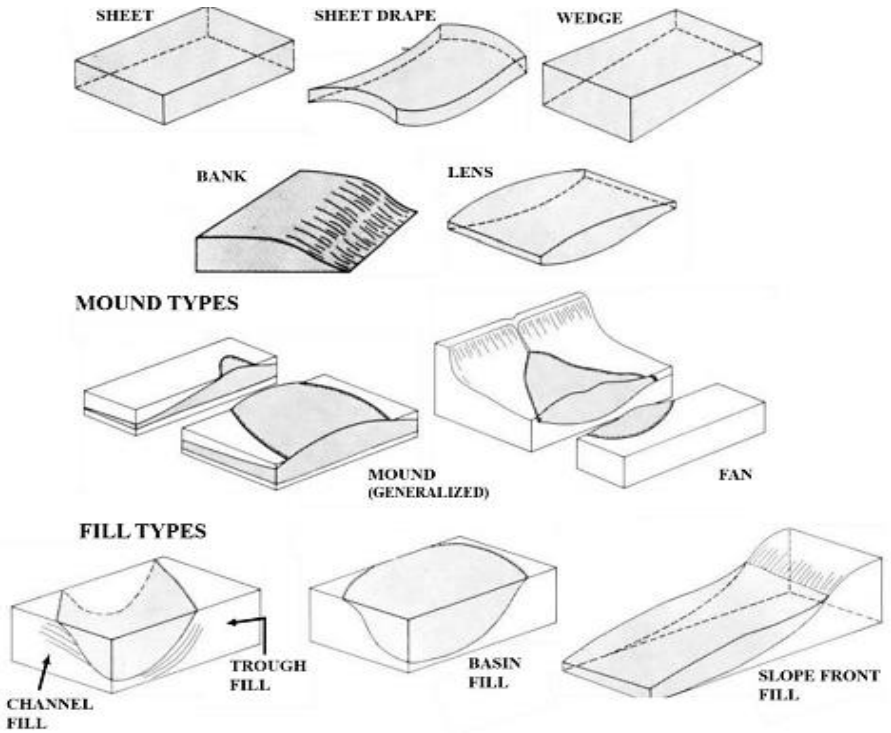

Figure 5.9 – External forms of seismic facies units. Extracted from Mitchum *et al*. (1977c).

5.3.2 Seismic Interpretation Procedure

The seismic interpretation procedure of a contourite depositional system is well-defined in Nielsen *et al*. (2008). This procedure can be applied on this study, since it orders the seismic interpretation by an increasing level of seismic detail (which are named seismic elements), and respects the previous seismostratigraphic concepts. The procedure is outlined as follows (Figure 5.10):

- First-order elements represent large-scale features, such as the architecture of the drift, with emphasis on the geometry and larger depositional units;
- Second-order elements are medium-scale features, which correspond to the internal architecture and focus on the sub-units of the large-scale depositional units;
- Third-order elements consist of small-scale features, related to seismic attributes and the seismic facies configuration of the depositional sub-units.

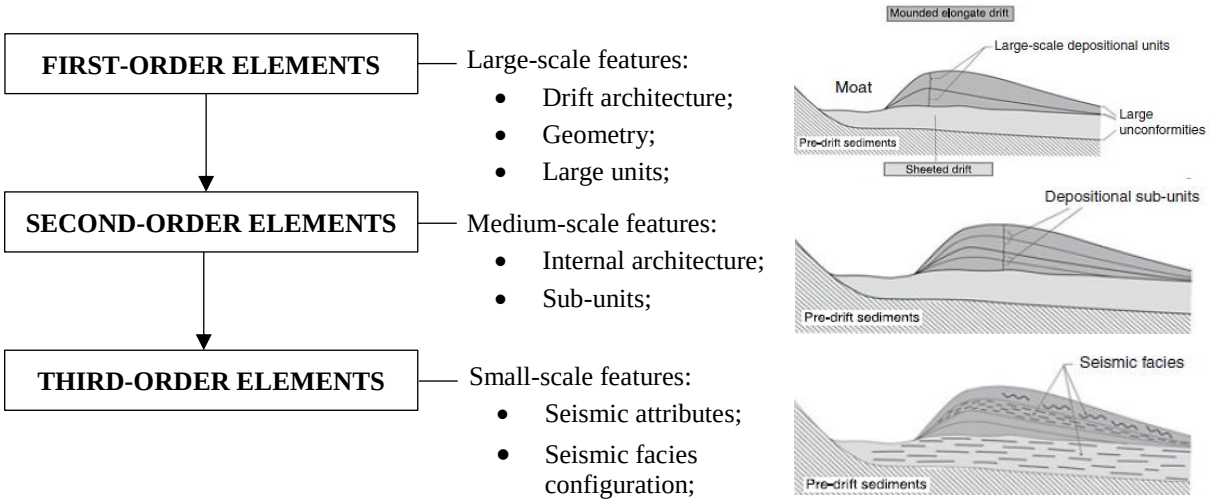

Figure 5.10 – Illustration of the seismic interpretation procedure applied to contourite studies, according to Nielsen *et al.* (2008).

5.3.3 Software

Landmark – Landmark developed by Landmark Graphic Corporation was used for the interpretation of seismic data, with the application of *SeisWorks* and *PowerView* tools. *SeisWorks* was used to view and interpret seismic profiles, through mapping of seismic horizons and faults. *PowerView* was used to view and create isobaths and isopachs maps, which represent the spatial distribution of a selected horizon's depth and the spatial variation of a unit's thickness. Also, a seismostratigraphic correlation of Site U1391 with the crossing seismic profiles was applied through Landmark Openworks Database Management.

ArcGIS – the ArcGIS software developed by Environmental Systems Research Institute **(**ESRI) is a geographic information system (GIS) with different modules. The main module, *ArcMap*, was used for the compilation of data and creation of the isobaths and isopachs maps rendered in this study. Also, the *ArcScene* module was used to generate 3D displays of a few selected maps.

Kingdom – the Kingdom software from IHS Corporation has multiple modules. *SynPAK* was used to create synthetic seismograms, using IODP well data and seismic data. This method generates a model, which can calibrate the seismic time data (in milliseconds) with depth data (meters) and the correct positioning of the well.

CHAPTER 6

RESULTS

6.1 General description of main morphological features

The joint analysis of SWIM multibeam bathymetry and seismic reflection profiles allowed the identification of three main morphological features in the study area, which are: i) the Sines Contourite Drift (SD) and moat; ii) submarine canyons and channels; iii) scarps and structural highs.

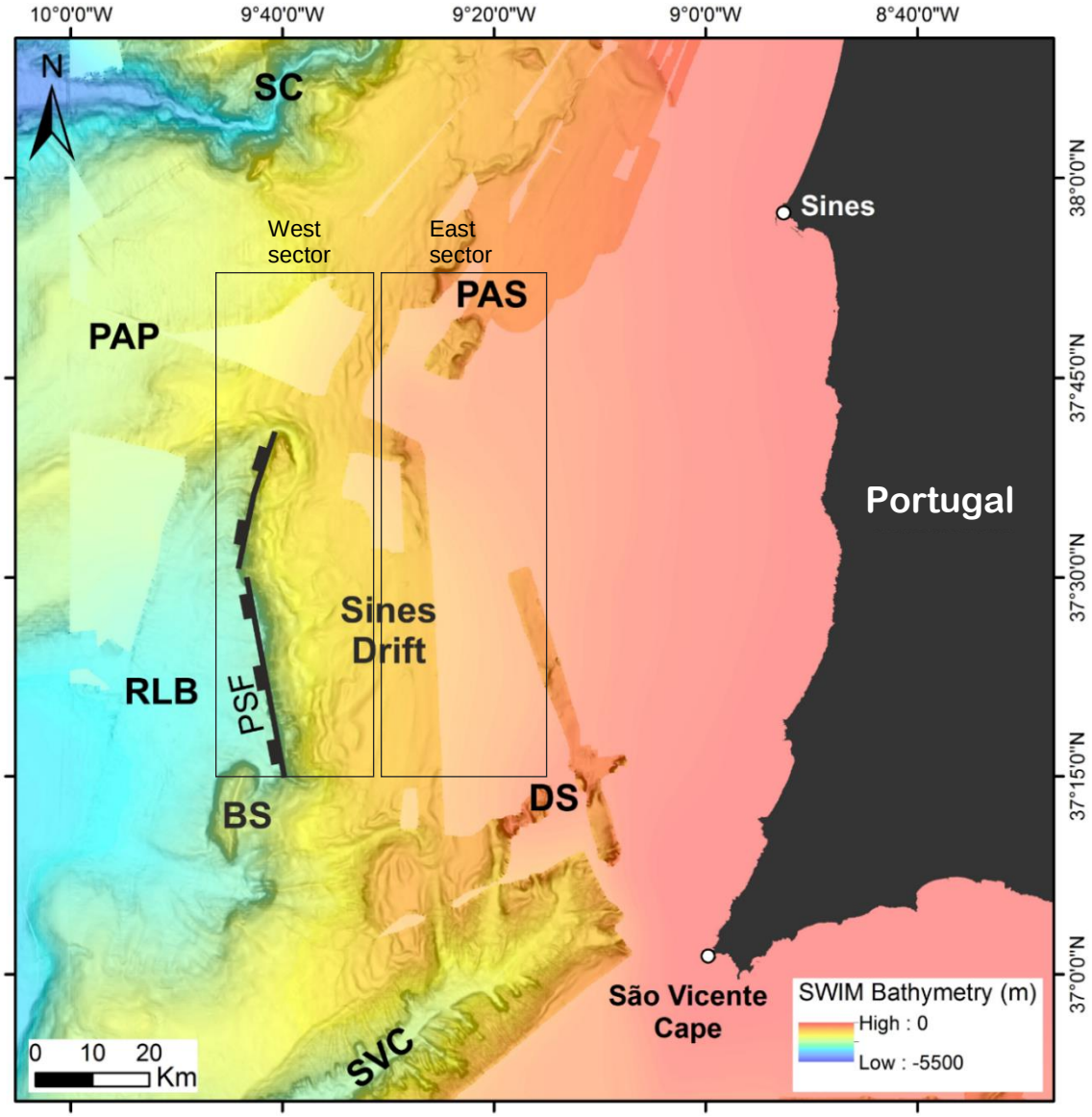

Figure 6.1 – Bathymetric map of the study area with SWIM multibeam bathymetry (100 m cell grid from Zitellini *et al*., 2009) to show the main morphostructures. The global GEBCO (2003) data was used to fill in the gaps of the SWIM dataset. BS – Bow Spur; DS – Descobridores Seamounts; PAP – Príncipe de Avis Plateau; PAS – Príncipe de Avis Seamounts; PSF – Pereira de Sousa Fault; RLB – Rincão do Lebre Basin; SVC – São Vicente Canyon; SC – Setúbal Canyon.

The SD is located between 1000 and 2000 m water depth on the Alentejo continental slope and has approximately 70 km of extension and 40 km of width. In general, the SD displays an asymmetric shape with a steeper western slope (0-5ºW) and plastered morphology. The seafloor morphology on the SD can be divided in east and west sectors due to the presence of different morphologic features.

The east sector is characterized by a smooth seafloor morphology. Also, the SD has an eastern moat, 70 km long, 0.5-1 km wide and 150 m deep, located between 1000 m and 1250 m depth with NNW-SSE to NNE-SSW orientation. The moat starts at the south, from the SVC, and curves around the continental shelf towards the SC. The moat is probably scoured by the MOW's upper core (MU) that flows between 600-1000 m water depths (Bower *et al.*, 2002; Llave *et al*., 2007b).

The western sector is marked by numerous depressions at the Pereira de Sousa Scarp (approximately 20º gradient, dip towards west, 50 km length and 1400 m height) between 1500 m and 2000 m depth. These occurrences are characterized by amphitheater shapes and head scarps, staggered till the slope (Figure 6.1) and were therefore interpreted as landslide scars and MTD from slope failure and gravity-driven events.

The SD is located between the distal segments of two canyons: the São Vicente at south and the Setúbal at north (Figure 6.1). Furthermore, the SD is seated on the steep scarp of the PSF and confined towards east by structurally controlled basement highs (<1000 m depth). The São Vicente Canyon is characterized by a NE-SW orientation and extends from 200 m close to the shore to 4900 m depths at the Horseshoe Abyssal Plain. The Setúbal Canyon is characterized by a meander shape and reaches depths around 5000 m at the Tagus Abyssal Plain.

The SD is located east of the Rincão do Lebre Basin (RLB). The passage from the SD (at 1000 m depth) to the RLB (at 3200 m depth) is marked by the abrupt N-S slope of the Pereira de Sousa Scarp. The RLB is an inner basin of the Infante Dom Henrique Basin, located between 3200 and 4000 m depth and confined to the north and to the south by the Príncipe de Avis Plateau (PAP) and the Marquês de Pombal Plateau (MPP), respectively. The RLB gives the seafloor a smooth morphology, except near the base of the Pereira de Sousa Scarp where it receives gravity-driven deposits from the nearby relief.

The SD is also surrounded by other morphostructures, which are from north to south (Figure 6.1): the Príncipe de Avis Seamounts and Plateau (PAS and PAP), the Bow Spur, and the Descobridores Seamounts (DS). The PAP is located between 1500 and 5000 m depth with an E-W elongated shape. The PAS separate the margin into two sub-basins, between the Setúbal and the São Vicente canyons. The Bow Spur is a relief advanced towards west (about 10 km), related to the Pereira de Sousa Scarp. Little can be said about the DS due to the absence of bathymetric data in this area, but the DS have been described by several authors as tectonic uplifted structures (e.g. Mougenot, 1989; Zitellini *et al.*, 2004).

6.2 Chronostratigraphic constraints

An important aspect to better understand contourites is a detailed sedimentological work, which will aid in the identification of contourite facies. Therefore, based on acquired well data we can: i) correlate seismic units with contourite successions, ii) identify any diagnostic criteria for contourite deposits and iii) associate the resulting observations with contourite formation factors on the SW Portuguese margin. Well Pescada-1 and Site U1391 data gave the depths and ages of the main discontinuities (Table 6.1). The synthetic seismogram created in the Kingdom software to make a chronostratigraphic correlation is presented below, despite no editing applied.

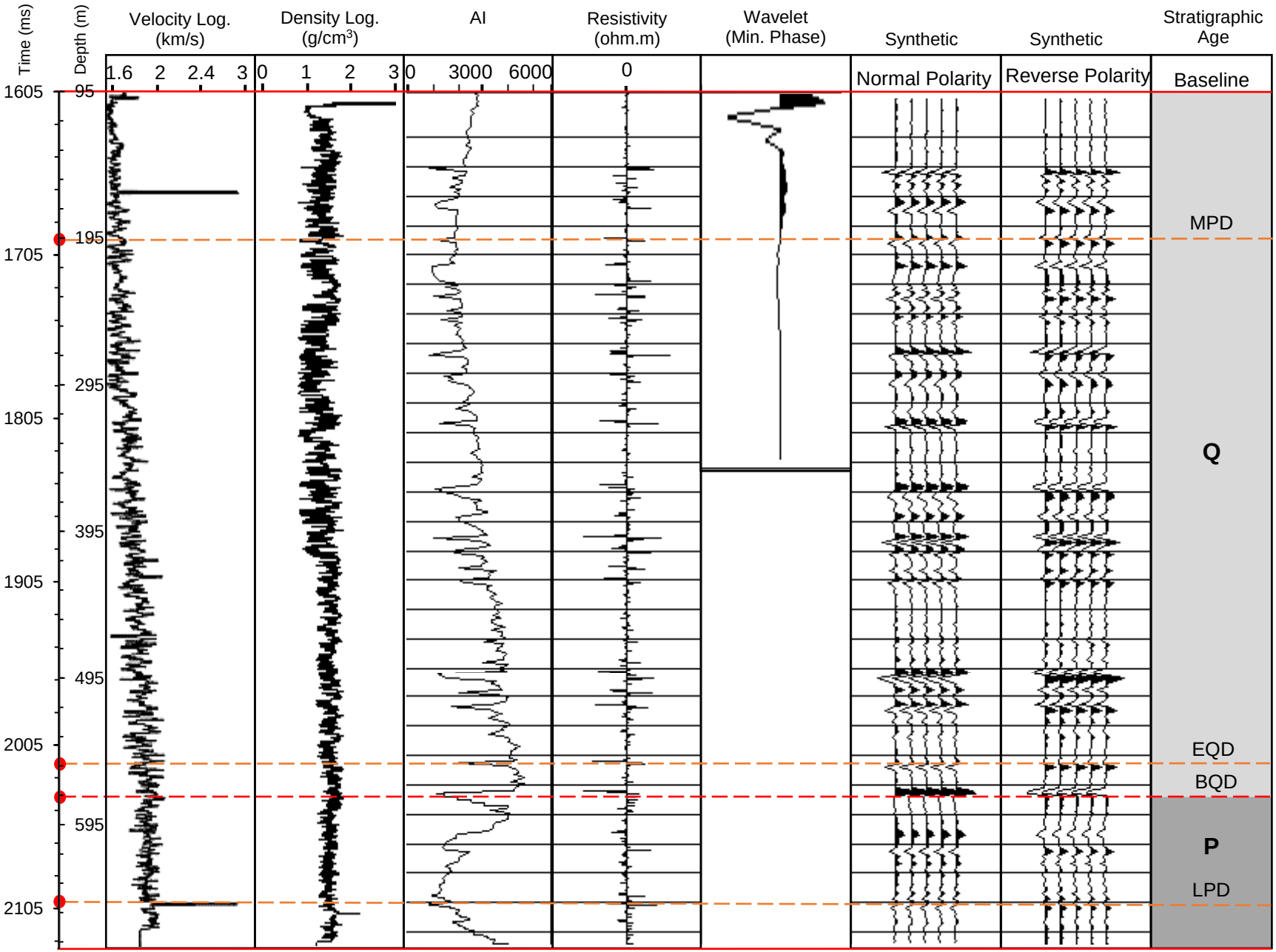

Figure 6.2 – Synthetic seismogram (normal and reverse polarities) based on velocity (km/s, from DSI Tool) and density (g/cm^3) logs and the convolution of the resistivity (ohm.m) with a minimum phase wavelet. Despite no editing and calibration, the main stratigraphic discontinuities (Expedition 339 Scientists, 2012; Hernández-Molina *et al*., 2015) are represented to the right.

6.2.1 Correlation with Pescada-1 oil-well

Oil industry well Pescada-1 data was correlated to the older seismic horizons. Pescada-1 well correlated the B unconformity, the lower boundary of the SD, to the Late Miocene (Figure 6.3). Therefore, seismic unit U1 is inferred as Late Miocene deposits.

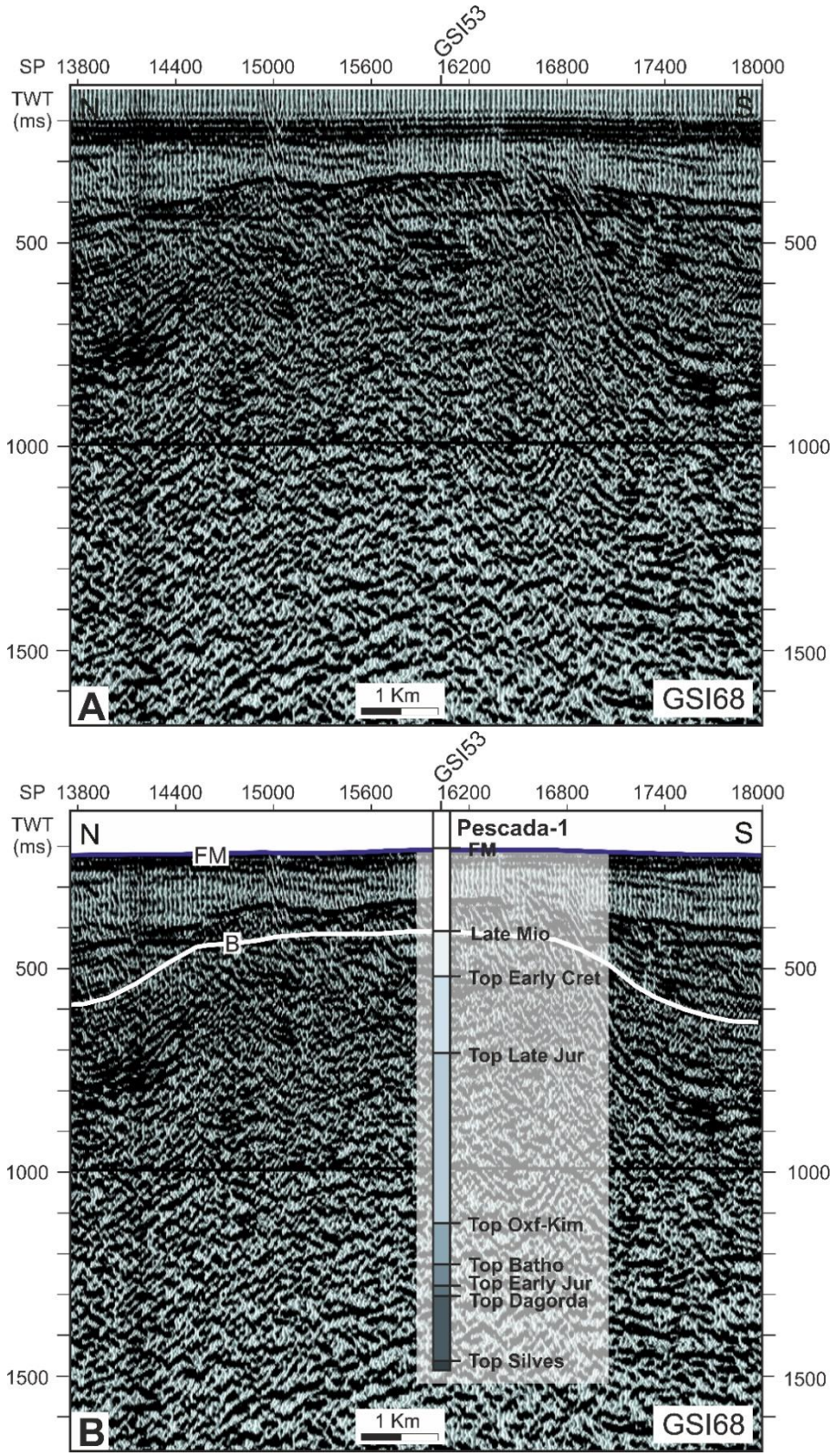

Figure 6.3 – Un-interpreted (A) and interpreted (B) section of seismic profile GSI68 displaying well Pescada-1 and the B unconformity. B: seismic horizon; FM: seafloor horizon. Location of seismic profile in Figure 6.5.

6.2.2 Correlation with IODP Expedition 339 data

This section focus on well data acquired at IODP Expedition 339 Site U1391, which targeted the SD. The well data provide a wide-variety of information regarding lithology, downhole logging and physical properties (Chapter 5, Point 5.1.3). Therefore, a correlation between seismic horizons and units identified in the present work and the stratigraphic hiatus, lithology and physical properties variations found at Site U1391 was made. The crossing seismic reflection profiles BS19 and CL06 were calibrated using Site U1391 data (Figure 6.4).

The bottom of the U1391C borehole at 671.5 mbsf reached Late Pliocene sediments (estimated to span 3.31-3.5 Ma) below horizon H3, which corresponds to the top of seismic unit U2. Hence, a Late Pliocene age was assigned to the uppermost part of seismic unit U2 deposits (Figure 6.4 and Table 6.1).

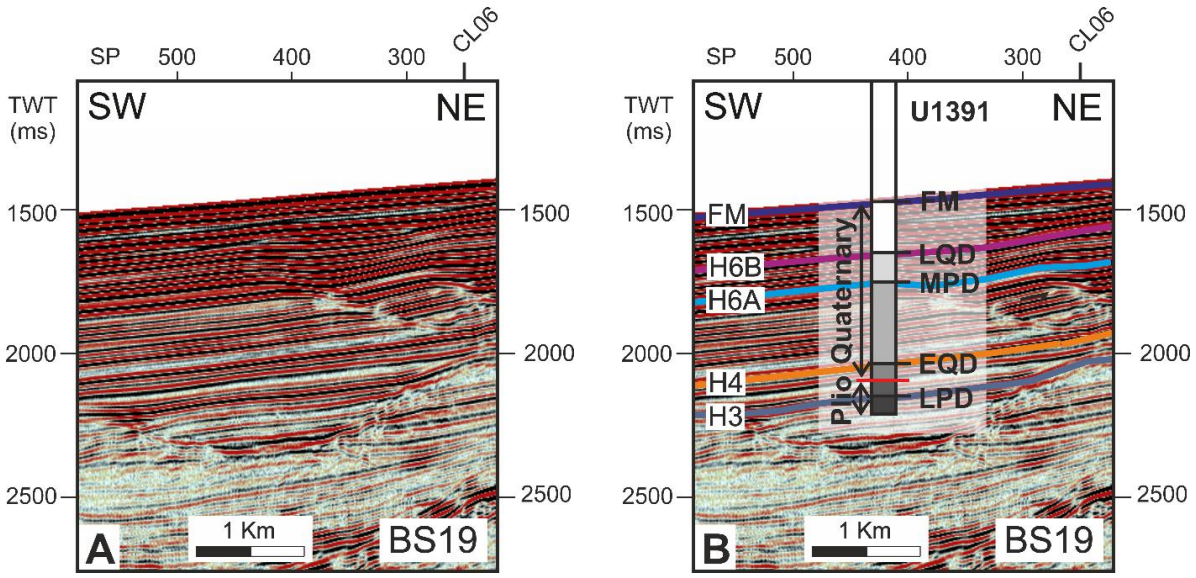

Figure 6.4 – Un-interpreted (A) and interpreted (B) section of seismic profile BS19 with Site U1391 and the correlated discontinuities. H3, H4, H6A and H6B: seismic horizons; FM: seafloor horizon. Location of seismic profile in Figure 6.5.

To determine the ages of the seismic units, the seismic horizons were correlated with the main discontinuities of the Pliocene-Quaternary succession of Site U1391. The correlations are: horizon H3 corresponds to the Late Pliocene Discontinuity (LPD); horizon H4 correlates to the Early Quaternary Discontinuity (EQD); horizon H6A corresponds to the Middle Pleistocene Discontinuity (MPD); and horizon H6B corresponds to the Late Quaternary Discontinuity (LQD). The seismostratigraphic correlation is presented in Figure 6.4 and Table 6.1.

Table 6.1 – Correlation between the main seismic horizons identified in the present work and the stratigraphic hiatus and unconformities found at well Pescada-1 (Matias, 2002; Batista, 2009) and at IODP Expedition 339 Site U1391 (Expedition 339 Scientists, 2012; Hernández-Molina *et al*., 2015). LPD – Late Pliocene Discontinuity; EQD – Early Quaternary Discontinuity; MPD – Middle Pleistocene Discontinuity; LQD – Late Quaternary Discontinuity.

Wells	**This Study** **Seismic discontinuities**	**Hernández-Molina *et al*. (2015)** **Stratigraphic discontinuities**	**Age**
Site U1391	H6B	LQD	0.4 Ma
	H6A	MPD	0.7 – 0.78 Ma
	H4	EQD	2.1 – 2.4 Ma
	H3	LPD	3 – 3.2 Ma
Pescada-1	B	-	Late Miocene

6.3 Seismic Stratigraphy

Seismic reflection profiles acquired in the BIGSETS, CONDRIBER, STEAM and GSI surveys were interpreted using the seismic stratigraphic methodology presented in Chapter 5 (Figure 6.5). The seismic datasets were interpreted to assess the main depositional environmental changes and controlling factors, through the relation between seismic facies and the main structures and depocenters. This work focused on the Late Neogene through Quaternary sedimentary record, where six seismic units were identified (U1 to U6), bound by important seismic horizons (B to H6). See Appendix 10.3 for the complete interpreted seismic profiles.

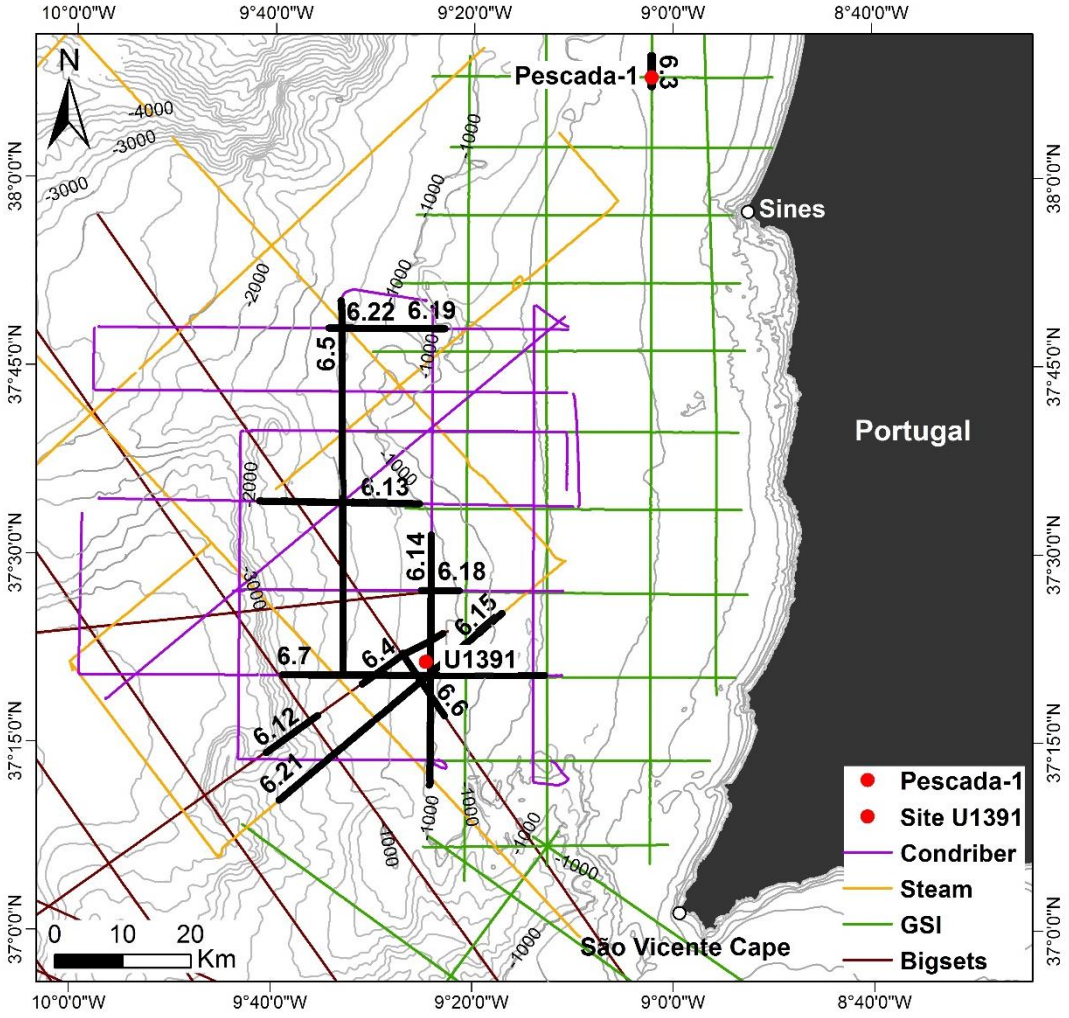

Figure 6.5 – Location of the seismic reflection profiles, IODP Expedition 339 Site U1391 and well Pescada-1. The black lines and numbers indicate the sections of the seismic profiles shown in this Chapter.

The Neogene sedimentary succession is bounded by an important basal discontinuity, named in this work the B unconformity (Figure 6.6). The B unconformity is interpreted as an erosive and irregular surface, with high amplitude and excellent lateral continuity at the scale of the basin (Figure 6.8). The B unconformity is marked by truncation terminations of the older deposits (deformed and sometimes poorly imaged reflections) and by downlap terminations for the overlying unconformable sequence (characterized as quasi-conformable units).

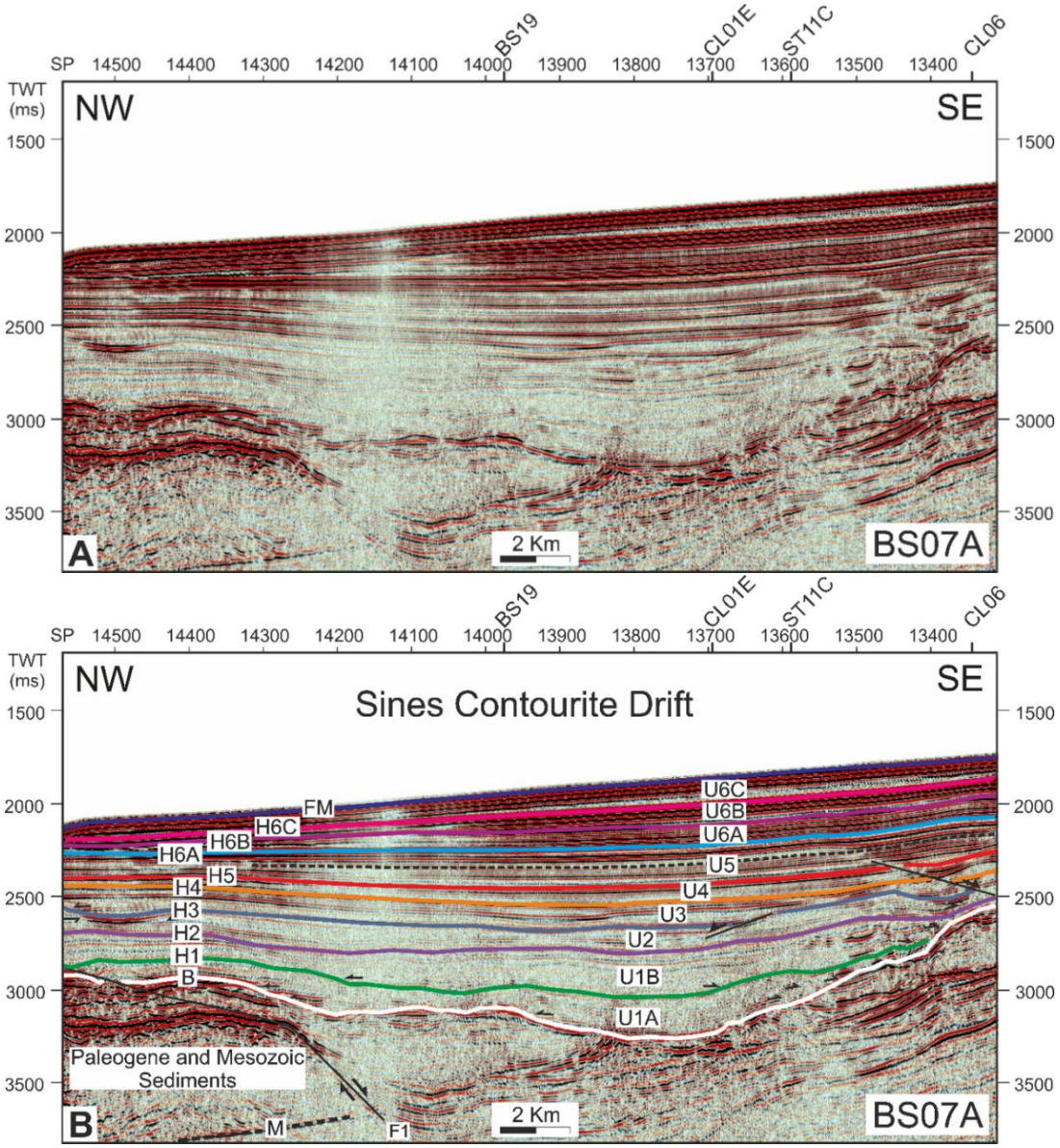

Figure 6.6 – Un-interpreted (A) and interpreted (B) section of seismic profile BS07A. (U1 to U6): seismic units; B and H1 to H6C: seismic horizons; FM: seafloor horizon. F: faults; **black arrows**: reflections terminations; **M**: multiple. Location of seismic profile in Figure 6.5.

6.3.1 Seismic Unit U1

The older seismic unit identified in this study is U1 of Late Miocene deposits, which lies on the B unconformity and is topped by horizon H2 (Figure 6.6). Horizon H2 shows high amplitude and good lateral continuity, marked by reflections of U1 with toplap terminations. Horizon H2 is generally conformable with the overlying seismic unit U2.

Seismic unit U1 is characterized by parallel low amplitude and continuous reflections with onlap terminations towards SE, with semi-transparent facies and a wedge configuration (Figure 6.7). In the north sector, this unit is thicker over the western horst **h1**, bounded by the PSF, with average thickness of 200 ms TWT and maximum thickness of 530 ms TWT (Figure 6.8). This unit is further subdivided into two seismic sub-units, U1A and U1B, since it is possibly to identify reflections with toplap terminations on U1A and onlap terminations on U1B, marking a local discontinuity identified as horizon H1. Horizon H1 marks a vertical amplitude decrease from U1A (characterized by semi-transparent facies) to U1B (with transparent facies).

6.3.2 Seismic Unit U2

Seismic unit U2 of Early Pliocene deposits is bounded at the base by horizon H2 and at the top by horizon H3. Horizon H3 is a high amplitude reflection, laterally continuous and marked by toplap terminations of U2 (Figure 6.6).

Seismic unit U2 shows a similar facies (transparent) and configuration when compared to seismic unit U1, with low amplitude, continuous and subparallel reflections and divergent reflections when it counters structural highs at the boundaries of the basin (Figure 6.7). Unit U2 is characterized as a thick and widespread unit, with lens configuration and average thickness of 220 ms TWT and maximum thickness of 250 ms TWT.

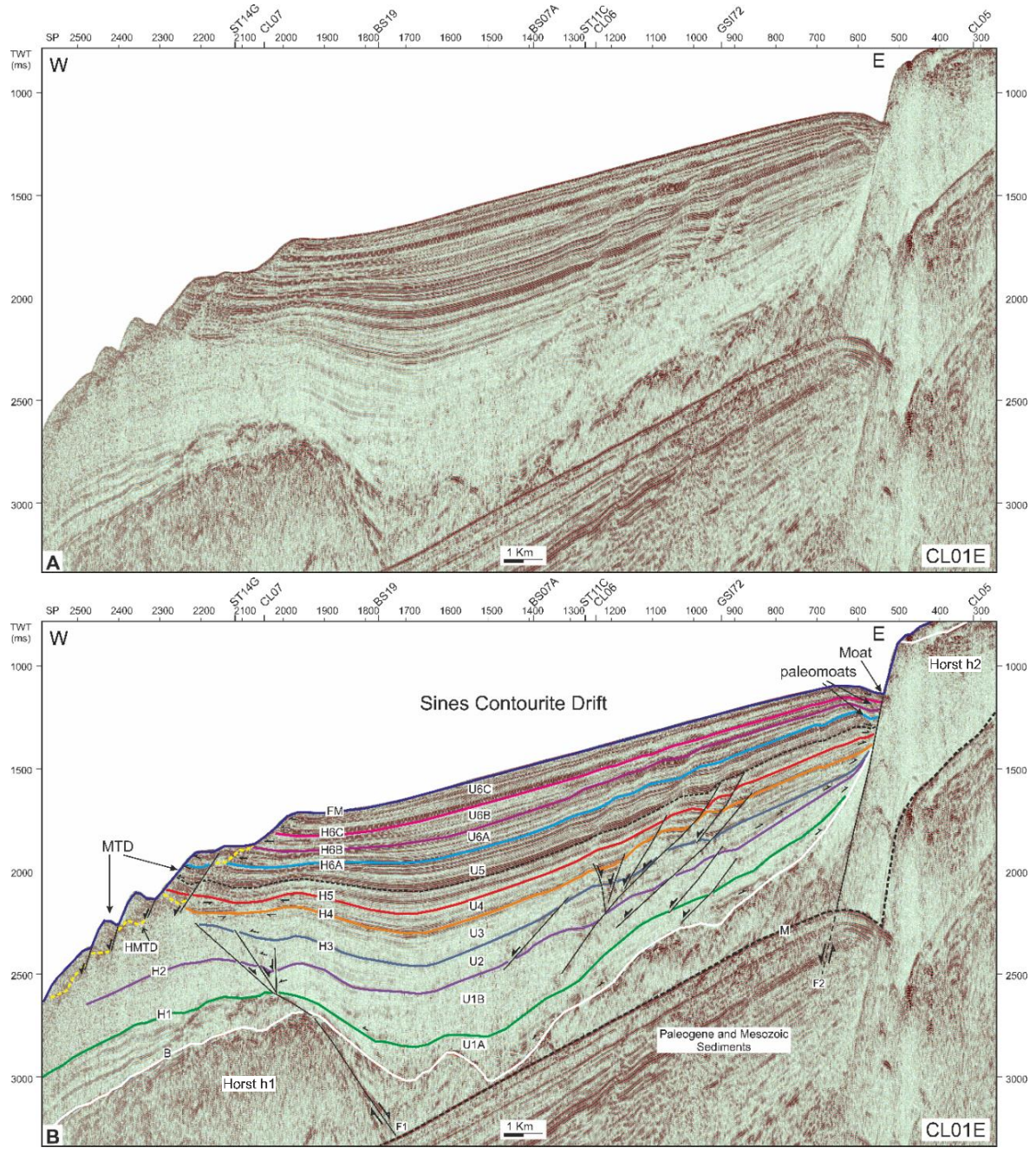

Figure 6.7 – Un-interpreted (A) and interpreted (B) seismic profile CL01E displaying the drift's asymmetric shape and MTD identified in the west. U1 to U6: seismic units; B and H1 to H6C: seismic horizons; HMTD: base of MTD; FM: seafloor horizon. F: faults; **black arrows**: reflections terminations; **shaded areas**: paleomoats; **M**: multiple. Location of seismic profile in Figure 6.5.

6.3.3 Seismic Unit U3

Seismic unit U3, of Late Pliocene age, lies on top of H3 and is topped by H4. Horizon H4 is a high amplitude and laterally continuous reflection, marked by toplap and truncation reflections of the underlying units (U1 to U3), denoting, respectively, its non-depositional and erosive character (Figure 6.7). Horizon H4 changes laterally to concordance with the overlying seismic unit (U4) in the middle of the basin.

Seismic unit U3 shows variable low to medium amplitude, parallel reflections with good lateral continuity and semi-transparent facies. The distribution of unit U3 is extensive laterally, in a lens configuration, with average thickness of 130 ms TWT and maximum thickness of 150 ms TWT.

6.3.4 Seismic Unit U4

Seismic unit U4, of Early Pleistocene deposits, is bound by horizon H4 at the base and horizon H5 at the top. Horizon H5 is a high amplitude reflection with good lateral continuity, marked by toplap terminations of U4 internal reflections and downlap terminations of U5 reflections. Horizon H5 changes laterally to conformable with the subsequently deposited unit, seismic unit U5.

Seismic unit U4 is characterized by a significant change in acoustic facies, with stratified facies and high amplitude, parallel and laterally continuous reflections (Figure 6.8). Although this unit is also characterized by highly chaotic and irregular reflections in the east, with multiple erosive surfaces, related to the erosion and fill of a channel feature interpreted as a paleomoat (Figure 6.19). This unit reaches an average thickness of 110 ms TWT and maximum thickness of 280 ms TWT.

6.3.5 Seismic Unit U5

Seismic unit U5 of Early Pleistocene deposits is bound by horizon H5 at the base and horizon H6A at the top. Horizon H6A is a high amplitude, continuous and parallel reflection. Horizon H6A is marked by toplap terminations of unit U5 (Figure 6.7).

Unit U5 has stratified facies with high amplitude and continuous reflections in the center of the basin and chaotic to semi-transparent reflections related to the fill of a paleomoat. This unit has an average thickness of 190 ms TWT and maximum thickness of 330 ms TWT. Units U4 and U5 mark the beginning of the build-up of a mounded drift towards south, with a small upslope progradation of the unit towards the continental shelf and a prominent paleomoat along the continental shelf (Figure 6.19).

6.3.6 Seismic Unit U6

The most recent seismic unit is U6, of Middle Pleistocene to Holocene age, which is bound by horizon H6A at the base and by the seafloor at the top (horizon FM). Unit U6 is defined as a widespread unit with stratified facies characterized by parallel and high amplitude internal reflections, defining a sheet configuration (Figure 6.7). Unit U6 reaches a maximum thickness of 340 ms TWT with an average of 280 ms TWT.

Seismic unit U6 can be divided into three sub-units (from bottom to top, U6A, U6B and U6C) separated by two internal discontinuities, horizons H6B and H6C, both marked by toplap terminations on the underlying sub-units and downlap terminations on the overlying sub-units. These discontinuities represent erosional unconformities on the basin margins, close to the flanks of structural highs, changing laterally to concordance in the middle of the basins. This unit is characterized by small paleomoats in the east, marked by toplap terminations of the underlying sub-units and semi-transparent facies.

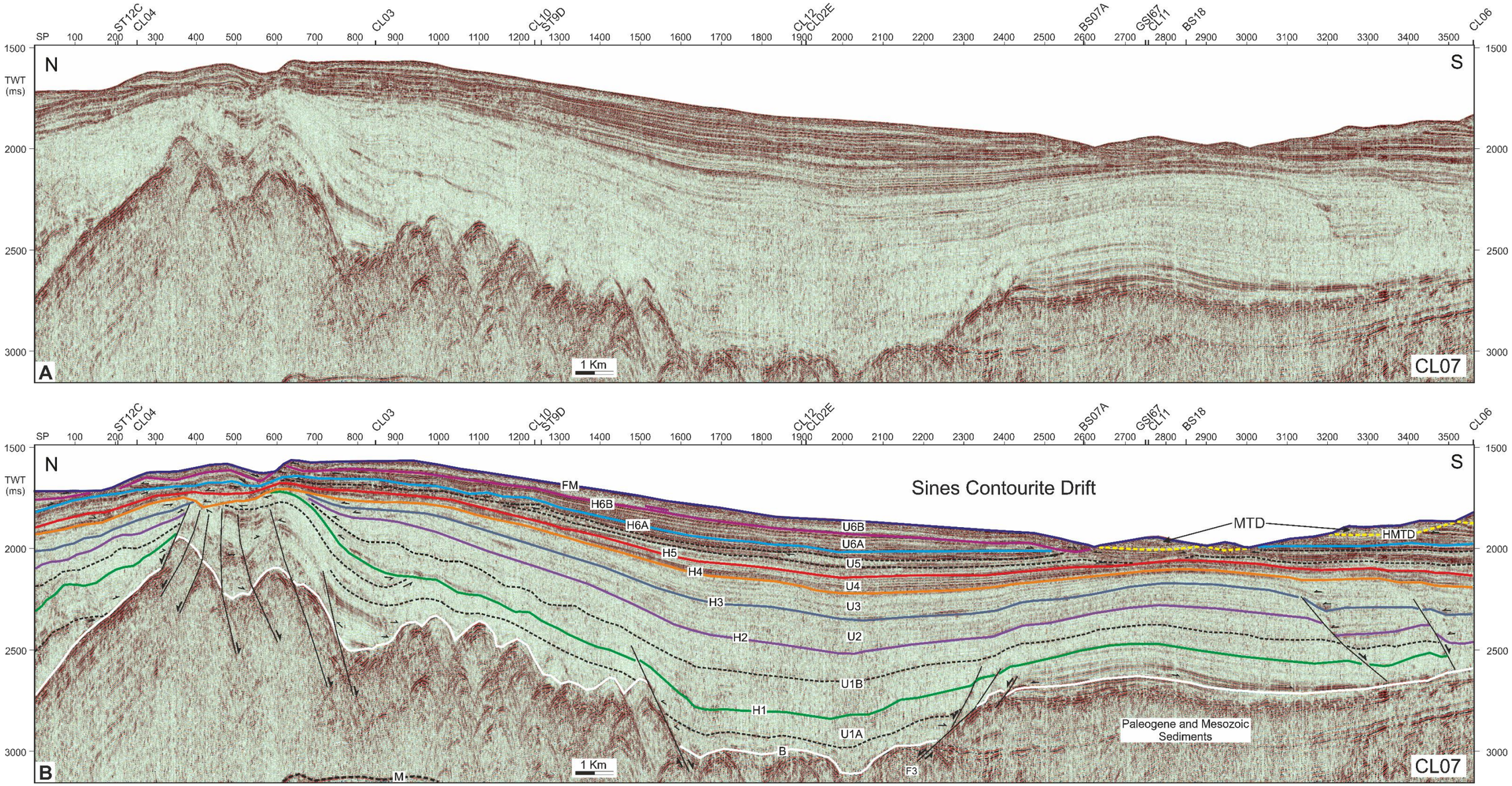

Figure 6.8 – Un-interpreted (A) and interpreted (B) seismic profile CL07 showing the seismic character of the seismic units and their configuration. U1 to U6: seismic units; B and H1 to H6C: seismic horizons; HMTD: base of MTD; FM: seafloor horizon. F: faults; **black arrows**: reflections terminations; **M**: multiple. Location of seismic profile in Figure 6.5.

6.4 Lithostratigraphy of Site U1391

The lithological and physical properties characterization of seismic horizons and units was also made by correlation with IODP Expedition 339 data provided at IODP's online database: http://iodp.tamu.edu/index.html. Visual description of cores and high-resolution photos taken during the Expedition 339 allowed a lithological and facies variations characterization. The main lithology recognized at Site U1391 was calcareous silty mud with few intervals of coarse-grained deposits, namely calcareous silty sand, mostly in the first 200 mbsf, and a debrite (~0.35 m) at 604 mbsf with muddy intraclasts and matrix (Figure 6.10 A to C). These lithologies are associated with bigradational contourite depositional successions with gradational contacts and bioturbation, which coarsens upwards from nannofossil muds through calcareous silty muds to calcareous silty sands and then fine up in the opposite order to calcareous silty mud and nannofossil muds, between 0 and 196.1 mbsf (Figure 6.10 C). Sharp contacts or rarer discontinuities occur between 0 and 196.1 mbsf and cut the contourite depositional successions and therefore partial bigradational, normal or reverse grading are also common (Appendix 10.2). Other sediments also occur interbedded with the contourites, such as calcareous muds between 196.1 and 566 mbsf, hemipelagites from 196.1 to 671.5 mbsf, biosiliceous muds between 562 and 671.5 mbsf and a dolomitic mudstone of ~0.87 m at 632 mbsf.

6.4.1 Downhole Logging

The downhole logging data obtained at Site U1391 was analysed in the present work to better characterize the spatial and temporal variability of the depositional record in the given sedimentological context. The physical parameters used in this characterization were resistivity (ohm.m), density (g/cm^3), gamma ray (gAPI) and sonic velocity (km/s). The grain size rank was also used to determine potential correlations with referred logging properties. The resistivity log is used to characterize the sediments by measuring their electrical resistivity (Cannon, 2016). The resistivity log shows highly variable values, 0.2 to 3 ohm.m, between 107 and 153 mbsf (Figure 6.9). These increased values probably mark the presence of coarse-grained sediments. In general, the resistivity log shows an increase with depth, from 1.5 to 5.5 ohm.m, between 153 and 562 mbsf.

The sonic velocity and density logs track rock composition changes and the effective stress (Cannon, 2016). If effective stress increases, sediment compaction occurs and the logs show increasing values. Low values of sonic velocity and density can indicate an increase of clay minerals, organic matter or porosity. At Site U1391, the sonic velocity and density logs show a general increase with depth, reaching, respectively, 1.6 to 2.2 km/s and 1.4 to 2.1 g/cm^3 between 96 and 562 mbsf (Figure 6.9). These increased values show the effect of compaction and a sequence characterized by silt to clay mud facies.

All rocks possess some natural gamma radioactivity, due to the presence of potassium, thorium or uranium (Ellis and Singer, 2007). Gamma ray is used mainly to track clay content in the sediment, since high gamma ray values usually identify fine-grained sediments with potassium rich clay minerals and absorbed uranium and thorium components (Cannon, 2016). Conversely, low values indicate no radioactive elements and usually identify quartz and calcite (Lofi *et al.*, 2016). The gamma ray downhole logging values obtained at site U1391 range between 30 and 65 gAPI until 153 mbsf, and between 30 and 75 gAPI from 153 to 562 mbsf (Figure 6.9). The higher values are probably tracking the clay content. Resistivity, density and gamma ray logs show a decrease at 562 mbsf, with no high values of gamma ray below (30-50 gAPI), which indicates a decrease in clay content and probable presence of sandy intervals, especially between 562-582 mbsf and 593-605 mbsf with 30 gAPI lows (Figure 6.8). This indicates a change in sediment facies at 562 mbsf and therefore separates the sediment column into two sub-units, IA and IB. This limit could be placed in the transition from seismic unit U3 to U4 and corresponds to seismic horizon H4, which is close to the Quaternary-Pliocene boundary (Table 6.2). Higher values of resistivity (3 ohm.m), density (2.5 g/cm^3) and velocity (2.9 km/s) and low values of gamma ray occur at 632 mbsf corresponding to a well-consolidated dolomite mudstone (Figure 6.10 B).

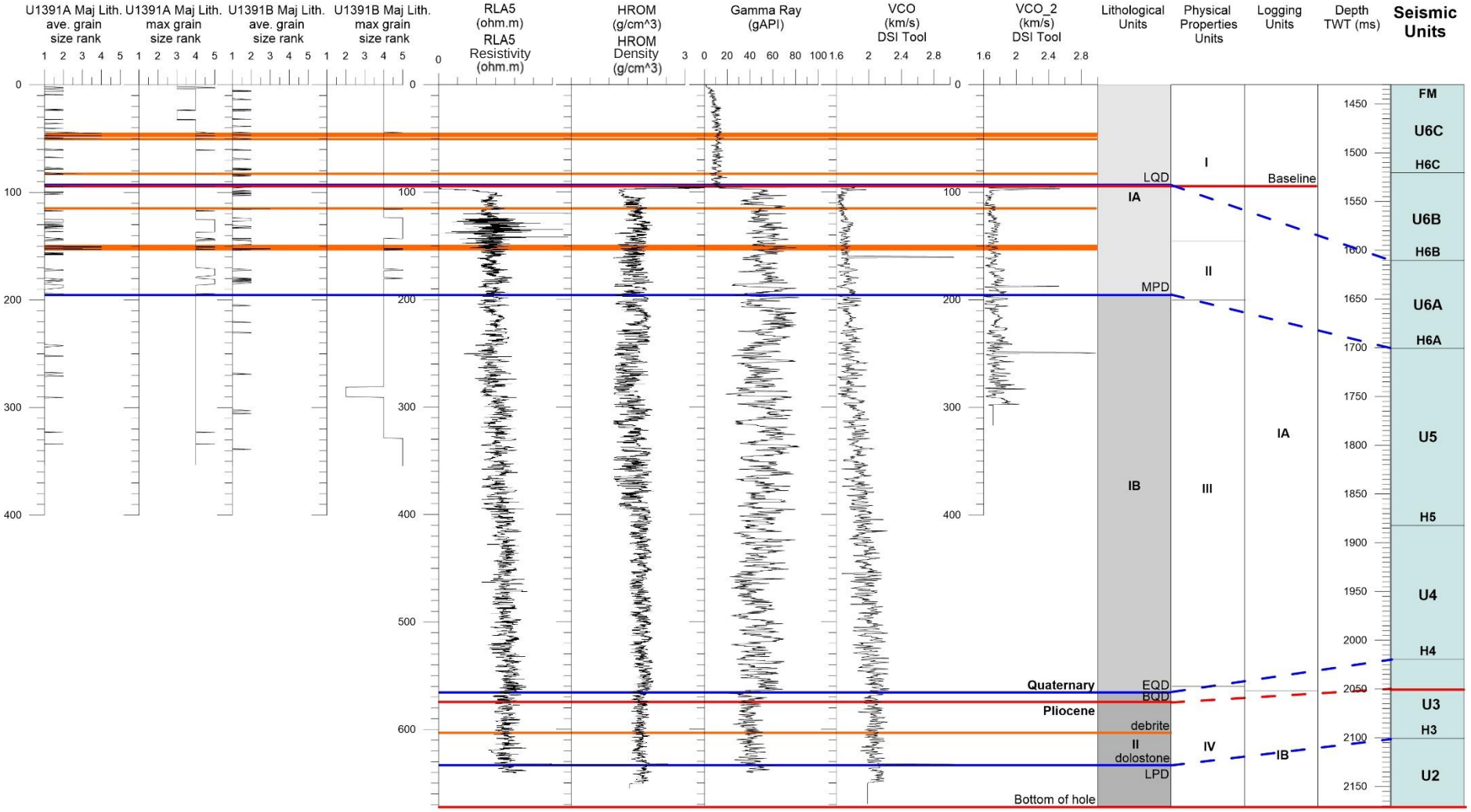

Figure 6.9 – U1391 logging and sedimentological properties, from left to right: U1391A and U1391B major lithology (average and maximum) grain size rank; resistivity log (ohm.m); HROM density (g/cm^3); gamma ray log (gAPI); U1391C and U1391A velocity (km/s) with DSI Tool; IODP U1391 lithological, physical properties and logging units; seismic units identified on this study. Orange lines: sand layers; blue lines: main stratigraphic discontinuities.

6.4.2 Physical Properties

The physical properties from Site U1391 were used in this work to study the sedimentological and mineralogical variations of the contouritic successions. The grain size rank, reflectance (L*, a* and b*), natural gamma ray total counts (cps), bulk density (g/cm^3) and magnetic susceptibility (instrumental units) were used to identify the main sedimentary units of the SD and their relation to the seismic units.

Grain size variations in contourites usually result from changes in the strength of the predominant bottom-current (Stow *et al*., 2013). However, it is still difficult to determine whether a change in mean grain size indicates variations in mean speed, frequency and amplitude of the current velocity or an increase of sediment supply by rivers and downslope processes (Mulder *et al*., 2013). In general, coarser grain size present higher gamma ray attenuation (GRA), density, magnetic susceptibility and a* measurements. The major lithology, calcareous silty mud, is interbedded by six sandy layers in the first 150 mbsf at 2, 50, 83, 96, 115 and 150 mbsf with variable thickness. The average grain size at Site U1391 is mostly clay to silt with bigradational, normal or reverse grading successions (Figure 6.11).

Magnetic susceptibility reveals changes in the mineralogical composition, mainly the concentration of ferromagnetic grains in the sediment (Blum, 1997). Measurement of this parameter at Site U1391 revealed cyclic variations between 5 x 10^{-5} SI and 60 x 10^{-5} SI with a decrease at 28 mbsf, from 65 x 10^{-5} SI to -10 x 10^{-5} SI. Also, the magnetic susceptibility is lower after 105 mbsf, under 20 x 10^{-5} SI in the first 100 mbsf and lower than 10 x 10^{-5} SI below that level (Figure 6.11). The natural gamma ray (NGR) trend mirrors the clay content, with values between 20 and 55 cps. NGR has regular values between 35 and 50 cps in the first 200 mbsf, which can be correlated to the higher number of sandy layers. Although at 560 mbsf, occurs a change to values between 30 and 45 cps which indicates facies variation and the separation of the lithostratigraphic column into two sub-units, III and IV.

Color and lightness changes in sediments are caused by the abundance and variations of different sedimentary phases (Blum, 1997). These variations can be seen in magnetic susceptibility, bulk density, and other physical parameters. Measurements of color reflectance at Site U1391 show an alternation of greenish and reddish intervals, with the disappearance of the reddish intervals below 200 mbsf (Figure 6.11). The values of a* are positive for the reddish intervals and negative and less variable below 200 mbsf. The color reflectance measurements (L*, a* and b*) show a positive relation for most of the Site, with a few intervals with slightly higher values. The bulk density has values ranging from 1.4 to 2.1 g/cm^3 and shows variations between 1.85 and 1.9 g/cm^3 from 250 to 400 mbsf. Bulk density is variable for the first 250 mbsf and this variation is also visible in the other measurements, indicating a possible separation of different sedimentary units. At 632 mbsf, bulk density reaches a maximum of 2.4 g/cm^3, related to the presence of a dolomitic mudstone.

Several correlations between the different physical properties described above were deduced in this work as follows: i) between 0-150 mbsf occurs a positive correlation between NGR, grain size, magnetic susceptibility and a* with low bulk density and widely fluctuating a* values; ii) a distinct second interval at 150-200 mbsf displays negative correlation between NGR and a* and reduced scatter of data; iii) a third interval from 200-560 mbsf has a positive correlation between NGR, magnetic susceptibility and bulk density with lower magnetic susceptibility; iv) a last interval from 560 mbsf to the bottom of the hole is clearly recognized by low NGR and magnetic susceptibility, and a considerably reduced scatter of data (Figure 6.11); v) at 604 mbsf, a ~35 cm debrite occurs, although its presence is not clear in the visual logs (Figure 6.10 A and 6.11); vi) at 632 mbsf, a dolomitic mudstone is identified by low NGR and bulk density and higher color reflectance measurements (L*, a* and b*).

During the IODP Expedition 339 the shipboard scientists divided the sedimentary record retrieved at Site U1391 into two lithological units based on visual core description, core logging and smear slides

analysis (Expedition 339 Scientists, 2012; Figure 6.9 and 6.11): i) Unit I (0-566.1 mbsf) and ii) Unit II (566.1-671.5 mbsf). Unit I is made of contourite rich layers with two sub-units separated by facies variation, IA and IB. Unit IA (0-196.1 mbsf) is clearly dominated by calcareous muds with few intervals of siliciclastic sediments, silty and sandy muds. In contrast, unit IB (196.1-353.5 mbsf) is characterized by calcareous mud, silty mud and very few sandy mud layers. Unit I has an estimated sedimentation rate of 17 cm/k.y from 2.58 to 1.5 Ma in the Pleistocene and 27 cm/k.y from ~1.5 Ma to the seafloor. Unit II has mixed facies with thin contourite beds with calcareous and bioclastic sediments, a debrite and a dolomitic mudstone and low sedimentation rate of 13 cm/k.y during the Pliocene.

The integration of the sedimentological and physical properties analysis with the seismic model shows a clear correlation between U1391 lithological units and the seismic units identified in this work. Unit IA corresponds to seismic unit U6, unit IB to seismic units U4 and U5 and unit II to seismic unit U3 and top of U2 (Table 6.2). The occurrence of lithological variations throughout the sedimentary record is related to the depositional environment. Therefore, we can probably infer that during the deposition of unit II (seismic units U2 and U3) in the Late Pliocene to Early Quaternary, the MOW probably flowed as a weak bottom-current and upwelling and downslope processes occurred intersected. Afterwards, during the deposition of unit IB (seismic unit U4 and U5) in the Early Pleistocene, upwelling occurred with an increase of the MOW, probably related to bottom-current enhancement. And finally, from the Middle Pleistocene to the Present, the deposition of unit IA (seismic unit U6) indicates the MOW had a slight increase of strength and velocity and possibly six episodes of bottom-current enhancement, related to the presence of the sandy intervals.

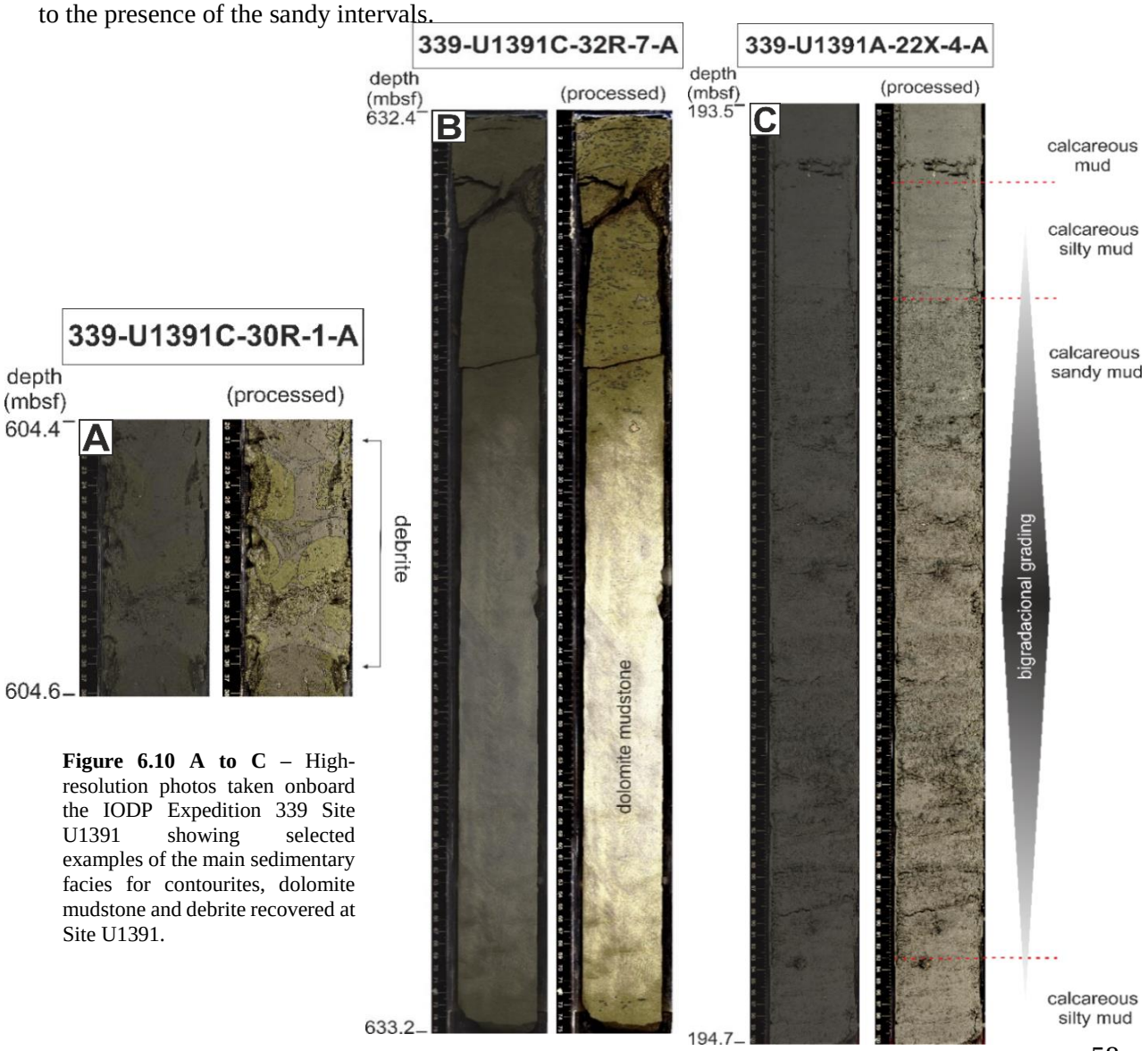

Figure 6.10 A to C – High-resolution photos taken onboard the IODP Expedition 339 Site U1391 showing selected examples of the main sedimentary facies for contourites, dolomite mudstone and debrite recovered at Site U1391.

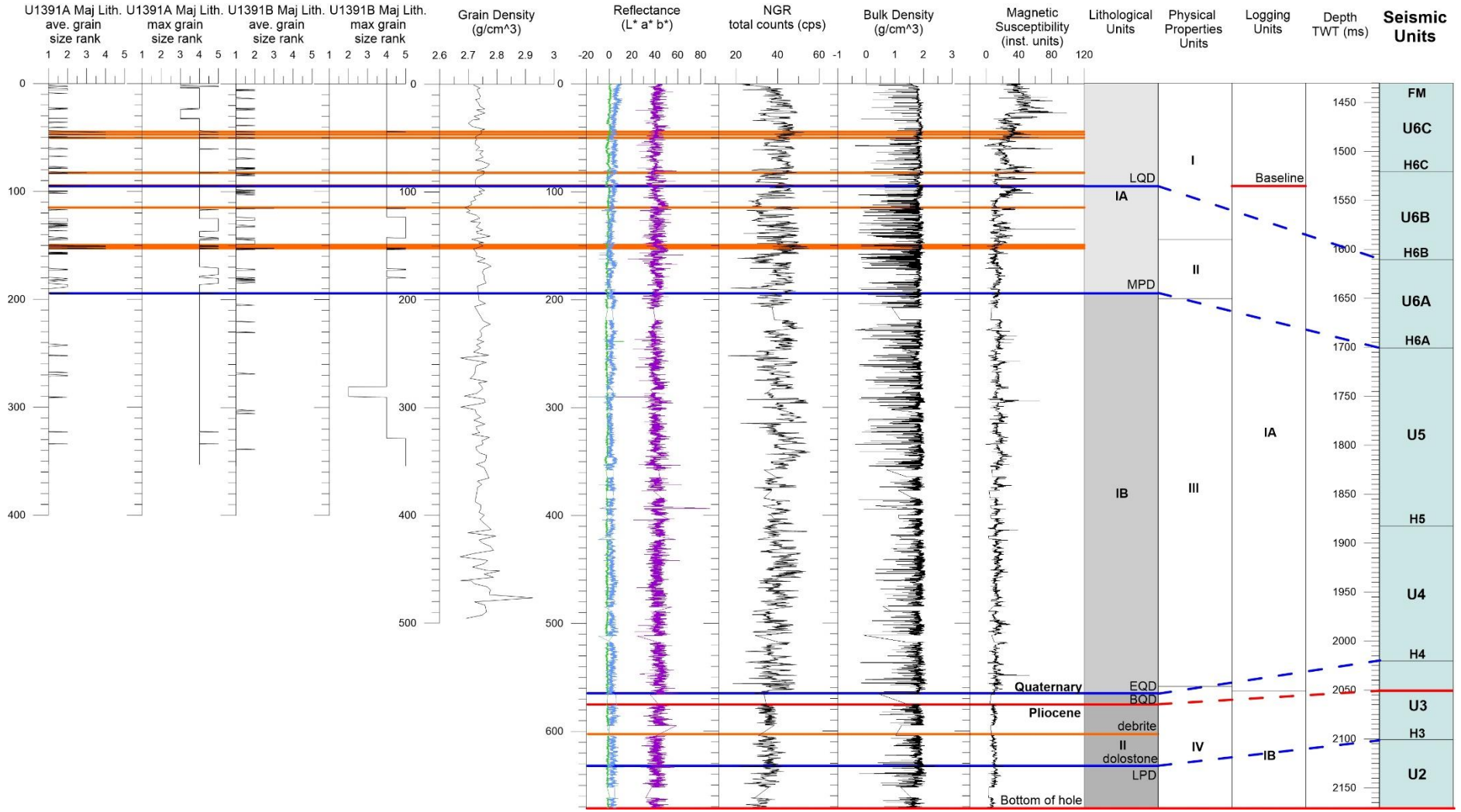

Figure 6.11 – U1391 physical and sedimentological properties, from left to right: U1391A and U1391B major lithology (average and maximum) grain size rank; U1391B grain density (g/cm^3); Reflectance (L*, a* and b*); natural gamma ray total counts (cps); bulk density (g/cm^3); magnetic susceptibility (instrumental units); IODP U1391 lithological, physical properties and logging units; seismic units identified on this study. Orange lines: sand layers; blue lines: main stratigraphic discontinuities.

Table 6.2 – Characterization of the main seismic units identified by seismic data, correlated with IODP U1391 well data. Legend: red line marks the bottom of the hole, while different colors indicate changes in lithology and dark grey denotes contourite beds; LPD – Late Pliocene Discontinuity; EQD – Early Quaternary Discontinuity; MPD – Middle Pleistocene Discontinuity; LQD – Late Quaternary Discontinuity.

			Seismic Units	Sub-units	Base of Unit TWT (ms)	Base of Seismic Unit Depth (mbsf)	Lithology Site U-1391	IODP Site U1391 Discontinuities
Quaternary	Pleistocene	Upper	U6	U6C / H6C	1521	-	**Contourites** Mud/Silt/Sand + muddy/sandy	Middle Pleistocene – Holocene
		Middle		U6B / H6B	1610	91		**LQD** (0.4 Ma)
				U6A / H6A	1700	196.1		**MPD** (0.7 – 0.78 Ma)
		Cala.	U5	H5	1882	-	**Contourites** Mud rich	Calabrian
		Gelasian	U4	H4	2020	566.1		Gelasian
			U3	H3	2100	633.2	**Mixed system** Mud-rich contourites, biosiliceous muds, debrite, dolostone	Piacenzian – Gelasian
Neogene	Pliocene	Piacen.						**EQD** (2.1 – 2.4 Ma)
		Zancle.	U2	H2	2176	bottom of Site U1391 at 671.5 m - -		Zanclean – Piacenzian
								LPD (3 – 3.2 Ma)
	Miocene	Messinian	U1	U1B / H1	2345	-		Late Miocene
				U1A	2578	-		
				B unconformity				

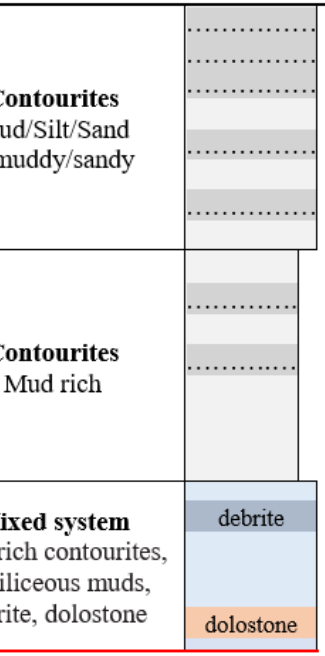

6.5 Structural Control of Sines Drift Deposition

The interpretation of the seismic datasets allowed the identification of several faults and structural highs, which played an important role controlling the evolution of the SD.

BIGSETS and GSI profiles have lower resolution, thus allow a better understanding of deeper and older structures, whereas higher-resolution CONDRIBER and STEAM profiles display shallower structures in great detail. The different but complementary resolutions of these profiles allowed a multi-scale analysis of the main tectonic structures in the study area.

6.5.1 Main tectonic structures

Two major structurally controlled basement highs were identified: the western horst **h1** limited by the PSF and the eastern horst **h2** limited by fault F2.

Horst **h1** is limited by the PSF at the west and by the fault F1 at the east. The PSF is a key feature of this study area and is characterized by a NNE-SSW orientation, steep ~1400 m high scarp wall and 50 km of extension (Figure 6.12). F1 is a normal NNE-SSW trending fault with 40 km length.

The horst **h1**, bounded by PSF and F1, controlled the deposition of seismic units U1 through U6 (Late Miocene to Holocene deposits) reducing the accommodation space available for the Sines Contourite Drift development. Therefore, this drift is thinner above the horst. Other smaller NNE-SSW steep normal and reverse faults offset the older seismic units, U1 to U3 (Late Miocene to Early Pleistocene) (Figure 6.13 and 6.14).

The referred normal faults illustrate the Mesozoic extensional architecture and the segmentation of the West Iberian margin and later a few were reversed by the tectonic inversion events related to the Alpine Orogeny, since they affected the sedimentary succession. Fault F1 is a structure buried under the post-rift sequence, while the PSF shows a well-developed scarp, suggesting passive exhumation (Figure 6.12).

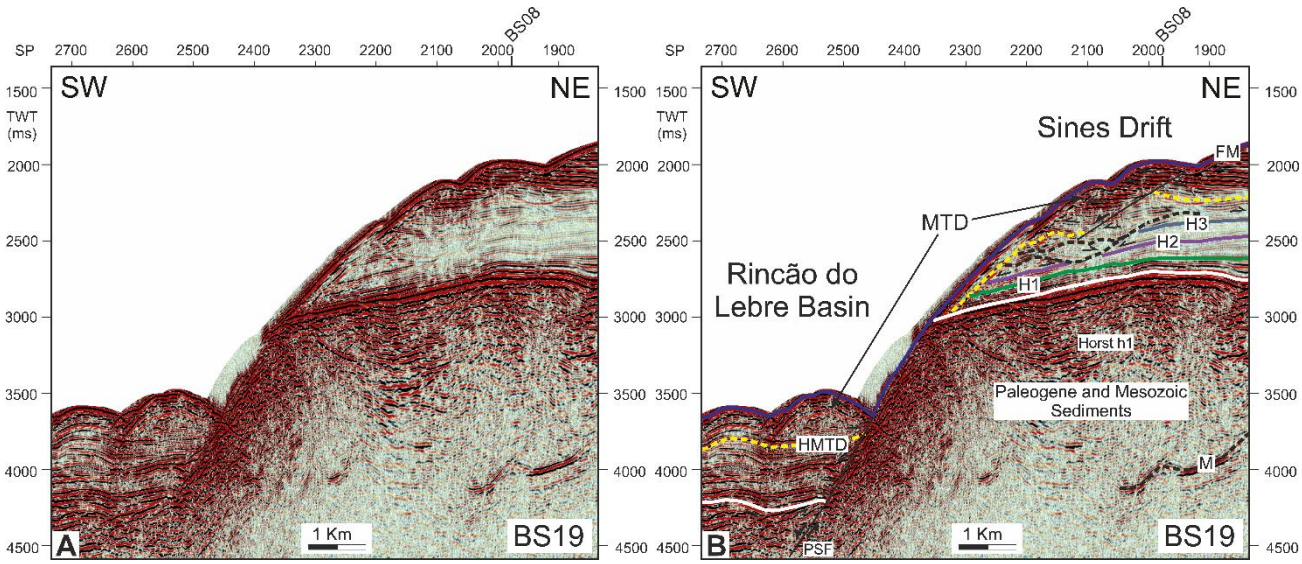

Figure 6.12 – Un-interpreted (A) and interpreted (B) section of seismic profile BS19 displaying the PSF and associated MTD accumulation. U1 to U6: seismic units; B and H1 to H6C: seismic horizons; HMTD: base of MTD; FM: seafloor horizon. F: faults; **black arrows**: reflections terminations; **shaded areas**: paleomoats; **M**: multiple. Location of seismic profile in Figure 6.5.

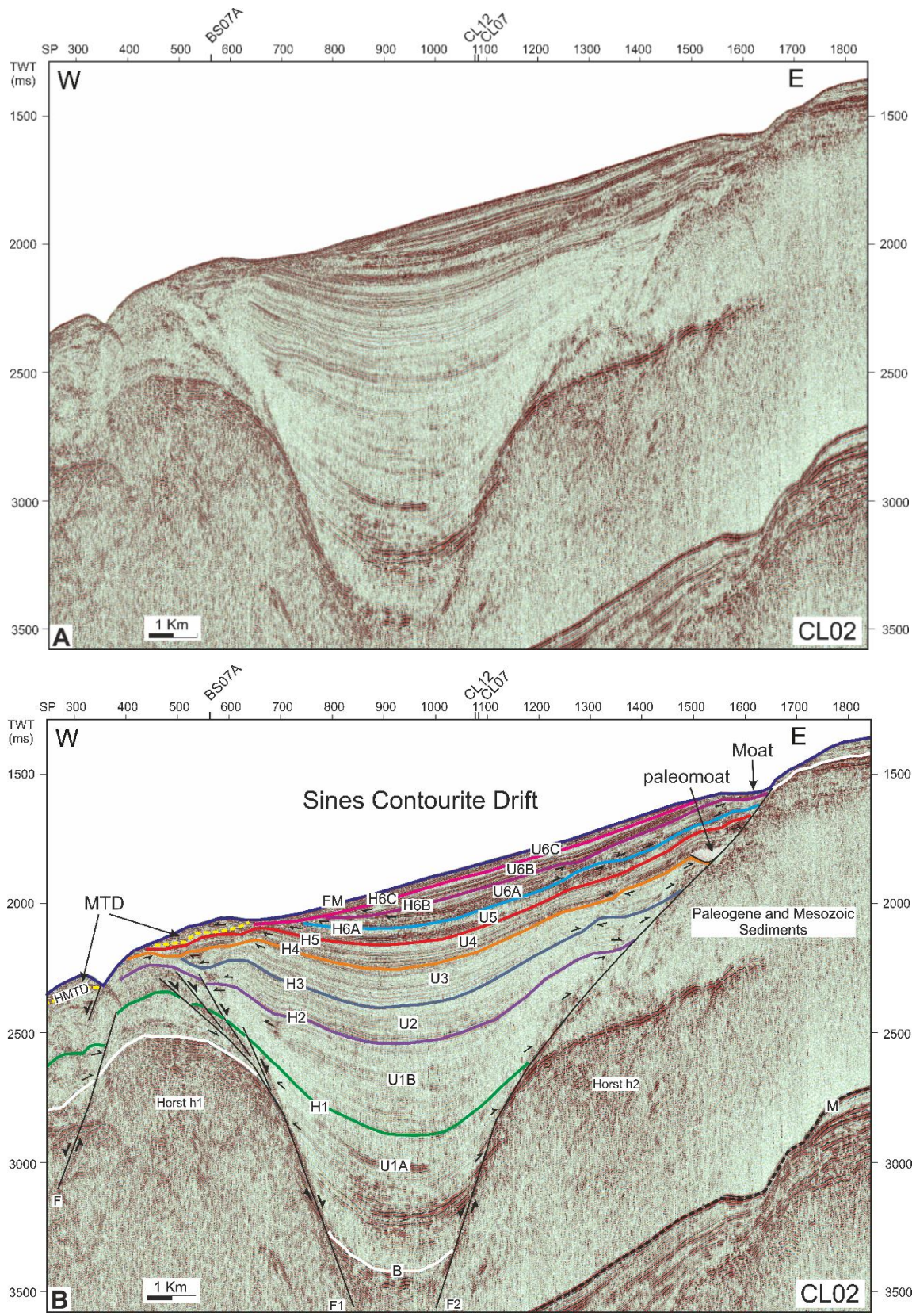

Figure 6.13 – Un-interpreted (A) and interpreted (B) seismic profile CL02 displaying two main faults, F1 and F2, which constrict the drift's development. U1 to U6: seismic units; B and H1 to H6C: seismic horizons; HMTD: base of MTD; FM: seafloor horizon. F: faults; **black arrows**: reflections terminations; **shaded areas**: paleomoats; **M**: multiple. Location of seismic profile in Figure 6.5.

The horst **h2** is a structural high limited by normal fault F2 of NNW-SSE orientation and 75 km of extension (Figure 6.13). This fault was inherited from the Mesozoic rifting of the West Iberian margin, which segmented the margin into multiple planes.

The fault F2 is also responsible for a block uplift at the southwest, since the sediments on its hanging wall show signs of a NE-SW compressive event (see Appendix 10.3). Fault F2 was reactivated as a reverse fault and deformed seismic units U1 to U5 (Late Miocene to Middle Pleistocene deposits), which suggests the NE-SW compressive event occurred in the Middle Pleistocene. This compressive event does not disturb the most recent seismic unit U6 of Middle Pleistocene to Holocene age and is therefore probably related to neotectonics on the Iberian margin.

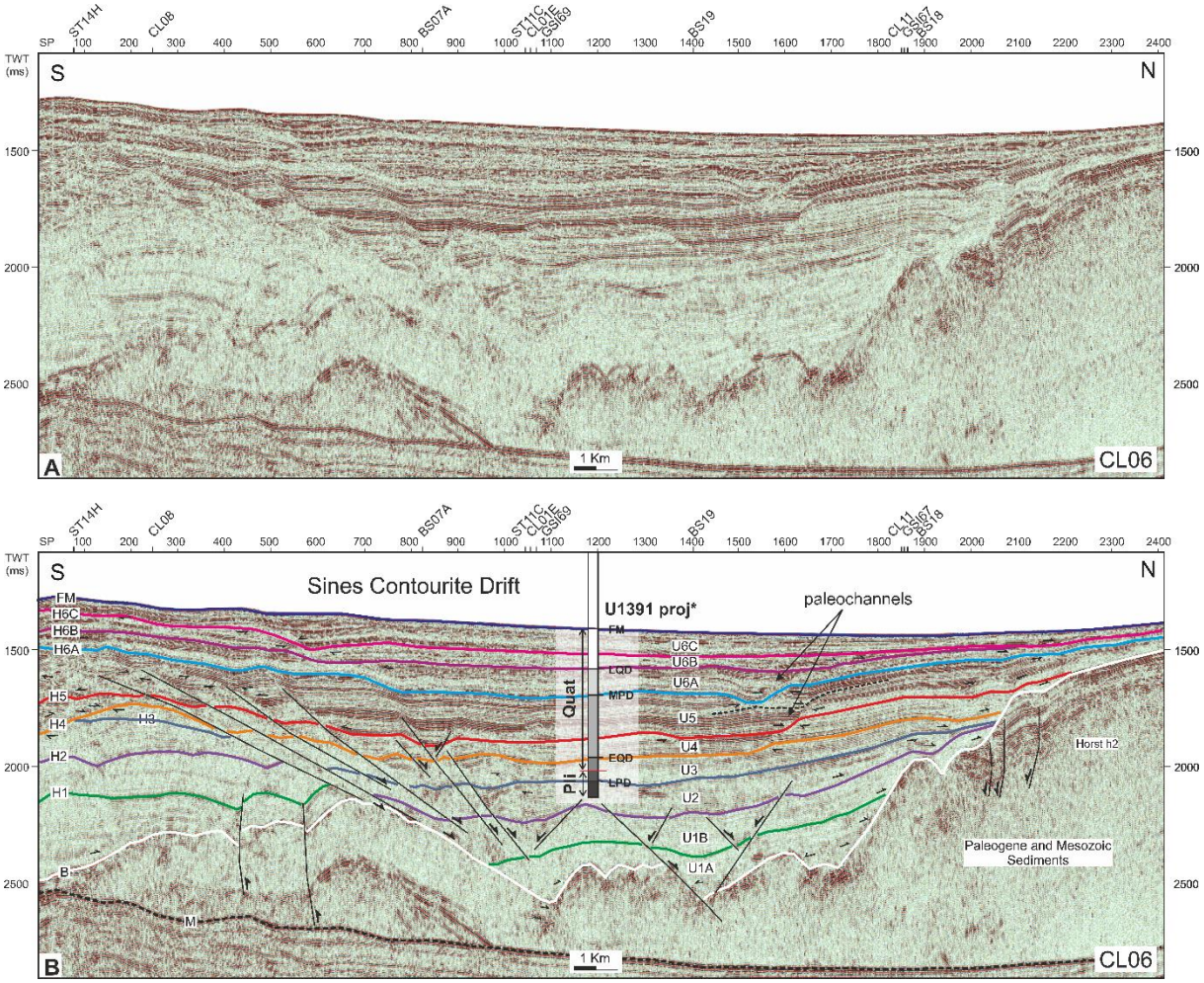

Figure 6.14 – Un-interpreted (A) and interpreted (B) seismic profile CL06 with Site U1391 projected and numerous normal faults affect units U1 to U5. U1 to U6: seismic units; B and H1 to H6C: seismic horizons; FM: seafloor horizon. F: faults; **black arrows**: reflections terminations; **M**: multiple. Location of seismic profile in Figure 6.5.

Seismic unit U6 shows little to almost no deformation, while U1 to U5 were affected by numerous N-S steep normal faults with variable slope, located close to the SVC, the continental shelf and the Príncipe de Avis Seamounts (Figure 6.15). These faults that dip west are buried in the sedimentary column and rooted in the normal faults F2 and F1 (Figure 6.15). These are interpreted as growth faults which deformed the sedimentary cover.

The development of the SD was restricted to the west and to east by horsts **h1** and **h2**, respectively. Thus, this contourite drift developed in a north-south elongated corridor.

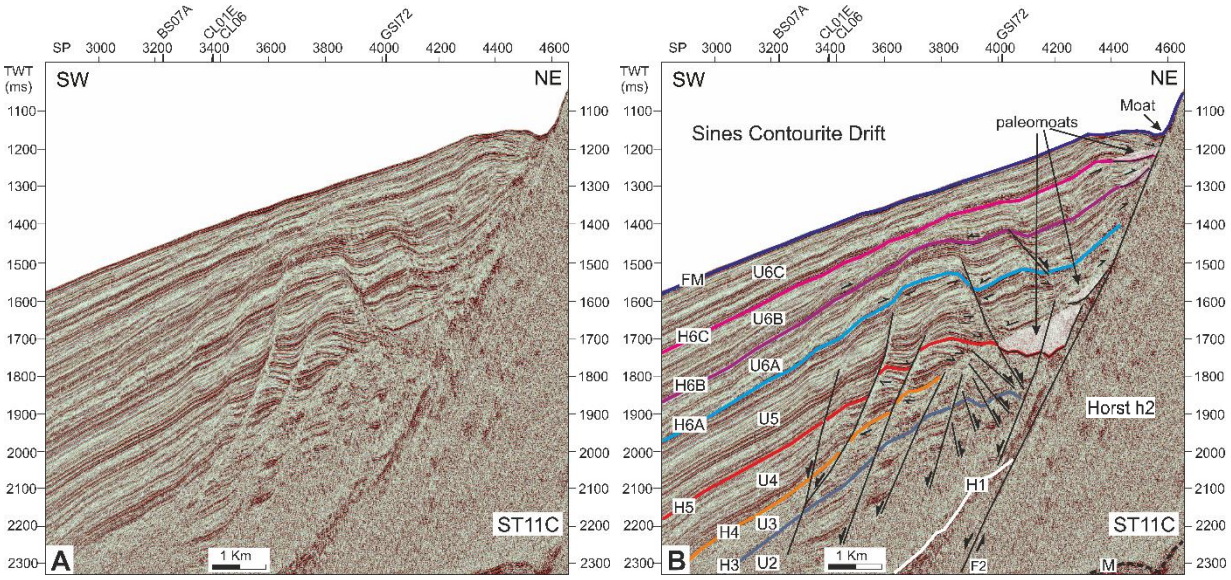

Figure 6.15 – Un-interpreted (A) and interpreted (B) section of seismic profile ST11C with numerous normal faults. U1 to U6: seismic units; B and H1 to H6C: seismic horizons; FM: seafloor horizon. F: faults; **black arrows**: reflections terminations; **shaded areas**: paleomoats; **M**: multiple. Location of seismic profile in Figure 6.5.

- ***Horizons isobaths and structural mapping***

Isobath maps are depth maps, usually given in TWT units that allow for the interpretation of morphology and tectonic deformation of a selected horizon. Thus, they could be interpreted as the paleotopographic surface prior to the deposition of the overlying seismic unit. This representation is illustrated in a colored scale, where the deeper zones are blue and the shallower zones are red. Maps for all horizons interpreted in this work were generated, including the seafloor. Isobaths maps for each seismic horizon and respective interpretation are shown in Figure 6.17.

The isobath map for horizon B, corresponding to the base of the SD and lower boundary of the older seismic unit U1, provides information about the preserved paleomorphology at the Late Miocene (Figure 6.16). An inspection of the map allowed the identification of deeper basins to the west consisting of the RLB and the PAP.

Faults PSF and F1 limit the western NNE-SSW oriented horst **h1**. Towards east of horst **h1**, faults F1 and F2 limit a graben **g1** and create space accommodation, registered as elongated NNW-SSE depressions in the center of the continental slope (Figure 6.16). This depression is observed in BS19, CL01E, and CL02 seismic profiles and reaches a maximum depth of 2578 ms TWT. The graben **g1** is bounded towards east by horst **h2** and by its associated fault F2 (inherited from the Mesozoic rifting episodes). The NNW-SSE normal fault switches to NNE-SSW as it crosses the PAS. These morphological features are also conveyed by a related structure, the Príncipe de Avis Ridge. The Príncipe de Avis Ridge is the expression of a ENE-WSW strike-slip fault, responsible for the displacement of the normal faults orientation. The strike slip fault extends over 60 km and is the submarine prolongation of the Sines promontory (Batista, 2009).

The isobath map of seismic horizon H2 (Early Pliocene) shows a diminution of the N-S middle depressions, probably related to sediment accumulation of the overlying seismic unit U2 (Figure 6.17 B). The isobath map of seismic horizon H3 (Late Pliocene) follows the same trend with the near disappearance of the central depressions. This isobath map shows that horizon H3 is still affected by the paleo-reliefs created by horsts **h1** and **h2** (Figure 6.17 C).

The isobath map of horizon H4 (Early Pleistocene) is characterized by the burial of the western horst **h1**. This development is visible in the seismic profiles (see Appendix 10. 3) where the deposition of the overlying seismic unit U4 covered the relief created by the horst. This isobath map starts to show resemblance with present-day seafloor morphology, with a smooth paleomorphology (Figure 6.17 D). The isobath map of seismic horizon H5 (Early Pleistocene) is quite similar to the map of horizon H4 (Figure 6.17 D and E), with an even paleotopography.

The isobaths maps of the younger seismic horizon H6A (Middle Pleistocene), H6B (Middle Pleistocene) and H6C (Upper Pleistocene) show a close resemblance with present-day seafloor morphology (Figure 6.17 F to H). The isobaths maps display a similar evolution from horizon H6A to horizon H6C, with the complete disappearance of the central depressions associated with graben **g1**.

In synthesis, the analysis of the precedent isobaths maps indicated that the construction of the Sines Contourite Drift through time was controlled by the existence of paleotopographic features and structures, such as the PSF, structural highs, seamounts and the SVC. The SD was deposited over the existing paleomorphology (Figure 6.16), despite its early construction being restricted by the structural highs (horsts **h1** and **h2**) which implicated a higher vertical growth for the drift, with little to no lateral migration.

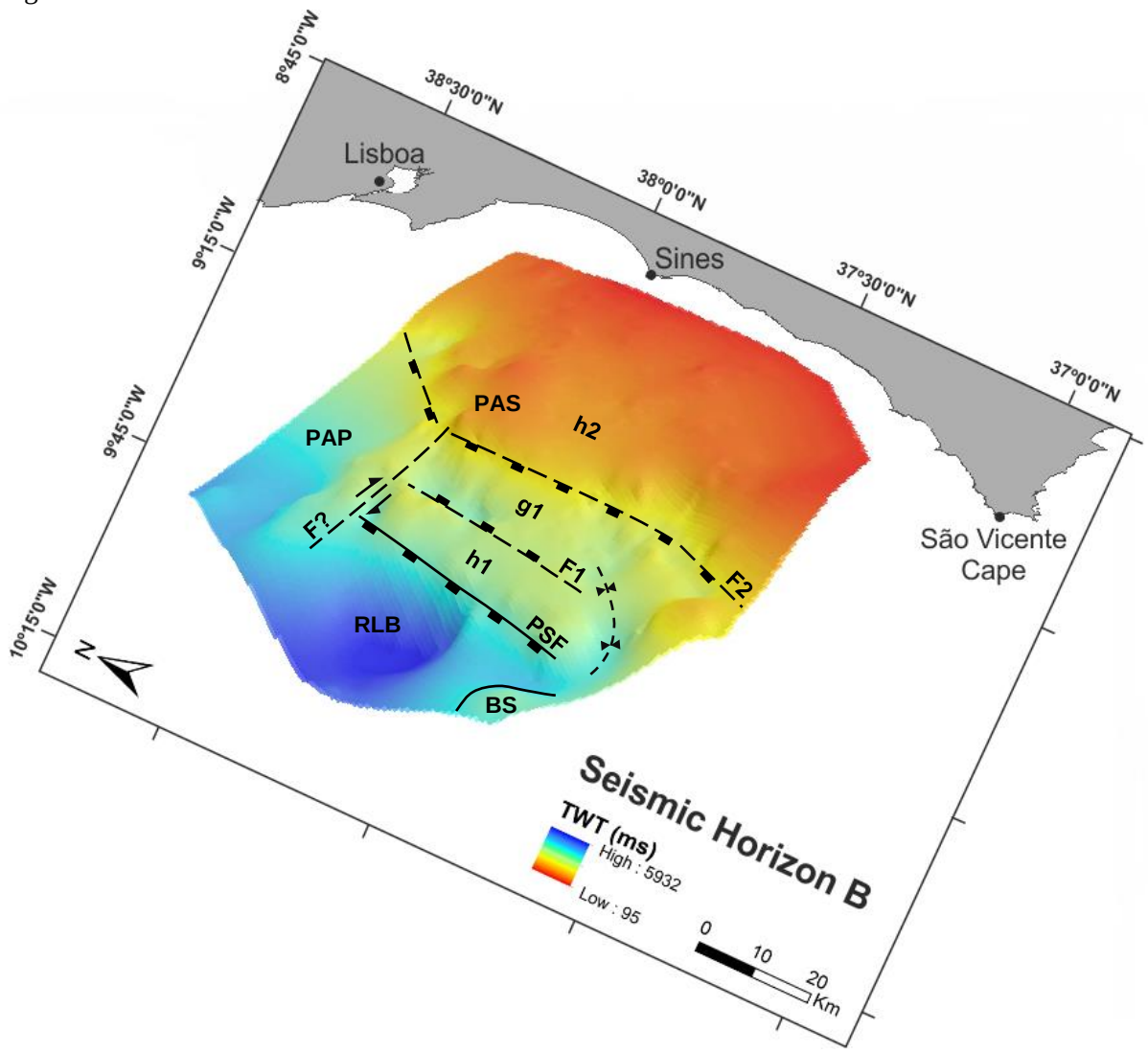

Figure 6.16 – 3D representation of the isobath map of seismic horizon B (Late Miocene) and main structures (5 times vertical amplification). BS – Bow Spur; PAP – Príncipe de Avis Plateau; PAS – Príncipe de Avis Seamounts; PSF – Pereira de Sousa Fault; RLB – Rincão do Lebre Basin.

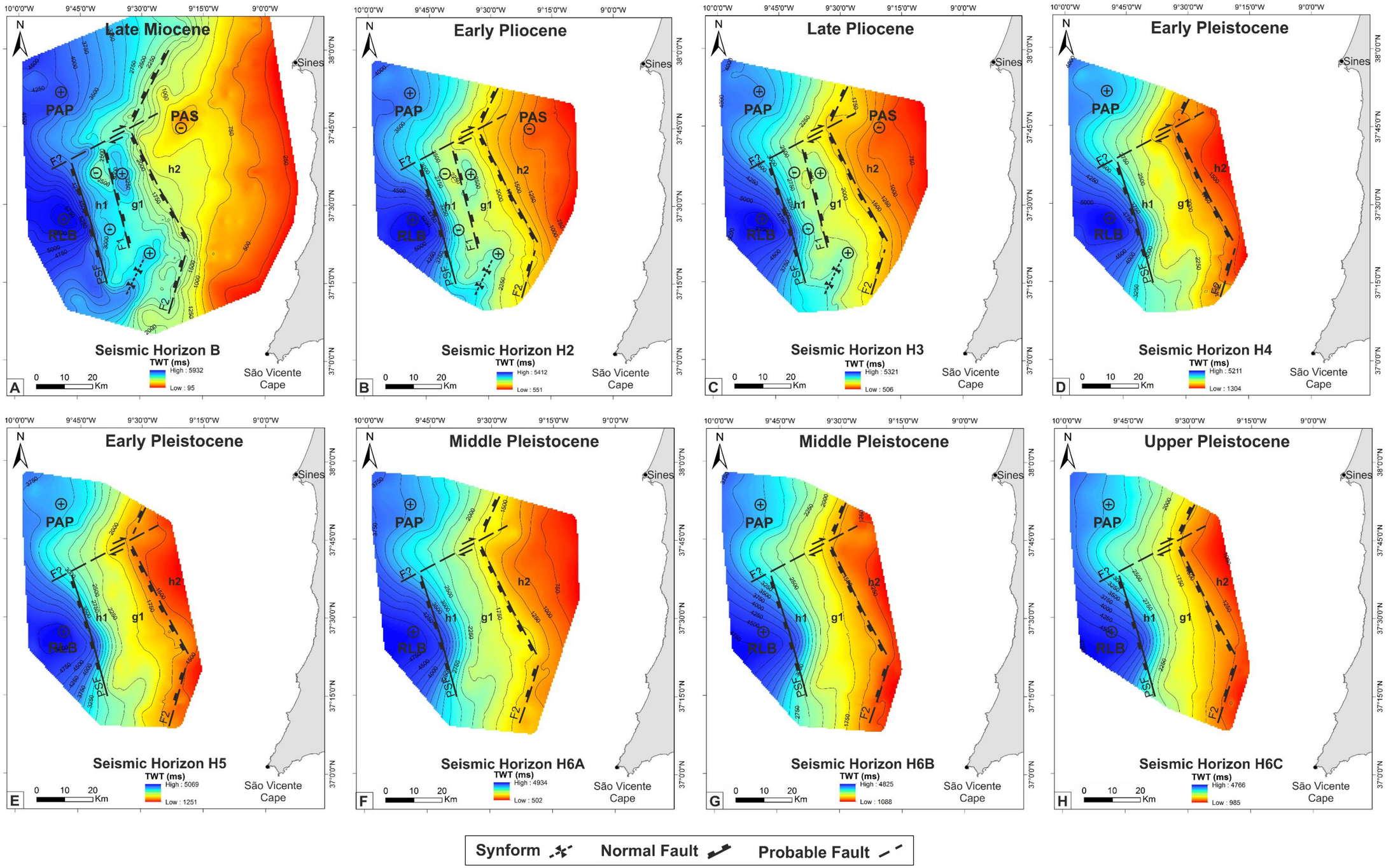

Figure 6.17A to H – Isobath maps for all seismic horizons (B to H6C). **Legend:** plus and minus signs mark depressions and elevations; **h1** and **h2** correspond to horsts and **g1** to a graben; BS – Bow Spur; PAP – Príncipe de Avis Plateau; PAS – Príncipe de Avis Seamounts; PSF – Pereira de Sousa Fault. RLB – Rincão do Lebre Basin. Equidistance: 250 ms.

6.6 Depositional evolution

The spatial distribution of the SD deposits from Late Miocene to Holocene age was established through the analysis of seismic units isopachs mapping, which represent the thickness in TWT units (ms) of one or more seismic units. These maps reveal the location and shape of the main depocenters and erosional areas, as well as their migration pattern and evolution through time.

6.6.1 Late Miocene

The isopach map of seismic unit U1 (Upper Miocene deposits) shows variable thickness from 200 to 560 ms TWT (Figure 6.20 A). This map shows two main depocenters in the west, (D1 and D2) corresponding to the RLB and the PAP respectively. This map also reveals the existence of two other minor depocenters, D1 in the south and D2 in the north. The southern depocenter D1 is divided by a NNE-SSW basement high. This is probably a buried horst, which controlled the area available for deposition of the first units. Also, at the east of said structural high, the seismic units are folded as a synform with N-S axis, as a result of compressive neotectonic events (see Appendix 10.3). Depocenters D1 and D2 correspond to the earliest development of the SD, a sheeted drift onlapping seismic horizon B (Figure 6.6). The deposition of the drift is restricted by the horsts **h1** and **h2**, with deeper and thicker accumulation in D1 and shallower above the horsts (100 ms TWT) (Figure 6.20 A). In the northern sector, the continental shelf gains relevance and seismic unit U1 has a thinner depocenter D2 (200 ms TWT), which lines around the continental shelf with variable configuration (from NW-SE to NE-SW). This configuration is also visible for fault F2, since its orientation goes from NNW-SSE to NNE-SSW (Figure 6.17 A to H). This deviation occurs as a manifestation of the NE-SW strike-slip fault previously mentioned, associated with the PAS.

The configuration of the margin is responsible for the SD's deepest depocenter D1 (to the west of it) with approximately 1 km depth (Figure 6.13) and the deposition of a sheeted drift. The continental slope relays considerable leverage over sediment deposition, since it forces the drift to develop in the south and north (depocenters D1 and D2), where there is space accommodation thanks to graben **g1** (Figure 6.20 A to H). The drift reaches its maximum thickness with 1612 ms TWT in an N-S elongation. Despite being a barrier to contourite development, a small upslope progradation of the SD was observed in the seismic profiles (Figure 6.18 and 6.19).

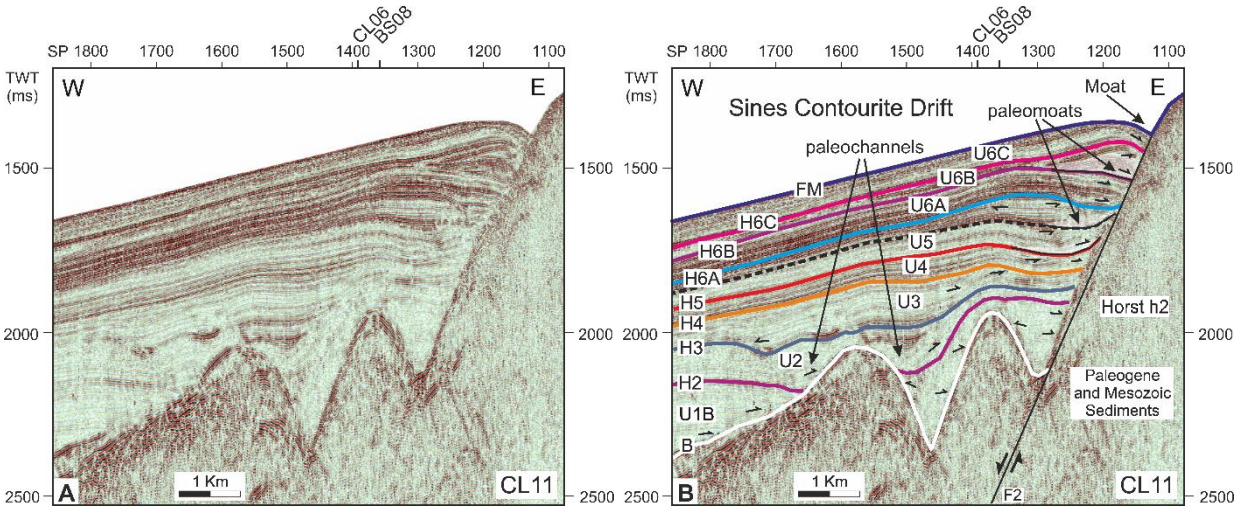

Figure 6.18 – Un-interpreted (A) and interpreted (B) section of seismic profile CL11 displaying paleo-channels and paleomoats against the continental shelf. U1 to U6: seismic units; B and H1 to H6C: seismic horizons; FM: seafloor horizon. F: faults; **black arrows**: reflections terminations; **shaded areas**: paleomoats. Location of seismic profile in Figure 6.5.

6.6.2 Early Pliocene

The isopach map of seismic unit U2 (Early Pliocene) shows variable but overall thickening of sediments in the south (depocenter D1) and small build up over structural highs (50 ms TWT). Unit U2 was partially eroded in the north, due to the formation of a NNW-SSE elongated paleomoat, during the deposition of the upper units (Figure 6.20 B). This suggests a N-S migration of the main depocenter through time, related to the development and initiation of drift formation. The construction of the drift begun in the south sector of the map since Late Miocene and it developed vertically and towards north. The structural restrictions channeled the MOW's pathways, thus aiding in the development of drift bodies along the SW Portuguese margin.

In the study area, erosive features mark the construction of the SD, such as the paleochannels located south, near the continental shelf (Figure 6.18). These paleochannels were incised during the deposition of units U1 and U2. The paleochannels are filled by low amplitude to semi-transparent facies, with a discontinuity which marks the boundary between units U1 and U2, designed horizon H2. The paleochannels mark a local increase of bottom-current strength as a result of abutting against the paleo-reliefs of the inherited structures. The deposition of seismic unit U3 sealed the paleochannels, which are the expression of a bottom-current system at work.

A current erosive channel is located north of the PSF. This channel curves over an area of 15 km width and 20 km length (Figure 6.1). This channel was carved at least since the deposition of seismic unit U1. The formation of this channel results from the passage of bottom-currents and shows a probable alignment with PSF and F1 N-S orientation. (Figure 6.1). The channel is being carved in the lineation of the PSF, thus suggests water passage was favored by the relief created by the Pereira de Sousa Scarp.

6.6.3 Late Pliocene-Early Pleistocene

The isopach map of seismic unit U3 (Late Pliocene to Early Pleistocene) is similar to the map of U2, due to the thicker accumulation in D1 and the northward migration of said depocenter (Figure 6.20 C). This unit smoothens the sharp cuts of the paleo-reliefs and, as U1 and U2, was also eroded by the formation of the eastern paleomoat.

The isopach map of seismic unit U4 (Early Pleistocene deposits) shows a widespread thickness with 310 ms TWT (Figure 6.20 D). An important characteristic is the paleomoats along the continental shelf. These paleomoats were carved by a bottom-current, which eroded the older units (U1 to U3), in ~70 km of extension and were subsequently filled during the deposition of U4 and U5. The paleomoats are an evidence of a previous mounded morphology of the drift.

6.6.4 Early-Middle Pleistocene

The isopach map of seismic unit U5 (Early-Middle Pleistocene) has 391 ms TWT thickness (Figure 6.20 E). This map shows the fill and seal of the paleomoat, which translates to a deeper depocenter D2 towards east. Paleomoats began to develop during the deposition of seismic units U4 and U5, which extended for 70 km along the continental shelf. Seismic units U1 to U3 were eroded by the paleomoats, prior to the deposition of the overlying units U4 and U5 (Figure 6.19). The paleomoats are filled by highly chaotic and irregular reflections and multiple erosive surfaces. The fill itself is characterized by an increase of amplitude for the internal seismic facies, separated by an erosive surface. This surface designed horizon H5 shows a decrease in acoustic turbidity and marks the boundary between units U4 and U5 (Figure 6.18 and 6.19). The paleomoats are wider and deeper due to higher incision when bottom-currents were constrained by morphological features (~2 km wide near the SVC; ~2.5 km wide near the PAS).

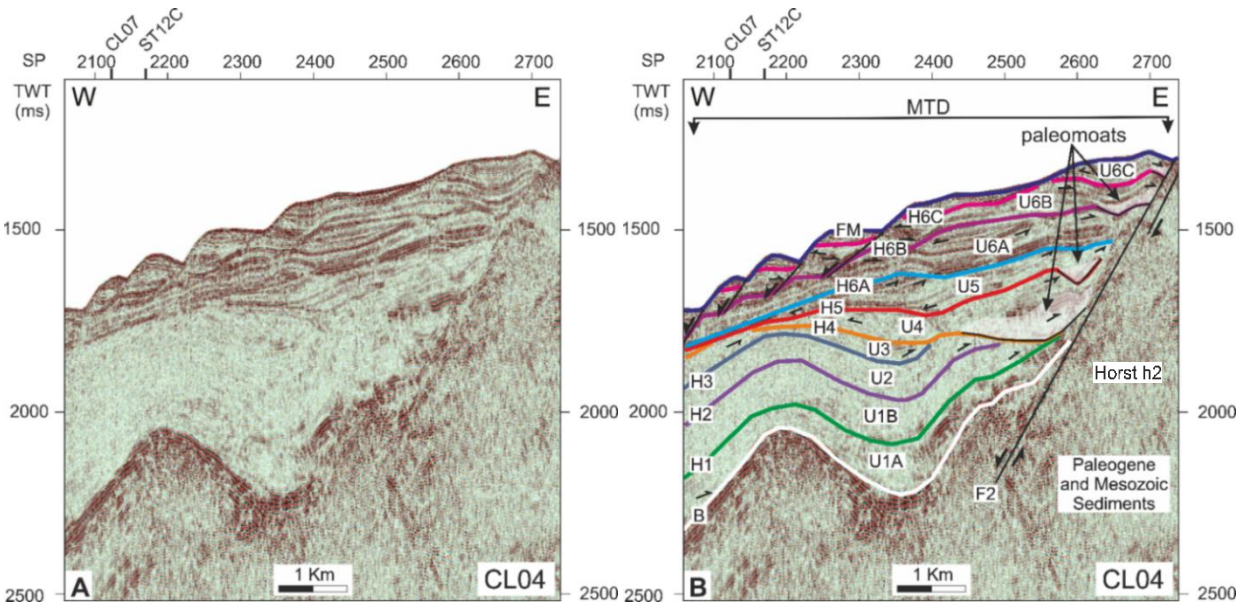

Figure 6.19 – Un-interpreted (A) and interpreted (B) section of seismic profile CL04 displaying the erosion of seismic units U1 to U3 with paleomoats formed during the deposition of U4 and U5. U1 to U6: seismic units; B and H1 to H6C: seismic horizons; HMTD: base of MTD; FM: seafloor horizon. F: faults; **black arrows**: reflections terminations; **shaded areas**: paleomoats. Location of seismic profile in Figure 6.5.

6.6.5 Middle Pleistocene-Holocene

The isopach maps for the sub-units of U6 have a much higher thickness, reaching 190 ms TWT (Figure 6.20 F to H). Seismic unit U6 (Middle Pleistocene-Holocene) has a fuller depocenter in the north. This unit has variations among its sub-units, due to water current variations and the incision of the current moat (which is an extension of the previous paleomoats). Although all sub-units were deposited in a widespread manner (following the main inclination of the SD with migration of the depocenters towards north) (Figure 6.20 A to H). At the present time, the SD is characterized by a plastered morphology, an asymmetric shape and a smooth western slope. Seismic unit U6 also has small paleomoats towards northeast, 40 km long along the continental shelf (Figure 6.18 and 6.19). These paleomoats developed during the deposition of seismic sub-units U6B and U6C and eroded the underlying sub-units, U6A and U6B, respectively. The paleomoats have a fill of high amplitude subparallel reflections (Figure 6.18 and 6.19). The paleomoats suggest the presence of a semi-permanent bottom-current, which contours the continental shelf since Late Miocene times. These paleomoats (created since unit U4) are the precursor for the present-day SD moat. The SD moat is carved by the northward flowing upper core of the MOW.

From the interpretation of the isopach maps, all units show higher deposition in the south depocenter D1, with thinner deposition in the north (depocenter D2) due to a decrease in accommodation space (Figure 6.20 A to H). Sediment accumulation is restricted by the inherited topography, such as the barrier created by the continental shelf. As time progressed, there was a northward migration of D1. The evolution of the Pliocene-Quaternary sequence is probably related to the MOW's passage and incision, with the formation of paleomoats along the continental shelf and higher sedimentation for recent units. This trend is misleading further up north, near the SC and towards southeast, near the SVC. Both canyons do not allow sediment accumulation and provoke slope failure due to canyon incision and the sharp slant of the canyon walls. The seismic units are also affected by multiple landslide events along the PSF (Figure 6.21 and 6.22). Overall, the SD is characterized by a plastered morphology. In seismic units U4 to U5, the SD had a different configuration, with mounded morphology towards south and sheeted in the north. The change from mounded to plastered is indication of a strong MOW bottom-current with diminuition of its strength towards north.

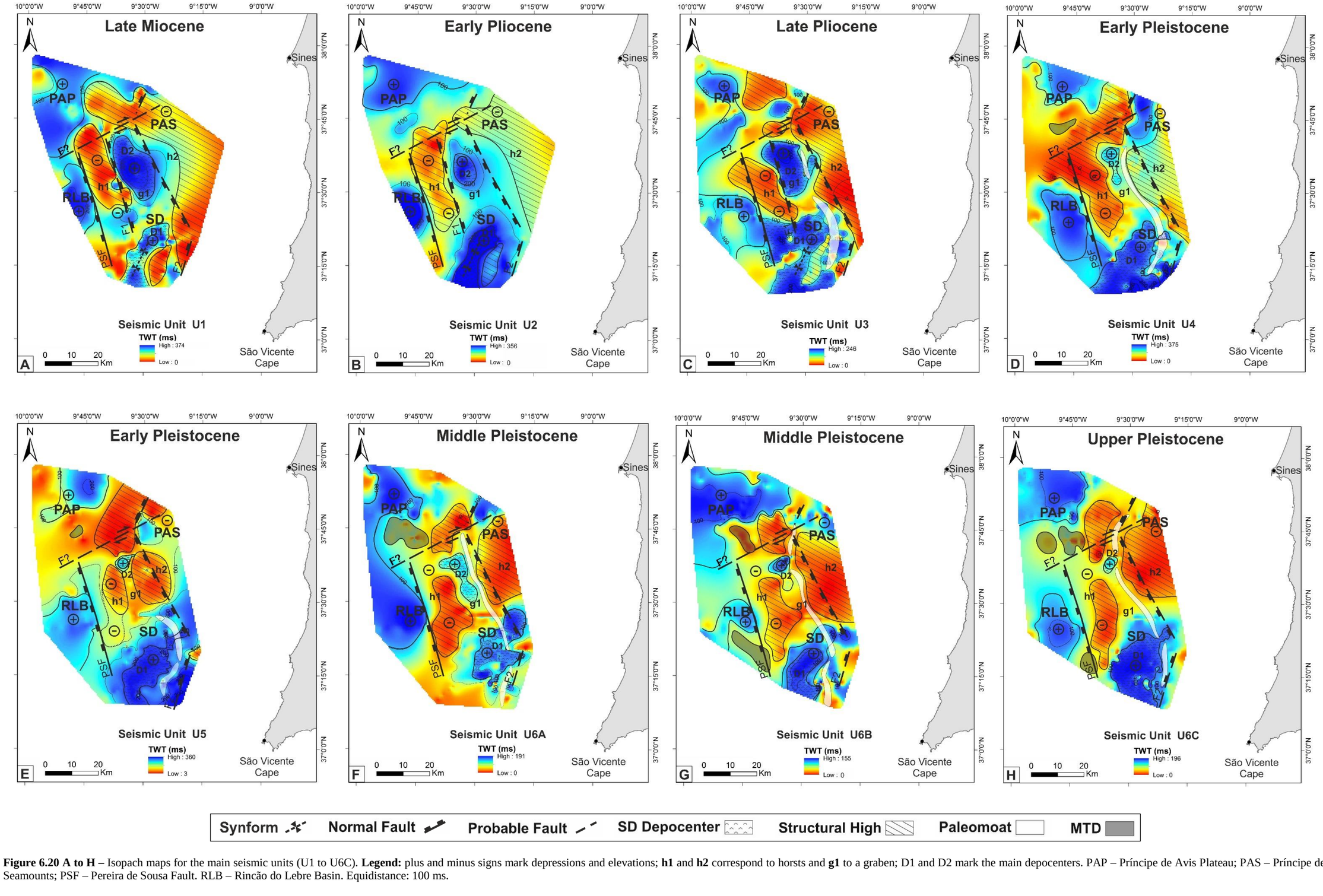

Figure 6.20 A to H – Isopach maps for the main seismic units (U1 to U6C). **Legend:** plus and minus signs mark depressions and elevations; **h1** and **h2** correspond to horsts and **g1** to a graben; D1 and D2 mark the main depocenters. PAP – Príncipe de Avis Plateau; PAS – Príncipe de Avis Seamounts; PSF – Pereira de Sousa Fault. RLB – Rincão do Lebre Basin. Equidistance: 100 ms.

6.7 Slope failure and Mass Transport Deposits

The term mass transport deposits (MTDs) includes gravity-driven deposits identified in seismic record, which could correspond to slides, slumps and debris flows. The Early Pleistocene-Holocene sedimentary record of the SD corresponding to seismic units U4 to U6 has been affected by slope failure processes. Several mass transport deposits were recognized either within the sedimentary column or affecting the present-day seafloor as describe previously on Chapter 6, Point 6.1.

The MTDs were recognized by their typical chaotic acoustic facies on the west flank of the SD and associated with major topographic reliefs, such as the Pereira de Sousa Scarp, the PAS and the SVC. The MTDs occupy an area of 50 km by 20 km, along the N-S PSF (Figure 6.1).

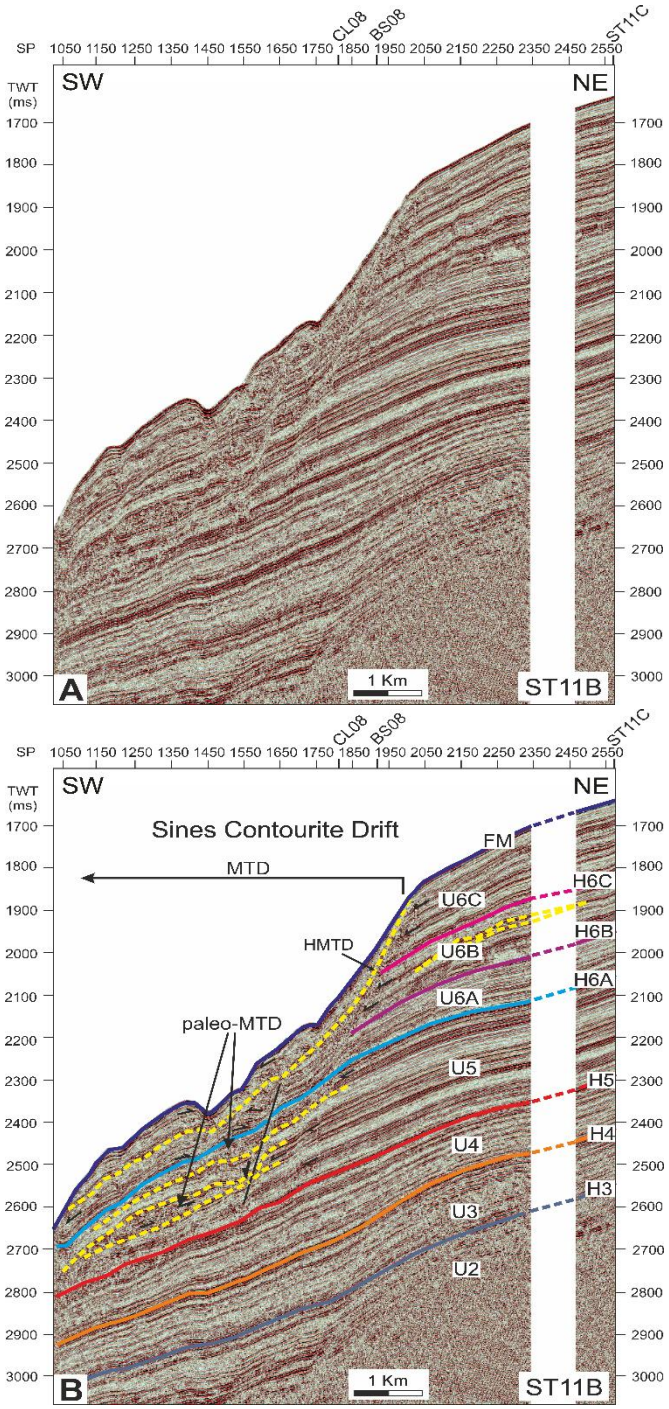

Figure 6.21 – Un-interpreted (A) and interpreted (B) section of seismic profile ST11B with MTD and paleo-MTD, which have occurred on the west flank of the SD since seismic unit U5. U1 to U6: seismic units; B and H1 to H6C: seismic horizons; HMTD: base of MTD; FM: seafloor horizon. F: faults; **black arrows**: reflections terminations. Location of seismic profile in Figure 6.5.

Present-day and past MTDs concentrate on the hanging wall and footwall of the PSF (Figure. 6.21), which affect an area over 50 km long with a western slope towards the inner basin (RLB). The landslide scars are located between 1250-2500 m depth in a staggered succession and were identified by their asymmetric and amphitheater shapes, with variable dimensions and head scarps. These occurrences seem to affect mostly seismic units U4 to U6 deposited above horst **h1** bound by the PSF (Figure. 6.21).

Near the PAS, landslides move westward in a step pattern, separated by N-NE normal slope failure faults (Figure 6.22). This slope failure is related to the west dip of the SD and the current configuration of the seafloor morphology, with deeper basins RLB and PAP in the west.

The SVC is another preferential site for the accumulation of several slumps and slides, probably resulting from slope instability on the southern flank of the SD. Besides that, the steep flanks of SVC (ranging between 5º and 30º) acted since Late Miocene (Valadares, 2012) as a source for gravity-driven deposits, which have been deposited at the axis and walls of the canyon and carried further south into the Horseshoe Abyssal Plain (Valadares, 2012).

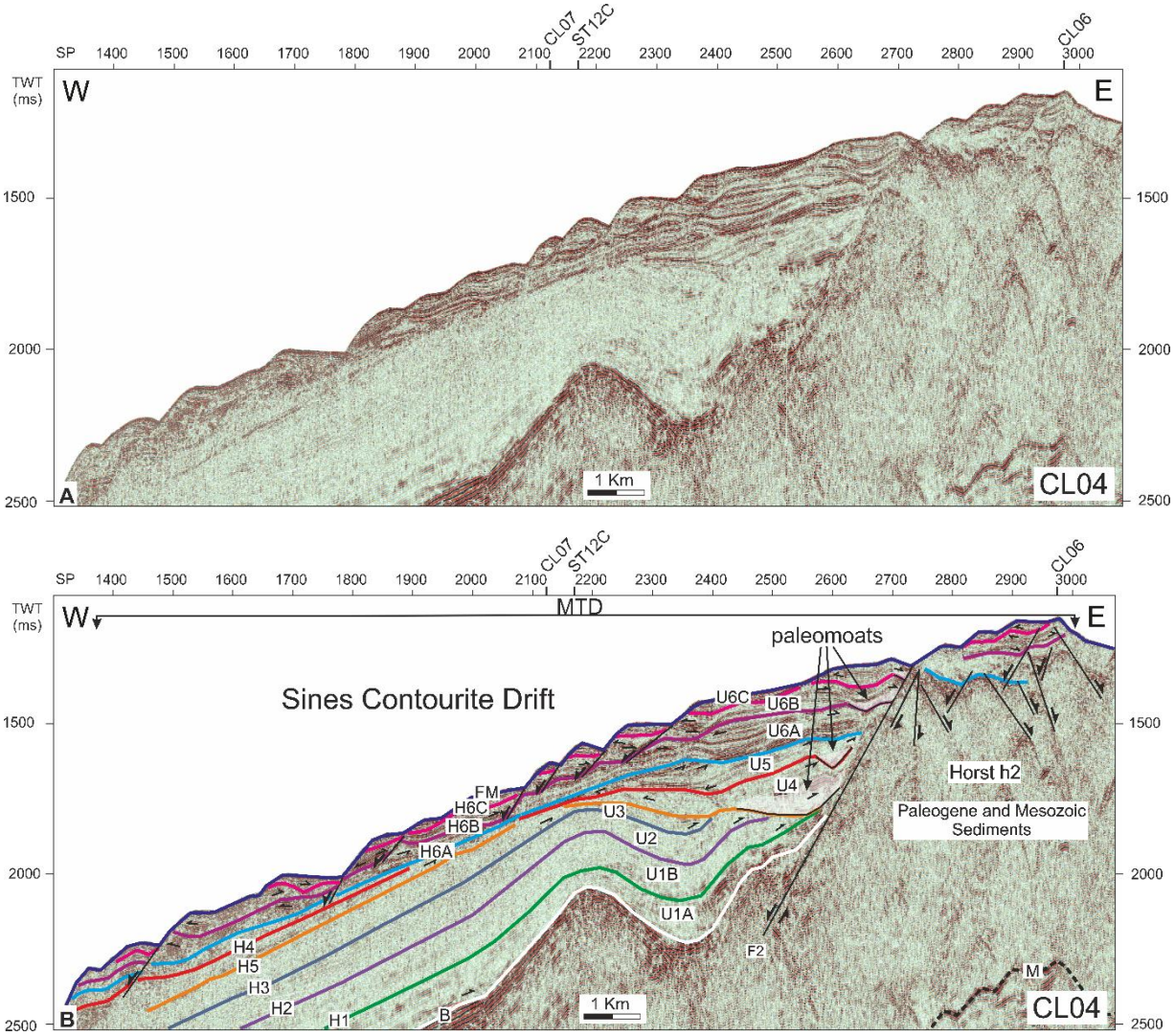

Figure 6.22 – Un-interpreted (A) and interpreted (B) section of seismic profile CL04 shows several MTD affecting the upper units, north of the SD. U1 to U6: seismic units; B and H1 to H6C: seismic horizons; HMTD: base of MTD; FM: seafloor horizon. F: faults; **black arrows**: reflections terminations; **M**: multiple. Location of seismic profile in Figure 6.5.

CHAPTER 7

DISCUSSION

Based on the results presented in Chapter 6, a depositional model for the SD development is proposed. The conception of any depositional model needs to consider the different controls which influence either its preservation or erosion (Faugères and Stow, 2008). This chapter will discuss said model, assessing the role of tectonic, paleoceanographic, sediment supply, climatic and sea-level changes on the development of the depositional architecture shown by the SD.

7.1 Depositional Model of the Sines Drift

Through seismic stratigraphy interpretation and mapping of seismic units, three main phases of contourite sedimentation have been identified, being characterized by different morphologies and stacking patterns: 1) sheeted-contourite-drift phase, 2) mounded-contourite-drift phase and 3) plastered-contourite-drift phase. These phases are described herein.

1. Phase 1: Sheeted-Contourite-Drift (Late Miocene to Late Pliocene, at least <5.3-3.2 Ma)

The sheeted-contourite-drift phase is represented by seismic units U1 and U2 and interpreted as a precursor phase of contourite formation (Figure 7.1). This phase occurred from Late Miocene to the Late Pliocene, after an erosional event during the Late Miocene (seismic horizon B). This was an erosive episode which changed the seafloor morphology of the Alentejo Basin. Although the precise age of this event remains unknown, it could be linked to regional tectonic and paleoceanographic changes that took place during the end of Late Miocene. Among them, are the closure and opening of the Mediterranean and Atlantic gateways (Flecker *et al*., 2015). The closure of the Rifian and Betic gateways at 5.96 Ma led to the Messinian Salinity Crisis (5.96-5.33 Ma) (Hsü *et al*., 1973; Sierro *et al*., 2008; Flecker *et al*., 2015). According to Duggen *et al.* (2003), vertical movements at lithospheric scale were responsible for the closure of the Atlantic and Mediterranean gateways in the Late Miocene, thereby causing the Messinian Salinity Crisis.

The end of the Late Miocene signifies the Messinian Salinity Crisis and the opening of the Strait of Gibraltar (Maldonado *et al*., 1999; Estrada *et al*., 2011), which allowed the MOW to flow through the Atlantic (5.33 Ma) and cause the Zanclean flooding (Garcia-Castellanos *et al*., 2009; Estrada *et al*., 2011). Therefore, the onset of contourite drift accumulation along the Iberia margin begins associated with significant changes of oceanic circulation patterns (Hernández-Molina *et al*., 2002, 2006; Rogerson *et al*., 2012; Van der Schee *et al*., 2016) and the oldest phases seems to be well preserved on the SD.

Phase 1 was dominated by deposition of a sheeted drift, indicating that a weak bottom-current flowed northward. This is corroborated by the recovery at site U1391 of mixed facies with mud rich contourites, biosiliceous muds, dolomite mudstone and a debrite, for seismic unit U2 (Table 6.2). The MOW would be initially weak and probably flowed as a single core along the continental margin (Stow *et al*., 2013; Hernández-Molina *et al*., 2014a). Therefore, a semi-permanent MOW begun flowing to deposit contourite sediments and construct a sheeted drift, which was restricted by the paleo-reliefs (horsts **h1** and **h2**, Figure 7.1). During this phase, upwelling events probably occurred along the West Iberian margin, responsible for the deposition of the biosiliceous muds and assemblages of benthic foraminifers

seen in Site U1391 (high amounts of *Brizalina* spp. or *Cibicides*/*Cibicidoides* spp. or *Siphonodosaria* spp. associated with variable amounts of *Cibicidoides* cf. *wuellerstorfi, Melonis* spp., *Sigmoilopsis schlumbergeri* and *Uvigerina* spp.; Expedition 339 Scientists, 2012). Gravity driven processes also occurred, marked by the debrite of ~35 cm thickness with muddy intraclasts and matrix (Figure 6.10 A).

2. Phase 2: Mounded-Contourite-Drift (Late Pliocene to Early Quaternary, 3.2-0.7 Ma)

The second phase of sedimentation is characterized by the development of a mounded-contourite-drift which is constituted by seismic units U4 and U5 (Figure 7.1). The transition from sheeted drift to mounded drift is marked by a hiatus (seismic horizon H4), small upslope migration and incision of prominent and precursory paleomoats (Figure 7.1). This change is not only seen in drift morphology and stacking pattern, from sheeted to mounded, but also in Site U1391 lithologic and physical properties data. The lithologic character shows a shift from mixed system (debrite and mud rich contourites) that dominated Phase 1 to muddy contourites which predominate during Phase 2. Therefore, this shift reflects a significant variation of the oceanic circulation patterns and its beginning was correlated to the LPD (seismic horizon H3, 3-3.2 Ma) and its ending to the EQD (seismic horizon H4, 2-2.4 Ma), recognized by Hernández-Molina *et al*. (2015).

The LPD and EQD events coincide with a regional compression due to the reorganization of Eurasia (Iberia)-Africa (Nubia) plate boundary from NW-SE to WNW-ESSE during the Early Quaternary (Rosas *et al*., 2009; Zitellini *et al*., 2009; Duarte *et al*., 2013). This affected the sediments in some regions, most notably in the east of the study area with the reactivation of NNW-SSE normal faults, rooted in the Mesozoic faults that bound structural highs (Figure 6.8 and 6.14).

As for the MOW, the period between the LPD and EQD marks an intensification of its strength from 3.2 Ma to 2.4 Ma (Hernández-Molina *et al*., 2015). The LPD event is marked by a lower sedimentation rate during the Pliocene, with 13 cm/k.y (Expedition 339 Scientists, 2012), associated with the higher erosive action of the MOW. This suggests the MOW's main core flowed through in a persistent northward direction (Figure 7.2 and 7.3). This intensification is attributed to a prominent rise in Mediterranean summer aridity, which translates to enhanced deep-water convection in the Mediterranean Sea and active circulation in the North Atlantic Ocean (Khélifi *et al*., 2009, 2011, 2014). The MOW enhancement also improved the Thermohaline Circulation, AMOC and Northern Hemisphere deep-water formation due to its contribution of saline and warm waters to the intermediate depths in the northern Atlantic waters (Hernández-Molina *et al*., 2014a). The LPD and EQD events also coincide with the final intensification of the Northern Hemisphere Glaciations, marked by global cooling and sea-level fall (Bartoli *et al*., 2005; Miller *et al*., 2011).

3. Phase 3: Plastered-Contourite-Drift (Middle Pleistocene to Present, 0.7 Ma)

The third and final phase of sedimentation led to the build-up of a plastered contourite drift from Middle Pleistocene to the present-day, which is represented by seismic unit U6 (Figure 7.1). The transition from the mounded-contourite-drift phase to the plastered-contourite-drift phase is marked by an important change in drift architecture (Figure 6.22). The SD stacking pattern shifts from mounded to plastered, with higher sedimentation rate at 27 cm/k.y (Expedition 339 Scientists, 2012). Site U1391 data shows that this change is marked by an increase of coarser-grained intervals and the presence of bigradational contourite successions. Phase 3 is also characterized by small precursory paleomoats along the continental shelf (Figure 7.1). Therefore, this phase is characterized by the formation of a moat and thick accumulation, which suggests more vigorous bottom-currents and substantial MOW outflow into the Atlantic Ocean (Sierro *et al*., 1991; Flinch and Vail, 1998).

The development of the present-day MOW occurs during this last stage with two phases of MOW intensification, marked by two important discontinuities: the MPD (0.7-0.9 Ma) and the LQD (~0.4 Ma) (Hernández-Molina *et al.*, 2002, 2015; Llave *et al.*, 2007b; Lofi *et al.*, 2016). Hernández-Molina *et al.* (2015) attributes the formation of the MOW pathways to tectonic constriction and deformation in the Gulf of Cadiz. The SW Portuguese margin shows the exact opposite, with the absence of deformation and tectonic influence since the Middle Pleistocene (Pereira and Alves, 2011, 2013; Hernández-Molina *et al.*, 2015). The plastered contourite drift phase is not affected by deformation, thus indicating that tectonics do not play a major role in the evolution of this depositional phase.

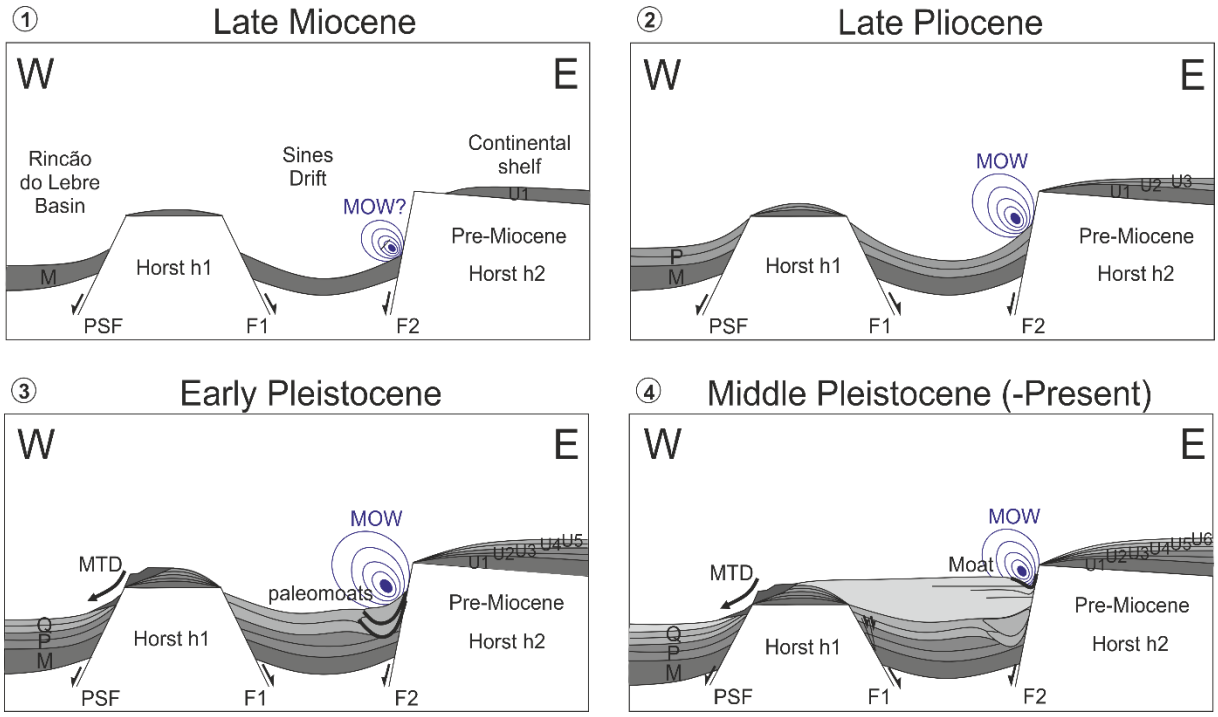

Figure 7.1 – Representation of the depositional evolution of the SD and possible changes in MOW intensification and drift architecture.

The first phase of MOW intensification is marked by the MPD (seismic horizon H6A), which shows the change in drift morphology and the increase of sandier deposits. The MPD is related to an important climatic change, the Middle Pleistocene Revolution (0.7-0.78 Ma) (Hayward *et al.*, 2009; Hernández-Molina *et al.*, 2015). Several authors show this is the most important hiatus for the Quaternary deposits (Hernández-Molina *et al.*, 2006, 2015; Llave *et al.*, 2007b, 2011; Lofi *et al.*, 2016) which is also verified for the SD Quaternary deposits.

The second phase of MOW intensification is marked by the LQD (seismic horizon H6B), which is also related to an important climatic change at ~0.4 Ma (Hayward *et al.*, 2009; Lofi *et al.*, 2016). The MPD and the LQD coincide with eustatic falls of the sea-level (Miller *et al.*, 2005; Rogerson *et al.*, 2012; Table 7.1) and enhancement of the AMOC (Knutz, 2008). Hence, since the Middle Pleistocene, two episodes of MOW intensification increased bottom-current strength. The second phase of MOW intensification matches one coarse-grained interval at Site U1391 in the Middle Pleistocene. However, Site U1391 has a total of six coarser-grained intervals from the Middle Pleistocene to the Present (see Chapter 6, Point 6.4), which suggests at least six episodes of bottom-current enhancement during this stage.

Overall, the MOW was capable of constructing the SD on the left and its moat on the right side. The SD did not migrate considerably since Late Miocene, as the flow pathway remained almost unchanged due

to the paleomorphologic constraints. Therefore, a long-term MOW current has consistently been flowing along the SW Portuguese margin since that time till the present-day.

7.2 Controls of Sines Drift Edification

7.2.1 Structural Control

Tectonic activity can influence the available accommodation space and confine drift growth. During the Mesozoic, the multiple rifting phases segmented the Southwest Portuguese margin into continental shelf, upper slope (Alentejo Basin) and distal slope (Rincão do Lebre Basin) (Figure 7.2). The growth of the SD was constrained by the seafloor morphologies that resulted from the Mesozoic rifting processes, inherited from the Mesozoic rifting phases. The paleomorphologies provided accommodation space for drift growth and conditioned its overall architecture. The N-S horsts built during the Mesozoic rifting did not allow a lateral migration and instead permitted a more vertical growth (Figure 7.2). The paleomorphologies also contributed to bottom-current acceleration. The boundary input by the continental slope probably aids the acceleration of the MOW current as it turns São Vicente Cape and flows northward. This generates alongslope current erosion and contributes for drift growth, with the MOW flowing along and eroding the continental slope.

The construction of the drift begun after a major erosive event in the Late Miocene, which affected the seafloor morphology of the Alentejo Basin. Although the precise age of this event is unknown, it could be related to regional tectonic and paleoceanographic changes that occurred during the end of Late Miocene, such as the closure and opening of the Mediterranean and the Atlantic gateways (Flecker *et al.*, 2015).

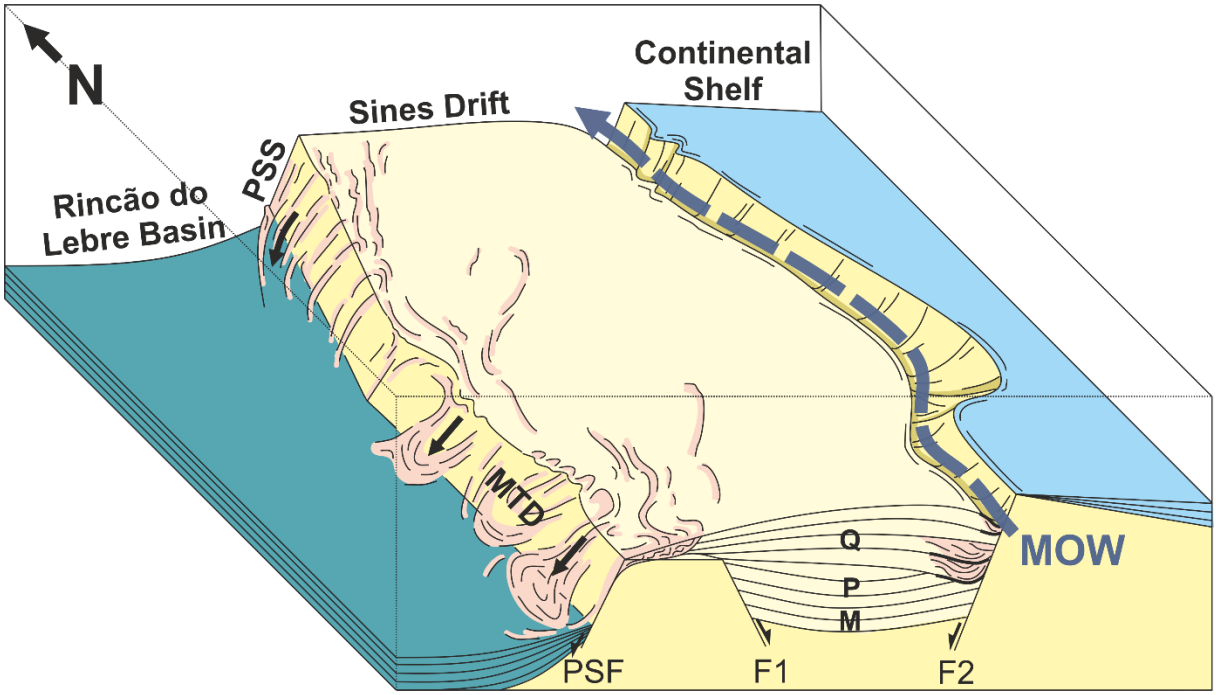

Figure 7.2 – Model of the SD and the factors that control its depositional evolution: tectonics, paleomorphology, paleoceanography and slope instability.

7.2.2 Paleoceanographic Implications

Paleoceanographic changes can control contourite drift growth and its internal configuration (i.e. progradation and/or aggradation). The construction of the SD was influenced by variations in the MOW,

which shows distinct behavior under different climatic and eustatic conditions and under different bottom-current regime in the Mediterranean and the Atlantic.

The deposition of contourites on the GCCDS only occurred after the end of the Messinian Salinity Crisis, when the interaction between the Atlantic and the Mediterranean was rekindled. The Messinian Salinity Crisis affected the Mediterranean between 5.96 and 5.33 Ma (Cita, 2001; Bache *et al*., 2012) and had drastic consequences for the bottom-current circulation between the Mediterranean and the Atlantic. The Messinian Salinity Crisis occurred as a result of the closure of the Rifian and Betic gateways at 5.96 Ma (Hsü *et al*., 1973; Sierro *et al*., 2008; Flecker *et al*., 2015) due to tectonic movements between the Eurasian and the African plates (Duggen *et al*., 2003). This led to the progressive isolation of the Mediterranean region and caused desiccation and precipitation of massive evaporites (Krijgsman *et al*., 1999).

The end of the Messinian Salinity Crisis occurred near the Early Pliocene with the Zanclean flood, which was the inundation of the Mediterranean Basin by Atlantic waters (Garcia-Castellanos *et al*., 2009). There is a general agreement that the circulation between the Atlantic and the Mediterranean was fully established in the Early Pliocene, allowing the MOW to flow along the Iberian margin and interact with the seafloor to create contourite sheeted drifts.

Therefore, the first phase of the SD, which is characterized by the formation of a sheeted drift since the Late Miocene, suggests the existence of enhanced bottom-current circulation to aid the incipient MOW with the deposition of contourites.

Several works show that humid climate conditions prevailed in the Mediterranean until 3.4 Ma (Béthoux and Pierre, 1999), until it changed to cold and arid, which triggered enhanced production of cooler, saltier and oxygenated Mediterranean deep water (Hayward *et al*., 2009; Khélifi *et al*., 2009). The first phase of development of the SD is also characterized by assemblages of benthic foraminifers in a carbonated biogenic system (in the Late Pliocene at Site U1391), which marks the occurrence of upwelling events on the Southwest Portuguese margin. At the present time, upwelling events usually occur over the continental shelf and slope of the West Portuguese margin in the summer and carry cold nutrient-rich NACWp in the north and colder nutrient-poor NACWt in the south (Mason *et al*., 2006). During the Early to Late Pliocene times, there were warmer waters in the Mediterranean and Atlantic, although upwelling events also occurred under similar oceanographic conditions to today's (Dowsett *et al*., 1996, 1999; Silva *et al*., 2008).

The transition to the Quaternary is characterized by the development of a mounded drift since 3.2 Ma and a plastered drift since 0.7 Ma, with erosional contourite features (moats and paleomoats). The formation of these features is associated with several events of MOW intensification and climatic and eustatic fluctuations (Hernández-Molina *et al*., 2002, 2015; Llave *et al*., 2007b; Lofi *et al*., 2016).

The location of the moats/paleomoats allowed the reconstruction of the MOW's pathway along the Southwest Portuguese margin, from the Early Quaternary to the Present (Figure 7.3). It is possible to observe that the MOW remained in a persistent and semi-permanent pathway towards north and along the contours of the upper continental slope. The constant pathway of the MOW is probably related to the paleomorphology of the Alentejo margin, which was inherited from the Mesozoic rifting phases.

In the past, the MOW flowed as a single core along the South and West Iberian margin. Therefore, it is not possible to recreate or separate the pathways of the MOW's Upper Core (MU) from the MOW's Lower Core (ML).

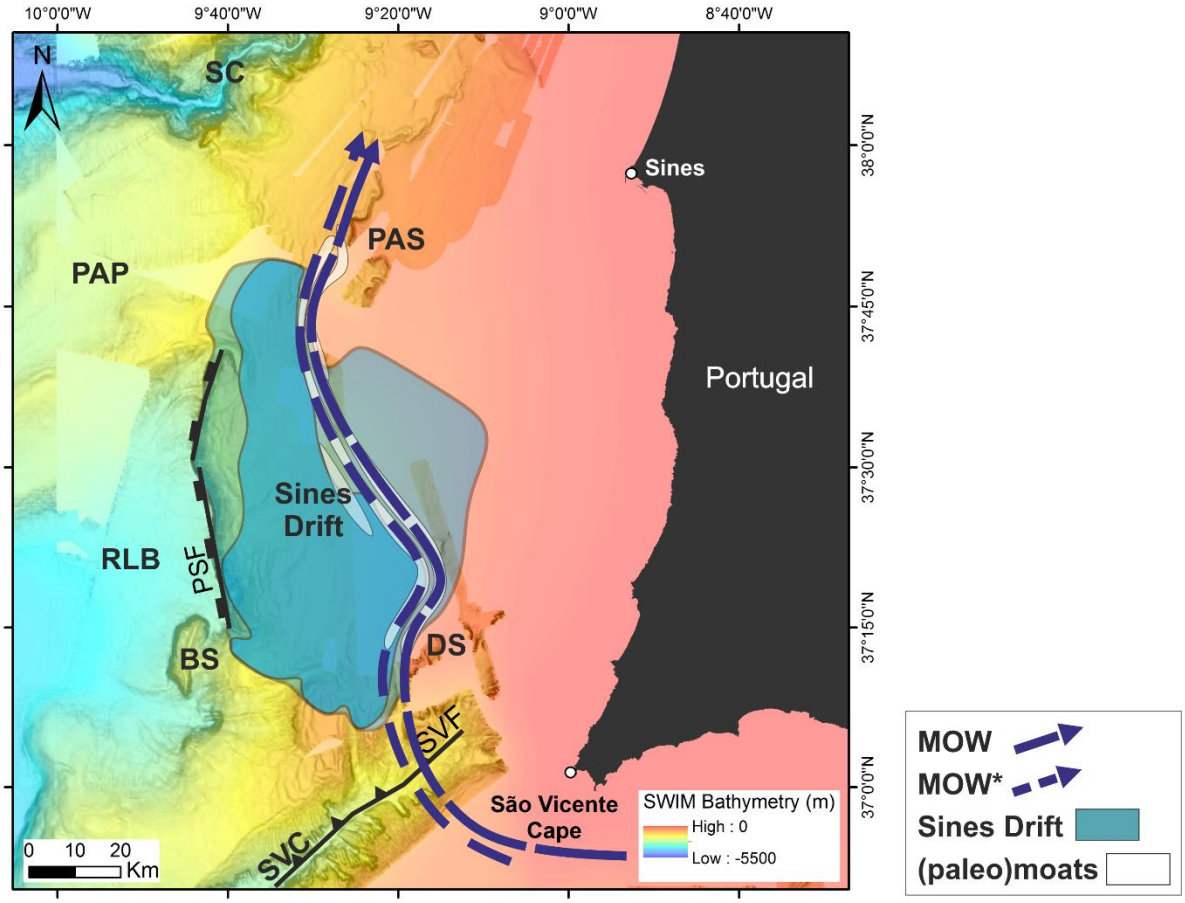

Figure 7.3 – Reconstruction from the Early Quaternary (MOW*) to the Present (MOW) of the paleoceanographic pathways of the MOW along the SW Portuguese margin, inferred by the seafloor morphology and moat/paleomoats formed since seismic units U4 to U6 (Early Quaternary to Holocene age). Bathymetric map with SWIM bathymetry (100 m cell grid from Zitellini *et al*., 2009) and GEBCO (2003) data. BS – Bow Spur; DS – Descobridores Seamounts; PAP – Príncipe de Avis Plateau; PAS – Príncipe de Avis Seamounts; PSF – Pereira de Sousa Fault; RLB – Rincão do Lebre Basin; SVC – São Vicente Canyon; SC – Setúbal Canyon.

7.2.3 Sedimentary record and bottom-current circulation

Contourite drift formation is also controlled by sediment influx and consequently certain conditions must be maintained over a prolonged period of time for deposition to take place. In general, the sediment supply by bottom-currents must be greater than background pelagic and hemipelagic accumulation for contourite development to occur (Rebesco and Camerlenghi, 2008). Bottom-currents are capable of reworking and transporting sediments, so sediment influx can be provided by turbidity currents, pro-delta plumes, slope spillover, hemipelagic and pelagic settling both upstream, downstream and directly at the drift's location (Stow *et al*., 2008).

Bottom-currents are capable of eroding the continental slope and reworking previously deposited sediments. Therefore vigorous and persistent bottom-currents are required for the deposition of contourites and particularly contourite sands (Stow *et al*., 2008). Not only are strong bottom-currents required, but their persitence over geological timescales is imperative for any significant thickness to accumulate. Also, sediment influx, distance and type of transportation plays a major role for contourite deposition (Stow *et al*., 2008; Figure 7.4). For example, larger grain size sediments can have a higher biogenic component, such as foraminifera, which are significantly lighter than clasts, and require lower velocities for transportation (McCave, 1984), and fine-grained sediments (mud or silt) could be

deposited by pelagic settling, since contourites have a combination of sediments sourced by alongslope, downslope and pelagic or hemipelagic processes (Rebesco and Camerlenghi, 2008).

The sediment supply for the edification of the SD was inferred based on the lithological character and physical properties at Site U1391 and the paleomorphology of the SW Portuguese margin.

The lithological record at Site U1391 showed a predominantly calcareous mud rich facies (Figure 6.8 in Chapter 6). The mud-dominated contourites have interbedded pelagic and hemipelagic muds, since these processes can occur at the same time. The first phase of contourite drift deposition (Late Pliocene) was characterized by a mixed system at Site U1391, composed of fine-grained sediments (mainly calcareous and biogenic components) with a debrite and a dolomitic mudstone, with low amplitude reflections in the seismic data (seismic units U1 to U3; Figure 6.7). These characteristics suggest a low energy system, with almost no gradational successions and multiple ongoing depositional processes, with interbedded sediments derived both from downslope and alongslope.

The second phase (mounded-contourite-drift, from the Late Pliocene to the Early Quaternary) was marked by muddy contourites and calcareous muds (Figure 6.10 C). During this stage, the formation of a mounded drift with a succession of paleomoats was probably associated with intensification of the MOW from the Late Pliocene to the Early Quaternary. This observation does not take into account the grain size of the sediments which fill the paleomoats, since Site U1391 is located on the center of the study area. Although, it is possible to speculate that the paleomoats probably hold coarser-grained sediments (marked by low to high amplitude reflections in seismic units U4 and U5) as a result of enhanced bottom-current velocity.

The transition to the plastered-contourite-drift stage in the Middle Pleistocene is marked by a change in sedimentation. This is testified by an increase to six sandy contourite layers and numerous bigradational contourite successions of calcareous and siliciclastic natures (Figure 6.10 C in Chapter 6). On seismic data, this phase has high amplitude reflections (seismic unit U6), which reflects the coarse-grained nature of the sediments. This phase is also characterized by a cyclic pattern of transparent facies with thick reflective facies at the top and minor erosional surfaces (Figure 6.14). This variation is probably correlated with the alternations from fine- to coarse-grained contourite deposits and the bigradational contourite successions. The alternations could indicate periods of strengthening and waning bottom-current velocity and probably result from climatic and sea-level changes, observed mainly since the Middle Pleistocene. This shows sediment supply has varied at numerous timescales, with variations of sediment grain size as a result of bottom-current fluctuations. Therefore, in the SD a relation exists between bottom-current velocity and average grain size.

The relation between sediment input and bottom-currents for the SD should also consider the Gulf of Cadiz Contourite Depositional System (GCCDS), since the SD is formed by the MOW, which comes from the Strait of Gibraltar.

The GCCDS is characterized as a silici-bioclastic system since the Early Pliocene to the Present, with mean grain sizes of 6 μm to ~1000 μm (Brackenbrige, 2014; Alonso *et al*., 2016; Nishida *et al*., 2016). The GCCDS is characterized by a reduction of grain size away from the Strait of Gibraltar (Stow *et al*., 2013; Figure 7.4) and away from the main bottom-currents (Nelson *et al*., 1993; Brackenridge, 2014; Hernández-Molina *et al*., 2014a). This CDS also has a broad relation between the accumulation of coarse-grained sediments in zones of bottom-current acceleration (channels, valleys) or in zones of bottom-current deceleration (exit of a channel) (Stow *et al*., 2013; Figure 7.4). Also, shelf spillover plays an important role in the GCCDS, with sand spilling off the shelf closer to the Strait of Gibraltar and being entrained into the MOW (Stow *et al*., 2013; Brackenridge, 2014; Hernández-Molina *et al*.,

2014a; Ducassou *et al*., 2015; Figure 7.4). This sand can be transported alongslope for many kilometers before being deposited.

The SD is constituted by a mixed carbonated-bioclastic system from the Late Pliocene to the Present, with a higher siliciclastic component for the plastered-contourite drift stage from the Mid-Pleistocene till the present-day. The difference between the SD carbonated-bioclastic system and the Gulf of Cadiz silici-bioclastic system is probably related to the location of the SD, which slightly changes the main processes involved in sediment deposition. The difference also implicates different clast transport thresholds and a different response to bottom-current fluctuations. Although the change in the SD from a carbonated-bioclastic system to a more siliciclastic occurrence denotes the existence of bottom-current variations and enhancements.

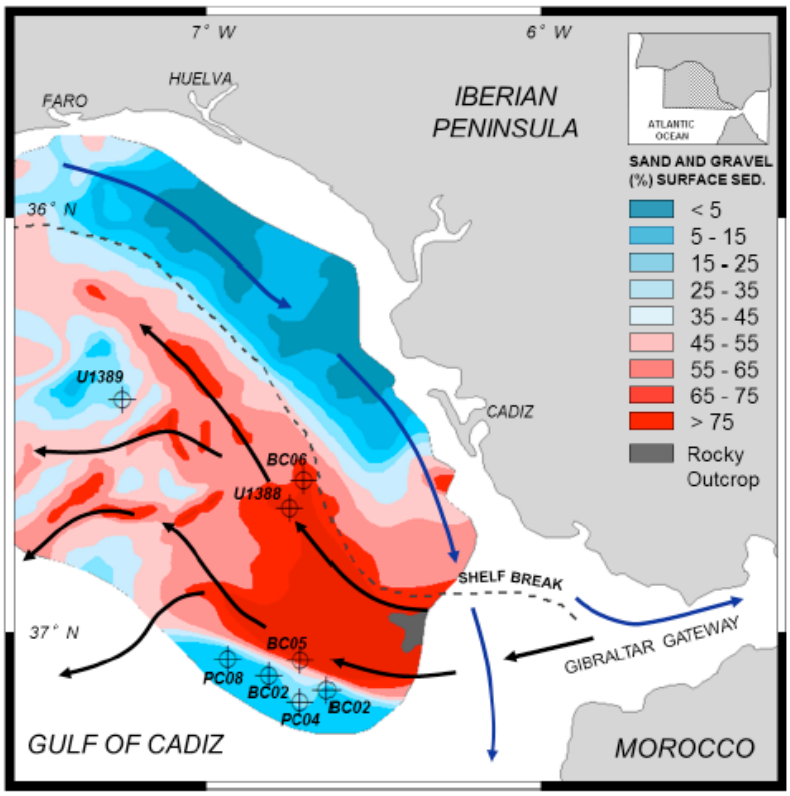

Figure 7.4 – Actual sand distribution across the Gulf of Cadiz. Brackenridge (2014) modified from Nelson *et al*. (1993).

7.2.4 Climatic Fluctuations

As previously mentioned, contourite formation is associated with intensifications and variations of bottom-currents (Stow *et al*., 2008, 2009). Bottom-current strength and velocity controls drift morphology and facies, in addition to the erosion or deposition of the seafloor. Bottom-currents need to be stable and semi-permanent to have effective re-working, transportation and deposition of sediments. Velocities at > 0.1 ms^{-1} establish this premise and velocities < 0.5 ms^{-1} force seafloor erosion and non-deposition (Stow *et al*., 2009). This variation of velocities translates to long or short-term cyclicity in the seismic facies. The cyclicity has been interpreted as related to climatic and sea-level changes, which induce bottom-current fluctuations.

The conventional depositional model usually shows second- and third-order changes of sea-level (1-10 Ma duration), while parasequences show third- and fourth-order changes (100 ky to 1 Ma duration), and internal variations of the successions reflect higher frequency (10 to 100 ky intervals) (Myers and

Milton, 1996). Drift systems can however span two or more normal depositional successions (Fulthorpe *et al*., 2010).

The GCCDS was developed in the last 5 Ma due to the MOW's outflow (Hernández-Molina *et al*., 2003, 2006; Llave *et al*., 2007b). The contourite drifts of the GCCDS have cyclical facies with numerous seismic successions and sub-successions (Llave *et al*., 2001, 2006; Stow *et al*., 2002c). This cyclicity is also observed in the stacking pattern of the SD. Therefore, climatic and eustatic variations have affected the SD since the establishment of the MOW in the Early Pliocene.

In the Late Pliocene, the period between the LPD and the EQD (seismic horizon H3 to H4, 3.2-2.4 Ma) marks a major enhancement of the MOW with higher salinity and density (Hernández-Molina *et al*., 2015). This event is characterized by enhanced bottom-current circulation, derived from the growth and southward advance of ice-sheets in the Northern Hemisphere and increasing arid and cold conditions in the Mediterranean and Atlantic regions (Hayward *et al*., 2009; Khélifi *et al*., 2009, 2014). These conditions triggered the formation of saltier and intense MOW and a shift from sheeted to mounded drift in the SD, with considerable paleomoat formation (Table 7.1).

Although other influential climatic and sea-level changes also occurred in the Middle Pleistocene, which generated MOW intensifications. In the Middle Pleistocene, two important climatic events seem to have affected the SD depositional evolution: the MPR (0.7-0.78 Ma) and the LQD (~0.4 Ma) (Miller *et al*., 2005; Llave *et al*., 2007b; Lofi *et al*., 2016). The MPR, marked by seismic horizon H6A, is considered as one of the most important climatic changes in the Northern Hemisphere (Hernández-Molina *et al*., 2014a). The MPR occurred due to the growth of ice sheets in the Northern Hemisphere and coincided with a shift to longer glaciations and shorter interglaciations (Hayward *et al*., 2009; Lofi *et al*., 2016). Seismic data shows the MPR is marked by a change in drift architecture, from mounded to plastered, as well as highly cyclical facies with high to low amplitude reflections and minor erosive surfaces (Figure 6.14 and Figure 6.22). At Site U1391, the MPR is characterized by an increase of coarser-grained sediments and bigradational contourite successions. The LQD, marked by seismic horizon H6B, coincides with a cold period in the Mediterranean region during the Pleistocene, formed by the advance of ice sheets towards lower latitudes (Hayward *et al*., 2009; Lofi *et al*., 2016). Seismic data shows the LQD is characterized by a small paleomoat and high amplitude basal reflections. Therefore, the cyclicity of the SD seismic facies have been interpreted as a result of major long-term variations of bottom-current intensity and depth, controlled by climatic-eustatic fluctuations (Table 7.1).

The available evidence suggests that the greatest contourite accumulation occurred during times of glacio-eustatic lowstand with sediment directly supplied to the slope from the continental shelf and a vigorous deep and dense MOW flowing along the margin. Several authors have described a saltier, denser and enhanced MOW during glacial times, settling at 700 m deeper than today (the MOW's main core flows at ~800 m depth in the Present and flowed at 1600-2200 m depth in the past) (Cacho *et al*., 2000, 2002; Rogerson *et al*., 2005, 2012; Voelker *et al*., 2006; Toucanne *et al*., 2007; García *et al*., 2009; Hernández-Molina *et al*., 2014a). The enhancement of the MOW probably occurred during Heinrich events, Dansgaard-Oeschger stadials and Younger Dryas (Sierro *et al*., 2005, Llave *et al*., 2006, Voelker *et al*., 2006). By contrast, during the interglacials and warm-water highstands the MOW was weaker and sub-divided into several branches, with the upper branch flowing at 600-1000 m depth (Stow *et al*., 2002c; Rogerson *et al*., 2005). The present circulation was established after the Younger Dryas, between 7.5 and 5.5 ka (Rogerson *et al*., 2005, 2006; García *et al*., 2009).

Table 7.1. – Late Miocene to Quaternary evolution of the SD, characterized by three growth phases with distinct seismic and lithological character. Paleogeographic events, glacio-eustatic sea-level changes and transgressive-regressive cycles associated with the formation of the SD are also included. Glacio-eustatic data and T-R cycles extracted from Haq *et al*. (1987), Llave *et al*. (2007b), Hernández-Molina *et al*. (2002, 2015), Ogg and Ogg (2008), De Boer *et al*. (2010) and Miller *et al*. (2011).

SINES DRIFT

Age (Ma)		Glacio-Eustatic Sea-Level Changes (m)	T-R cycles			Seismic characteristics	Drift Construction	
0.0117	Holo	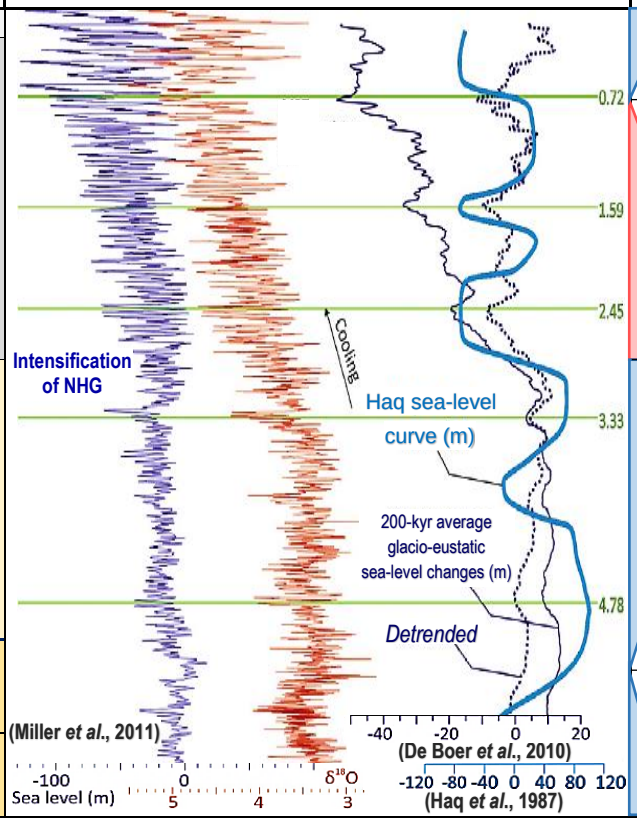		U6	QIV	Continuous high reflections	Plastered Drift	Drift aggradation
					QIII	**LQD** Sandy/muddy		Moat and small paleomoats
0.72	Pleistocene					**MPD** contourites		**Plastered drift**
				U5	QII	Subparallel high to low amplitude reflections	Mounded Drift	Southward drift progradation Northward drift aggradation
				U4	QI	Mud rich contourites		Paleomoats development
2.4						**EQD**		**Mounded drift**
				U3	PII	**LPD**		
3.3								
	Pliocene			U2	PI	Divergent continuous low amplitude reflections Mud rich contourites Mixed system	Sheeted Contourite Drift	Drift aggradation Vertical growth stage **Sheeted drift** **DEVELOPMENT OF MOW**
5.33								
	Late Miocene			U1	M	**B Discontinuity**		Opening of the Gibraltar Strait **Messinian Salinity Crisis**
						Pre-drift deposits		

7.2.5 Slope Instability

The occurrence of MTD is usually related to slope instability. MTD can occur as a result of predispositioning and triggering factors that predispose the slope to become unstable (Leroueil *et al*., 2005). The formation of MTD can generate other hazards, although their danger depends on their size, type, scale, location and process (Rebesco and Camerlenghi, 2008). For example, tsunamis are a well-known associated risk. There are historical tsunamis attributed to the formation of slides or slumps: Grand Banks, 1929; Sagami Bay, Great Tokyo Earthquake, 1923; Port Royal, Jamaica, 1692; Ishigaki Island, Japan, 1771; Valdez, Alaska, 1964; Lituya Bay, Alaska, 1958 (Bryant, 2001).

From the several triggers of slope failure, we will only refer to the ones active in the study area: oversteepening and seismic activity (Leroueil *et al*., 2005).

The joint analysis of the multibeam bathymetry and the seismic profiles showed that the western sector of the SD is affected by slope failure while resulting MTD accumulated at the footwall of the PSF, in the Rincão do Lebre Basin (Figure 7.5). The area of the SD affected by slope failure extends for over 50 km long and 20 km wide (Roque *et al*., 2015; Figure 6.1). It was previously seen in Chapter 6, Point 6.7 that the MTD occur mainly after the deposition of seismic unit U4 of Early Quaternary age. The MTD also seem to be associated with the steep slope of the PSF escarpment (~20º gradient, dipping towards west). The steepness of the PSF escarpment seems to favor the occurrence of slope failure (Figure 7.5).

The eastward extension of the SD is not significantly affected by downslope processes (notwithstanding the debrite of ~0.35 m in the Late Pliocene at Site U1391) due to the paleomorphology of the margin and due to the São Vicente and Setúbal canyons, which take most of the downslope sediment supply.

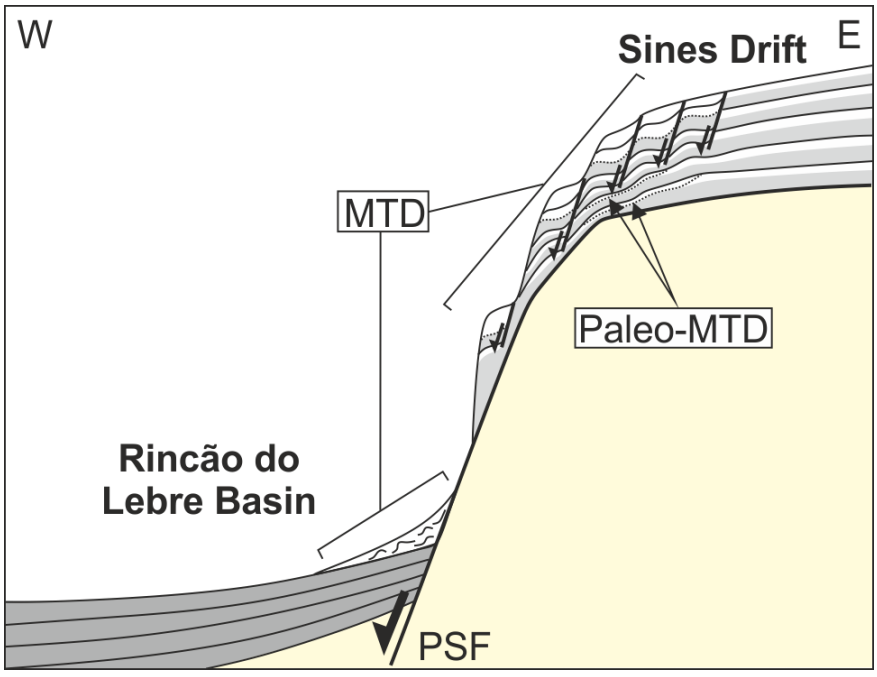

Figure 7.5 – Representation of the formation and accumulation of MTD and paleo-MTD, associated with the PSF escarpment.

Another triggering factor to take in consideration is seismic activity (Gràcia *et al*., 2003b; Masson *et al*., 2006; Stigall and Dugan, 2010; Urlaub *et al*., 2013). Instrumental seismic activity on the offshore SW Portugal is moderated (M<5) but this area has been stroked by higher magnitude events, such as the

1969's tsunami and earthquake (M=7.8; Fukao, 1973) and the Great Lisbon Earthquake and Tsunami on the 1st November 1755 (M=8,5-9; Johnston, 1996). Another important historical seismic event is the 1531 Lisbon Earthquake on the 26th January 1531, which was felt on the Lisbon and Tagus margin (Justo and Salwa, 1998; Miranda *et al*., 2012). It is not known if these events are associated with the formation of MTD, although it proves that high magnitude earthquakes can occur in the study area and potentially trigger downslope events (Terrinha *et al*., 2003).

Predispositioning factors also influence slope instability, such as the properties of the sediments, high sedimentation rates, excess pore pressure, unfavorable layering or weak layers (Leroueil *et al*., 2005). The joint occurrence of contourites and mass movement deposits is recognized in several geological and oceanographic settings (Bryn *et al*., 2005; Hernández-Molina *et al*., 2014a,b; Roque *et al*., 2015). This association has been studied for the development of the Storegga Slide in Norway. The Storegga Slide is the largest known submarine slide with ~3500 km^3 (Bondevik *et al*., 2003, 2006, 2012). This slide corresponds to a collapse of ~290 km along the Norwegian margin and a movement over 500 km with >50 m/s velocity (Bondevik *et al*., 2003, 2006, 2012). It is constituted by deposits with average and maximum thicknesses of 88 m and 450 m, respectively. According to Lisa (2014), this event occurred in the Holocene due to seismic activity, which caused dissociation of methane hydrates. However, the existence of contourite sediments was considered as a potential predisposition for the submarine slide (Bryn *et al*., 2005). The contourites are characterized by high mud contents, plasticity and water content, and therefore might have worked as weak predispositioning layers for the slide (Bryn *et al*., 2005). Also, the quick sedimentation of glacial deposits over the contourites could have caused a rapid increase of pore pressure inside the contouritic sediments and the occurrence of the submarine slide (Bondevik *et al*., 2003; Bünz *et al*., 2003).

In the case of the SD, it shows a considerable thickness (1000-1200 m) due to the paleomorphology of the margin and a moderate to high sedimentation rate, estimated at 13 cm/k.y during the Pliocene, 17 cm/k.y for the Early Pleistocene (2.588-1.5 Ma) and 27 cm/k.y for the Pleistocene (from ~1.5 Ma to the seafloor) (Expedition 339 Scientists, 2012). This thickness would create overloading and excessive pore pressure inside the contourites, overcoming the hydrostatic pressure (Iverson, 1997). The excess pore pressure supports most of the weight of the sedimentary column above and reduces tension, triggering an MTD (Iverson, 1997).

It was previously seen that seismic units U4 to U6 ranging from the Early Quaternary to the present-day are constituted by numerous bigradational contourite successions and six coarse to fine-grained sandy intervals (see Chapter 6, Point 6.4). These sandy intervals can be under excess pore pressure due to their own characteristics (density, porosity and water content) and due to unfavorable layering (dense material deposited above less dense material or loose sand under a low permeability layer). Therefore, the presence of contouritic sediments within the sedimentary column might act as a pre-conditioning factor for slope instability (Bryn *et al*., 2005; Roque *et al*., 2015).

CHAPTER 8

CONCLUSIONS

This work proposed an evolutionary model for the Sines Drift as well as the identification of its main driving mechanisms and constraints. The main conclusions of this study can be summarized as follows:

- Seismic stratigraphy interpretation of a newly acquired seismic reflection dataset on the Sines Contourite Drift allowed the identification of six seismic units (U1 to U6) from Late Miocene to Holocene age: the Late Miocene unit (U1) overlaying the B unconformity; the Pliocene to Early Quaternary units (U2 and U3) characterized by a mixed system; the Early to Mid-Pleistocene units (U4 and U5) marked by muddy contourites and severe paleomoats along the east; and the Mid-Pleistocene to Holocene unit (U6) characterized by interbedded sandy-muddy contourites and moats;

- Three evolutionary phases are identified for the SD development: 1) a sheeted-contourite-drift phase (<5.3-3.2 Ma) built since the Late Miocene by an initially weak flowing MOW; 2) a mounded-contourite-drift phase (3.2-0.7 Ma) from Late Pliocene to Early Quaternary times characterized by a mounded drift in the south and sheeted in the north, with a succession of sinuous N-S paleomoats in the east built as a result of MOW enhancement; and 3) a plastered-contourite-drift phase from Mid-Pleistocene (0.7 Ma) till the present-day, characterized by the present depositional (sandy-muddy drifts) and erosional (moats) contourite features associated with two major events of MOW intensification;

- The growth of the Sines Drift was constrained, in a long-term, by seafloor morphologies that resulted from the Mesozoic rifting processes of the Southwest Portuguese margin. The paleomorphology provided ample accommodation space for drift growth and conditioned its overall architecture. The N-S horsts (h1 and h2) built during the Mesozoic rifting, confined drift formation and did not allow lateral migration. This indicates that past-tectonics considerably restrained general basin geometry and contourite drift deposition and edification;

- The formation of the Sines Drift has been influenced, in short-term, by climatic fluctuations and sea-level changes, especially during the Quaternary. Since the Mid-Pleistocene the architecture of the drift was mainly influenced by climatic and sea-level changes instead of tectonics, since there is no tectonic deformation during this stage and the drift presents a change in morphology (from mounded to plastered) with a higher number of sandy contourite layers (six in total), probably related to several episodes of bottom-current enhancement and therefore associated with climatic and sea-level changes;

- The higher thickness of the Late Miocene unit U1 may point to the occurrence of enhanced bottom-current circulation. Since the Early Pliocene, the exit of the warmer and more saline MOW from the Strait of Gibraltar into the intermediate depths of the North Atlantic Ocean probably enhanced bottom water generation and aided the initially weak MOW to construct the sheeted drift;

- The occurrence in the Early to Late Quaternary (seismic units U4 to U6) of a succession of staking N-S paleomoats beneath the present-day moat suggests a persistent and semi-permanent, northward flowing MOW with several phases of enhancement;
- Sediment supply was mainly sourced by alongslope and pelagic processes, as well as erosion of the continental slope by the MOW and its interaction with the seafloor. It was also perceived that the São Vicente and Setúbal canyons took most of the downslope sediment supply since they bound the drift to the south and north, respectively;
- The occurrence of mass-movement processes in the west is mainly associated with the steep gradient of the Pereira de Sousa Scarp. These processes occurred since the deposition of seismic units U4 to U6, which are characterized by sandy-muddy contourites and these sediments could act as a predispositioning factor. However, a complex mix of triggering and predispositioning factors are at work, such as seismicity, oversteepening, the properties of the sediments, high sedimentation rates and excess pore pressure.

All these results suggest the Sines Drift had a complex evolution from the Late Miocene to the Present, controlled by several factors at different scales and by the interactions between them. Therefore, the build-up of the Sines Drift in the Alentejo margin has been controlled by a complex combination of tectonics, bottom-current circulation, variations of sediment supply, climatic fluctuations and sea-level changes.

8.1 Future Work

This work was a step forward, to better understand the evolution of the distal sector of the Gulf of Cadiz Contourite Depositional System in the framework of the Mediterranean-Atlantic exchanges previously, during and after the Messinian Salinity Crisis. Hence, there is a need to investigate the questions that remained unanswered: i) how was the MOW circulation in the bottom-current system of the Late Miocene, ii) are there drifts further north, associated with the MOW or with another bottom-current system, iii) what is the lithology of the Late Miocene units, and iv) what is the age of the MTD accumulated along the Pereira de Sousa Scarp? In order to answer these questions, a few works will be needed:

- New data as seismic reflection profiles and wells for a detailed chronologic and lithologic study of the Miocene sedimentary record;
- A detailed microscopic and geochemical characterization of the sandy contourite layers, as well as the debrite and the dolomitic mudstone observed in the cores of Expedition 339 Site U1391, to understand their genesis;
- Construction of computational models to predict the pathway of the MOW along the western Portuguese margin to investigate the formation of other distal and older drifts.

9. BIBLIOGRAPHIC REFERENCES

Anderson P. and Newric R. (2008) – Strange but true stories of synthetic seismograms. *CSEG Recorder*, 33, 10, 51-56 pp.

Alonso, B.; Ercilla, G.; Casas, D.; Stow, D., Rodríguez-Tovar, F.; Dorador, J. and Hernández-Molina, F. (2016) – Contourite vs gravity-flow deposits of the Pleistocene Faro Drift (Gulf of Cadiz): Sedimentological and mineralogical approaches. *Marine Geology*, 377, 77-94 pp.

Alves, T. M.; Gawthorpe, R. L.; Hunt, D. and Monteiro, J. H. (2000) – Tertiary evolution of the São Vicente and Setúbal submarine canyons, Southwest Portugal: insights from seismic stratigraphy. *Ciências da Terra*, 14, 243-256 pp.

Alves, T. M.; Gawthorpe, R. L.; Hunt, D. W. and Monteiro, J. H. (2002) – Jurassic tectono-sedimentary evolution of the Northern Lusitanian Basin (offshore Portugal). *Marine and Petroleum Geology*, 19, 727-754 pp.

Alves, T. M.; Gawthorpe, R. L.; Hunt, D. W. and Monteiro, J. H. (2003) – Cenozoic tectono-sedimentary evolution of the western Iberian margin. *Marine Geology*, 195, 75-108 pp.

Alves, T. M.; Moita, C.; Sandes, F.; Cunha, C.; Monteiro, J. H. and Pinheiro, L. M. (2006) – Mesozoic-Cenozoic evolution of North Atlantic continental-slope basins: The Peniche basin, western Iberian margin. *American Association of Petroleum Geologists Bulletin*, 90 (1), 31-60 pp.

Alves, T. M.; Moita, C.; Cunha, T.; Ullnaess, M.; Myklebust, R.; Monteiro, J. and Manuppella, G. (2009) – Diachronous evolution of late Jurassic-cretaceous continental rifting in the northeast Atlantic (west Iberian margin). *Tectonics*, 28 (TC4003), 32 pp.

Alves, T. M.; Cunha, T. A.; Moita, C.; Terrinha, P.; Hipólito, M. J. and Manupella, G. (2013) – A evolução de bacias sedimentares tipo-rift em margens continentais passivas: o exemplo da Margem Ocidental Ibérica. *In:* R. Dias; A. Araújo; P. Terrinha and J. C. Kullberg (Eds.), *Geologia de Portugal, Volume II: Geologia Meso-cenozóica de Portugal*, Escolar Editora, Lisboa, III.4., 349-404 pp.

Ambar, I. (1983) – A shallow core of Mediterranean water off western Portugal. *Deep-Sea Research*, Vol. 30 (6A), 677-680 pp.

Ambar, I. and Howe, M. R. (1979) – Observations of the Mediterranean outflow-II. The deep circulation in the vicinity of the Gulf of Cadiz. *Deep-Sea Research*, 26(A), 555-568 pp.

Ambar, I.; Serra, N.; Brogueira, M. J.; Cabeçadas, G.; Abrantes, F.; Freitas, P.; Gonçalves, C. and Gonzalez, N. (2002) – Physical, chemical and sedimentological aspects of the Mediterranean outflow off Iberia. *Deep-Sea Research Part I: Oceanographic Research Papers*, 49, 4163-4177 pp.

Ambar, I.; Serra, N.; Neves, F. and Ferreira, T. (2008) – Observations of the Mediterranean undercurrent and eddies in the gulf of cádiz during 2001. *Journal of Marine Systems*, 71 (1-2), 195-220 pp.

Azerêdo, A. C.; Ramalho, M. M. and Wright, V. P. (1998) – The Middle-Upper Jurassic disconformity in the Lusitanian Basin, Portugal: preliminary facies analysis and evidence for palaeoclimatic fluctuation. *Cuadernos de Geologia Ibérica*, 29, 99-119 pp.

Azerêdo, A. C.; Wright, V. P. and Ramalho, M. M. (2002) – The Middle-Late Jurassic forced regression and disconformity in central Portugal: eustatic, tectonic and climatic effects on a carbonate ramp system. *Sedimentology*, 49 (6), 1339-1370 pp.

Azerêdo, A.C.; Duarte, L. V.; Henriques, M. H. and Manupella, G. (2003) – Da dinâmica continental no Triásico aos mares do Jurássico Inferior e Médio. *Cadernos de Geologia de Portugal, Instituto Geológico e Mineiro*, Lisboa, 43 pp.

Bache, F.; Popescu, S.-M.; Rabineau, M.; Gorini, C.; Suc, J.-P.; Clauzon, G.; Olivet, J.-L.; Rubino, J.-L.; Melinte-Dobrinescu, M.; Estrada, F.; Londeix, L.; Armijo, R.; Meyer, B.; Jolivet, L.; Jouannic, G.; Leroux, E.; Aslanian, D.; Tadeu Dos Reis, A.; Mocochain, L.; Dumurdzanov, N.; Zagorchev, I.; Lesic, V.; Tomic, D.; Catagay, M.; Brun, J.-P.; Sokoutis, D.; Csato, I.; Ucarkus, G. and

Cakir, Z. (2012) – A two step process for the reflooding of the Mediterranean after the Messinian Salinity Crisis. *Basin Research*, 24, 125-153 pp.

Badagola, A. P. L. (2008) – Evolução morfo-tectónica da plataforma continental do Esporão da Estremadura. MSc thesis, Universidade de Lisboa, Lisboa, 171 pp.

Baringer, M. and Price, J. (1997) – Mixing and spreading of the Mediterranean outflow. *Journal of Physical Oceanography*, 27 (8), 1654-1677 pp.

Baringer, M. and Price, J. (1999) – A review of the physical oceanography of the Mediterranean outflow. *Marine Geology*, 155, 63-82 pp.

Bartoli, G.; Sarnthein, M.; Weinelt, M.; Erlenkeuser, H.; Garbe-Schönberg, D. and Lea, D.W. (2005) – Final closure of panama and the onset of northern hemisphere glaciation. *Earth and Planetary Science Letters*, 237, 33-44 pp.

Batista., L. (2009) – Cartografia da Deformação Tectónica de Idade Pliocénica e Quaternária na Planície Abissal do Tejo, Talude e Plataforma Continental Adjacentes com Base na Interpretação de Perfis Sísmicos de Reflexão e Batimetria Multifeixe. MSc thesis, Universidade de Lisboa, Lisboa, 84 pp.

Becker, J.; Lourens, L. J. and Raymo, M. E. (2006) – High-frequency climate linkages between the North Atlantic and the Mediterranean during marine oxygen isotope stage 100 (MIS100). *Paleoceanography*, 21 (PA3002), 1-14 pp.

Béthoux, J.-P. and Pierre, C. (1999) – Mediterranean functioning and sapropel formation: respective influences of climate and hydrological changes in the Atlantic and the Mediterranean. *Marine Geology*, 153, 29-39 pp.

Blum, P. (1997) – Physical properties handbook: a guide to the shipboard measurement of physical properties of deep-sea cores. *ODP Technical Note*, 26

Bondevik, Stein; Dawson, Sue; Dawson, Alastair; Lohne, Øystein; Dawson, Sue; Dawson, Alastair and Lohne, Øystein (2003) – Record-breaking Height for 8000-Year-Old Tsunami in the North Atlantic. *Eos, Transactions of the American Geophysical Union*, 84 (31), 289-300 pp.

Bondevik, S.; Lovholt, F.; Harbitz, C.; Stormo, S. and Skjerdal, G. (2006) – The Storegga Slide Tsunami – Deposits, Run-up Heights and Radiocarbon Dating of the 8000-Year-Old Tsunami in the North Atlantic. *American Geophysical Union meeting*, 87 (52), 0S34C-01.

Bondevik, S.; Stormo, S. K. and Skjerdal, G. (2012) – Green mosses date the Storegga tsunami to the chilliest decades of the 8.2 ka cold event. *Quaternary Science Reviews*, 45, 1-6 pp.

Bower, A. S.; Armi, L. and Ambar, I. (1994) – Direct evidence of meddy formation off the southwestern coast of Portugal. *Deep-Sea Research Part I: Oceanographic Research Papers*, 42 (9), 1621-1630 pp.

Bower, A.; Serra, N. and Ambar, I. (2002) – Structure of the Mediterranean undercurrent and Mediterranean water spreading around the southwestern Iberian Peninsula. *Journal of Geophysical Research*, 107 (C10), 1-19 pp.

Brackenridge, R. E. (2014) – Contourite Sands in the Gulf of Cadiz: Characterisation, Controls and Wider Implications for Hydrocarbon Exploration. PhD thesis, Heriot-Watt University, Institute of Petroleum Engineering, Edinburgh, 257 pp.

Brackenridge, R.; Stow, D. and Hernández-Molina, F. (2011) – Contourites within a deep-water sequence stratigraphic framework. *Geo-Marine Letters*, 31, 343-360 pp.

Brackenridge, R. A.; Hernández-Molina, F. J.; Stow, D. A. V. and Llave, R. (2013) – A Pliocene mixed contourite-turbidite system offshore the Algarve Margin, Gulf of Cadiz: Seismic response, margin evolution and reservoir implications. *Marine and Petroleum Geology*, 46, 36-50 pp.

Bronner, A.; Sauter, D.; Manatschal, G.; Péron-Pinvidic, G. and Munschy, M. (2011) – Magmatic breakup as an explanation for magnetic anomalies at magma-poor rifted margins. *Nature Geoscience*, 4, 549-553 pp.

Bryant, E. A. (2001) – *Tsunami. The underrated hazard*. Springer, Verlag Berlin Heidelberg, 2, 330 pp.

Bryn, P.; Berg, K.; Stoker, M. S.; Haflidason, H. and Solheim, A. (2005) – Contourites and their relevance for mass wasting along the Mid-Norwegian Margin. *Marine and Petroleum Geology*, 22, 85-96 pp.

Bünz, S.; Mienert, J. and Berndt, C. (2003) – Geological controls on the Storegga gas hydrate system of the mid-Norwegian continental margin. *Earth and Planetary Science Letters*, 209, 291-307 pp.

Cacho, I.; Grimalt, J. O.; Sierro, F. J.; Shackleton, N. J. and Canals, M. (2000) – Evidence of enhanced Mediterranean thermohaline circulation during rapid climatic coolings. *Earth and Planetary Science Letters*, 183, 417-429 pp.

Cacho, I.; Grimalt, J. O. and Canals, M. (2002) – Response of the Western Mediterranean Sea to rapid climatic variability during the last 50,000 years: a molecular biomarker approach. *Journal of Marine Systems*, 33-34, 253-272 pp.

Cacho, I.; Shackleton, N.; Elderfield, H.; Sierro, F. J. and Grimaltd, J. O. (2006) – Glacial rapid variability in deep-water temperature and δ18O from the Western Mediterranean Sea. *Quaternary Science Reviews*, 25, 3294-3311 pp.

Cannon, S. (2016) – *Petrophysics: A Practical Guide*. Wiley-Blackwell, 224 pp.

Cita, M. B. (2001) – The Messinian salinity crisis in the Mediterranean. *In:* U. Briegel and W. Xiao (Eds.), *Paradoxes in Geology*. Elsevier Science, 353-360 pp.

Criado-Aldeanueva, F.; García-Lafuentea, J.; Vargas, J. M.; Del Río, J.; Vázquez, A.; Reul, A. and Sánchez, A. (2006) – Distribution and circulation of water masses in the Gulf of Cadiz from in situ observations. *Deep-Sea Research Part II: Topical Studies in Oceanography*, 53, 1144-1160 pp.

Cunha, T. A.; Watts, A. B.; Pinheiro, L. M. and Alves, T. M. (2009) – West Iberia Margin Subsidence-Uplift History: Constraints from Seismic Data and Well and Pseudo-well Backstripping. *6º Simposio sobre el Margen Ibérico Atlántico*, Oviedo, Spain, 29-32 pp.

Cunha, T. A.; Watts, A. B.; Pinheiro, L. M. and Myklebust, R. (2010) – Seismic and gravity anomaly of large-scale compressional deformation of SW Portugal. *Earth and Planetary Science Letters*, 293 (1-2), 171-179 pp.

Cunha, T. A.; Matias, L. M.; Terrinha, P.; Negredo, A. M.; Rosas, F.; Fernandes, R. M. S. and Pinheiro, L. M. (2012) – Neotectonics of the SW Iberia margin, Gulf of Cadiz and Alboran Sea: a reassessment including recent structural, seismic and geodetic data. *Geophysics Journal International*, 188, 850-872 pp.

Cunningham, A. D. and Droxler, A. W. (2000) – Synthetic seismogram generation and seismic facies to core lithology correlation for Sites 998, 1000, and 1001. *In:* R. M. Leckie; H. Sigurdsson; G. D. Acton and G. Draper (Eds.), *Proceedings of the Ocean Drilling Program, Scientific Results*, 165, 205-217 pp.

De Boer, B.; Van de Wal, R. S. W.; Bintanja, R.; Lourens, L. J. and Tuenter, E. (2010) – Cenozoic global ice-volume and temperature simulations with 1-D ice-sheet models forced by benthic δ18O records. *Annals of Glaciology*, 51 (55), 23-33 pp.

Dowsett, H. J.; Cronin, T. M.; Poore, R. Z.; Thompson, R. S.; Whatley, R. C. and Wood, A.M. (1992) – Micropaleontological evidence for increased meridional heat transport in the North Atlantic Ocean during the Pliocene. *Science*, 258, 1133-1135 pp.

Dowsett, H. J.; Barron, J. A.; Poore, R. Z.; Thompson, R. S.; Cronin, T. M.; Ishman, S. E. and Willard, D. A. (1999) – Middle Pliocene palaeoenvironmental reconstruction: PRISM2. *US Geological Survey Open File Report*, 99-535 pp.

Dowsett, H. J.; Robinson, M. M. and Foley, K. M. (2009) – Pliocene three-dimensional global ocean temperature reconstruction. *Climate of the Past*, 5, 769-783 pp.

Duarte, J. C.; Rosas, F. M.; Terrinha, P.; Gutscher, M.-A.; Malavieille, J.; Silva, S. and Matias, L. (2011) – Thrust-wrench interference tectonics in the gulf of Cadiz (Africa-Iberia plate boundary in the north-east Atlantic): insights from analog models. *Marine Geology*, 289, 135-149 pp.

Duarte, J. C.; Rosas, F. M.; Terrinha, P.; Schellart, W. P.; Boutelier, D.; Gutscher, M.-A. and Ribeiro, A. (2013) – Are subduction zones invading the Atlantic? Evidence from the southwest Iberia margin. *Geology*, 41, 839-842 pp.

Ducassou, E.; Fournier, L.; Sierro, F. J.; Alvarez Zarikian, C. A.; Lofi, J.; Flores, J. A. and Roque, C. (2015) – Origin of the large Pliocene and Pleistocene debris flows on the Algarve margin. *Marine Geology*, 377, 58-76.

Duggen, S.; Hoernle, K.; Van den Bogaard, P.; Rüpke, L. and Morgan, J. P. (2003) – Deep roots of the Messinian salinity crisis. *Nature*, 422 (6932), 602-606 pp.

Ellis, D. V. and Singer, J. M. (2007) – *Well Logging for Earth Scientists*. Springer, Dordrecht, Netherlands, 2, 692 pp.

Estrada, F.; Ercilla, G.; Gorini, C.; Alonso, B.; Vázquez, J. T.; García-Castellanos, D.; Juan, C.; Maldonado, A.; Ammar, A. and Elabbassi, M. (2011) – Impact of pulsed Atlantic water inflow into the alboran basin at the time of the zanclean flooding. *Geo-Marine Letters*, 31, 361-376 pp.

Expedition 339 Scientists (2012) – Mediterranean outflow: environmental significance of the Mediterranean outflow water and its global implications. *Proceedings of the Integrated Ocean Drilling Program, Scientific Results*, 339, 106 pp.

Faugères, J.-C. and Stow, D. A. V. (2008) – Contourite Drifts: Nature, Evolution and Controls. *In:* M. Rebesco and A. Camerlenghi (Eds.), *Contourites*. Developments in Sedimentology, Elsevier, Amsterdam, 60, 257-288 pp.

Faugères, J.; Gonthier, E. and Stow, D. (1984) – Contourite drift molded by deep Mediterranean Outflow. *Geology*, 12 (5), 296-300 pp.

Faugères, J.; Mezerais, M. and Stow, D. (1993) – Contourite drifts types and their distribution in the North and South-Atlantic Ocean Basins. *Sedimentary Geology*, 82 (1-4), 189-203 pp.

Faugères, J.-C.; Stow, D. A. V.; Imbert, P. and Viana, A. R. (1999) – Seismic features diagnostic of contourite drifts. Marine Geology, 162, 1-38 pp.

Fiúza, A.; Hamann, M.; Ambar, I.; Díaz del Río, G.; Gonzaléz, N. and Cabanas, J. (1998) – Water masses and their circulation off western Iberia during May 1993. *Deep-Sea Research Part I: Oceanographic Research Papers*, 45, 1127-1160 pp.

Flecker, R.; Krijgsman, W.; Capella, W.; Martins, C.; De, C.; Demitrieva, E.; Mayser, J. P.; Marzocchi, A.; Modestu, S.; Ochoa Lozano, D.; Simon, D.; Tulbure, M.; Van den Berg, B.; Van der Schee, M.; de Lange, G.; Ellam, R.; Govers, R.; Gutjahr, M.; Hilgen, F.; Kouwenhoven, T.; Lofi, J.; Meijer, P.; Sierro, F. J.; Bachiri, N.; Barboun, N.; Chakor Alami, A.; Chacon, B.; Flores, J. A.; Gregory, J.; Howard, J.; Lunt, D.; Ochoa, M.; Pancost, R.; Vincent, S. and Yousfi, M. Z. (2015) – Evolution of the late Miocene Mediterranean-Atlantic gateways and their impact on regional and global environmental Change. *Earth-Science Reviews*, 150, 365-392 pp.

Flinch, J. and Vail, P. (1998) – Plio-Pleistocene sequence stratigraphy and tectonics of the Gibraltar Arc. *In:* P. De Graciansky; J. Hardenbol; T. Jacquin and P. Vail (Eds.), *Mesozoic and Cenozoic Sequence Stratigraphy of European Basins*, Society for Sedimentary Geology, 60, 199-208 pp.

FLTC Services Ltd. (2009) – Seismic Surveys. Accessed at: http://fishsafe.eu/en/offshorestructures/seismic-surveys.aspx on 16/12/2015.

Fukao, Y. (1973) – Thrust faulting at a lithospheric plate boundary the Portugal earthquake of 1969. *Earth and Planetary Science Letters*, 18 (2), 205-216 pp.

Fulthorpe, C.; Lu, H. and IODP Expedition Shipboard Scientific Party (2010) – Contourites and slope progradation: Canterbury Basin, New Zealand. *Geo-Temas*, 11, 45-46 pp.

García, M.; Hernández-Molina, F. J.; Llave, E.; Stow, D. A. V.; León, R.; Fernández-Puga, M. C.; Díaz del Río, V. and Somoza, L. (2009) – Contourite erosive features caused by the Mediterranean outflow water in the gulf of Cadiz: Quaternary tectonic and oceanographic implications. *Marine Geology*, 257, 24-40 pp.

García, M.; Hernández-Molina, F. J.; Alonso, B.; Vázquez, J. T.; Ercilla, G.; Llave, E. and Casas, D. (2015) – Erosive sub-circular depressions on the Guadalquivir Bank (Gulf of Cadiz): Interaction between bottom current, mass-wasting and tectonic processes. *Marine Geology*, 378, 5-19 pp.

Garcia-Castellanos, D.; Estrada, F.; Jiménez-Munt, I.; Gorini, C.; Fernàndez, M.; Vergés, J. and De Vicente, R. (2009) – Catastrophic flood of the Mediterranean after the Messinian salinity crisis. *Nature*, 462 (7274), 778-781 pp.

Garcia-Mondejar, J. (1989) – Strike-slip subsidence of the Basque-Cantabrian Basin of northern Spain and its relationship to Aptian-Albian opening of Bay of Biscay. *In:* A. J. Tankard and H. R. Balkwill (Eds.), *Extensional tectonics and stratigraphy of the North Atlantic margins*, American Association of Petroleum Geologists, 46, 395-409 pp.

Gebco (2003) – British Oceanographic Data Centre on behalf of IOC and IHO. GEBCO Digital Atlas.

Gómez, C.; González, E.; Sanchez, H. and Olivé, J. (2014) – Informe Técnico Campaña Mower 2014, 82 pp.

Gonthier, E. G.; Faugères, J.-C. and Stow, D. A. V. (1984) – Contourite facies of the faro drift, gulf of Cadiz. *In:* D. Stow and D. Piper (Eds.), *Fine-Grained Sediments, Deep-Water Processes and Facies.* Geological Society, London, Special Publications, 15, 275-292 pp.

Gràcia, E.; Dañobeitia, J.; Vergés, J.; Bartolomé, R. and Córdoba, D. (2003a) – Crustal architecture and tectonic evolution of the gulf of Cadiz, SW Iberia, at the convergence of the Eurasian and African plates. *Tectonics*, 22 (4), 24 pp.

Gràcia, E.; Dañobeitia, J.; Vergés, J. and PARSIFAL Team (2003b) – Mapping active faults offshore Portugal (36ºN-38ºN): Implications for seismic hazard assessment along the southwest Iberian margin. *Geology*, 31 (1), 83-86 pp.

Grange, M.; Schärer, U.; Cornen, G. and Girardeau, J. (2008) – First alkaline magmatism during Iberia–Newfoundland rifting. *Terra Nova*, 20 (6), 494-503 pp.

Grange, M.; Scharer, U.; Merle, R.; Girardeau, J. and Cornen, G. (2010) – Plume–Lithosphere Interaction during Migration of Cretaceous Alkaline Magmatism in SW Portugal: Evidence from U–Pb Ages and Pb–Sr–Hf Isotopes. *Journal of Petrology*, 51 (5), 1143-1170 pp.

Gutscher, M.-A.; Malod, J.; Rehault, J.-P.; Contrucci, I.; Klingelhoefer, F.; Mendes-Victor, L. and Spakman, W. (2002) – Evidence for active subduction beneath Gilbraltar. *Geology*, 30 (2), 1071-1074 pp.

Gutscher, M.; Dominguez, S.; Westbrook, G.; Gente, P.; Babonneau, N.; Mulder, T.; Gonthier, E.; Bartolome, R.; Luis, J.; Rosas, F.; Terrinha, P. and Delila and DelSis Scientifc Teams (2009) – Tectonic shortening and gravitational spreading in the Gulf of Cadiz accretionary wedge: Observations from multi-beam bathymetry and seismic profiling. *Marine and Petroleum Geology*, 26 (5), 647-659 pp.

Gutscher, M.-A.; Dominguez, S.; Westbrook, G. K.; Le Roy, P.; Rosas, F.; Duarte, J. C.; Terrinha, P.; Miranda, J. M.; Graindorge, D.; Gailler, A.; Sallares, V. and Bartolome, R. (2012) – The Gilbraltar subduction: A decade of new geophysical data. *Tectonophysics*, 574-575, 72-91 pp.

Hanquiez, V.; Mulder, T.; Toucanne, S.; Lecroart, P.; Bonnel, C.; Marchès, E. and Gonthier, E. (2010) – The sandy channel-lobe depositional systems in the Gulf of Cadiz: gravity processes forced by contour current processes. *Sedimentary Geology*, 229, 110-123 pp.

Haq, B. U.; Hardenbol, J. and Vail, P. R. (1987) – Chronology of Fluctuating Sea Levels Since the Triassic. *Science*, 235, 1156-1167 pp.

Hardage, B. A. (2007) – Fundamentals of Geophysics. *In:* E. D. Holstein (Ed.), *Volume V: Reservoir Engineering and Petrophysics*, Society of Petroleum Engineers, Texas, USA, 33 pp.

Harvey, J. (1982) – θ-S relationships and water masses in the eastern North Atlantic. *Deep-Sea Research*, 29 (8A), 1021-1033 pp.

Hay, W. W. (1996) – Tectonic and climate. *Geol. Rundsch*, 85, 409-437 pp.

Hayward, B. W.; Sabaa, A. T.; Kawagata, S. and Grenfell, H. R. (2009) – The Early Pliocene recolonisation of the deep Mediterranean Sea by benthic foraminifera and their pulsed Late Pliocene-Middle Pleistocene decline. *Marine Micropaleontology*, 71, 97-112 pp.

Haywood, A. M.; Sellwood, B. W. and Valdes, P. J. (2000) – Regional warming: Pliocene (3 Ma) paleoclimate of Europe and the Mediterranean. *Geology*, 28 (12), 1063-1066 pp.

Haywood, A. M.; Valdes, P. J. and Sellwood, B. W. (2002) – Magnitude of climate variability during middle Pliocene warmth: a palaeoclimate modelling study. *Palaeogeography, Palaeoclimatology, Palaeoecology*, 188, 1-24 pp.

Heezen, B. and Hollister, C. (1964) – Deep sea current evidence from abyssal sediments. *Marine Geology*, 1, 141-174 pp.

Hernández-Molina, F. J.; Somoza, L.; Vázquez, J. T.; Lobo, F.; Fernández-Puga, M. C.; Llave, E. and Díaz del Río, V. (2002) – Quaternary stratigraphic stacking patterns on the continental shelves of the southern Iberian peninsula: their relationship with global climate and palaeoceanographic changes. *Quaternary International*, 92 (1), 5-23 pp.

Hernández-Molina, F. J.; Llave, E.; Somoza, L.; Fernández-Puga, M. C.; Maestro, A.; León, R.; Barnolas, A.; Medialdea, T.; García, M.; Vázquez, J. T.; Díaz del Río, V.; Fernández- Salas, L. M.; Lobo, F.; Alveirinho Dias, J. M.; Rodero, J. and Gardner, J. (2003) – Looking for clues to paleoceanographic imprints: a diagnosis of the gulf of Cadiz contourite depositional systems. *Geology*, 31 (1), 19-22 pp.

Hernández-Molina, F. J.; Llave, E.; Stow, D. A. V.; García, M.; Somoza, L.; Vázquez, J. T.; Lobo, F. J.; Maestro, A.; Díaz del Río, V.; León, R.; Medialdea, T. and Gardner, J. (2006) – The contourite depositional system of the gulf of Cadiz: a sedimentary model related to the bottom current activity of the Mediterranean outflow water and its interaction with the continental margin. *Deep-Sea Research Part II: Topical Studies in Oceanography*, 53 (11-13), 1420-1463 pp.

Hernández-Molina, F. J.; Serra, N.; Stow, D. A. V.; Llave, L.; Ercilla, E. and Van Rooij, D. (2011) – Along-slope oceanographic processes and sedimentary products around the Iberian margin. *Geo-Marine Letters*, 31 (5), 315-341 pp.

Hernández-Molina, F. J.; Stow, D. A. V.; Alvarez-Zarikian, C.; Acton, G.; Bahr, A.; Balestra, B.; Ducassou, E.; Flood, R.; Flores, J. A.; Furota, S.; Grunert, P.; Hodell, D.; Jimenez-Espejo, F.; Kim, J. K.; Krissek, L., Kuroda, J.; Li, B.; Llave, E.; Lofi, J.; Lourens, L., Miller, M., Nanayama, F.; Nishida, N.; Richter, C.; Roque, C.; Pereira, H.; Sanchez Goñi, M. F.; Sierro, F. J.; Singh, A. D., Sloss, C., Takashimizu, Y., Tzanova, A., Voelker, A.; Williams, T. and Xuan, C. (2014a) – Onset of Mediterranean outflow into the north Atlantic. *Science*, 344, 1244-1250 pp.

Hernández-Molina, F. J.; Llave, E.; Preu, B.; Ercilla, G.; Fontan, A.; Bruno, M.; Serra, N.; Gomiz, J. J., Brackenridge, R. E.; Sierro, F. J.; Stow, D. A. V.; García, M.; Juan, C., Sandoval, N. and Arnáiz, A. (2014b) – Contourite processes associated to the Mediterranean outflow water after its exit from the Gibraltar strait: global and conceptual implications. *Geology*, 42, 227–230 pp.

Hernández-Molina, F. J.; Sierro, F. J.; Llave, E.; Roque, C.; Stow, D. A. V.; Williams, T.; Lofi, J.; Van der Schee, M.; Arnáiz, A.; Ledesma, S.; Rosales, C.; Rodríguez-Tovar, F. J.; Pardo-Igúzquiza, E. and Brackenridge, R. E. (2015) – Evolution of the gulf of Cadiz margin and southwest Portugal contourite depositional system: Tectonic, sedimentary and paleoceanographic implications from IODP expedition 339. *Marine Geology*, 377, 7-39 pp.

Hiscott, R. N.; Wilson, R. C. L.; Gradstein, F. M.; Pujalte, V.; García-Mondéjar, J.; Boudreau, R. R. and Wishart, H. A. (1990) – Comparative stratigraphy and subsidence history of Mesozoic rift basins of North Atlantic. *American Association of Petroleum Geologists Bulletin*, 74, 60-76 pp.

Hodell, D.; Lourens, L.; Crowhurst, S.; Konijnendijk, T.; Tjallingii, R. and the Shackleton Site Project Members (2015) – A reference time scale for Site U1385 (Shackleton Site) on the Iberian Margin. *Global and Planetary Change*, 133, 49-64 pp.

Hollister, C. D. (1967) – Sediment distribution and deep circulation in the western North Atlantic. PhD thesis, Columbia University, New York, 467 pp.

Holstein, E. D. (Ed.) (2007) – *Volume V: Reservoir Engineering and Petrophysics*. *In:* L. W. Lake (Ed.), *Petroleum Engineering Handbook*, Society of Petroleum Engineers, Texas, USA, 1640 pp.

Hsü, K.; Ryan, W. and Cita, M. (1973) – Late Miocene dessication of Mediterranean. *Nature*, 242 (5395), 240-244 pp.

Hüneke, H. and Stow, D. (2008) – Identification of Ancient Contourites: Problems and Palaeoceanographic Significance. *In:* M. Rebesco and A. Camerlenghi (Eds.), *Contourites*. Developments in Sedimentology, Elsevier, Amsterdam, 60, 323-344 pp.

Inverno, C. M. C.; Manupella, G.; Zbyszewski, G.; Pais, J. and Ribeiro, M. L. (1993) – Notícia explicativa da folha 42-C, Santiago do Cacém, 1:50.000. *Serviços geológicos de Portugal*, Lisboa, Portugal, 75 pp.

Iverson, R. M. (1997) – The physics of debris flows. *Reviews of Geophysics*, 35 (3), 245-296 pp.

Johnson, J.; Ambar, I.; Serra, N. and Stevens, I. (2002) – Comparative studies of the spreading of Mediterranean Water through the Gulf of Cadiz. *Deep-Sea Research Part II: Topical Studies in Oceanography*, 49, 4179-4193 pp.

Johnston, A. C. (1996) – Seismic moment assessment of earthquakes in stable continental regions – III, New Madrid 1811-1812, Charleston 1886, and Lisbon 1755, *Geophysical Journal International*, 126, 314-344 pp.

Justo, J. L. and Salwa, C. (1998) – The 1531 Lisbon Earthquake. *Bulletin of the Seismological Society of America*, Seismological Society of America, 88 (2), 319-328 pp.

Kaboth, S.; Bahr, A.; Reichart, G.-J.; Jacobs, B. and Lourens, L. J. (2016) – New insights into upper MOW variability over the last 150 kyr from IODP 339 site U1386 in the Gulf of Cadiz. *Marine Geology*, 377, 136-145 pp.

Kenyon, N. and Belderson, R. (1973) – Bed forms of the Mediterranean undercurrent observed with side-scan sonar. *Sedimentary Geology*, 9, 77-99 pp.

Khélifi, N.; Sarnthein, M.; Andersen, N.; Blanz, T.; Frank, M.; Garbe-Schönberg, D.; Haley, B. A.; Stumpf, R. and Weinelt, M. (2009) – A major and long-term Pliocene intensification of the Mediterranean outflow, 3.5-3.3 Ma ago. *Geology*, 37, 811-814 pp.

Khélifi, N.; Sarnthein, M.; Frank, M.; Andersen, N. and Garbe-Schönberg, D. (2014) – Late Pliocene Variations of the Mediterranean Outflow. *Marine geology*, 357, 182-194 pp.

Knutz, P. C. (2008) – Palaeoceanographic significance of contourite drifts. *In:* M. Rebesco and A. Camerlenghi (Eds.), *Contourites*. Developments in Sedimentology, Elsevier, Amsterdam, 60, 511-535 pp.

Krijgsman W.; Hilgen F. J.; Raffi I.; Sierro F. J. and Wilson D. S. (1999) – Chronology, causes and progression of the Messinian salinity crisis. *Nature*, 400 (6745), 652-655 pp.

Laberg, J. and Camerlenghi, A. (2008) – The Significance of Contourites for Submarine Slope Stability. *In:* M. Rebesco and A. Camerlenghi (Eds.), *Contourites*. Developments in Sedimentology, Elsevier, Amsterdam, 60, 537-556 pp.

Laberg, J. S.; Stoker, M. S.; Torbjørn Dahlgren, K. I.; De Haas, H.; Haflidason, H.; Hjelstuen, B. O.; Nielsen, T.; Shannon, P. M.; Vorren, T. O.; Van Weering, T. C. E. and Ceramicola, S. (2005) –

Cenozoic alongslope processes and sedimentation on the NW European Atlantic margin. *Marine and Petroleum Geology*, 22, 1069-1088 pp.

Lebreiro, S. M.; Antón, L.; Reguera, M. I.; Fernández, M.; Conde, E.; Barrado, A. I. and Yllbera, A. (2015) – Zooming into the Mediterranean outflow fossil moat during the 1.2-1.8 million years period (Early-Pleistocene) - Na approach by radiogenic and stable isotopes. *Global and Planetary Change*, 135, 104-118 pp.

Lisa, M. (2014) – An Inconvenient Ice. *Scientific American*, 311, 82-89 pp.

Llave, E.; Hernández-Molina, F. J.; Somoza, L.; Díaz del Río, V.; Stow, D. A. V.; Maestro, A. and Alveirinho Dias, J. M. (2001) – Seismic stacking pattern of the faro-albufeira contourite system (gulf of Cadiz): a Quaternary record of paleoceanographic and tectonic influences. *Marine Geophysical Research*, 22, 487-508 pp.

Llave, E.; Schönfeld, J.; Hernández-Molina, F. J.; Mulder, T.; Somoza, L.; Díaz del Río, V. I. and Sánchez-Almazo, I. (2006) – High-resolution stratigraphy of the Mediterranean outflow contourite system in the gulf of Cadiz during the late Pleistocene: the impact of Heinrich events. *Marine Geology*, 227, 241-262 pp.

Llave, E.; Hernández-Molina, F. J.; Somoza, L.; Stow, D. A. V. and Díaz del Río, V. (2007a) – Quaternary evolution of the contourite depositional system in the gulf of Cadiz. *In:* A. R. Viana and M. Rebesco (Eds.), *Economic and Palaeoceanographic Significance of Contourite Deposits*. Geological Society, London, Special Publications, 276, 49-79 pp.

Llave, E.; Hernández-Molina, F. J.; Stow, D.; Fernández-Puga, M. C.; García, M.; Vázquez, J. T.; Maestro, A.; Somoza, L. and Díaz del Río, V. (2007b) – Reconstructions of the Mediterraneanoutflow water during the Quaternary since the study of changes in buried mounded drift stacking pattern in the gulf of Cadiz. *Marine Geophysical Research*, 28 (4), 379-394 pp.

Llave, E.; Matias, H.; Hernández-Molina, F.; Ercilla, G.; Stow, D. and Medialdea, T. (2010) – Pliocene and Quaternary seismic stacking pattern and distribution of contourites in the Algarve margin (Northern Gulf of Cadiz, Spain). *Geo-Temas*, 11, 103-104 pp.

Llave, E.; Matias, H.; Hernández-Molina, F. J.; Ercilla, G.; Stow, D. A. V. and Medialdea, T. (2011) – Pliocene–Quaternary contourites along the northern gulf of Cadiz margin: sedimentary stacking pattern and regional distribution. *Geo-Marine Letters*, 31 (5-6), 377-390 pp.

Llave, E.; Hernández-Molina, F. J., Ercilla, G.; Roque, C.; Van Rooij, D.; García, M.; Juan, C.; Mena, A.; Brackenridge, R.; Jané, G.; Stow, D. and Gómez-Ballesteros, M. (2015) – Bottom current processes along the Iberian continental margin. *Boletín Geológico y Minero*, 126 (2-3), 219-256 pp.

Lofi, J.; Voelker, A. H. L.; Ducassou, E.; Hernández-Molina, F. J.; Sierro, F. J.; Bahr, A.; Galvani, A.; Lourens, L. J.; Pardo-Igúzquiza, E.; Pezard, P.; Rodríguez-Tovar, F. J. and Williams, T. (2016) – Quaternary chronostratigraphic framework and sedimentary processes for the Gulf of Cadiz and Portuguese Contourite Depositional Systems derived from Natural Gamma Ray records. *Marine Geology*, 377, 40-57 pp.

Maldonado, A.; Somoza, L. and Pallares, L. (1999) – The betic orogen and the Iberian-African boundary in the gulf of Cadiz, geological evolution central north Atlantic. *Marine Geology*, 155, 9-43 pp.

Marchès, E.; Mulder, T.; Cremer, M.; Bonnel, C.; Hanquiez, V.; Gonthier, E. and Lecroart, P. (2007) – Contourite drift construction influenced by capture of Mediterranean outflow water deep-sea current by the portimao submarine canyon (gulf of Cadiz, south Portugal). *Marine Geology*, 242, 247-260 pp.

Marchès, E.; Mulder, T.; Gonthier, E.; Cremer, M.; Hanquiez, V.; Garlan, T. and Lecroart, R. (2010) – Perched lobe formation in the gulf of Cadiz: interactions between gravity processes and contour currents (Algarve margin, southern Portugal). *Sedimentary. Geology*, 229, 81-94 pp.

Martins, L. T.; Madeira, J.; Youbi, N.; Munhá, J.; Mata, J. and Kerrich, R. (2008) – Rift-related magmatism of the Central Atlanticmagmatic province in Algarve, Southern Portugal. *Lithos*, 101 (1-2), 102-124 pp.

Mason, E.; Coombs, S. and Oliveira, P. B. (2006) – An overview of the literature concerning the oceanography of the eastern North Atlantic region. *Relatórios Cientifícos e Técnicos IPIMAR série digital*, 33, 58 pp.

Masson, D. G.; Harbitz, C. B.; Wynn, R. B.; Pedersen, G. and Lovholt, F. (2006) – Submarine landslides: processes, triggers and hazard prediction. *In:* H. E. Huppert and R. S. J. Sparks (Eds.), *Discussion Meeting Issue Extreme natural hazards*, Philosophical Transactions of the Royal Society A, 364 (1845), 2009-2039 pp.

Matias, H. (2002) – Interpretação tectono-estratigráfica da área do Marquês de Pombal, a oeste do cabo de São Vicente. MSc thesis, Universidade de Lisboa, Lisboa, 114 pp.

McCave, I. (1984) – Erosion, transport and deposition of fine-rained marine sediments, *In:* D. Stow and D. Piper (Eds.), *Fine-Grained Sediments: Deep-Water Processes and Facies*. Geological Society, London, Special Publications, 15, 35-69 pp.

McCave, I. (2008) – Size sorting during transport and deposition of fine sediments: sortable silt and flow speed., *In:* M. Rebesco and A. Camerlenghi (Eds.), *Contourites*. Developments in Sedimentology, Elsevier, Amsterdam, 60, 121-142 pp.

McCave, I. N. and Tucholke, B. E. (1986) – Deep current controlled sedimentation in the western North Atlantic. *In:* P. R. Vogt and B. E. Tucholke (Eds.), *The Geology of North America: The Western North Atlantic Region*. Geological Society of America, Boulder (CO), 451-468 pp.

Miller, K. G.; Kominz, M. A.; Browning, J. V.; Wright, J. D.; Mountain, G. S.; Katz, M. E.; Sugarman, P. J.; Cramer, B. S.; Christie-Blick, N. and Pekar, S. F. (2005) – The phanerozoic record of global sea-level change. *Science*, 310, 1293-1298 pp.

Miller, K. G.; Mountain, G. S.; Wright, J. D. and Browning, J. V. (2011) – A 180-million-year record of sea level and ice volume variations from continental margin and deep-sea isotopic records. Oceanography 24 (2), 40-53 pp.

Millot, C. (1999) – Circulation in the Western Mediterranean Sea outflow. *Progress in Oceanography*, 20, 423-442 pp.

Millot, C. (2009) – Another description of the Mediterranean Sea outflow. *Progress in Oceanography*, 82 (2), 101-124 pp.

Miranda, R.; Valadares, V.; Terrinha, P.; Mata, J.; Azevedo, M. R.; Gaspar, M.; Kullberg, J. C. and Ribeiro, C. (2009) – Age constraints on the Late Cretaceous alkaline magmatism on the West Iberian Margin. *Cretaceous Research*, 30, 575-586 pp.

Miranda, J.; Batlló, J.; Ferreira, H.; Matias, L. M. and Baptista, M. A. (2012) – The 1531 Lisbon earthquake and tsunami. 15 *World Conference on Earthquake Engineering*, Lisbon, Portugal, 9 pp.

Mitchum, R. M. Jr.; Vail, P. R. and Thompson III, S. (1977a) – Seismic stratigraphy and global changes of sea level, part 1: Overview. *In:* C. E. Payton (Ed.), *Seismic Stratigraphy - Applications to Hydrocarbon Exploration*. American Association of Petroleum Geologists, Memoirs, 26, 51-52 pp.

Mitchum, R. M. Jr.; Vail, P. R. and Thompson III, S. (1977b) – Seismic stratigraphy and global changes of sea level, part 2: The depositional sequence as a basic unit for stratigraphic analysis. *In:* C. E. Payton (Ed.), *Seismic Stratigraphy - Applications to Hydrocarbon Exploration*. American Association of Petroleum Geologists, Memoirs, 26, 53-62 pp.

Mitchum, R. M. Jr.; Vail, P. R. and Sangree, J. B. (1977c) – Seismic stratigraphy and global changes of sea level, part 6: Stratigraphic interpretation of seismic reflection patterns in depositional sequences. *In:* C. E. Payton (Ed.), *Seismic Stratigraphy - Applications to Hydrocarbon Exploration.* American Association of Petroleum Geologists, Memoirs, 26, 117-133 pp.

Mitchum, R. M. Jr.; Sangree, J. B.; Vail, P. R. and Wornardt, W. W. (1994) – Recognizing sequences and systems tracts from well logs, seismic data, and biostratigraphy: Examples from the Late Cenozoic of the Gulf of Mexico. *In:* P. Weimer and H. W. Posamentier (Eds.), *Siliciclastic sequence stratigraphy*. American Association of Petroleum Geologists, Memoirs, 58, 163-197 pp.

Mougenot, D. (1976) – Géologie du plateau continental portugaise (entre le cap Carvoeiro et le cap de Sines). Fascicule 1 et 2, Thèse 3ème cycle. Univ. Rennes, 76 pp. (not published)

Mougenot, D. (1989) – Geologia da Margem Portuguesa. *Instituto Hidrográfico*, 32, 259 pp.

Mougenot, D. and Vanney, J. (1982) – Les rides de contourites Plio-Quaternaires de la pente continentale sud-portugaise. *Bulletin Institut Gèologie Bassin d'Aquitaine*, 31, 131-139 pp.

Mougenot, D.; Monteiro, J. H.; Dupeuble, P. A. and Malod, J. A. (1979) – La marge continentale sud-portugaise: évolution structurale et sédimentaire. *Ciências da Terra*, 5, 223-246 pp.

Mulder, T.; Voisset, M.; Lecroart, P.; Le Drezen, E.; Gonthier, E.; Hanquiez, V.; Faugères, J.-C.; Habgood, E.; Hernández-Molina, F. J.; Estrada, F.; Llave, E.; Poirier, D.; Gorini, C.; Fuchey, Y.; Voelker, A.; Freitas, P.; Lobo Sánchez, F.; Fernández, L. M. and Morel, J. (2003) – The gulf of Cadiz: an unstable giant contouritic levee. *Geo-Marine Letters*, 23 (1), 7-18 pp.

Mulder, T.; Lecroart, P.; Hanquiez, V.; Marchès, E.; Gonthier, E.; Guedes, J.-C.; Thiébot, E.; Jaaidi, B.; Kenyon, N.; Voisset, M.; Pérez, C.; Sayago, M.; Fuchey, Y. and Bujan, S. (2006) – The western part of the Gulf of Cadiz: contour currents and turbidity currents interactions. *Geo-Marine Letters*, 26, 31-41 pp.

Mulder, T.; Gonthier, E.; Lecroart, P.; Hanquiez, V.; Marchès, E. and Voisset, M. (2009) – Sediment failures and flows in the Gulf of Cadiz (eastern Atlantic). *Marine and Petroleum Geology*, 26 (5), 660-672 pp.

Mulder, T.; Hassan, R., Ducassou, E.; Zaragosi, S.; Gonthier, E.; Hanquiez, V.; Marchès, E. and Toucanne, S. (2013) – Contourites in the Gulf of Cadiz: a cautionary note on potentially ambiguous indicators of bottom current velocity. *Geo-Marine Letters*, 33, 357-367 pp.

Myers, K. and Milton, N. (1996) – Concepts and principles. *In:* D. Emery and K. Myers (Eds.), *Sequence stratigraphy*. Oxford, Blackwell, 11-44 pp.

Nelson, C. H., Baraza, J. and Maldonado, A. (1993) – Mediterranean undercurrent sandy contourites Gulf of Cadiz, Spain. *Sedimentary Geology*, 82, 103-131 pp.

Nelson, C. H.; Baraza, J.; Rodero, J.; Maldonado, A.; Escutia, C. and Barber Jr., J.H. (1999) – Influence of the Atlantic inflow and Mediterranean outflow currents on late Pleistocene and Holocene sedimentary facies of gulf of Cadiz continental margin. *Marine Geology*, 155, 99-129 pp.

Neves, M. C.; Terrinha, P.; Afilhado, A.; Moulin, M.; Matias, L. and Rosas, F. (2009) – Response of a multi-domain continental margin to compression: study from seismic reflection-refraction and numerical modelling in the Tagus Abyssal Plain. *Tectonophysics*, 468, 113-130 pp.

Nielsen, T.; Knutz, P. C. and Kuijpers, P. C. A. (2008) – Seismic expression of contourite depositional systems. *In:* M. Rebesco and A. Camerlenghi (Eds.), *Contourites*. Developments in Sedimentology, Elsevier, Amsterdam, 60, 301-322 pp.

Nishida, N. (2016) – Microstructure of muddy contourites from the Gulf of Cádiz. *Marine Geology*, 377, 110-117 pp.

Ogg, J. and Ogg, G. (2008) – Neogene-Late Oligocene (0-33 Ma time-slice). Subcommission for Stratigraphic Information. Accessed at: http://stratigraphy.science.purdue.edu/charts/educational.html on 15/09/2016.

Oliveira, J. T. (1984) – Notícia explicativa da carta geológica de Portugal, folha 7, 1:200.000. *Serviços Geológicos de Portugal*, Lisboa, Portugal, 77 pp.

Padin, X. A.; Castro, C. G. and Pérez, F. F. (2011) – Oceanic CO_2 uptake and biogeochemical variability during the formation of the Eastern North Atlantic Central water under two contrasting NAO scenarios. *Journal of Marine Systems*, 84, 96-105 pp.

Payton, C. E. (1977) – *Seismic stratigraphy - Applications to hydrocarbon exploration*. American Association of Petroleum Geologists, Memoirs, 26, 516 pp.

Pereira, R. and Alves, T. M. (2010) – Multiphased syn-rift segmentation on the SW Iberian margin. *II Central and North Atlantic Conjugate Margins Conference*, Lisbon, Portugal, 224-227 pp.

Pereira, R. and Alves, T. M. (2011) – Margin segmentation prior to continental break-up: a seismic–stratigraphic record of multiphased rifting in the North Atlantic. *Tectonophysics*, 505, 17-34 pp.

Pereira, R. and Alves, T. M. (2013) – Crustal deformation and submarine canyon incision in a Meso-Cenozoic first-order transfer zone (SW Iberia, North Atlantic Ocean). *Tectonophysics*, 601, 148-162 pp.

Pérez, F. F.; Mouriño, C.; Fraga, F. and Rios, A. F. (1993) – Displacement of water asses and remineralization rates off the Iberian Peninsula by nutrient anomalies. *Journal of Marine Research*, 51 (4), 869-892 pp.

Pinheiro, L. M.; Wilson, R. C. L.; Pena dos Reis, R.; Whitmarsh, R. B. and Ribeiro, A. (1996) – The Western Iberia Margin: A Geophysical and Geological overview. *In:* R. B. Whitmarsh; D. S. Sawyer; A. Klaus and D. G. Masson (Eds.), *Proceedings of the Ocean Drilling Program, Scientific Results*, 149, 3-23 pp.

Rahmstorf, S. (2002) – Ocean circulation and climate during the past 120,000 years. *Nature*, 419, 207-214 pp.

Rahmstorf, S. (2006) – Thermohaline ocean circulation. *In:* S. Elias (Ed.), *Encyclopedia of Quaternary Sciences*. Elsevier, Amsterdam, 1-10 pp.

Rasmussen, E. S.; Lomholt, S.; Andersen, C. and Vejbæ k, O. V. (1998) – Aspects of the structural evolution of the Lusitanian Basin in Portugal and the shelf and slope area offshore Portugal. *Tectonophysics*, 300, 199-225 pp.

Ravelo, A. C.; Andreasen, D. H.; Lyle, M.; Lyle, A. O. and Wara, M. W. (2004) – Regional climate shifts caused by gradual cooling in the Pliocene epoch. *Nature*, 429, 263-267 pp.

Raymo, M. E.; Lisiecki, L. E. and Nisancioglu, K. H. (2006) – Plio-Pleistocene ice volume, Antarctic climate, and the global $\delta^{18}O$ record, *Science*, 313 (5786), 492-495 pp.

Rebesco, M. (2005) – Contourites. *In:* C. Richard; R. C. Selley; L. R. Cocks and I. R. Plimer (Eds.), *Encyclopedia of Geology*, Elsevier, London, 4, 513-527 pp.

Rebesco, M. and Camerlenghi, A. (2008) – *Contourites*. Developments in Sedimentology, Elsevier, Amsterdam, 60.

Rebesco, M. and Stow, D. (2001) – Seismic expression of contourites and related deposits: a preface. *Marine Geophysical Research*, 22, 303-308 pp.

Rebesco, M.; Hernández-Molina, F. J.; Van Rooij, D. and Wåhlin, A. (2014) – Contourites and associated sediments controlled by deep-water circulation processes: state of the art and future considerations. *Marine Geology*, 352, 111-154 pp.

Reed, D. L.; Meyer, A. W.; Silver, E. A. and Prasetyo, H. (1987) – Contourite sedimentation in na intraoceanic forearc system: eastern Sunda Arc, Indonesia. *Marine Geology*, 76, 223-242 pp.

Reid, J. L. (1979) – On the contribution of the Mediterranean Sea out flow to the Norwegian-Greenland Sea. *Deep-Sea Research*, 26 (A), 1199-1223 pp.

Rey, J.; Dinis, J. L.; Callapez, P. and Cunha, P. P. (2006) – Da rotura continental à margem passiva: Composição e evolução do Cretácico de Portugal. *INETI*, Lisboa, Portugal, 75 pp.

Ribeiro, A. (2013a) – Evolução geodinâmica de Portugal; os ciclos ante-mesozóicos. *In:* R. Dias; A. Araújo; P. Terrinha and J. C. Kullberg (Eds.), *Geologia de Portugal, Volume I: Geologia Pré-mesozóica de Portugal*, Escolar Editora, Lisboa, II, 15-58 pp.

Ribeiro, A. (2013b) – Evolução geodinâmica de Portugal; os ciclos Meso-Cenozóicos. *In:* R. Dias; A. Araújo; P. Terrinha and J. C. Kullberg (Eds.), *Geologia de Portugal, Volume II: Geologia Meso-cenozóica de Portugal*, Escolar Editora, Lisboa, III, 9-28 pp.

Ribeiro, A.; Antunes, M. T.; Ferreira, M. P.; Rocha, R. B.; Soares, A. F.; Zbyszewski, G.; Almeida, F. M.; Carvalho, D. and Monteiro, J. H. (1979) – Introduction à la géologie générale du Portugal. *Serviços Geológicos de Portugal*, Lisboa, Portugal, 114 pp.

Ribeiro, A.; Oliveira, J. T.; Ramalho, M. ; Ribeiro, M. L. and Silva, L. (1987) – Notícia explicativa da folha 48-D, Bordeira, 1:50.000. *Serviços Geológicos de Portugal*, Lisboa, Portugal, 30 pp.

Ribeiro, A.; Kullberg, M. C.; Kullberg, J. C.; Manuppella, G. and Phipps, S. (1990) – A review of Alpine tectonics in Portugal: Foreland detachment in basement and cover rocks. *Tectonophysics*, 184 (3-4), 357-366 pp.

Rogerson, M.; Rohling, E.; Weaver, P. and Murray, J. (2005) – Glacial to interglacial changes in the settling depth of the Mediterranean Outflow plume. *Paleoceanography*, 20 (3), 1-12 pp.

Rogerson, M.; Rohling, E. and Weaver, P. (2006) – Promotion of meridional overturning by Mediterranean-derived salt during the last deglaciation. *Paleoceanography*, 21 (PA4101), 1-8 pp.

Rogerson, M.; Schönfeld, J. and Leng, M. (2011) – Qualitative and quantitative approaches in palaeohydrography: A case study from core-top parameters in the Gulf of Cadiz. *Marine Geology*, 280 (1-4), 150-167 pp.

Rogerson, M.; Rohling, E.; Bigg, G.R. and Ramirez, J. (2012) – Paleoceanography of the Atlantic-Mediterranean exchange: Overviewand first quantitativeassessment of climatic forcing. *Reviews of Geophysics*, 50 (RG2003), 1-32 pp.

Roque, C. (2007) – *Tectonostratigrafia do Cenozóico das margens continentais sul e sudoeste portuguesas: um modelo de correlação sismostratigráfica*. PhD thesis, Universidade de Lisboa, Lisboa, 348 pp.

Roque, C.; Duarte, H.; Terrinha, P.; Valadares, V.; Noiva, J.; Cachão, M.; Ferreira, J.; Legoinha, P. and Zitellini, N. (2012) – Pliocene and Quaternary depositionalmodel of the Algarve margin contourite drifts (gulf of Cadiz, SW Iberia): seismic architecture, tectoni control and paleoceanographic insights. *Marine Geology*, 303-306, 42-62 pp.

Roque, C.; Hernández-Molina, F. J.; Ercilla, G.; Casas, D.; Quartau, R.; Llave, E.; Alonso, B.; Ferran, M.; Mena, A.; Francés, G. and MOWER Cruise Party (2015) – Slope failure and mass movement in the Sines Contourite Drift (West Portuguese Margin): preliminary results. *In:* V. Díaz del Río; P. Bárcenas; L. M. Fernández-Salas; N. López-González; D. Palomino; J. L. Rueda; O. Sánchez-Guillamón and J. T. Vázquez (Eds.), *Volumen de Comunicaciones presentadas en el VIII Simposio sobre el Margem Iberico Atlántico*, 579-581 pp.

Rosas, F.; Duarte, J.; Terrinha, P.; Valadares, V.; Matias, L. and Gutscher, M. A. (2009) – Major bathymetric lineaments and soft sediment deformation in NW gulf of Cadiz (Africa-Iberia plate boundary): new insights from high resolution multibeam bathymetry data and analogue modelling experiments. *Marine Geology*, 261 (1-4), 33-47 pp.

Sánchez Goñi, M.; Llave, E.; Oliveira, D.; Naughton, F.; Desprat, S.; Ducassou, E.; Hodell, D. and Hernández-Molina, F. (2016) – Climate changes in south western Iberia and Mediterranean Outflow variations during two contrasting cycles of the last 1 Myrs: MIS 31-MIS 30 and MIS 12-MIS 11. *Global and Planetary Change*, 136, 18-29 pp.

Scholz, N. A.; Riedel, M.; Bahk; J.-J.; Yoo, D.-G. and Ryu, B.-J. (2012) – Mass transport deposits and gas hydrate occurrences in the Ulleung Basin, East Sea - Part 1: Mapping sedimentation patterns using seismic coherency. *Marine and Petroleum Geology*, 35, 91-104 pp.

Serra, N. and Ambar, I. (2002) – Eddy generation in the Mediterranean undercurrent. *Deep-Sea Research Part II: Topical Studies in Oceanography*, 49 (19), 4225-4243 pp.

Serra, N.; Ambar, I. and Käse, R. H. (2005) – Observations and numerical modelling of the Mediterranean outflow splitting and eddy generation. *Deep-Sea Research Part II: Topical Studies in Oceanography*, 52, 383-408 pp.

Shanmugam, G. (2006) – *Deep-water Processes and Facies Models: Implications for Sandstone Petroleum Reservoirs*. Handbook of Petroleum Exploration and Production, Elsevier Science, 5, 496 pp.

Shanmugam, G. (2008) – Deep-water bottom currents and their deposits. *In:* M. Rebesco and A. Camerlenghi (Eds.), *Contourites*. Developments in Sedimentology, Elsevier, Amsterdam, 60, 59-81 pp.

Sheriff, R. E. and Geldart, L. P. (1995) – *Exploration Seismology (Second Edition)*. Cambridge University Press, Cambridge, United Kingdom, 592 pp.

Sierro, F. J.; Glez Delgado, J. A.; Dabrio, C.; Flores, J. A. and Civis, J. (1991) – The Neogene of the Guadalquivir basin. *Paleontologia y Evolució Mem. Especial 2: Iberian Neogene basins*, 209-250 pp.

Sierro, F. J.; Flores, J. A.; Civis, J.; González-Delgado, J. A. and Francés, G. (1993) – Late Miocene globorotaliid event-stratigraphy and biogeography in the NE Atlantic and Mediterranean. *Marine Micropaleontology*, 21, 143-168 pp.

Sierro, F. J.; Flores, J. A.; Zamarreño, I.; Vázquez, A.; Utruilla, R.; Francés, G.; Hilgen, F.J. and Krigsman, W. (1999) – Messinian climatic oscilations, astronomic cyclicity and reef growth in the western Mediterranean. *Marine Geology*, 153, 137-146 pp.

Sierro, F. J.; Ledesma, S.; Flores, J. A.; Torrescusa, S. and Martínez del Olmo, W. (2000) – Sonic and gamma-ray astrochronology: cycle to cycle calibration of Atlantic climatic toMediterranean sapropels and astronomical oscillations. *Geology*, 28 (8), 695-698 pp.

Sierro, F. J.; Ledesma, S. and Flores, J. A. (2008) – Astrobiochronology of late neogene deposits near the strait of Gibraltar (SW Spain). Implications for the tectonic control of the messinian salinity crisis. *In:* F. Biand (Ed.), *The messinian salinity crisis from mega-deposits to microbiology, CIESM workshop monographs*, Monaco, 45-48 pp.

Silva, C. M.; Landau, B.; Domènech, R. and Martinell, J. (2006) – Pliocene Atlanto-Mediterranean biogeography of Patella pellucida (Gastropoda, Patellidae): Palaeoceanographic implications. *Palaeogeography, Palaeoclimatology, Palaeoecology*, Amsterdam, 233 (3-4), 225-234 pp.

Silva, P. F.; Henry, B.; Marques, F. O.; Font, E.; Mateus, A.; Vegas, R.; Miranda, J. M.; Palomino, R. and Palencia-Ortas, A. (2008) – Magma flow, exsolution processes and rock metasomatism in the Great Messejana–Plasencia dyke (Iberian Peninsula). *Geophysics Journal International*, 175 (2), 806-824 pp.

Sinclair, I. K. (1995) – Sequence stratigraphic response to Aptian-Albian rifting in conjugate margin basins: a comparison of the Jeanne d'Arc Basin, offshore Newfoundland, and the Porcupine Basin, offshore Ireland. Geological Society, London, Special Publications 1995, 90, 29-49 pp.

Singh, A.; Verma, K.; Jaiswal, S.; Alonso-Garcia M.; Li, B. and Abrantes, F. (2015) – Planktic foraminiferal responses to orbital scale oceanographic changes off the western Iberian margin over the last 900 kyr: Results from IODP site U1391. *Global and Planetary Change*, 135, 47-56 pp.

Sloss, L. L. (1963) – Sequences in the cratonic interior of North America. *Geological Society of America Bulletin*, 74, 93-114 pp.

Snedden, J. W. and Sarg, J. F. (2008) – Seismic Stratigraphy - A Primer on Methodology. American Association of Petroleum Geologists Search and Discovery Website, Article #40270. Accessed at: www.searchanddiscovery.org on 15/1/2016.

Stapel, G.; Cloetingh, S. and Pronk, B. (1996) – Quantitative subsidence analysis of the Mesozoic evolution of the Lusitanian Basin (western iberian margin). *Tectonophysics*, 266 (1-4), 493-507 pp.

Stigall, J. and Dugan, B. (2010) – Overpressure and earthquake initiated slope failure in the Ursa region, northern Gulf of Mexico. *Journal of Geophysical Research: Solid Earth*, 115 (B4), 2156-2202 pp.

Stow, D. A. V. and Faugères, J.-C. (2008) – Contourites facies and the facies model. *In:* M. Rebesco and A. Camerlenghi (Eds.), *Contourites*. Developments in Sedimentology, Elsevier, Amsterdam, 60, 223-256 pp.

Stow, D. A. V. and Lovell, J. P. B. (1979) – Contourites: their recognition in modern and ancient sediments. *Earth Science Reviews*, 14, 251-291 pp.

Stow, D. A. V.; Pudsey, C. J.; Howe, J. A.; Faugères, J.-C. and Viana, A. R. (2002a) – *Deep-Water Contourite Systems: Modern Drifts and Ancient Series, Seismic and Sedimentary Characteristics*. Geological Society, London, Memoirs, 22.

Stow, D. A. V.; Faugères, J.-C.; Howe, J. A.; Pudsey, C. J. and Viana, A. R. (2002b) – Bottom currents, contourites and deep-sea sediment drifts: current state-of-the-art. *In:* D. A. V. Stow; C. J. Pudsey; J. A. Howe; J.-C. Faugères and A. R. Viana (Eds.), *Deep-Water Contourite Systems: Modern Drifts and Ancient Series, Seismic and Sedimentary Characteristics*. Geological Society, London, Memoirs, 22, 7-20 pp.

Stow, D. A. V.; Faugères, J.-C.; Gonthier, E.; Cremer, M.; Llave, E.; Hernández-Molina, F. J.; Somoza, L. and Díaz del Río, V. (2002c) – Faro-Albufeira Drift Complex, Northern Gulf of Cadiz. *In:* D. A. V. Stow; C. J. Pudsey; J. A. Howe; J.-C. Faugères and A. R. Viana (Eds.), *Deep-Water Contourite Systems: Modern Drifts and Ancient Series, Seismic and Sedimentary Characteristics*. Geological Society, London, Memoirs, 22, 137-154 pp.

Stow, D.; Hunter, S.; Wilkinson, D. and Hernández-Molina, F. (2008) – The nature of contourite deposition, *In:* M. Rebesco and A. Camerlenghi (Eds.), *Contourites*. Developments in Sedimentology, Elsevier, Amsterdam, 60, 143-156 pp.

Stow, D.; Hernández-Molina, F.; E, L.; Sayago-Gil, M.; Díaz del Río, V. and Branson, A. (2009) – Bedform-velocity matrix: The estimation of bottom current velocity from bedform observations. *Geology*, 37, 327-330 pp.

Stow, D. A. V.; Hernández-Molina, F. J.; Llave, E.; Bruno, M.; García, M.; Díaz del Río, V.; Somoza, L. and Brackenridge, R. E. (2013) – The Cadiz contourite channel: sandy contourites, bedforms and dynamic current interaction. *Marine Geology*, 343, 99-114 pp.

Stow, D. A. V.; Hernández-Molina, J.; Alvarez-Zarikian, C. and the Expedition 339 Shipboard Scientists (2014) – New Advances in the Contourite Paradigm: IODP Expedition 339, Gulf of Cadiz. *In:* D. Van Rooji and A. Rüggeberg (Eds.), *2nd Deep Water Circulation Congress: The Contourite Log-book*, Ghent, Belgium, VLIZ Special Publication 69, 11-12 pp.

Stumpf, R.; Frank, M.; Schönfeld, J. and Haley, B. A. (2010) – Late Quaternary variability of Mediterranean Outflow Water from radiogenic Nd and Pb isotopes. *Quaternary Science Reviews*, 29, 2462-2472 pp.

Tankard, A. J. and Balkwill, H. R. (1989) – Extensional tectonics and stratigraphy of the North Atlantic margins: Introduction. *In:* A. J. Tankard and H. R. Balkwill (Eds.), *Extensional tectonics and stratigraphy of the North Atlantic margins*, American Association of Petroleum Geologists, 46, 1-6 pp.

Terrinha, P.; Ribeiro, C.; Kullberg, J. C.; Lopes, C.; Rocha, R. and Ribeiro, A. (2002) – Compressive Episodes and Faunal Isolation during Rifting, Southwest Iberia. *The Journal of Geology*, 110, 101-113 pp.

Terrinha, P.; Pinheiro, L. M.; Henriet, J.-P.; Matias, L.; Ivanov, M. K.; Monteiro, J. H.; Akhmetzhanov, A.; Volkonskaya, A.; Cunha, T.; Shaskin, P. and Rovere, M. (2003) – Tsunamigenic-seismogenic structures, neotectonics, sedimentary processes and slope instability on the southwest Portuguese margin. *Marine Geology*, 195, 55-73 pp.

Terrinha, P.; Matias, L.; Vicente, J.; Duarte, J.; Luís, J.; Pinheiro, L.; Lourenço, N.; Diez, S.; Rosas, F.; Magalhães, V.; Valadares, V.; Zitellini, N.; Roque, C.; Mendes Víctor, L. and MATESPRO Team (2009) – Morphotectonics and strain partitioning at the Iberia-Africa plate boundary from multibeam and seismic reflection data. Marine Geology Vol. 267, 156-174 pp.

Terrinha, P.; Rocha, R. B.; Rey, J.; Cachão, M.; Moura, D.; Roque, C.; Martins, L.; Valadares, V.; Cabral, J.; Azevedo, M. R.; Barbero, L.; Clavijo, E.; Dias, R. P.; Matias, H.; Matias, L.; Madeira, J.; Silva, C. M.; Munhá, J. R.; Rebelo, L.; Ribeiro, C.; Vicente, J.; Noiva, J.; Youbi, N. and Bensalah, M. K. (2013a) – A Bacia do Algarve: Estratigrafia, Paleogeografia e Tectónica. *In:* R. Dias; A. Araújo; P. Terrinha and J. C. Kullberg (Eds.), *Geologia de Portugal, Volume II: Geologia Meso-cenozóica de Portugal*, Escolar Editora, Lisboa, III.1., 29-166 pp.

Terrinha, P; Matias, L.; Valadares, V.; Roque, C.; Duarte, J.; Rosas, F.; Silva, S.; Cunha, T.; Batista, L.; Duarte, H.; Garrara, G.; Gràcia, E.; Zitellini, N.; Lourenço, N. and Pinto de Abreu, M. (2013b) – A Margem Sul Portuguesa Profunda. *In:* R. Dias; A. Araújo; P. Terrinha and J. C. Kullberg (Eds.), *Geologia de Portugal, Volume II: Geologia Meso-cenozóica de Portugal*, Escolar Editora, Lisboa, III.2., 167-194 pp.

Toucanne, S.; Mulder, T.; Schönfeld, J.; Hanquiez, V.; Gonthier, E.; Duprat, J.; Cremer, M. and Zaragosi, S. (2007) – Contourites of the gulf of Cadiz: a high-resolution record of the paleocirculation of the Mediterranean outflow water during the last 50,000 years. *Palaeogeography, Palaeoclimatology, Palaeoecology*, 246, 354-366 pp.

Tucholke, B. E.; Sawyer, D. S. and Sibuet, J. C. (2007) – Breakup of the Newfoundland Iberia rift. *In:* G.D. Karner; G. Manatschal and L. M. Pinheiro (Eds.), *Imaging, Mapping and Modelling Continental Lithosphere Extension and Breakup*. Geological Society, London, Special Publications, 282 (1), 9-46 pp.

Tzanova, A. and Herbert, T. (2015) – Regional and global significance of Pliocene sea surface temperatures from the Gulf of Cadiz (Site U1387) and the Mediterranean. *Global and Planetary Change*, 133, 371-377 pp.

Urlaub, M.; Talling, P. J. and Masson, D. G. (2013) – Timing and frequency of large submarine landslides: implications for understanding triggers and future geohazard. *Quaternary Science Reviews*, 72, 63-82 pp.

Vail, P. R.; Mitchum Jr., R. M. and Thomson III, S. (1977) – Global cycles of relative changes of sea level. *In:* C. E. Payton (Ed.), *Seismic stratigraphy - Applications to hydrocarbon exploration*, American Association of Petroleum Geologists, Memoirs, 26, 83-98 pp.

Vail, P. R. (1987) – Seismic stratigraphy interpretation using sequence stratigraphy: Part 1, Seismic stratigraphy interpretation procedure. *In:* A. W. Bally (Ed.), *Atlas of Seismic Stratigraphy*, American Association of Petroleum Geologists, Studies in Geology, 1 (27), 1-10 pp.

Van der Schee, M.; Sierro, F. J.; Jiménez-Espejo, F. J.; Hernández- Molina, F. J.; Flecker, R.; Flores, J. A.; Acton, G.; Gutjahr, M.; Grunert, P.; García-Gallardo, A. and Andersen, N. (2016) – Evidence of early bottom water current flow after the Messinian Salinity Crisis in the Gulf of Cadiz. *Marine Geology*, 380, 315-329 pp.

Vandorpe, T.; Van Rooij, D. and Haas, H. (2014) – Stratigraphy and paleoceanography of a topography-controlled contourite drift in the Pen Duick area, southern Gulf of Cádiz. *Marine Geology*, 349, 136-151 pp.

Vandorpe, T.; Martins, I.; Vitorino, J.; Hebbeln, D.; García, M. and Van Rooij, D. (2015) – Bottom currents and their influence on the sedimentation pattern in the El Arraiche mud volcano province, southern Gulf of Cadiz. *Marine Geology*, 378, 114-126 pp.

Vanney, J. R. and Mougenot, D. (1981) – *La Plate-forme Continentale du Portugal et les Provinces adjacentes: Analyse Geomorphologique*. Memórias dos Serviços Geológicos de Portugal, Lisboa, 28, 86 pp.

Valadares, V. (2012) – The morphotectonics offshore Southwest Iberia and the origin of the South Portuguese submarine canyons. PhD thesis, Universidade de Lisboa, Lisboa, 346 pp.

Verati, C.; Rapaille, C.; Feraud, G.; Marzoli, A.; Bertrand, H. and Youbi, N. (2007) – Ar-40/Ar-39 ages and duration of the Central Atlantic Magmatic Province volcanism in Morocco and Portugal and its relation to the Triassic-Jurassic boundary. *Palaeogeography, Palaeoclimatology, Palaeoecology*, 244 (1-4), 308-325 pp.

Viana, A. R. (2008) – Economic relevance of contourites. *In:* M. Rebesco and A. Camerlenghi (Eds.), *Contourites*. Developments in Sedimentology, Elsevier, Amsterdam, 60, 493-510 pp.

Viana, A. R. and Rebesco, M. (2007) – *Economic and Palaeoceanographic Significance of Contourite Deposits*, Geological Society, London, Special Publications, 276.

Viana, A.; Almeida Jr., W.; Nunes, M. and Bulhões, E. (2007) – The Economic importance of contourites. *In:* A. R. Viana and M. Rebesco (Eds.), *Economic and Palaeoceanographic Significance of Contourite Deposits*. Geological Society, London, Special Publications, 276, 1-23 pp.

Voelker, A. H. L.; Lebreiro, S. M.; Schönfeld, J.; Cacho, I.; Erlenkeuser, H. and Abrantes, F. (2006) – Mediterranean outflow strengthening during northern hemisphere coolings: a salt source for the glacial Atlantic? *Earth and Planetary Science Letters*, 245 (1–2), 39-55 pp.

Voelker, A. H. L.; Salgueiro, E.; Rodrigues, T.; Jimenez-Espejo, F.; Bahr, A.; Alberto, A.; Loureiro, I.; Padilha, M.; Rebotim, A. and Röhl, U. (2015) – Mediterranean Outflow and surface water variability off southern Portugal during the early Pleistocene: A snapshot at Marine Isotope Stages 29 to 34 (1020-1135 Ka), *Global and Planetary Change*,133, 223-237 pp.

Welsink, H. J.; Dwyer, J. D. and Knight, R. J. (1989) – Tectono-stratigraphy of the passive margin off Nova Scotia. *In:* A. J. Tankard and H. R. Balkwill (Eds.), *Extensional tectonics and stratigraphy of the North Atlantic margins*, American Association of Petroleum Geologists, 46, 215-231 pp.

Zenk, W. (1970) – On the temperature and salinity structure of the Mediterranean water in the Northeast Atlantic. *Deep-Sea Research*, 17, 627-631 pp.

Zenk, W. (1975) – On the Mediterranean outflow west of Gibraltar. *Meteor Forschungsergebnisse, Deutsche Forschungsgemeinschaft, Reihe A Allgemeines, Physik und Chemie des Meeres, Gebrüder Bornträger, Berlin, Stuttgart*, A16, 23-34 pp.

Zenk, W. (2008) – Abyssal and contour currents. *In:* M. Rebesco and A. Camerlenghi (Eds.), *Contourites*. Developments in Sedimentology, Elsevier, Amsterdam, 60, 37-57 pp.

Yilmaz, Öz (1987) – *Seismic Data Processing*. Investigations in Geophysics, 2, Society of Exploration Geophysicists, 526 pp.

Zitellini, N.; Mendes, L. A.; Cordoba, D.; Danobeitia, J.; Nichols, R.; Pellis, G.; Ribeiro, A.; Sartori, R.; Torelli, L.; Bartolome, R.; Bortoluzzi, G.; Calafato, A.; Carrilho, F.; Casoni, L.; Chierici, F.; Corela, C.; Correggiari, A.; Vedova, B. D.; Gracia, E.; Jornet, P.; Landuzzi, M.; Ligi, M.; Magagnoli, A.; Marozzi, G.; Matias, L.; Penitenti, D.; Rodriguez, P.; Rovere, M.; Terrinha, P.; Vigliotti, L. and Ruiz, A. Z. (2001) – Source of 1755 Lisbon earthquake and tsunami investigated. *Eos, Transactions American Geophysical Union*, 82 (26), 290-291 pp.

Zitellini, N.; Rovere, M.; Terrinha, P.; Chierici, F.; Matias, L. and BIGSETS Team (2004) – Neogene Through Quaternary Tectonic Reactivation of SW Iberian Passive Margin. *Pure and Applied Geophysics*, 161 (3), 565-587 pp.

Zitellini, N.; Gràcia, E.; Matias, L.; Terrinha, P.; Abreu, M.A.; DeAlteriis, G.; Henriet, J.P.; Dañobeitia, J.J.; Masson, D.G.; Mulder, T.; Ramella, R.; Somoza, L. and Diez, S. (2009) – The quest for the Africa-Eurasia plate boundary west of the Strait of Gibraltar. *Earth and Planeraty Science Letters*, 280 (1-4), 13-50 pp.

10. APPENDIX

10.1 Seismic Data Acquisition

Acquisition parameters and processing flow of the CONDRIBER seismic data.

Table 10.1 – Technical specifications of the CONDRIBER seismic survey during the MOWER/CONDRIBER cruise (from Informe Técnico Campaña Mower, 2014).

CONDRIBER	**Acquisition Parameters**
Year	2014
Source	8 G-GunII airguns
Total volume	610 and 910 in^3 (150+150, 110+110, 45+45 in^3)
Record length	4, 6 and 9 s (controlled by time)
Shot Interval	50 m
Sample Rate	0.5 ms
Source depth	5 m
Synchronization Error	+/- 0.1 ms
Source compressors	2 LMF25/138-207E
Entry air pressure	1.013 bar – 14.65 psi
Working air pressure	140 bar – 2000 psi
Maximum air volume	25 m^3/min – 900 cfm
Streamer configuration	3-channel SIG 16.3 x 40.175
Active section	150 m
Total length	250 m
Streamer depth	0.5 – 1.5 m
Penetration	50 – 4500 m
Vertical Resolution	High/medium
Channels	3
Channel interval	50 m
Hydrophones sensibility	SIG 16 – 90 dB, re 1 V/µbar
Hydrophones per channel	40
Frequency range	10 – 1000 Hz +/- 1 dB

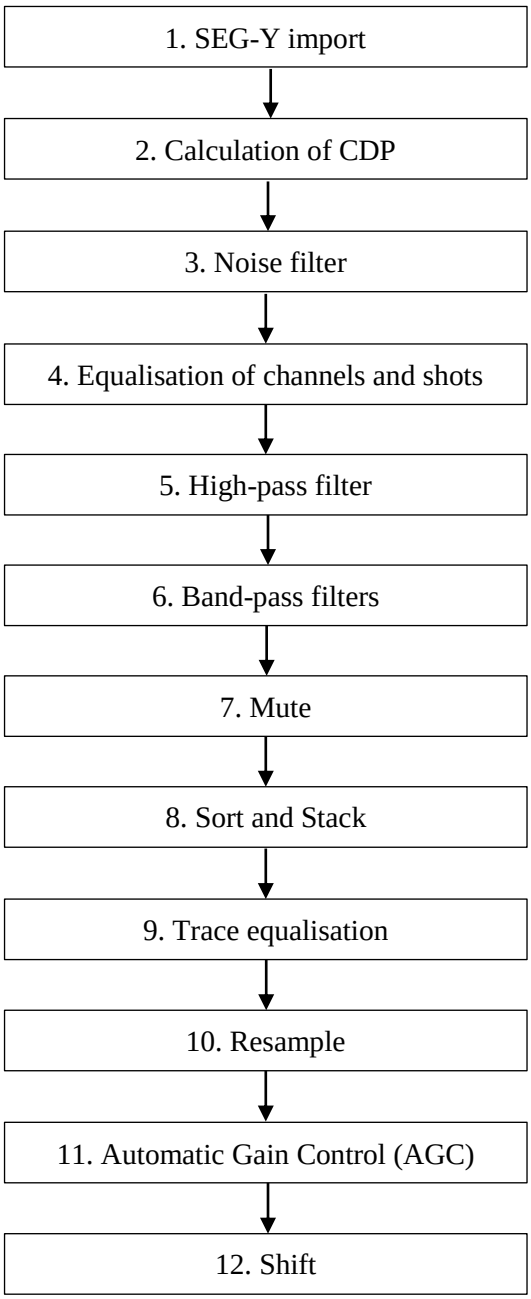

Figure 10.1 – Processing steps applied to the CONDRIBER seismic data, based on Informe Técnico Campaña Mower (2014).

10.2 Site U1391 Core Images

Selected examples of high-resolution photos taken onboard the IODP Expedition 339 Site U1391 to illustrate the gradational contourite successions and their facies variations.

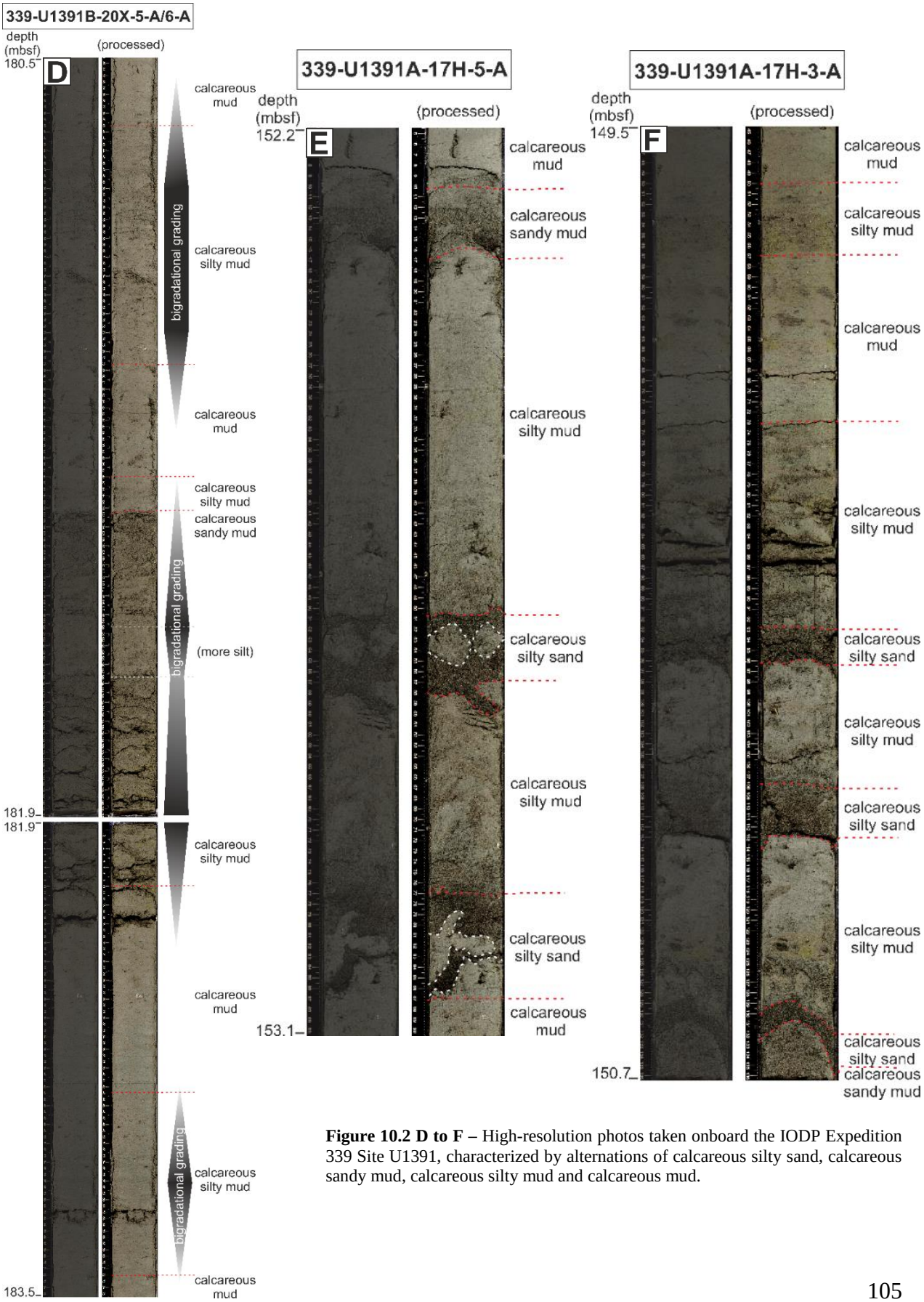

Figure 10.2 D to F – High-resolution photos taken onboard the IODP Expedition 339 Site U1391, characterized by alternations of calcareous silty sand, calcareous sandy mud, calcareous silty mud and calcareous mud.

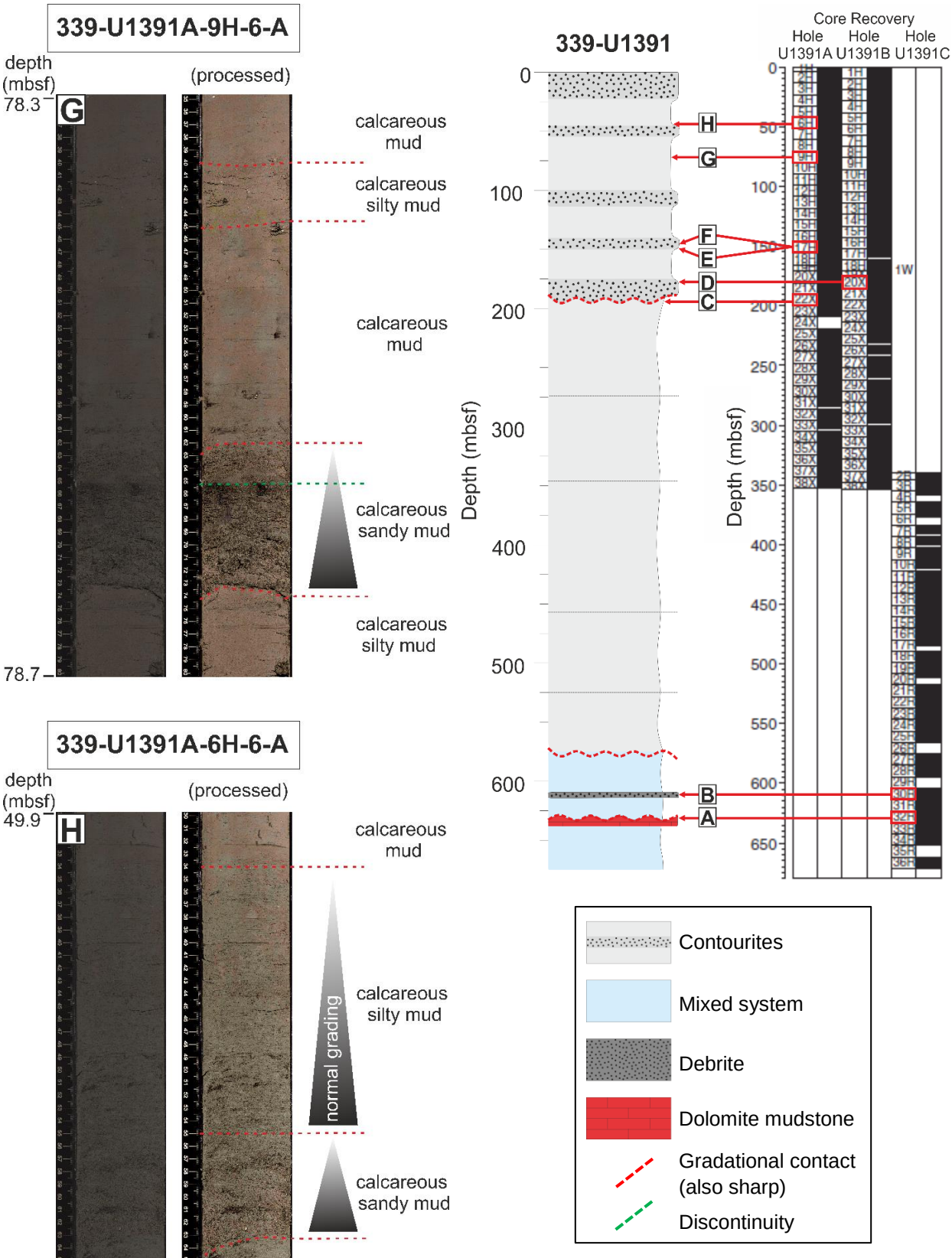

Figure 10.2 G and H – High-resolution photos from IODP Expedition 339 Site U1391, displaying contourite gradational successions. The photos analyzed in this study represent different core sections and depths, as shown in the lithostratigraphic column.

10.3 Seismic Reflection Profiles

Seismic reflection profiles from the CONDRIBER, STEAM, BIGSET, and GSI surveys with seismic stratigraphic interpretations.

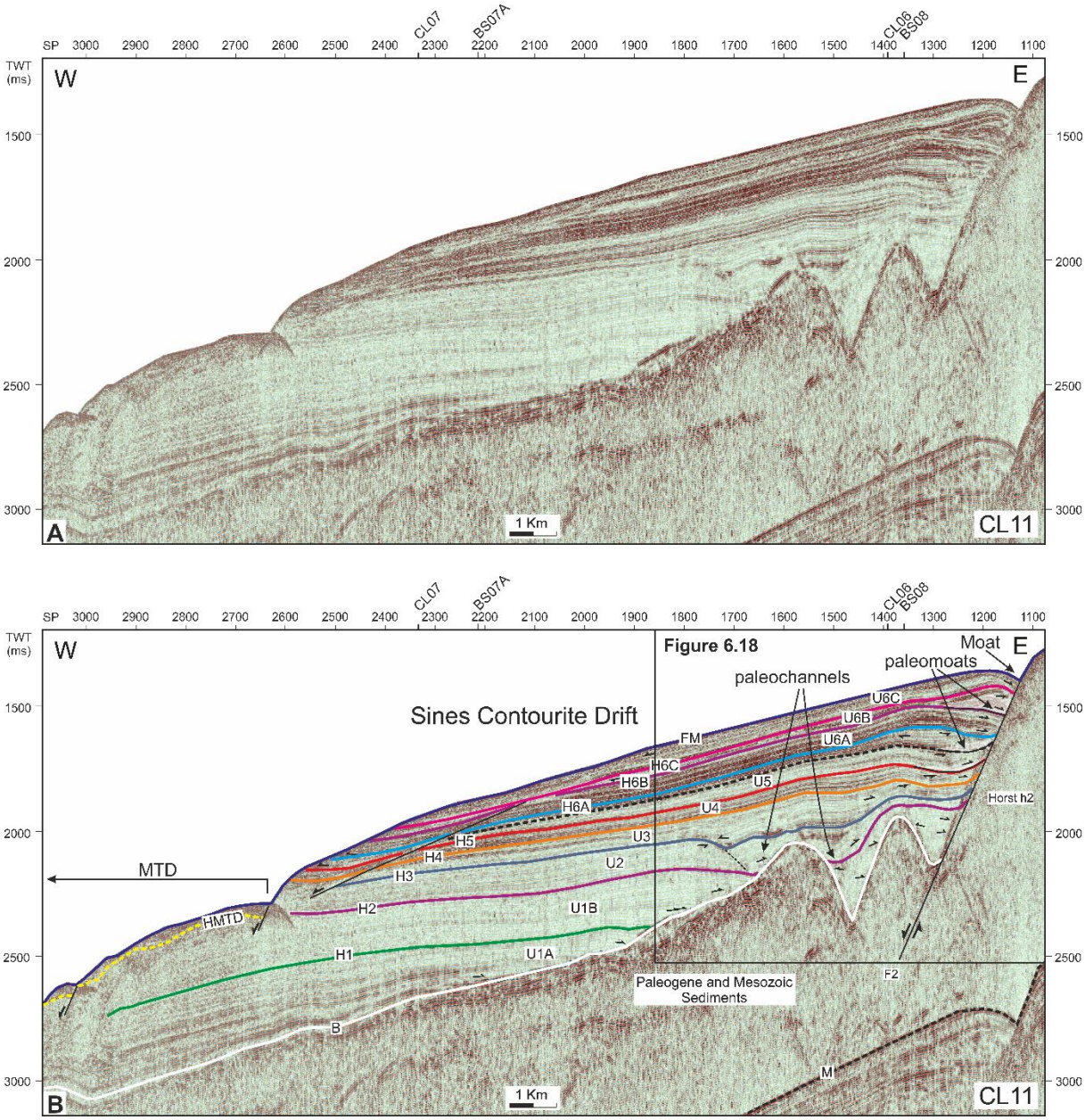

Figure 10.3 – Un-interpreted (A) and interpreted (B) seismic profile CL11, showing the paleomoats formed since seismic unit U4 and paleochannels affecting seismic units U1 to U3. U1 to U6: seismic units; B and H1 to H6C: seismic horizons; HMTD: base of MTD; FM: seafloor horizon. F: faults; **black arrows**: reflections terminations; **shaded areas**: paleomoats; **M**: multiple.

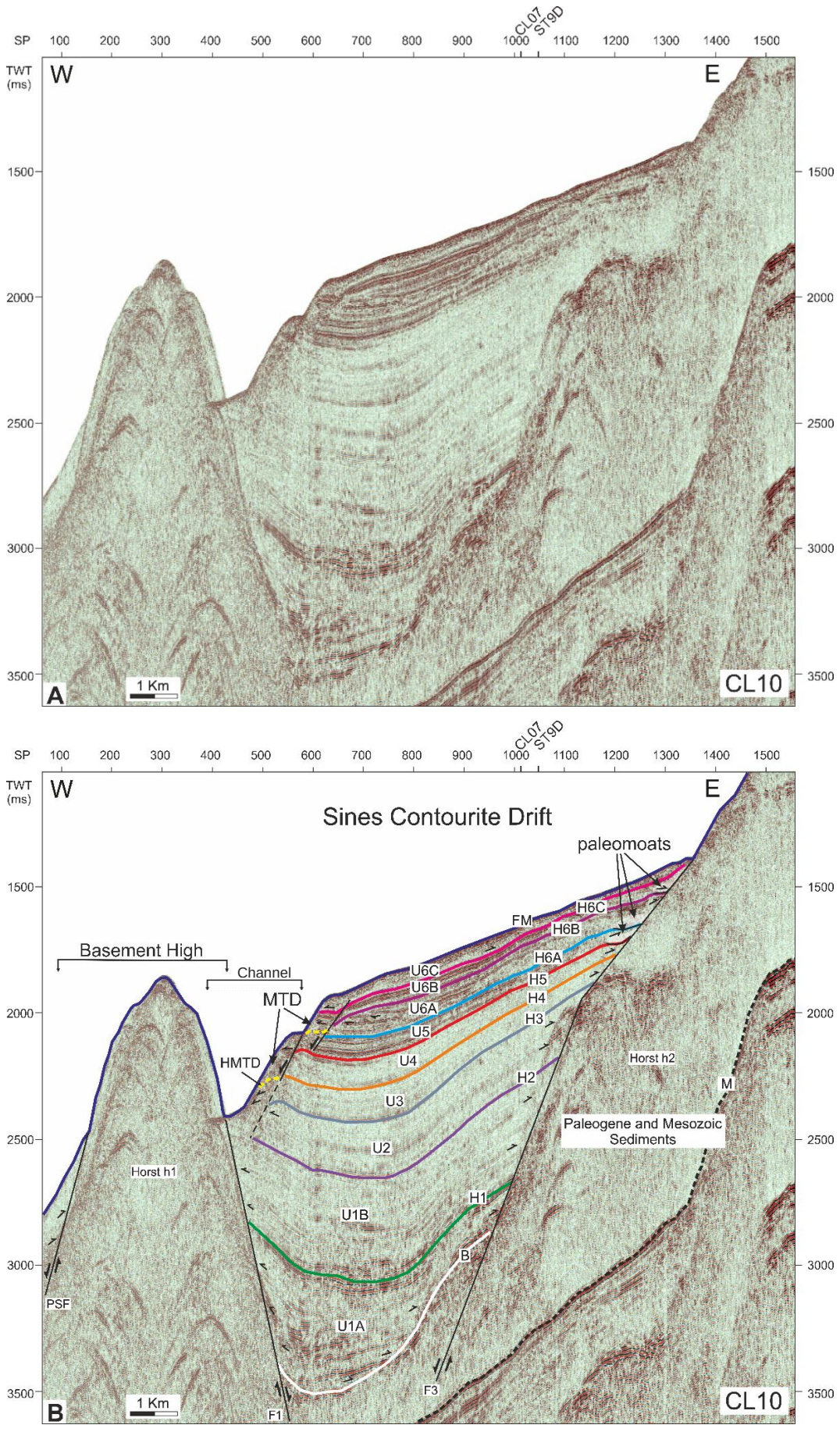

Figure 10.4 – Un-interpreted (A) and interpreted (B) seismic profile CL10, showing a basement high west of the SD, with an associated channel and MTD accumulation. U1 to U6: seismic units; B and H1 to H6C: seismic horizons; HMTD: base of MTD; FM: seafloor horizon. F: faults; **black arrows**: reflections terminations; **shaded areas**: paleomoats; **M**: multiple.

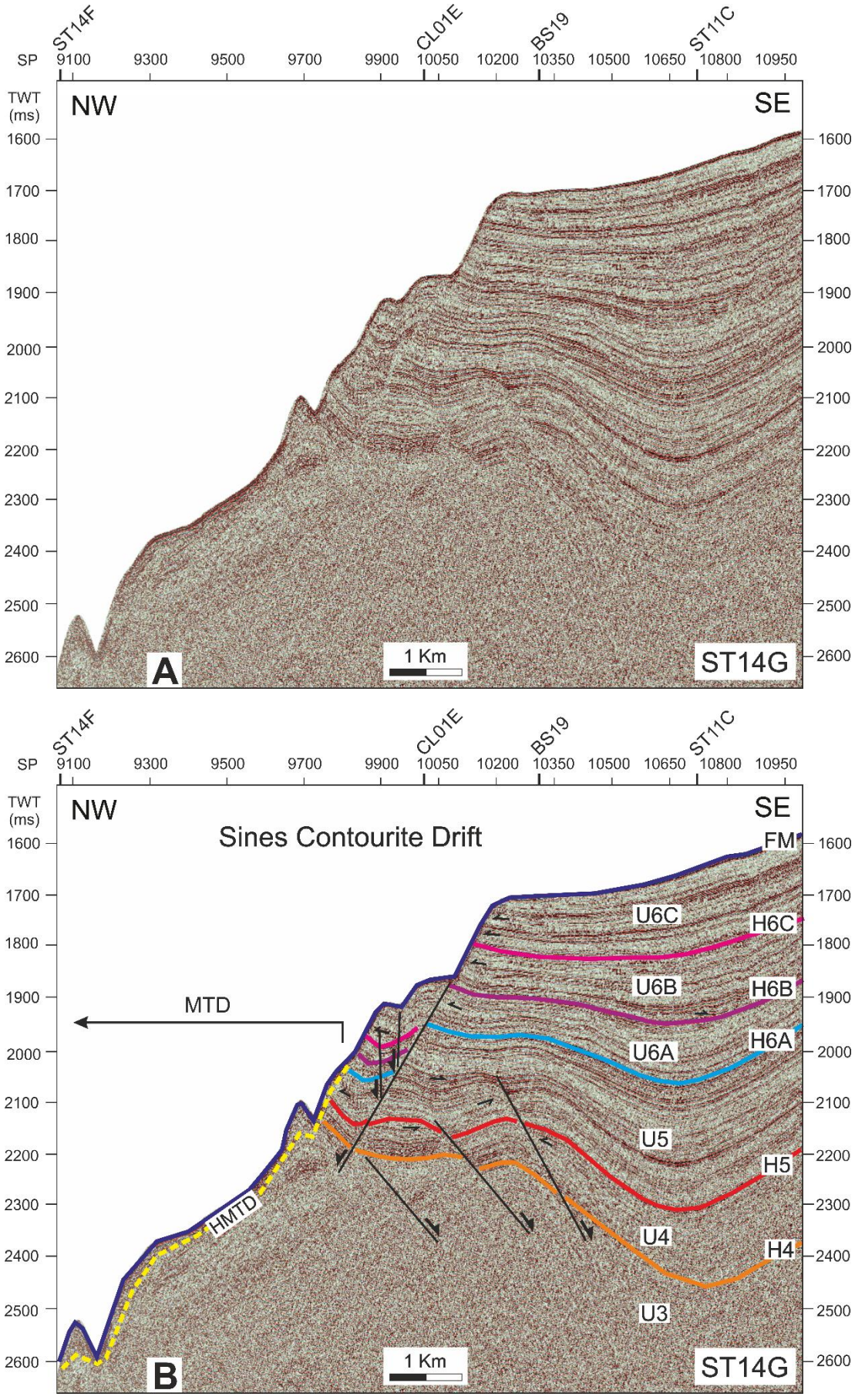

Figure 10.5 – Un-interpreted (A) and interpreted (B) seismic profile ST14G shows MTD accumulation and slope failure related faults. U1 to U6: seismic units; B and H1 to H6C: seismic horizons; HMTD: base of MTD; FM: seafloor horizon. F: faults; **black arrows**: reflections terminations.

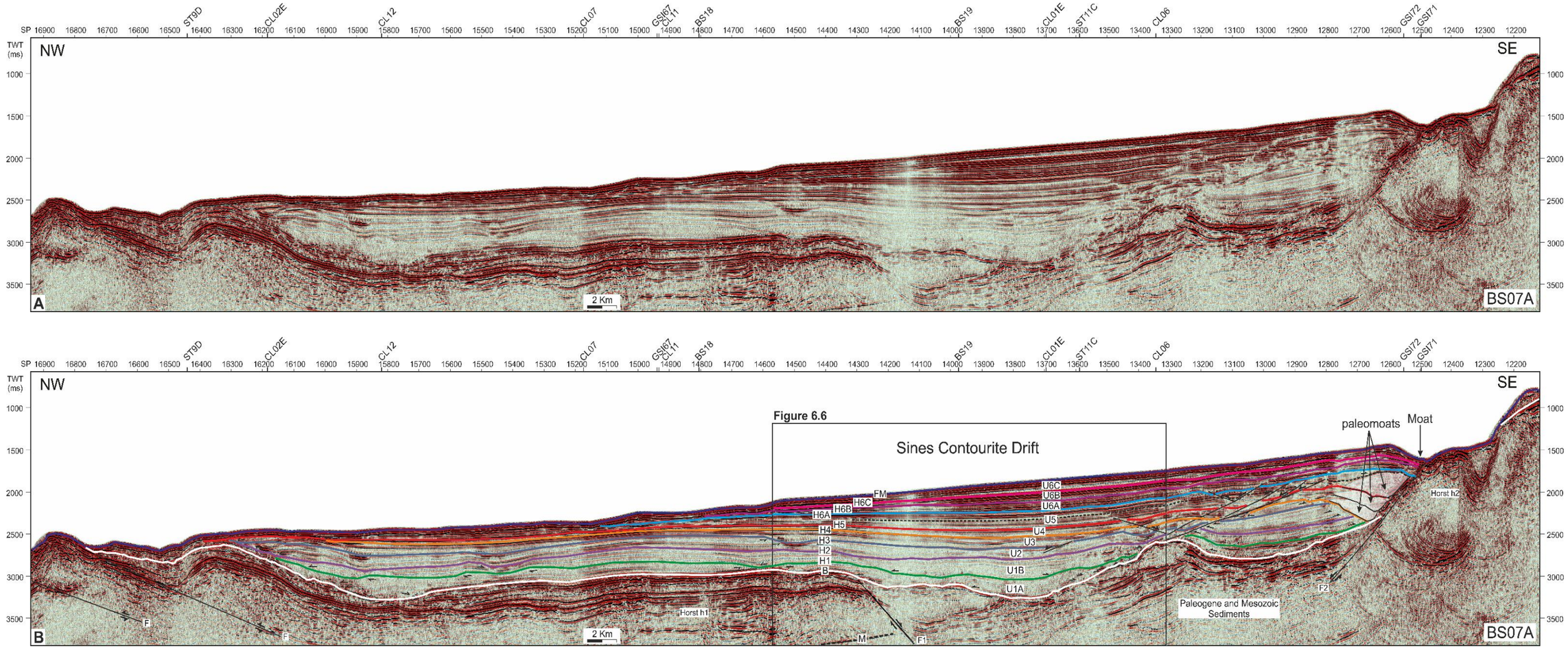

Figure 10.6 – Un-interpreted (A) and interpreted (B) seismic profile BS07A displaying the internal configurations of the SD seismic units. U1 to U6: seismic units; B and H1 to H6C: seismic horizons; FM: seafloor horizon. F: faults; **black arrows**: reflections terminations; **shaded areas**: paleomoats; **M**: multiple.

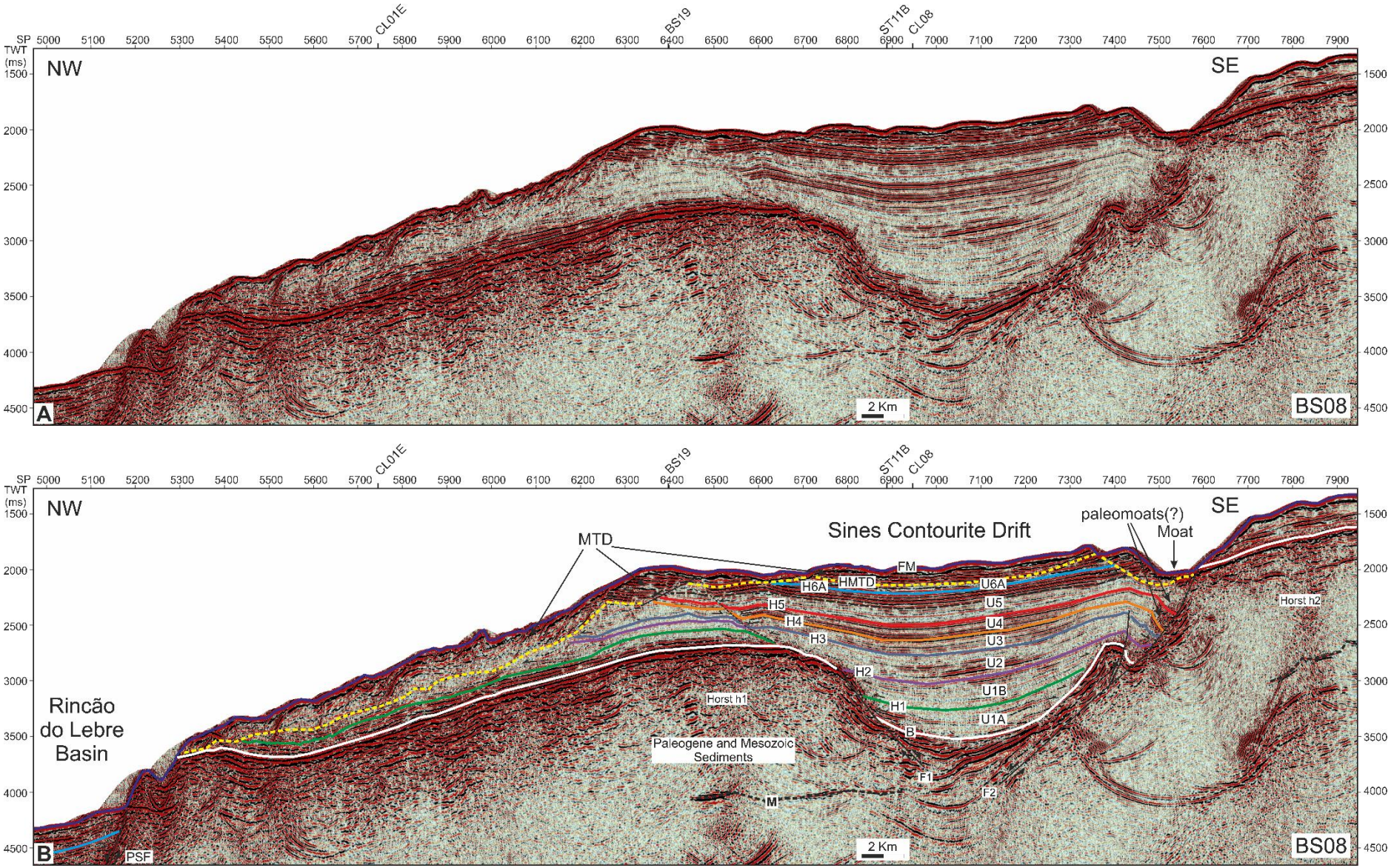

Figure 10.7 – Un-interpreted (A) and interpreted (B) seismic profile BS08 displaying MTD accumulation and a compressive event related to fault F2. U1 to U6: seismic units; B and H1 to H6C: seismic horizons; HMTD: base of MTD; FM: seafloor horizon. F: faults; **black arrows**: reflections terminations; **M**: multiple.

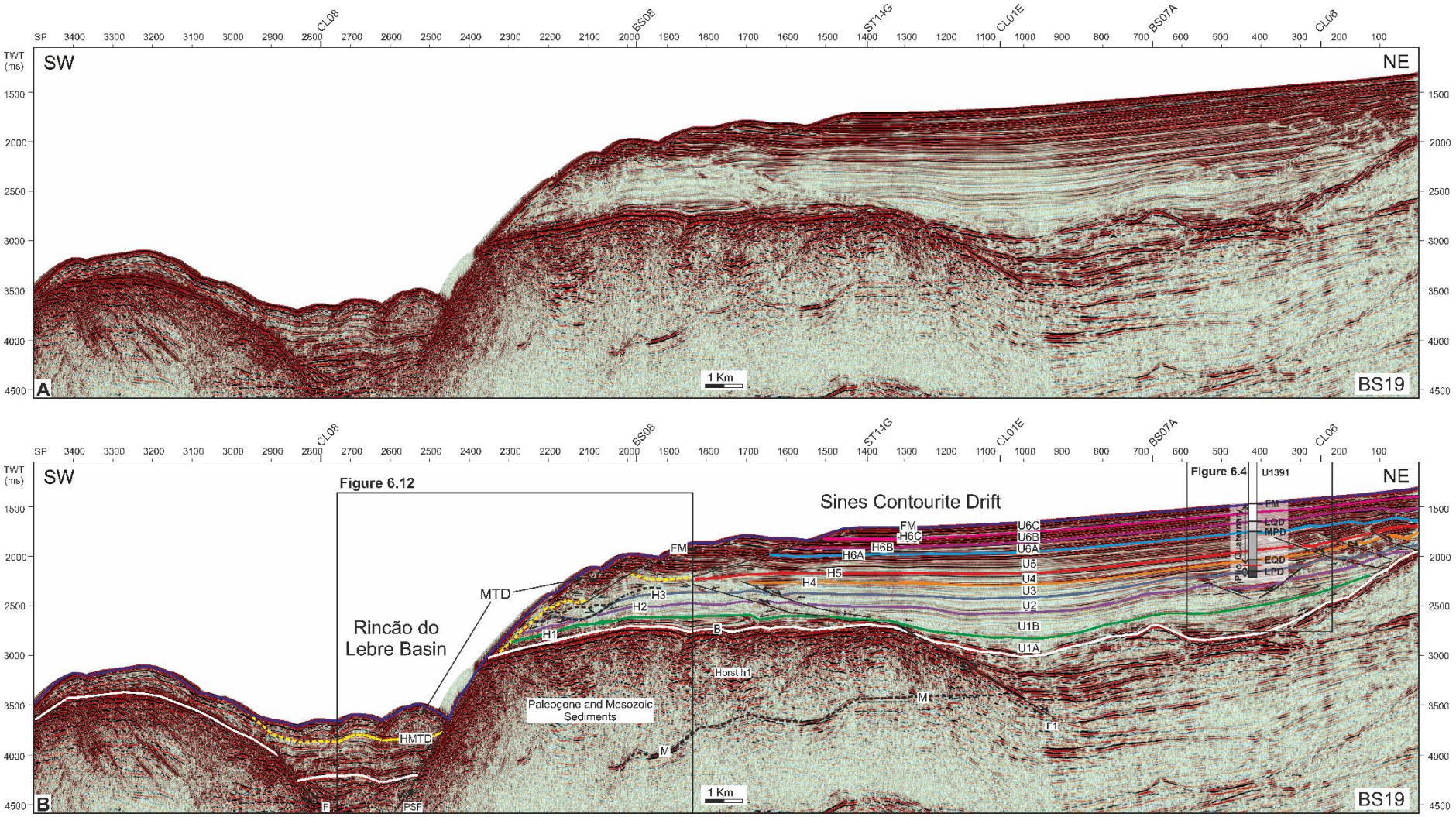

Figure 10.8 – Un-interpreted (A) and interpreted (B) seismic profile BS19 shows MTD accumulation related to the Pereira de Sousa escarpment and the correlation with Site U1391 stratigraphic discontinuities. U1 to U6: seismic units; B and H1 to H6C: seismic horizons; HMTD: base of MTD; FM: seafloor horizon. F: faults; **black arrows**: reflections terminations; **M**: multiple.

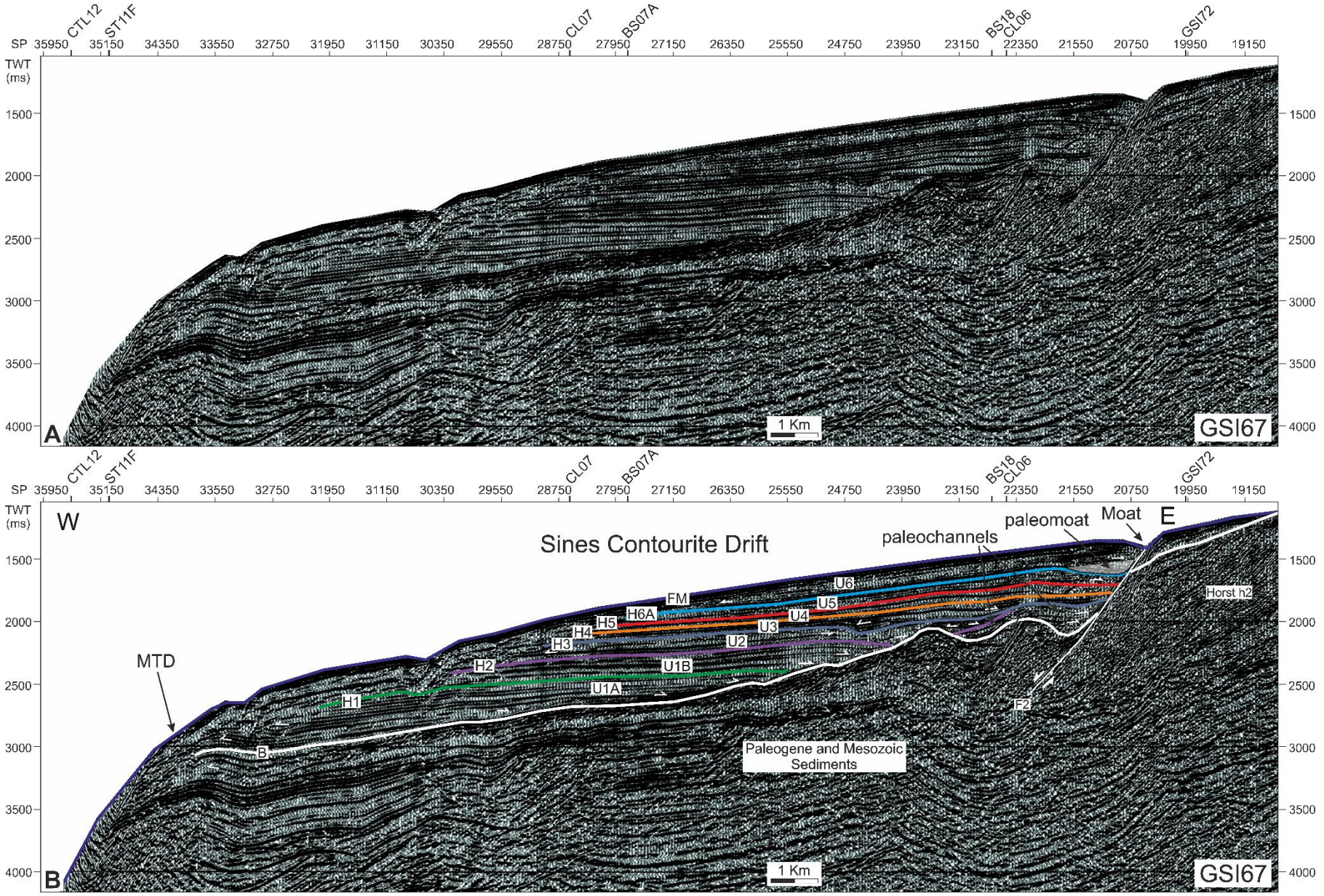

Figure 10.9 – Un-interpreted (A) and interpreted (B) seismic profile GSI67 displaying the seismic character of the SD seismic units. U1 to U6: seismic units; B and H1 to H6C: seismic horizons; HMTD: base of MTD; FM: seafloor horizon. F: faults; **black arrows**: reflections terminations; **shaded areas**: paleomoats.

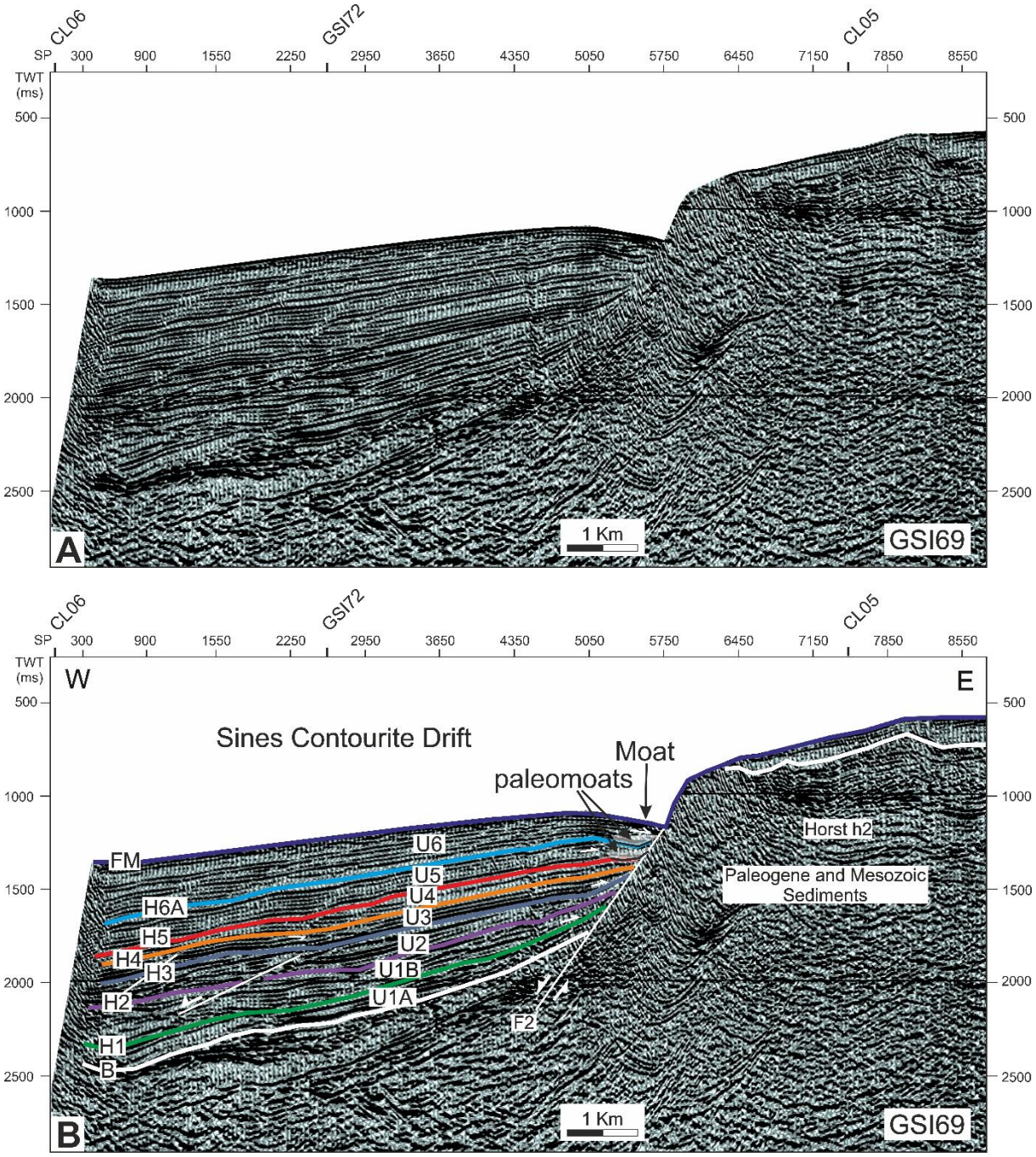

Figure 10.10 – Un-interpreted (A) and interpreted (B) seismic profile GSI69 displaying the internal reflection configurations of seismic units U1 to U6. U1 to U6: seismic units; B and H1 to H6C: seismic horizons; HMTD: base of MTD; FM: seafloor horizon. F: faults; **black arrows**: reflections terminations; **shaded areas**: paleomoats.

10.4 Isopach Maps

Isopach maps of the thickness for the Sines Drift total sedimentary package and for the MTD.

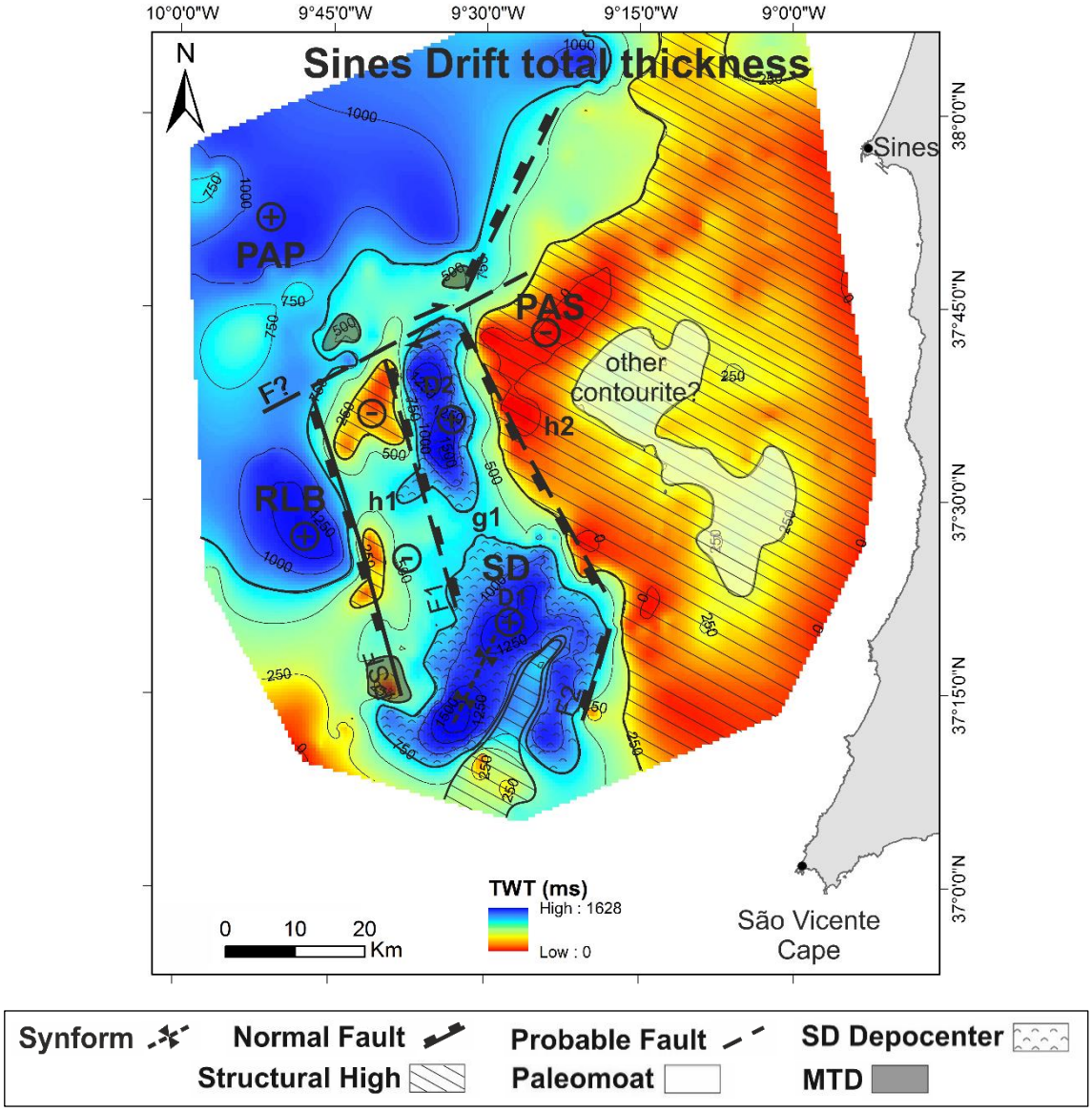

Figure 10.11 – Isopach map of the SD total thickness (comprises seismic units U1 to U6). **Legend:** plus and minus signs mark depressions and elevations; **h1** and **h2** correspond to horsts and **g1** to a graben; D1 and D2 mark the main depocenters; PAP – Príncipe de Avis Plateau; PAS – Príncipe de Avis Seamounts; PSF – Pereira de Sousa Fault. RLB – Rincão do Lebre Basin. Equidistance: 250 ms.

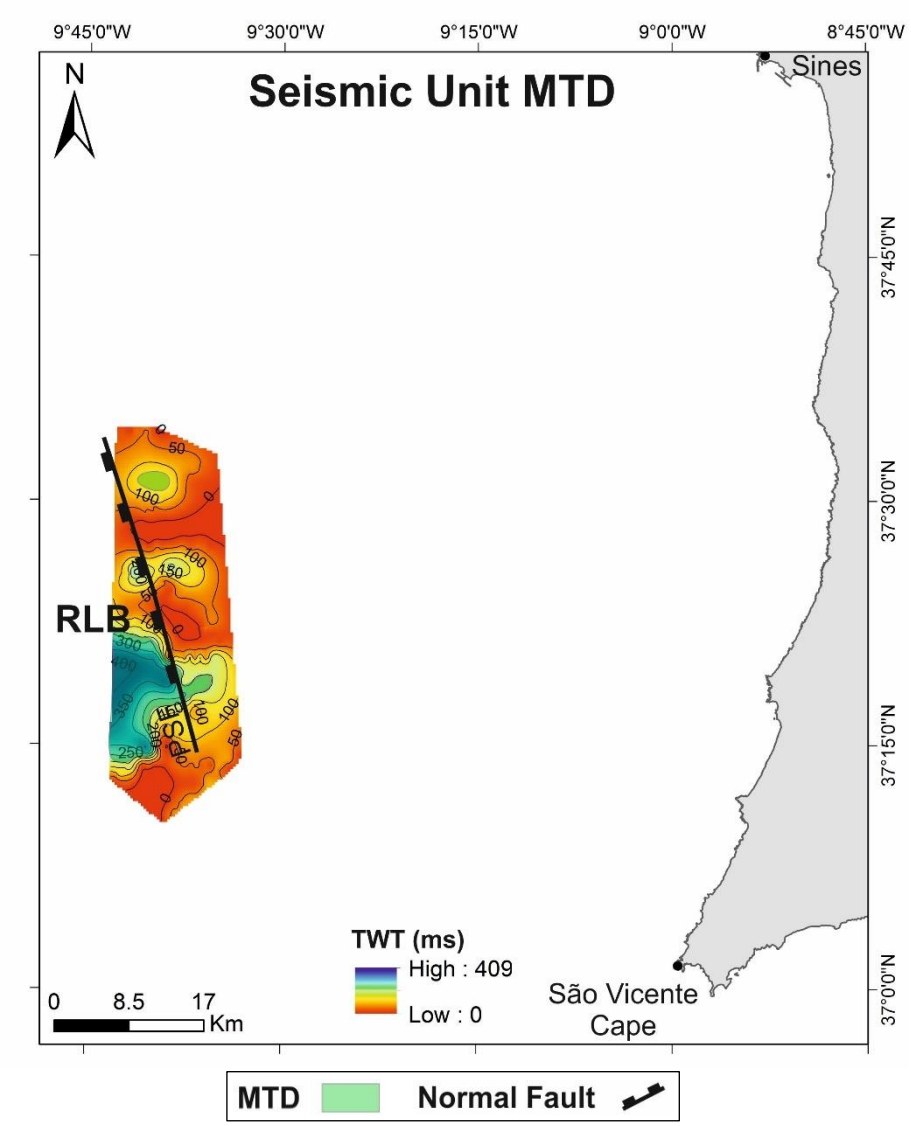

Figure 10.12 – Isopach map for the MTD. **Legend:** PSF – Pereira de Sousa Fault. RLB – Rincão do Lebre Basin. Equidistance: 50 m.